Title

Investigation of the Endoplasmic Reticulum-Mitochondria Encounter Structure in Regulating Coenzyme Q Biosynthesis

Author

Novales, Noelle Alexa Villasin

Publication Date

2024

Peer reviewed|Thesis/dissertation

UNIVERSITY OF CALIFORNIA

Los Angeles

Investigation of the Endoplasmic Reticulum-Mitochondria Encounter Structure in Regulating Coenzyme Q Biosynthesis

A dissertation submitted in partial satisfaction of the requirements for

the degree Doctor of Philosophy

in Biochemistry, Molecular & Structural Biology

by

Noelle Alexa Villasin Novales

2024

ABSTRACT OF THE DISSERTATION

Investigation of the Endoplasmic Reticulum-Mitochondria Encounter Structure in Regulating Coenzyme Q Biosynthesis

by

Noelle Alexa Villasin Novales

Doctor of Philosophy in Biochemistry, Molecular & Structural Biology

University of California, Los Angeles, 2024

Professor Catherine F. Clarke, Chair

Coenzyme Q (CoQ_n or ubiquinone) is an essential lipid molecule containing a redox-active benzoquinone head group and polyisoprenoid tail of varying length, denoted by *n*. The structural features of CoQ afford its ability to perform its role as a mobile electron carrier in the mitochondrial electron transport chain. Its synthesis is driven by the nuclear-encoded Coq polypeptides, several of which are required to assemble into a protein-lipid complex, the CoQ synthome. The formation of the CoQ synthome is coordinated by the endoplasmic reticulum-mitochondria encounter structure (ERMES), a membrane contact site that bridges the ER and mitochondria. CoQ deficiency results in various clinical manifestations, therefore it is imperative to have a holistic understanding of how CoQ is endogenously synthesized and distributed, and how these processes are regulated. We utilize *Saccharomyces cerevisiae* as a model organism given the high functional conservation of *COQ* genes and mitochondrial membrane contact sites with humans. Chapter 1 details an overview of the members required for CoQ biosynthesis and

discusses the relationship between the CoQ synthome and ERMES. Chapter 2 focuses on the recharacterization of Coq10 using nonfunctional Coq10 isoforms. The *COQ10* gene is positioned adjacent to *MDM12*, which encodes the cytosolic subunit of ERMES. Due to this arrangement, we discovered that deletion of *COQ10* impacts *MDM12* expression, resulting in diminished Mdm12 protein content and ERMES dysfunction. We use CRISPR-Cas9 to introduce mutations within *COQ10* that preserve *MDM12* expression, thereby maintaining ERMES. We show that Coq10 is not required for CoQ synthome assembly, and phenotypes associated with the *coq10*Δ mutant were due to the impact on ERMES. Considering ERMES may have a specific role in CoQ synthome assembly, Chapter 3 evaluates if *ERMES*Δ mutants can be rescued by deleting *COQ11*. The *COQ11* gene product is proposed to be a negative modulator of CoQ synthome assembly, indicated by the ability of the *COQ11* deletion to rescue complex stability in the *coq10*Δ*coq11*Δ double mutant. With Dr. Maya Schuldiner, we show that select *ERMES*Δ mutants can be rescued by deleting *COQ11*, indicating the role of ERMES in regulating CoQ synthome assembly can be circumvented when ERMES is absent. Chapter 4 examines how the expression of an artificial tether affects CoQ biosynthesis. Artificial tethers have been used to study membrane contact sites *in vivo*, and we report that the act of physical tethering does not bolster CoQ biosynthesis, and instead may impact trafficking and degradation. The results from Chapter 4 support the notion that ERMES has a direct role in CoQ synthesis and distribution, which an artificial tether cannot fulfill. Appendices I-III contain previous publications, including: characterization of the *coq10*Δ*coq11*Δ phenotype, an enzymology study from my undergraduate research published during my graduate program, and a structural analysis of clinically relevant single nucleotide variants in human *COQ* genes. Together, this work helps to clarify the roles of Coq10 and ERMES in the regulation of CoQ biosynthesis and distribution.

The dissertation of Noelle Alexa Villasin Novales is approved.

Carla M. Koehler

Joseph A. Loo

Alexander M. van der Bliek

Catherine F. Clarke, Committee Chair

University of California, Los Angeles

2024

This work is dedicated to my parents,

who have made countless sacrifices to support my dreams.

TABLE OF CONTENTS

LIST OF TABLES AND FIGURES

ACKNOWLEDGEMENTS

To start, I am immensely appreciative of the support and guidance I have received from my advisor, Dr. Catherine Clarke, throughout my doctoral program. Cathy has provided me with countless opportunities to challenge myself as a scientist, and I am grateful for the creative independence I have developed under her mentorship. I am fortunate to have had an advisor who was extremely supportive of my various extracurricular activities during my graduate studies. Cathy gave me so much freedom and space to constantly learn and create, and without her support, I wouldn't have known what I was, and will be, capable of achieving.

I am grateful for the members of my thesis committee, Dr. Carla Koehler, Dr. Alexander van der Bliek, and Dr. Joseph Loo, as they provided me with endless support in my research as well as in my career development. I looked forward to our periodic updates, as my committee always matched my level of excitement whenever I talked about my science or my teaching. It brought me so much joy to know I had these individuals in my corner, supporting me and encouraging me to do great things.

Chapter 2 is a reprint of an article under review in *The Journal of Biological Chemistry* (2024), and I thank my co-author, Kelsey Feustel, for generating the CRISPR mutants and partnering with me in the biochemical characterization of those mutants. Chapter 3 is a manuscript in preparation that I worked on with several tremendous scientists; I thank Dr. Hadar Meyer and Dr. Yeynit Asraf, who performed imaging analyses, and Dr. Zachary Hemminger, who processed RNA sequencing data. For the synthetic biology experiments outlined in Chapter 4, I thank Dr. Maya Schuldiner for gifting the artificial tether constructs. In addition to collaborating on these projects, Maya was also a constant supporter throughout my degree; her willingness to help me succeed has truly been a gift.

Appendix I is a reprint of an article in *The Journal of Biological Chemistry* (2020) 295: 6023-6042; I would like to thank the American Society for Biochemistry and Molecular Biology and the primary author Dr. Michelle Bradley for permission to use this copyrighted material. Appendix II is a reprint of an article in *Analytical Biochemistry* (2022) 654: 114796; I would like to thank Elsevier for permission to use this copyrighted material. Appendix III is a reprint of an article in *Antioxidants* (2022) 11: 2308; I would like to thank the Multidisciplinary Digital Publishing Institute and the primary authors Sining Wang and Akash Jain for permission to use this copyrighted material.

To the former members of the Clarke lab, Dr. Michelle Bradley and Dr. Lucia Fernández-del-Río, thank you for being valuable mentors during my rotation and teaching me the foundational skills that I would use in my research. To the current members, Michael Guile, Sining Cindy Wang, and Kelsey Feustel, thank you for your friendship, for making the lab a healthy environment, and for teaching me new things every day. To all the undergraduates I have worked with, thank you for reminding me why I continue to work with emerging scientists and for being a positive light throughout my academic career. I want to highlight and thank two former lab members in particular, Audrey Nashner and Miranda Kelly, for being constant motivators in my career. Working with them and seeing their successes today inspires me, as they are fantastic female scientists who will go so far in their careers. I am particularly grateful for the kindness, friendship, and mentorship from Dr. Danielle Schmitt, who offered so much advice on navigating this career path, and frequently reminded me how amazing we are as women in science! I want to give a special acknowledgement to Maya Cornejo, who afforded me a friendship that holds a special place in my heart. Maya is an extremely talented scientist and kindhearted person, and I will always be rooting for her success.

To the teaching faculty I have worked with, I treasure the community we have built, which has left a lasting impression on me. I would like to acknowledge Dr. Agape Awad and Dr. James Gober, the first instructors I worked with, who allowed me to have the creative independence that blossomed my passion for teaching. To Dr. Margaret Davis and Dr. Laurel Westrup, thank you for offering instrumental advice throughout my Graduate Certificate in Writing Pedagogy. I want to acknowledge the faculty at Saint Monica Catholic High School that I worked with as a teacher; I particularly want to thank Dr. Laura Haney and Principal James Spellman for taking a chance on a graduate student for this teaching opportunity. I want to thank the hundreds of students I've had the pleasure to teach; you all have made my work in the educational sector so rewarding and fulfilling. To the phenomenal instructional faculty in the UCLA Department of Chemistry and Biochemistry, I am honored to have had the opportunity to learn from you. To Dr. Arlene Russell, Dr. Anne Hong-Hermesdorf, Dr. Johnny Pang, and Dr. Ryan Lannan: thank you for your camaraderie, and for believing in me and my teaching abilities.

To my best friends, Amara Pouv, Christian Loo, and Jordan Ngo: my heart is so full knowing our friendship has persisted despite us being all over the country now. I appreciate that when we reunite, it's like nothing has changed. To my undergraduate advisor, Dr. Jason Schwans, thank you for teaching me the foundations of biochemistry and inspiring me to pursue higher education. Thank you for always highlighting my best qualities, because too often I couldn't see them on my own. To Dr. Paul Buonora, thank you for always believing in me, even when I didn't believe in myself. It is astoundingly rare to find a mentor with as much patience as these professors, and I am lucky to have had them both supporting me, even after parting from Long Beach. It took quite some time to build up my confidence as a scientist and as a person, but they remained patient throughout, and never stopped supporting me.

To my sister and brother-in-law, Nicole and Kurt, thank you for always making me laugh, reminding me to give myself a break when I need to, and lending an ear during difficult times. Thank you for visiting me every now and then; I know I don't come home as often as I should, but I appreciate when you're able to bring a little bit of home here to LA. To my dad, who has worked tirelessly to provide for the life I have today, I appreciate your sacrifices and help whenever I needed it. To my mom, whose phone calls I look forward to every Sunday, I cannot thank you enough for supporting me and encouraging me to support my dreams. I value the relationship we have built since I started college, and I know it will only get stronger with time.

Finally, I want to thank my rescue pup (a.k.a. my son), Rambo, for being a constant force of positivity in my life. I'm so glad your dad and I adopted you and have been able to give you the life and love you are so deserving of. To my husband, Dr. Zachary Hemminger, thank you for being at Boyer Patio for the QCBio gathering that I crashed during my first week of graduate school, because that led me to meeting you. Unironically, I attribute most, if not all, of the fortunate events in my life to serendipity, simply being at the right place at the right time, but I'm almost certain that meeting you wasn't by chance. Every day I am in awe of the person that you are, and I am so lucky that I got to experience the entirety of grad school with you by my side. Your unwavering love and support are things I cherish deeply and cannot express enough gratitude for. I am thrilled that we got this opportunity to grow as scientists and as people together here at UCLA, and I can't wait for our next adventure!

VITA

2016 – 2019	Undergraduate Student Researcher Department of Chemistry and Biochemistry California State University, Long Beach Long Beach, CA
2016 – 2017	NIH Building Infrastructure Leading to Diversity (BUILD) Fellow California State University, Long Beach Long Beach, CA
2017 – 2019	NIH Research Initiative for Scientific Enhancement (RISE) Fellow California State University, Long Beach Long Beach, CA
2018	Summer Training Academy for Research Success (STARS) Fellow University of California, San Diego La Jolla, CA
2019	B.S. Biochemistry, Cum Laude California State University, Long Beach Long Beach, CA
2019 – 2024	Graduate Student Researcher and Teaching Fellow Department of Chemistry and Biochemistry University of California, Los Angeles Los Angeles, CA
2021	M.S. Biochemistry and Molecular Biology University of California, Los Angeles Los Angeles, CA
2022	Excellence in Second Year Research and Academics Award Department of Chemistry and Biochemistry University of California, Los Angeles Los Angeles, CA
2022	Michael E. Jung Excellence in Teaching Award Department of Chemistry and Biochemistry University of California, Los Angeles Los Angeles, CA
2022 – 2023	Chemistry Teacher and Senior Class Advisor Saint Monica Catholic High School Santa Monica, CA

2023 – 2024 Instructor and Course Creator
Undergraduate Education Initiatives Unit
University of California, Los Angeles
Los Angeles, CA

2023 Ralph and Charlene Bauer Award
University of California, Los Angeles
Los Angeles, CA

2024 CIRTL Certified Associate
University of California, Los Angeles
Los Angeles, CA

2024 Graduate Certificate in Writing Pedagogy
University of California, Los Angeles
Los Angeles, CA

2024 Roberts A. Smith Dissertation Award
University of California, Los Angeles
Los Angeles, CA

PUBLICATIONS

Novales, N.A., Hemminger, Z.E., Meyer, H., Asraf, Y., Schuldiner, M., Clarke, C.F. Deletion of *COQ11* rescues the respiratory deficiency of yeast lacking *MMM1*, a component of the ERMES complex. **Manuscript in preparation.**

Novales, N.A.‡, Feustel, K.J.‡, Clarke, C.F. Nonfunctional *coq10* mutants maintain the ERMES complex and reveal true phenotypes associated with the loss of the coenzyme Q chaperone protein Coq10. *Journal of Biological Chemistry*, **In review.**

Wang, S.‡, Jain, A.‡, **Novales, N.A.**, Nashner, A.N., Tran, F., Clarke, C.F. Predicting and understanding the pathology of single nucleotide variants in human *COQ* genes. *Antioxidants*. 2022, *11*, 2308.

Novales, N.A., Schwans, J.P. Comparing the Effects of Organic Cosolvents on Acetylcholinesterase and Butyrylcholinesterase Activity. *Analytical Biochemistry*. 2022, *654*, 114796.

Bradley, M.C., Yang, K., Fernández-del-Río, L., Ngo, J., Ayer, A., Tsui, H.S., **Novales, N.A**., Stocker, R., Shirihai, O.S., Barros, M.H., Clarke, C.F. *COQ11* Deletion Mitigates Respiratory Deficiency Caused by Mutations in the Gene Encoding the Coenzyme Q Chaperone Protein Coq10. *Journal of Biological Chemistry.* 2020, *295*, 6023–6042.

‡ These authors contributed equally to this work.

Chapter 1

Introduction to Coenzyme Q:

Function, Biosynthesis, and Regulation

WHAT IS COENZYME Q?

Coenzyme Q (ubiquinone, CoQ, or Q) is an essential redox-active lipid molecule found in the plasma membranes and endomembranes of all eukaryotic species (1–3). Proper function of CoQ is dependent on its hydrophobic tail, which enables its localization within the midplane of lipid bilayers (Fig. 1A). The number of isoprene units is species dependent, denoted by *n* in CoQ_n: humans synthesize a polyisoprenyl tail with ten isoprene units, forming CoQ_{10}, yeast synthesize CoQ_6, *E. coli* synthesize CoQ_8, and mice synthesize a mixture of CoQ_9 and CoQ_{10} (4). Its fully decorated quinone head group affords its ability to serve as a single electron and proton carrier, shifting redox states from ubiquinone, to the radical semiubiquinone (CoQH•), and subsequently ubiquinol ($CoQH_2$) (Fig. 1B) (4).

The canonical role of CoQ takes place in the mitochondrial electron transport chain (ETC), where the fully oxidized CoQ accepts electrons and protons from NADH or succinate via complex I or II, respectively, forming the reduced $CoQH_2$, and donates them to cytochrome *c* at complex III, restarting the CoQ redox cycle (Fig. 1C) (5). This electron transfer allows for proton pumping via the ETC and subsequent production of ATP via complex V, or ATP synthase (6). Yeast lack complex I; instead they possess NADH:ubiquinone oxidoreductases that reside on the inner mitochondrial membrane facing the matrix (Ndi1) or facing the intermembrane space (Nde1 and Nde2) (7, 8). While these alternative electron donors do not participate in proton translocation that typically occurs at complex I, the transport of electrons via the CoQ cycle still contributes ATP synthesis at complex V. In general, CoQ serves as a cofactor for several metabolic processes, such as choline metabolism, sulfide detoxification, and pyrimidine biosynthesis, which in turn provides several entryways for the acceptance of electrons at complex III (1, 3).

Reduced $CoQH_2$ is the only endogenously synthesized lipid-soluble antioxidant in animal cells (9). Membrane lipids can be subject to lipid peroxidation via the radical-mediated abstraction of bis-allylic hydrogens (10), a phenotype that can be emulated in yeast treated with exogenous polyunsaturated fatty acids (PUFAs), which rapidly autoxidize (11). Reduced $CoQH_2$ in conjunction with α-tocopherol is capable of serving as a chain-breaking antioxidant, which alleviates peroxidative damage (9). In accordance with this, yeast that are deficient in CoQ synthesis are not viable upon treatment with exogenous PUFAs, given the lack of the $CoQH_2$-mediated antioxidant protection (12, 13). This has been more broadly explored in the context of ferroptosis, a form of cell death caused by iron-dependent lipid peroxidation (14, 15). Namely, ferroptosis suppressor protein 1 (FSP1) has been identified as an oxidoreductase required to reduce plasma membrane CoQ to the hydroquinone in order to combat lipid hydroperoxides (16, 17). Importantly, this role of $CoQH_2$ in non-mitochondrial membranes suggests that the modulation of CoQ redox pools is paramount for cellular function; such redox regulatory mechanisms have yet to be elucidated.

ESSENTIAL GENES FOR COENZYME Q BIOSYNTHESIS

Mutations in the genes encoding COQ polypeptides lead to primary CoQ_{10} deficiency, a rare condition typically caused by autosomal recessive mutations that results in a variety of clinical manifestations in humans (18, 19). While clinical variants of *COQ* genes are well documented and broadly available from numerous databases and published literature (20–23), the clinical significance is poorly understood. Recently, the structural and functional consequences of several single nucleotide variants found in *COQ* genes was characterized using structural analyses with AlphaFold predicted models or available solved structures (24). The

results spotlight the importance in elucidating the mechanisms performed in the biosynthetic pathway, as they may reveal insight in how these clinical manifestations from primary CoQ_{10} deficiency arise.

Human *PDSS1*, *PDSS2*, *COQ2* (Yeast *COQ1*, *COQ2*)

The primary aromatic ring precursor molecule in the CoQ biosynthetic pathway is 4-hydroxybenzoic acid (4HB) (4). In humans, 4HB is generated from tyrosine, however many of the steps in converting tyrosine to 4HB remain elusive (2, 4). Yeast is also capable of synthesizing 4HB from tyrosine, however it is preferentially generated via the shikimate pathway (4). In yeast, Hfd1 catalyzes the dehydrogenation of 4-hydroxybenzaldehyde (4-HBz) to 4HB (25); yeast lacking the *HFD1* gene (*hfd1*Δ) are able to perform this conversion when complemented with the human homolog *ALDH3A1* (26), however the gene product has not been confirmed in fulfilling this role in humans. As an alternative head group precursor, para-aminobenzoic acid (pABA), derived from chorismate, can also be used for CoQ synthesis in yeast (27). The transport mechanism of 4HB or pABA from the cytosol into the mitochondrial matrix, where CoQ biosynthesis takes place exclusively, remains unclear.

The synthesis of the polyisoprenoid tail requires polyprenyl diphosphate synthase (comprised of two subunits, PDSS1 and PDSS2) in humans (28), or Coq1 in yeast (29, 30). These proteins are responsible for isoprene polymerization via condensation of dimethylallyl pyrophosphate (DMAPP) and isopentenyl pyrophosphate (IPP), which are both intermediates of the mevalonate pathway (3) (Fig. 2). Similar to the head group precursors, the mitochondrial import mechanism of the isoprenyl diphosphate precursors, IPP and DMAPP, have not been characterized. Upon import into the mitochondrial matrix, COQ2/Coq2 catalyzes the first

attachment onto the head group precursor at the C3 position, generating 3-polyprenyl-4-hydroxybenzoic acid (HPB) (31) (Fig. 2), or 3-hexaprenyl-4-aminobenzoic acid (HAB) when pABA is utilized as the precursor in yeast (27). Notably, expression of human *COQ2* in *coq2*Δ yeast permits the hexaprenyl tail attachment to the headgroup (32), indicating the reaction catalyzed by Coq2 is not specific to the tail length of the corresponding species. Of all the mitochondrial-associated proteins involved in CoQ biosynthesis, COQ2/Coq2 is the only integral membrane protein (33, 34); the rest of the CoQ biosynthetic proteins are peripherally associated to the inner mitochondrial membrane, facing the matrix (35).

Human *COQ3* (Yeast *COQ3*)

COQ3/Coq3 is an *S*-adenosylmethionine (AdoMet)-dependent methyltransferase that catalyzes the *O*-methylation reactions in CoQ biosynthesis (36–38). Specifically, it converts 4,5-dihydroxy-3-polyprenylbenzoic acid (DHPB) to 4-hydroxy-5-methoxy-3-polyprenylbenzoic acid (HMPB), as well as 3-methyl-6-methoxy-2-polyprenyl-1,4,5-benzenetriol ($DMeQH_2$) to the final product, $CoQH_2$ (Fig. 2). Four highly conserved motifs among class I methyltransferases, motifs I-III and post-I, form a seven-strand twisted beta sheet capable of binding AdoMet (39–41). In yeast, Coq3 has been observed to be phosphorylated in a Coq8-dependent manner (39, 42); it is speculated that Coq8 modulates the stability and subsequent activity of Coq3 via this modification.

Human *COQ4* (Yeast *COQ4*)

The COQ4/Coq4 protein is required for CoQ synthesis, and was previously thought to serve solely as a scaffolding protein to ensure the stability of other Coq polypeptides, as yeast

coq4 mutants have diminished levels of the remaining Coq polypeptides (43, 44). Recently, the enzymatic function of COQ4 has been identified as an oxidative decarboxylase for the C1 modification (45), a step that previously remained elusive (as denoted by "???" in Fig. 2). COQ4 thus performs both the decarboxylation and hydroxylation steps required to convert 4-hydroxy-5-methoxy-3-polyprenylbenzoic acid (HMPB) to 6-methoxy-2-polyprenyl-1,4-benzenediol ($DDMQH_2$). An *in vitro* reconstitution of CoQ biosynthesis using ancestral COQ proteins and a monoprenylated ring precursor also demonstrated that COQ4 possesses decarboxylase activity (46), although it is most compelling in the work by Pelosi et al., where C1-decarboxylation and C1-hydroxylation catalyzed by COQ4 is observed in human cells, *E. coli*, and *C. glutamicum* (45).

Human *COQ5* (Yeast *COQ5*)

COQ5/Coq5 is another AdoMet-dependent methyltransferase required for CoQ biosynthesis, and is responsible for the *C*-methylation performed at the C2 position (47, 48). Namely, it performs the conversion of $DDMQH_2$ to 3-methyl-6-methoxy-2-polyprenyl-1,4-benzenediol ($DMQH_2$) (Fig. 2). The yeast Coq5 structure has been determined previously and reveals a characteristic seven β-strand AdoMet methyltransferase structure required for Coq5 activity (49). Indeed, yeast *coq5* mutants that harbor mutations in the methyltransferase motifs result in loss of *C*-methyltransferase activity despite maintaining normal polypeptide content (50). Akin to Coq3, the Coq5 polypeptide has also been shown to be phosphorylated in a Coq8-dependent manner (42).

Human *COQ6*, *FDX1*/*FDX2*, *FDXR* (Yeast *COQ6*, *YAH1*, *ARH1*)

COQ6/Coq6 is a flavin-dependent monooxygenase that contains a tightly bound FAD (51, 52). Unlike canonical flavin-dependent monooxygenases that can use NAD(P)H as a direct electron source, yeast Coq6 acquires electrons through ferredoxin (Yah1) and ferredoxin reductase (Arh1) in order to perform the hydroxylation reactions (53). This coupled electron transfer in tandem with Coq6's hydroxylase activity enable Coq6 to perform the C5-hydroxylation step in CoQ biosynthesis, converting HPB to DHPB (53) (Fig. 2). Additionally, these proteins are also required for the C4-deamination reaction when pABA is used as a precursor (54). While expression of human *COQ6* was able to rescue CoQ_6 synthesis in *coq6*Δ yeast (55), the human homologs of Yah1 (FDX1 and FDX2) and Arh1 (FDXR) have not been implicated in CoQ biosynthesis. Nicoll et al. have recently proposed that COQ6 is capable of performing the C1-hydroxylation based on the ancestral COQ6 performing this reaction on the monoprenylated CoQ intermediate (46), however this role seems unlikely given that yeast and mammalian cells harboring mutations in their respective COQ6 isoforms are still able to perform the C1-decarboxylation and hydroxylation steps (53, 56).

Human *COQ7*/*CAT5*/*CLK-1* (Yeast *COQ7*/*CAT5*)

COQ7/Coq7 is a hydroxylase that performs the penultimate reaction of CoQ biosynthesis, converting $DMQH_2$ to $DMeQH_2$ (57–59) (Fig. 2). Coq7 was initially predicted to be a di-iron carboxylate protein based on high sequence conservation across organisms (59), which was later confirmed via cryo-EM using a human COQ7:COQ9 complex expressed in *E. coli* (60). The human COQ7 structure revealed a hydrophobic channel, such that when the COQ7:COQ9 complex was purified, octaprenylphenol, a bacterial CoQ intermediate, was found bound to this

site (60). Yeast Coq7 is phosphorylated in a Coq8-dependent manner, a modification that regulates its hydroxylase activity (42, 61). The phosphatase responsible for dephosphorylating Coq7 is Ptc7 (62), which has two isoforms in yeast as a result of splicing (63, 64). Notably, the spliced form localizes to the mitochondria where it can dephosphorylate Coq7; expression of the spliced Ptc7 in *ptc7*Δ yeast has been shown to increase *de novo* CoQ_6 biosynthesis, indicating that Coq7 activity is promoted when dephosphorylated (63). Further, mutagenesis on several putative Coq7 phospho-sites from Ser to Ala confirmed that the active form of Coq7 is not phosphorylated, given that these mutant strains have significantly elevated CoQ_6 content (61). Despite the extensive studies on phosphorylation-mediated regulation of Coq7 activity in yeast, it is not known if human COQ7 activity is modulated by post-translational modification.

Human *COQ8A*/*ADCK3*, *COQ8B*/*ADCK4* (Yeast *COQ8*)

The Coq8 polypeptide and its human homologs, COQ8A and COQ8B, have been shown to rescue CoQ_6 biosynthesis in several *coq*Δ mutants (42). Coq8 is considered a member of the aarF-domain containing kinases (ADCK) superfamily, in which human COQ8A and COQ8B have also been named ADCK3 and ADCK4, respectively (65). Expression of COQ8A in yeast *coq8* mutants restores CoQ_6 biosynthesis and the phosphorylation state of Coq3, Coq5, and Coq7, indicating highly conserved function across the Coq8 homologs (42). Additionally, overexpression of Coq8 in select *coq*Δ mutants restores the steady state expression of Coq4, Coq7, and Coq9, which in turn enhances the stability of the CoQ metabolon (66, 67). Coq8 is considered to be an atypical protein kinase, and structural studies indicate that the protein kinase-like (PKL) subdomains of Coq8 are essential for its function (42, 65). Instead of protein kinase activity, the COQ8A polypeptide possesses ATPase activity that is activated by cardiolipin and

small molecules analogous to CoQ biosynthetic intermediates (68, 69). It is thereby predicted that the ATPase function serves to facilitate the assembly of the CoQ metabolon to promote CoQ biosynthesis. In support of this notion, the ancestral COQ8B polypeptide has been shown to streamline the assembly of the *in vitro* reconstituted CoQ metabolon through ATPase activity that is stimulated in the presence of all metabolon members (46).

Human *COQ9* (Yeast *COQ9*)

The COQ9/Coq9 protein has not been characterized to possess any enzymatic function, however it is required for CoQ biosynthesis (70–72). Strikingly, yeast lacking *COQ9* have significantly decreased levels of Coq3, Coq4, Coq6, and Coq7, suggesting the Coq9 polypeptide serves a structural stability role for several Coq polypeptides (71). Previous crystallography on human COQ9 revealed a membrane binding region required for anchoring the polypeptide to the inner mitochondrial membrane at sites enriched with cardiolipin (70), where COQ9 is proposed to accept prenylated intermediates from the membrane and "present" them to neighboring COQ proteins, such as its direct interacting partner, COQ7 (60). In terms of a functional role, it seems to serve more of a supporting role for the Coq6 and Coq7 polypeptides. Namely, the Coq6 deamination reaction when pABA is used as a precursor in yeast requires the presence of Coq9 (73), and the structural characterization of human COQ7 required the copurification with human COQ9 (60).

NONESSENTIAL GENES FOR COENZYME Q BIOSYNTHESIS

Human *COQ10A*, *COQ10B* (Yeast *COQ10*)

Humans possess two isoforms of the yeast Coq10, named COQ10A and COQ10B (74).

Deletion of *COQ10* in yeast results in respiratory incompetency, impaired *de novo* biosynthesis, and a destabilized CoQ synthome (74–77). Of these phenotypes, growth on respiratory medium is the only phenotype that is rescued upon expression of either COQ10A or COQ10B (74). The Coq10 homologs possess a steroidogenic acute regulatory protein-related lipid transfer (START) domain that has been shown to be capable of binding CoQ and its late-stage quinone intermediates *in vitro* (78, 79). Purified Coq10 from *S. cerevisiae* and *S. pombe* copurify with CoQ_6 or CoQ_{10}, respectively (75, 76), suggesting Coq10 functions as a CoQ chaperone, taking CoQ from its sites of synthesis to the respiratory complexes. It was previously thought that Coq10 was required for CoQ synthome assembly, as shown biochemically and with fluorescence microscopy (74, 80), however we have shown that the presence of Coq10 is only required for respiration, and not for CoQ_6 biosynthetic efficiency or stability of the CoQ synthome (Chapter 2).

Human *NDUFA9* (Yeast *COQ11*)

The Coq11 polypeptide was identified via proteomic analysis of tandem affinity purification eluates using CNAP-tagged Coq3, Coq6, and Coq9 (81). In yeast lacking *COQ11*, *de novo* CoQ_6 biosynthesis is impaired, however the *coq11* null mutant retains the ability to grow on nonfermentable medium and has oxygen consumption rates similar to that of wild-type yeast (81, 82). Coq10 and Coq11 exist as fusion proteins in several fungal species, suggesting the two may have some functional codependence or regulatory relationship (81). Considering the *coq10*Δ mutant is respiratory deficient, it was surprising to discover that the subsequent deletion of *COQ11* rescues respiratory capacity, which could be attributed to slightly increased CoQ biosynthetic efficiency compared to the *coq10*Δ (82). Considering the overexpression of *COQ8*

can also remedy defects in CoQ biosynthesis (67), it was intriguing to note that the overexpression of *COQ8* in the *coq10*Δ*coq11*Δ double mutant did not have an additive effect (82). This may indicate that the mechanism of rescue by Coq8 overexpression and deletion of *COQ11* are carried out in different manners, or rather the mechanism of Coq8-mediated rescue requires the presence of Coq11. Further, the deletion of *COQ11* results in elevated protein content of several Coq polypeptides, contributing to a stabilized CoQ synthome in the *coq10*Δ*coq11*Δ double mutant, and an enlarged complex in the *coq11*Δ single mutant (80, 82). Coq11 is proposed to serve as a negative modulator of CoQ synthome formation, whereby its deletion enhances the assembly of the complex. While the function of Coq11 is presently unknown, a protein similarity network has identified its closest human homolog to be NDUFA9, a subunit of complex I (81). Considering yeast do not possess complex I, it is tempting to speculate that the Coq11 polypeptide links respiration with CoQ production. In line with this notion, the Coq11 polypeptide also interacts with the mitochondrial organization of gene expression (MIOREX) complex, where it was named Mrx2 (83). The MIOREX complex is involved in the mitochondrial genetic expression system, and considering the mitochondrial genome encodes for several respiratory complex subunits, Coq11 may utilize its dual functional roles to coordinate CoQ biosynthesis with assembly of the respiratory complexes. Overall, further investigation on how Coq11 participates in CoQ biosynthesis is warranted.

THE COENZYME Q METABOLON

Efficient CoQ biosynthesis requires the formation of a large molecular weight protein-lipid complex, referred to as the CoQ synthome in yeast (43, 44, 71), or Complex Q in humans (6). The CoQ synthome is comprised of the polypeptides Coq3-Coq9 and Coq11 (2, 35) (Fig. 3).

Protein interactions within the CoQ synthome were revealed via co-immunoprecipitation experiments (71), and the identities of lipids that co-purified with tagged Coq polypeptides were determined using mass spectrometry (81). The CoQ synthome can be visualized biochemically using two-dimensional Blue Native/SDS-PAGE (71) and can also be detected as discrete puncta, termed CoQ domains, using fluorescence microscopy with Coq9-yEGFP as a marker for the complex (80, 84). Deletion of genes encoding for the essential core components of the CoQ synthome, Coq3-Coq9, result in loss of the domains (80), which can be attributed to the dependence on interacting partners to maintain stable steady state protein content and overall protein stability (43, 60, 67, 71). Importantly, stable formation of the CoQ synthome also requires the presence of the polyisoprenyl intermediates (4, 85), which is why the deletion of *COQ1* or *COQ2*, whose gene products are not associated with the CoQ synthome, also results in loss of CoQ domains, as all lipid intermediates are absent (80). Along these lines, it has been noted that bypassing defective steps of the CoQ biosynthetic pathway with substrate analogs can remedy complex destabilization (53, 80).

CONTACT SITES AND COENZYME Q: A PUTATIVE TRANSPORT MECHANISM

Located outside of the mitochondria, the endoplasmic reticulum-mitochondria encounter structure (ERMES) has been identified as a modulator of CoQ synthome formation and CoQ_6 biosynthesis (80, 84). ERMES is a cluster of four proteins (Mmm1, Mdm10, Mdm12, and Mdm34) that tethers the ER to the mitochondria and is essential for the biosynthesis and transport of phospholipids between these organelles (86–89). Considering that yeast harboring deletions in ERMES-encoding genes (*ERMES*Δ) exhibit respiratory deficiency (86, 90–92), Eisenberg-Bord et al. investigated the potential influence *ERMES* mutations may have on CoQ

biosynthesis and discovered that ERMES subunits are required for efficient CoQ biosynthesis (84). Additionally, the CoQ domains were found to selectively colocalize with ERMES contact sites marked by Mdm34-mCherry (84); given that contact sites are proposed to serve as platforms to mediate the transport of metabolites between organelles, it is speculated that the CoQ synthome assembles adjacent to ERMES (Fig. 3), denoted by the colocalization of the CoQ domains and Mdm34-mCherry, to facilitate in the stability of the CoQ synthome and subsequent CoQ biosynthesis. This was further corroborated using 2D BN/SDS-PAGE (84).

Given the presence of CoQ in all endomembranes (2), it is possible that the colocalization of the CoQ synthome and ERMES is to streamline CoQ export out of the mitochondria via ERMES. Structural analyses reveal that ERMES forms a hydrophobic channel comprised by the Mmm1, Mdm12, and Mdm34 polypeptides, which each possess synaptotagmin-like mitochondrial lipid binding protein (SMP) domains capable of transporting lipids (86–89). Because the Mdm34 subunit of ERMES resides on the outer mitochondrial membrane (92) and CoQ synthesis occurs exclusively within the mitochondrial matrix (2), it is unclear how the hydrophobic lipid is able to traverse the intermembrane space. One potential model is cristae junctions, formed between cristae and the inner leaflet of the outer mitochondrial membrane, are sufficient to close the intermembrane space gap, thereby bridging the CoQ synthome with ERMES; however this is not widely accepted as cristae junctions and contact sites seem to be randomly distributed and do not always colocalize (93). Alternatively, a few intermembrane space proteins have been identified as candidates for lipid transport proteins. Intra-mitochondrial phospholipid transport has been ascribed to the proteins Ups1 and Ups2, which have been shown to have genetic interaction with ERMES constituents (94), although their ability to bind and transport CoQ has not been evaluated. In regards to CoQ trafficking specifically, two Coq8

homologs located within the intermembrane space have been shown to reciprocally regulate the intracellular distribution of CoQ, as assayed by exogenous PUFA sensitivity (95) (Fig. 3). Prior to this study, where the Coq8 homologs were named CoQ distribution proteins 1 and 2 (Cqd1 and Cqd2), Cqd2 was known as Mdm10 complementing protein 2, or Mcp2 (87). Mcp2 has been shown to suppress *ERMES*Δ respiratory defects upon overexpression (87), which could be a result of altering CoQ distribution, although this hypothesis was not tested in this work. Surprisingly, Cqd2/Mcp2 has a third alias, Mrx13, as it also interacts with the MIOREX complex like Coq11 (83); considering this, the rescue of respiratory growth in *ERMES*Δ mutants when Mcp2/Cqd2 is overexpressed may be attributed to enhanced respiratory complex formation via MIOREX. However, given the genetic interactions with ERMES (87) and homology to Coq8 (95), Cqd2 is an attractive candidate to facilitate the transport of CoQ between the CoQ synthome and ERMES.

It is imperative to note that a direct human equivalent to ERMES has not been identified, however several contact sites in humans do exist and fulfill different roles that may be similar to ERMES functions (96). The mitochondrial fusion protein, mitofusin-2 (MFN2), has dual localization in the ER and mitochondria, such that when MFN2 dimerizes, can form a tether (97). Cardiomyocytes derived from *Mfn2* knockout mice have limited respiratory capacity, and mitochondria isolated from *Mfn2* knockout heart tissue contained significantly diminished CoQ_9 and CoQ_{10} content relative to wild-type mice (98). This indicates that the relationship between ER-mitochondrial contact sites and CoQ synthesis is profoundly conserved across organisms.

FIGURES

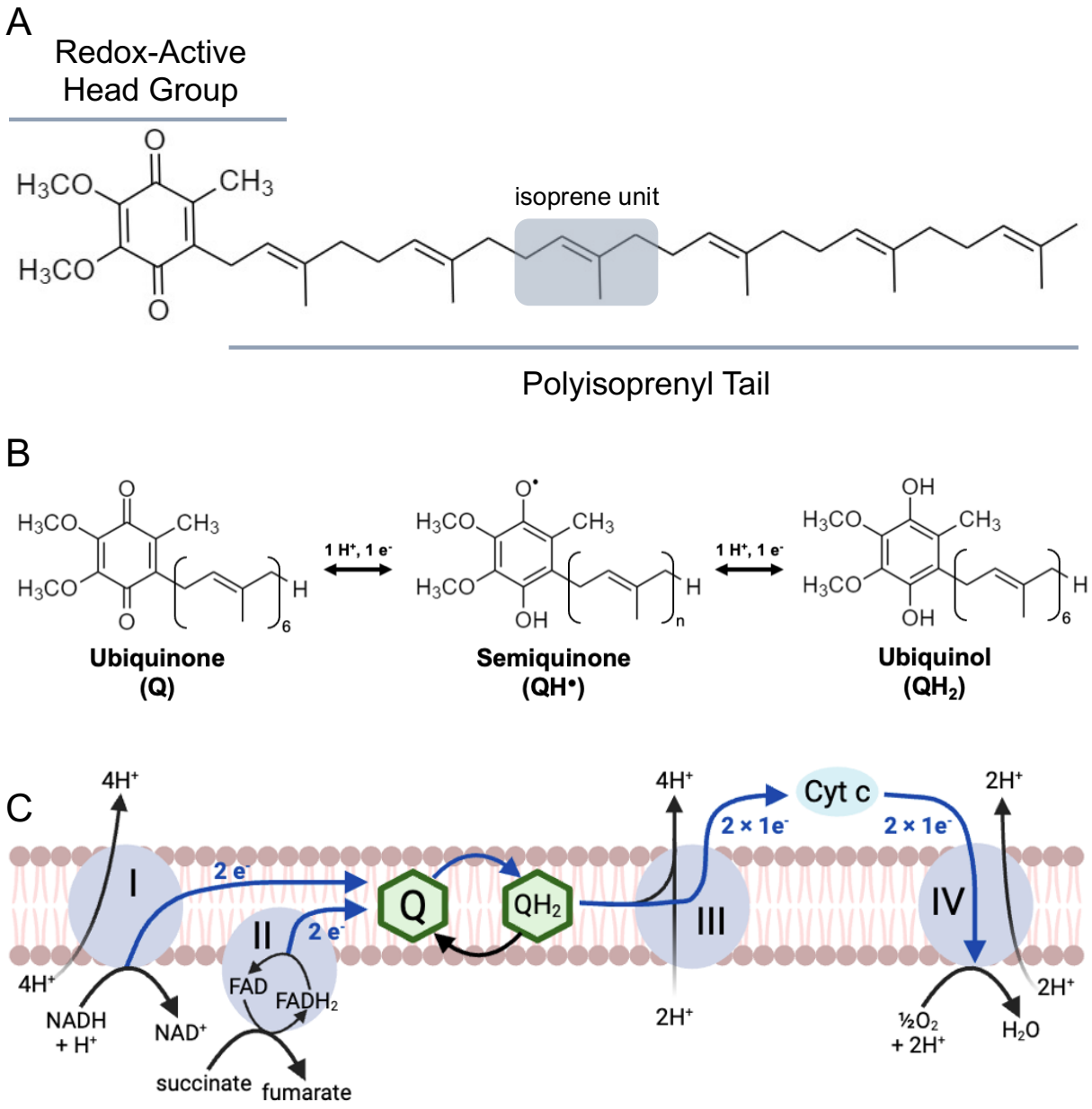

Figure 1. CoQ structure and function. *A,* CoQ is comprised of a redox-active head group and polyisoprenyl tail. The isoprenyl repeats of the tail affords its ability to lie within the midplane of lipid biolayers. Shown is the yeast isoform, CoQ_6, which contains six isoprene units. *B,* Redox forms of CoQ. *C*, Canonical function of CoQ in the mitochondrial electron transport chain. Blue arrows indicate direction of electron flow.

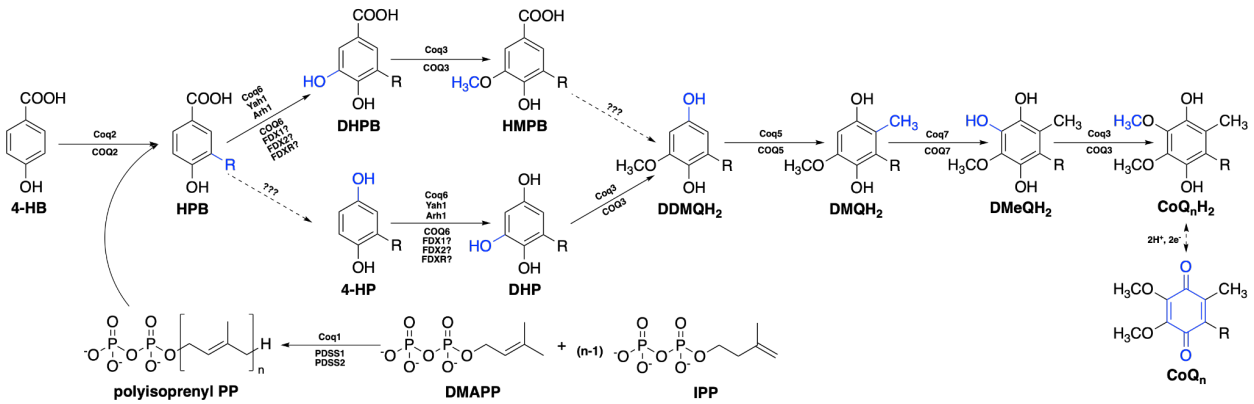

Figure 2. The CoQ biosynthetic pathway. Biosynthesis of coenzyme Q is largely homologous between yeast (polypeptide names above arrows) and humans (polypeptide names below arrows). CoQ intermediates in this figure are denoted broadly as bearing polyprenyl tails, however humans and yeast generate decaprenyl and hexaprenyl tails, respectively. This figure has been adapted from Wang & Jain et al. (24). Abbreviations: DMAPP, dimethylallyl pyrophosphate; IPP, isopentenyl pyrophosphate; HPB, 3-polyprenyl-4-hydroxybenzoic acid; DHPB, 4,5-dihydroxy-3-polyprenylbenzoic acid; HMPB, 4-hydroxy-5-methoxy-3-polyprenylbenzoic acid; DHP, 4,5-dihydroxy-3-polyprenylphenol; $DDMQH_2$, 6-methoxy-2-polyprenyl-1,4-benzenediol; $DMQH_2$, 3-methyl-6-methoxy-2-polyprenyl-1,4-benzenediol, $DMeQH_2$, 3-methyl-6-methoxy-2-polyprenyl-1,4,5-benzenetriol.

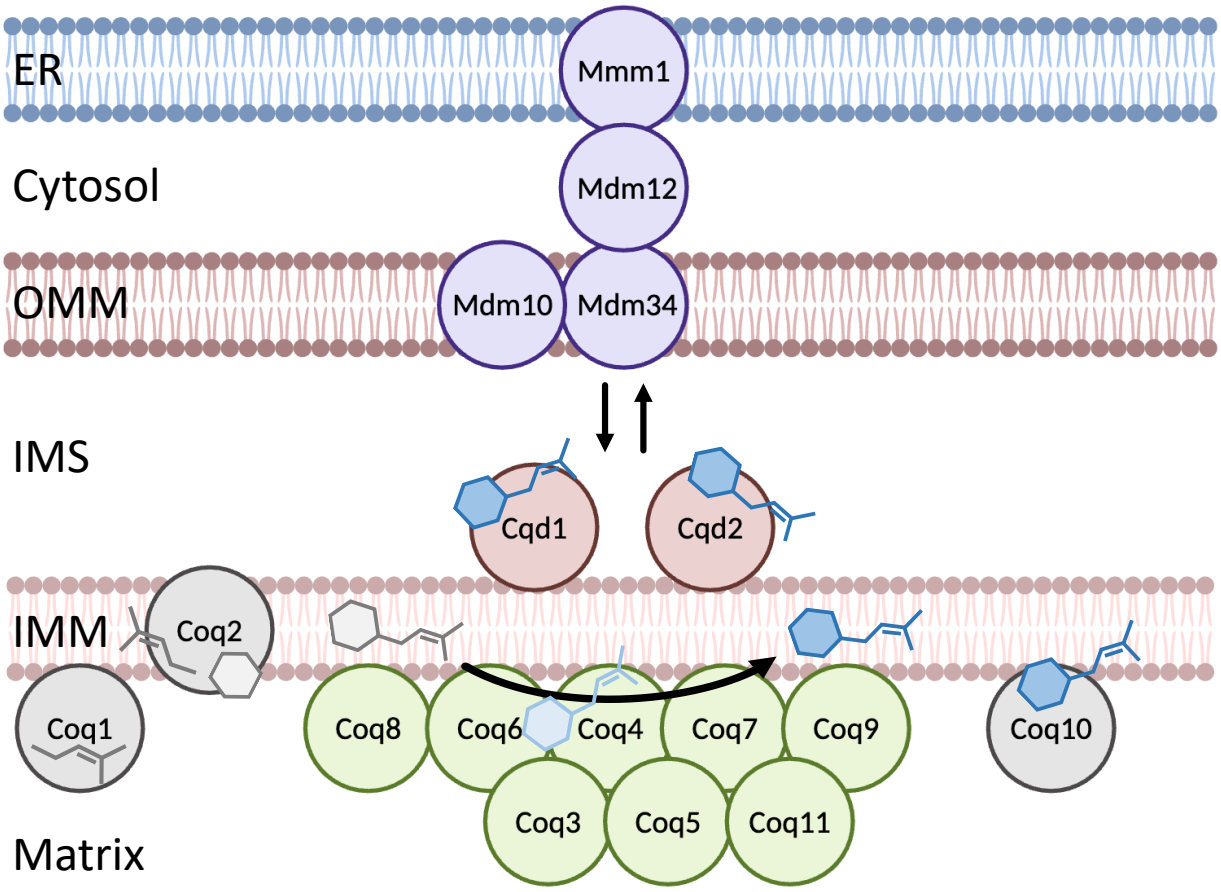

Figure 3. The CoQ synthome. In yeast, the CoQ synthome is comprised of the polypeptides Coq3-Coq9 and Coq11 (green). Coq1, Coq2, and Coq10 (gray) do not associate with the complex, but are required for complex assembly as they provide the prenylated precursor. The Coq8 polypeptide has been shown to promote the assembly of the CoQ synthome in select *coq* mutants. Deletion of *COQ11*, which encodes for the Coq11 polypeptide, also promotes the stability of the CoQ synthome. The endoplasmic reticulum-mitochondria encounter structure (ERMES, purple) has been shown to regulate the assembly of the CoQ synthome. The Coq8 homologs, Cqd1 and Cqd2, are inner membrane associated proteins that face the intermembrane space and are proposed to modulate mitochondrial CoQ distribution. The localization of the Cqd proteins in relation to ERMES or the CoQ synthome has not been determined.

REFERENCES

1. Banerjee, R., Purhonen, J., and Kallijärvi, J. (2022) The mitochondrial coenzyme Q junction and complex III: biochemistry and pathophysiology. *The FEBS Journal*. **289**, 6936–6958
2. Guerra, R. M., and Pagliarini, D. J. (2023) Coenzyme Q biochemistry and biosynthesis. *Trends in Biochemical Sciences*. **48**, 463–476
3. Turunen, M., Olsson, J., and Dallner, G. (2004) Metabolism and function of coenzyme Q. *Biochimica et Biophysica Acta (BBA) - Biomembranes*. **1660**, 171–199
4. Wang, Y., and Hekimi, S. (2019) The Complexity of Making Ubiquinone. *Trends in Endocrinology & Metabolism*. **30**, 929–943
5. Brandt, U., and Trumpower, B. (1994) The Protonmotive Q Cycle in Mitochondria and Bacteria. *Critical Reviews in Biochemistry and Molecular Biology*. **29**, 165–197
6. Stefely, J. A., and Pagliarini, D. J. (2017) Biochemistry of Mitochondrial Coenzyme Q Biosynthesis. *Trends in Biochemical Sciences*. **42**, 824–843
7. Grandier-Vazeille, X., Bathany, K., Chaignepain, S., Camougrand, N., Manon, S., and Schmitter, J.-M. (2001) Yeast Mitochondrial Dehydrogenases Are Associated in a Supramolecular Complex. *Biochemistry*. **40**, 9758–9769
8. Luttik, M. A. H., Overkamp, K. M., Kötter, P., De Vries, S., Van Dijken, J. P., and Pronk, J. T. (1998) The Saccharomyces cerevisiae NDE1 and NDE2 Genes Encode Separate Mitochondrial NADH Dehydrogenases Catalyzing the Oxidation of Cytosolic NADH. *Journal of Biological Chemistry*. **273**, 24529–24534
9. Frei, B., Kim, M. C., and Ames, B. N. (1990) Ubiquinol-10 is an effective lipid-soluble antioxidant at physiological concentrations. *Proceedings of the National Academy of*

Sciences. **87**, 4879–4883

10. Yin, H., Xu, L., and Porter, N. A. (2011) Free Radical Lipid Peroxidation: Mechanisms and Analysis. *Chem. Rev.* **111**, 5944–5972

11. Porter, N. A. (1986) Mechanisms for the autoxidation of polyunsaturated lipids. *Acc. Chem. Res.* **19**, 262–268

12. Do, T. Q., Schultz, J. R., and Clarke, C. F. (1996) Enhanced sensitivity of ubiquinone-deficient mutants of Saccharomyces cerevisiae to products of autoxidized polyunsaturated fatty acids. *Proc Natl Acad Sci U S A*. **93**, 7534–7539

13. Poon, W. W., Do, T. Q., Noelle Marbois, B., and Clarke, C. F. (1997) Sensitivity to treatment with polyunsaturated fatty acids is a general characteristic of the ubiquinone-deficient yeast coq mutants. *Molecular Aspects of Medicine*. **18**, 121–127

14. Dixon, S. J., Lemberg, K. M., Lamprecht, M. R., Skouta, R., Zaitsev, E. M., Gleason, C. E., Patel, D. N., Bauer, A. J., Cantley, A. M., Yang, W. S., Morrison, B., and Stockwell, B. R. (2012) Ferroptosis: An Iron-Dependent Form of Nonapoptotic Cell Death. *Cell*. **149**, 1060–1072

15. Jiang, X., Stockwell, B. R., and Conrad, M. (2021) Ferroptosis: mechanisms, biology and role in disease. *Nat Rev Mol Cell Biol*. **22**, 266–282

16. Bersuker, K., Hendricks, J. M., Li, Z., Magtanong, L., Ford, B., Tang, P. H., Roberts, M. A., Tong, B., Maimone, T. J., Zoncu, R., Bassik, M. C., Nomura, D. K., Dixon, S. J., and Olzmann, J. A. (2019) The CoQ oxidoreductase FSP1 acts parallel to GPX4 to inhibit ferroptosis. *Nature*. **575**, 688–692

17. Doll, S., Freitas, F. P., Shah, R., Aldrovandi, M., Da Silva, M. C., Ingold, I., Goya Grocin, A., Xavier Da Silva, T. N., Panzilius, E., Scheel, C. H., Mourão, A., Buday, K.,

Sato, M., Wanninger, J., Vignane, T., Mohana, V., Rehberg, M., Flatley, A., Schepers, A., Kurz, A., White, D., Sauer, M., Sattler, M., Tate, E. W., Schmitz, W., Schulze, A., O'Donnell, V., Proneth, B., Popowicz, G. M., Pratt, D. A., Angeli, J. P. F., and Conrad, M. (2019) FSP1 is a glutathione-independent ferroptosis suppressor. *Nature*. **575**, 693–698

18. Alcázar-Fabra, M., Trevisson, E., and Brea-Calvo, G. (2018) Clinical syndromes associated with Coenzyme Q10 deficiency. *Essays in Biochemistry*. **62**, 377–398

19. Mantle, D., Millichap, L., Castro-Marrero, J., and Hargreaves, I. P. (2023) Primary Coenzyme Q10 Deficiency: An Update. *Antioxidants*. **12**, 1652

20. Landrum, M. J., Lee, J. M., Benson, M., Brown, G., Chao, C., Chitipiralla, S., Gu, B., Hart, J., Hoffman, D., Hoover, J., Jang, W., Katz, K., Ovetsky, M., Riley, G., Sethi, A., Tully, R., Villamarin-Salomon, R., Rubinstein, W., and Maglott, D. R. (2016) ClinVar: public archive of interpretations of clinically relevant variants. *Nucleic Acids Res*. **44**, D862–D868

21. Karczewski, K. J., et al. (2020) The mutational constraint spectrum quantified from variation in 141,456 humans. *Nature*. **581**, 434–443

22. Khanna, T., Hanna, G., Sternberg, M. J. E., and David, A. (2021) Missense3D-DB web catalogue: an atom-based analysis and repository of 4M human protein-coding genetic variants. *Hum Genet*. **140**, 805–812

23. Alcázar-Fabra, M., Rodríguez-Sánchez, F., Trevisson, E., and Brea-Calvo, G. (2021) Primary Coenzyme Q deficiencies: A literature review and online platform of clinical features to uncover genotype-phenotype correlations. *Free Radical Biology and Medicine*. **167**, 141–180

24. Wang, S., Jain, A., Novales, N. A., Nashner, A. N., Tran, F., and Clarke, C. F. (2022) Predicting and Understanding the Pathology of Single Nucleotide Variants in Human COQ Genes. *Antioxidants*. **11**, 2308

25. Stefely, J. A., Kwiecien, N. W., Freiberger, E. C., Richards, A. L., Jochem, A., Rush, M. J. P., Ulbrich, A., Robinson, K. P., Hutchins, P. D., Veling, M. T., Guo, X., Kemmerer, Z. A., Connors, K. J., Trujillo, E. A., Sokol, J., Marx, H., Westphall, M. S., Hebert, A. S., Pagliarini, D. J., and Coon, J. J. (2016) Mitochondrial protein functions elucidated by multi-omic mass spectrometry profiling. *Nat Biotechnol*. **34**, 1191–1197

26. Payet, L.-A., Leroux, M., Willison, J. C., Kihara, A., Pelosi, L., and Pierrel, F. (2016) Mechanistic Details of Early Steps in Coenzyme Q Biosynthesis Pathway in Yeast. *Cell Chemical Biology*. **23**, 1241–1250

27. Marbois, B., Xie, L. X., Choi, S., Hirano, K., Hyman, K., and Clarke, C. F. (2010) para-Aminobenzoic Acid Is a Precursor in Coenzyme Q6 Biosynthesis in Saccharomyces cerevisiae. *Journal of Biological Chemistry*. **285**, 27827–27838

28. López, L. C., Schuelke, M., Quinzii, C. M., Kanki, T., Rodenburg, R. J. T., Naini, A., DiMauro, S., and Hirano, M. (2006) Leigh Syndrome with Nephropathy and CoQ10 Deficiency Due to decaprenyl diphosphate synthase subunit 2 (PDSS2) Mutations. *The American Journal of Human Genetics*. **79**, 1125–1129

29. Gin, P., and Clarke, C. F. (2005) Genetic Evidence for a Multi-subunit Complex in Coenzyme Q Biosynthesis in Yeast and the Role of the Coq1 Hexaprenyl Diphosphate Synthase. *Journal of Biological Chemistry*. **280**, 2676–2681

30. Ashby, M. N., and Edwards, P. A. (1990) Elucidation of the deficiency in two yeast coenzyme Q mutants. Characterization of the structural gene encoding hexaprenyl

pyrophosphate synthetase. *Journal of Biological Chemistry*. **265**, 13157–13164

31. Ashby, M. N., Kutsunai, S. Y., Ackerman, S., Tzagoloff, A., and Edwards, P. A. (1992) COQ2 is a candidate for the structural gene encoding para-hydroxybenzoate:polyprenyltransferase. *Journal of Biological Chemistry*. **267**, 4128–4136

32. Forsgren, M., Attersand, A., Lake, S., Grünler, J., Swiezewska, E., Dallner, G., and Climent, I. (2004) Isolation and functional expression of human *COQ2*, a gene encoding a polyprenyl transferase involved in the synthesis of CoQ. *Biochemical Journal*. **382**, 519–526

33. Desbats, M. A., Morbidoni, V., Silic-Benussi, M., Doimo, M., Ciminale, V., Cassina, M., Sacconi, S., Hirano, M., Basso, G., Pierrel, F., Navas, P., Salviati, L., and Trevisson, E. (2016) The *COQ2* genotype predicts the severity of coenzyme Q $_{10}$ deficiency. *Hum. Mol. Genet.* **25**, 4256–4265

34. Vargas-Pérez, M. D. L. Á., Devos, D. P., and López-Lluch, G. (2024) An AlphaFold Structure Analysis of COQ2 as Key a Component of the Coenzyme Q Synthesis Complex. *Antioxidants*. **13**, 496

35. Awad, A. M., Bradley, M. C., Fernández-del-Río, L., Nag, A., Tsui, H. S., and Clarke, C. F. (2018) Coenzyme Q10 deficiencies: pathways in yeast and humans. *Essays in Biochemistry*. **62**, 361–376

36. Poon, W. W., Barkovich, R. J., Hsu, A. Y., Frankel, A., Lee, P. T., Shepherd, J. N., Myles, D. C., and Clarke, C. F. (1999) Yeast and Rat Coq3 and Escherichia coli UbiG Polypeptides Catalyze Both O-Methyltransferase Steps in Coenzyme Q Biosynthesis. *Journal of Biological Chemistry*. **274**, 21665–21672

37. Jonassen, T., and Clarke, C. F. (2000) Isolation and Functional Expression of Human COQ3, a Gene Encoding a Methyltransferase Required for Ubiquinone Biosynthesis. *Journal of Biological Chemistry*. **275**, 12381–12387

38. Clarke, C. F., Williams, W., and Teruya, J. H. (1991) Ubiquinone biosynthesis in Saccharomyces cerevisiae. Isolation and sequence of COQ3, the 3,4-dihydroxy-5-hexaprenylbenzoate methyltransferase gene. *Journal of Biological Chemistry*. **266**, 16636–16644

39. Tauche, A., Krause-Buchholz, U., and Rödel, G. (2008) Ubiquinone biosynthesis in *Saccharomyces cerevisiae*: the molecular organization of *O* -methylase Coq3p depends on Abc1p/Coq8p. *FEMS Yeast Research*. **8**, 1263–1275

40. Niewmierzycka, A., and Clarke, S. (1999) S-Adenosylmethionine-dependent Methylation in Saccharomyces cerevisiae. *Journal of Biological Chemistry*. **274**, 814–824

41. Petrossian, T. C., and Clarke, S. G. (2009) Multiple Motif Scanning to Identify Methyltransferases from the Yeast Proteome. *Molecular & Cellular Proteomics*. **8**, 1516–1526

42. Xie, L. X., Hsieh, E. J., Watanabe, S., Allan, C. M., Chen, J. Y., Tran, U. C., and Clarke, C. F. (2011) Expression of the human atypical kinase ADCK3 rescues coenzyme Q biosynthesis and phosphorylation of Coq polypeptides in yeast coq8 mutants. *Biochimica et Biophysica Acta (BBA) - Molecular and Cell Biology of Lipids*. **1811**, 348–360

43. Marbois, B., Gin, P., Faull, K. F., Poon, W. W., Lee, P. T., Strahan, J., Shepherd, J. N., and Clarke, C. F. (2005) Coq3 and Coq4 Define a Polypeptide Complex in Yeast Mitochondria for the Biosynthesis of Coenzyme Q. *Journal of Biological Chemistry*. **280**, 20231–20238

44. Marbois, B., Gin, P., Gulmezian, M., and Clarke, C. F. (2009) The yeast Coq4 polypeptide organizes a mitochondrial protein complex essential for coenzyme Q biosynthesis. *Biochimica et Biophysica Acta (BBA) - Molecular and Cell Biology of Lipids*. **1791**, 69–75

45. Pelosi, L., Morbiato, L., Burgardt, A., Tonello, F., Bartlett, A. K., Guerra, R. M., Ferizhendi, K. K., Desbats, M. A., Rascalou, B., Marchi, M., Vázquez-Fonseca, L., Agosto, C., Zanotti, G., Roger-Margueritat, M., Alcázar-Fabra, M., García-Corzo, L., Sánchez-Cuesta, A., Navas, P., Brea-Calvo, G., Trevisson, E., Wendisch, V. F., Pagliarini, D. J., Salviati, L., and Pierrel, F. (2024) COQ4 is required for the oxidative decarboxylation of the C1 carbon of coenzyme Q in eukaryotic cells. *Molecular Cell*. **84**, 981-989.e7

46. Nicoll, C. R., Alvigini, L., Gottinger, A., Cecchini, D., Mannucci, B., Corana, F., Mascotti, M. L., and Mattevi, A. (2024) In vitro construction of the COQ metabolon unveils the molecular determinants of coenzyme Q biosynthesis. *Nat Catal*. **7**, 148–160

47. Barkovich, R. J., Shtanko, A., Shepherd, J. A., Lee, P. T., Myles, D. C., Tzagoloff, A., and Clarke, C. F. (1997) Characterization of the COQ5 Gene from Saccharomyces cerevisiae EVIDENCE FOR A C-METHYLTRANSFERASE IN UBIQUINONE BIOSYNTHESIS. *Journal of Biological Chemistry*. **272**, 9182–9188

48. Dibrov, E., Robinson, K. M., and Lemire, B. D. (1997) The COQ5 Gene Encodes a Yeast Mitochondrial Protein Necessary for Ubiquinone Biosynthesis and the Assembly of the Respiratory Chain. *Journal of Biological Chemistry*. **272**, 9175–9181

49. Dai, Y.-N., Zhou, K., Cao, D.-D., Jiang, Y.-L., Meng, F., Chi, C.-B., Ren, Y.-M., Chen, Y., and Zhou, C.-Z. (2014) Crystal structures and catalytic mechanism of the *C* -

methyltransferase Coq5 provide insights into a key step of the yeast coenzyme Q synthesis pathway. *Acta Crystallogr D Biol Crystallogr*. **70**, 2085–2092

50. Baba, S. W., Belogrudov, G. I., Lee, J. C., Lee, P. T., Strahan, J., Shepherd, J. N., and Clarke, C. F. (2004) Yeast Coq5 C-Methyltransferase Is Required for Stability of Other Polypeptides Involved in Coenzyme Q Biosynthesis. *Journal of Biological Chemistry*. **279**, 10052–10059

51. Gin, P., Hsu, A. Y., Rothman, S. C., Jonassen, T., Lee, P. T., Tzagoloff, A., and Clarke, C. F. (2003) The Saccharomyces cerevisiae COQ6 Gene Encodes a Mitochondrial Flavin-dependent Monooxygenase Required for Coenzyme Q Biosynthesis. *Journal of Biological Chemistry*. **278**, 25308–25316

52. Ismail, A., Leroux, V., Smadja, M., Gonzalez, L., Lombard, M., Pierrel, F., Mellot-Draznieks, C., and Fontecave, M. (2016) Coenzyme Q Biosynthesis: Evidence for a Substrate Access Channel in the FAD-Dependent Monooxygenase Coq6. *PLoS Comput Biol*. **12**, e1004690

53. Ozeir, M., Mühlenhoff, U., Webert, H., Lill, R., Fontecave, M., and Pierrel, F. (2011) Coenzyme Q Biosynthesis: Coq6 Is Required for the C5-Hydroxylation Reaction and Substrate Analogs Rescue Coq6 Deficiency. *Chemistry & Biology*. **18**, 1134–1142

54. Ozeir, M., Pelosi, L., Ismail, A., Mellot-Draznieks, C., Fontecave, M., and Pierrel, F. (2015) Coq6 Is Responsible for the C4-deamination Reaction in Coenzyme Q Biosynthesis in Saccharomyces cerevisiae. *Journal of Biological Chemistry*. **290**, 24140–24151

55. Doimo, M., Trevisson, E., Airik, R., Bergdoll, M., Santos-Ocaña, C., Hildebrandt, F., Navas, P., Pierrel, F., and Salviati, L. (2014) Effect of vanillic acid on COQ6 mutants

identified in patients with coenzyme Q10 deficiency. *Biochimica et Biophysica Acta (BBA) - Molecular Basis of Disease*. **1842**, 1–6

56. Acosta Lopez, M. J., Trevisson, E., Canton, M., Vazquez-Fonseca, L., Morbidoni, V., Baschiera, E., Frasson, C., Pelosi, L., Rascalou, B., Desbats, M. A., Alcázar-Fabra, M., Ríos, J. J., Sánchez-García, A., Basso, G., Navas, P., Pierrel, F., Brea-Calvo, G., and Salviati, L. (2019) Vanillic Acid Restores Coenzyme Q Biosynthesis and ATP Production in Human Cells Lacking *COQ6*. *Oxidative Medicine and Cellular Longevity*. **2019**, 1–11

57. Jonassen, T., Proft, M., Randez-Gil, F., Schultz, J. R., Marbois, B. N., Entian, K.-D., and Clarke, C. F. (1998) Yeast Clk-1 Homologue (Coq7/Cat5) Is a Mitochondrial Protein in Coenzyme Q Synthesis. *Journal of Biological Chemistry*. **273**, 3351–3357

58. Marbois, B. N., and Clarke, C. F. (1996) The COQ7 Gene Encodes a Protein in Saccharomyces cerevisiae Necessary for Ubiquinone Biosynthesis. *Journal of Biological Chemistry*. **271**, 2995–3004

59. Stenmark, P., Grünler, J., Mattsson, J., Sindelar, P. J., Nordlund, P., and Berthold, D. A. (2001) A New Member of the Family of Di-iron Carboxylate Proteins. *Journal of Biological Chemistry*. **276**, 33297–33300

60. Manicki, M., Aydin, H., Abriata, L. A., Overmyer, K. A., Guerra, R. M., Coon, J. J., Dal Peraro, M., Frost, A., and Pagliarini, D. J. (2022) Structure and functionality of a multimeric human COQ7:COQ9 complex. *Molecular Cell*. **82**, 4307-4323.e10

61. Martín-Montalvo, A., González-Mariscal, I., Padilla, S., Ballesteros, M., Brautigan, D. L., Navas, P., and Santos-Ocaña, C. (2011) Respiratory-induced coenzyme Q biosynthesis is regulated by a phosphorylation cycle of Cat5p/Coq7p. *Biochemical*

Journal. **440**, 107–114

62. Martín-Montalvo, A., González-Mariscal, I., Pomares-Viciana, T., Padilla-López, S., Ballesteros, M., Vazquez-Fonseca, L., Gandolfo, P., Brautigan, D. L., Navas, P., and Santos-Ocaña, C. (2013) The Phosphatase Ptc7 Induces Coenzyme Q Biosynthesis by Activating the Hydroxylase Coq7 in Yeast. *Journal of Biological Chemistry*. **288**, 28126–28137

63. Awad, A. M., Venkataramanan, S., Nag, A., Galivanche, A. R., Bradley, M. C., Neves, L. T., Douglass, S., Clarke, C. F., and Johnson, T. L. (2017) Chromatin-remodeling SWI/SNF complex regulates coenzyme Q6 synthesis and a metabolic shift to respiration in yeast. *Journal of Biological Chemistry*. **292**, 14851–14866

64. Juneau, K., Nislow, C., and Davis, R. W. (2009) Alternative Splicing of PTC7 in *Saccharomyces cerevisiae* Determines Protein Localization. *Genetics*. **183**, 185–194

65. Stefely, J. A., Reidenbach, A. G., Ulbrich, A., Oruganty, K., Floyd, B. J., Jochem, A., Saunders, J. M., Johnson, I. E., Minogue, C. E., Wrobel, R. L., Barber, G. E., Lee, D., Li, S., Kannan, N., Coon, J. J., Bingman, C. A., and Pagliarini, D. J. (2015) Mitochondrial ADCK3 Employs an Atypical Protein Kinase-like Fold to Enable Coenzyme Q Biosynthesis. *Molecular Cell*. **57**, 83–94

66. Xie, L. X., Ozeir, M., Tang, J. Y., Chen, J. Y., Jaquinod, S.-K., Fontecave, M., Clarke, C. F., and Pierrel, F. (2012) Overexpression of the Coq8 Kinase in Saccharomyces cerevisiae coq Null Mutants Allows for Accumulation of Diagnostic Intermediates of the Coenzyme Q6 Biosynthetic Pathway. *Journal of Biological Chemistry*. **287**, 23571–23581

67. He, C. H., Xie, L. X., Allan, C. M., Tran, U. C., and Clarke, C. F. (2014) Coenzyme Q

supplementation or over-expression of the yeast Coq8 putative kinase stabilizes multi-subunit Coq polypeptide complexes in yeast coq null mutants. *Biochimica et Biophysica Acta (BBA) - Molecular and Cell Biology of Lipids*. **1841**, 630–644

68. Reidenbach, A. G., Kemmerer, Z. A., Aydin, D., Jochem, A., McDevitt, M. T., Hutchins, P. D., Stark, J. L., Stefely, J. A., Reddy, T., Hebert, A. S., Wilkerson, E. M., Johnson, I. E., Bingman, C. A., Markley, J. L., Coon, J. J., Dal Peraro, M., and Pagliarini, D. J. (2018) Conserved Lipid and Small-Molecule Modulation of COQ8 Reveals Regulation of the Ancient Kinase-like UbiB Family. *Cell Chemical Biology*. **25**, 154-165.e11

69. Stefely, J. A., Licitra, F., Laredj, L., Reidenbach, A. G., Kemmerer, Z. A., Grangeray, A., Jaeg-Ehret, T., Minogue, C. E., Ulbrich, A., Hutchins, P. D., Wilkerson, E. M., Ruan, Z., Aydin, D., Hebert, A. S., Guo, X., Freiberger, E. C., Reutenauer, L., Jochem, A., Chergova, M., Johnson, I. E., Lohman, D. C., Rush, M. J. P., Kwiecien, N. W., Singh, P. K., Schlagowski, A. I., Floyd, B. J., Forsman, U., Sindelar, P. J., Westphall, M. S., Pierrel, F., Zoll, J., Dal Peraro, M., Kannan, N., Bingman, C. A., Coon, J. J., Isope, P., Puccio, H., and Pagliarini, D. J. (2016) Cerebellar Ataxia and Coenzyme Q Deficiency through Loss of Unorthodox Kinase Activity. *Molecular Cell*. **63**, 608–620

70. Lohman, D. C., Aydin, D., Von Bank, H. C., Smith, R. W., Linke, V., Weisenhorn, E., McDevitt, M. T., Hutchins, P., Wilkerson, E. M., Wancewicz, B., Russell, J., Stefely, M. S., Beebe, E. T., Jochem, A., Coon, J. J., Bingman, C. A., Dal Peraro, M., and Pagliarini, D. J. (2019) An Isoprene Lipid-Binding Protein Promotes Eukaryotic Coenzyme Q Biosynthesis. *Molecular Cell*. **73**, 763-774.e10

71. Hsieh, E. J., Gin, P., Gulmezian, M., Tran, U. C., Saiki, R., Marbois, B. N., and Clarke, C. F. (2007) Saccharomyces cerevisiae Coq9 polypeptide is a subunit of the

mitochondrial coenzyme Q biosynthetic complex. *Archives of Biochemistry and Biophysics*. **463**, 19–26

72. Johnson, A., Gin, P., Marbois, B. N., Hsieh, E. J., Wu, M., Barros, M. H., Clarke, C. F., and Tzagoloff, A. (2005) COQ9, a New Gene Required for the Biosynthesis of Coenzyme Q in Saccharomyces cerevisiae. *Journal of Biological Chemistry*. **280**, 31397–31404

73. He, C. H., Black, D. S., Nguyen, T. P. T., Wang, C., Srinivasan, C., and Clarke, C. F. (2015) Yeast Coq9 controls deamination of coenzyme Q intermediates that derive from para-aminobenzoic acid. *Biochimica et Biophysica Acta (BBA) - Molecular and Cell Biology of Lipids*. **1851**, 1227–1239

74. Tsui, H. S., Pham, NguyenV. B., Amer, B. R., Bradley, M. C., Gosschalk, J. E., Gallagher-Jones, M., Ibarra, H., Clubb, R. T., Blaby-Haas, C. E., and Clarke, C. F. (2019) Human COQ10A and COQ10B are distinct lipid-binding START domain proteins required for coenzyme Q function. *Journal of Lipid Research*. **60**, 1293–1310

75. Cui, T.-Z., and Kawamukai, M. (2009) Coq10, a mitochondrial coenzyme Q binding protein, is required for proper respiration in Schizosaccharomyces pombe: CoQ-binding protein in fission yeast. *FEBS Journal*. **276**, 748–759

76. Barros, M. H., Johnson, A., Gin, P., Marbois, B. N., Clarke, C. F., and Tzagoloff, A. (2005) The Saccharomyces cerevisiae COQ10 Gene Encodes a START Domain Protein Required for Function of Coenzyme Q in Respiration. *Journal of Biological Chemistry*. **280**, 42627–42635

77. Busso, C., Bleicher, L., Ferreira-Júnior, J. R., and Barros, M. H. (2010) Site-directed mutagenesis and structural modeling of Coq10p indicate the presence of a tunnel for

coenzyme Q6 binding. *FEBS Letters*. **584**, 1609–1614

78. Allan, C. M., Hill, S., Morvaridi, S., Saiki, R., Johnson, J. S., Liau, W.-S., Hirano, K., Kawashima, T., Ji, Z., Loo, J. A., Shepherd, J. N., and Clarke, C. F. (2013) A conserved START domain coenzyme Q-binding polypeptide is required for efficient Q biosynthesis, respiratory electron transport, and antioxidant function in Saccharomyces cerevisiae. *Biochimica et Biophysica Acta (BBA) - Molecular and Cell Biology of Lipids*. **1831**, 776–791

79. Shen, Y., Goldsmith-Fischman, S., Atreya, H. S., Acton, T., Ma, L., Xiao, R., Honig, B., Montelione, G. T., and Szyperski, T. (2005) NMR structure of the 18 kDa protein CC1736 from *Caulobacter crescentus* identifies a member of the "START" domain superfamily and suggests residues mediating substrate specificity. *Proteins*. **58**, 747–750

80. Subramanian, K., Jochem, A., Le Vasseur, M., Lewis, S., Paulson, B. R., Reddy, T. R., Russell, J. D., Coon, J. J., Pagliarini, D. J., and Nunnari, J. (2019) Coenzyme Q biosynthetic proteins assemble in a substrate-dependent manner into domains at ER–mitochondria contacts. *Journal of Cell Biology*. **218**, 1353–1369

81. Allan, C. M., Awad, A. M., Johnson, J. S., Shirasaki, D. I., Wang, C., Blaby-Haas, C. E., Merchant, S. S., Loo, J. A., and Clarke, C. F. (2015) Identification of Coq11, a New Coenzyme Q Biosynthetic Protein in the CoQ-Synthome in Saccharomyces cerevisiae. *Journal of Biological Chemistry*. **290**, 7517–7534

82. Bradley, M. C., Yang, K., Fernández-del-Río, L., Ngo, J., Ayer, A., Tsui, H. S., Novales, N. A., Stocker, R., Shirihai, O. S., Barros, M. H., and Clarke, C. F. (2020) COQ11 deletion mitigates respiratory deficiency caused by mutations in the gene encoding the coenzyme Q chaperone protein Coq10. *Journal of Biological Chemistry*. **295**, 6023–6042

83. Kehrein, K., Möller-Hergt, B. V., and Ott, M. (2015) The MIOREX complex - lean management of mitochondrial gene expression. *Oncotarget*. **6**, 16806–16807

84. Eisenberg-Bord, M., Tsui, H. S., Antunes, D., Fernández-del-Río, L., Bradley, M. C., Dunn, C. D., Nguyen, T. P. T., Rapaport, D., Clarke, C. F., and Schuldiner, M. (2019) The Endoplasmic Reticulum-Mitochondria Encounter Structure Complex Coordinates Coenzyme Q Biosynthesis. *Contact*. **2**, 2515256418825409

85. Tran, U. C., and Clarke, C. F. (2007) Endogenous synthesis of coenzyme Q in eukaryotes. *Mitochondrion*. **7**, S62–S71

86. Kornmann, B., Currie, E., Collins, S. R., Schuldiner, M., Nunnari, J., Weissman, J., and Walter, P. (2009) An ER-Mitochondria Tethering Complex Revealed by a Synthetic Biology Screen. *Science*. **325**, 477–481

87. Tan, T., Özbalci, C., Brügger, B., Rapaport, D., and Dimmer, K. S. (2013) Mcp1 and Mcp2, two novel proteins involved in mitochondrial lipid homeostasis. *Journal of Cell Science*. 10.1242/jcs.121244

88. AhYoung, A. P., Jiang, J., Zhang, J., Khoi Dang, X., Loo, J. A., Zhou, Z. H., and Egea, P. F. (2015) Conserved SMP domains of the ERMES complex bind phospholipids and mediate tether assembly. *Proc. Natl. Acad. Sci. U.S.A.* 10.1073/pnas.1422363112

89. Wozny, M. R., Di Luca, A., Morado, D. R., Picco, A., Khaddaj, R., Campomanes, P., Ivanović, L., Hoffmann, P. C., Miller, E. A., Vanni, S., and Kukulski, W. (2023) In situ architecture of the ER–mitochondria encounter structure. *Nature*. **618**, 188–192

90. Berger, K. H., Sogo, L. F., and Yaffe, M. P. (1997) Mdm12p, a Component Required for Mitochondrial Inheritance That Is Conserved between Budding and Fission Yeast. *Journal of Cell Biology*. **136**, 545–553

91. Hobbs, A. E. A., Srinivasan, M., McCaffery, J. M., and Jensen, R. E. (2001) Mmm1p, a Mitochondrial Outer Membrane Protein, Is Connected to Mitochondrial DNA (Mtdna) Nucleoids and Required for Mtdna Stability. *J Cell Biol*. **152**, 401–410

92. Youngman, M. J., Hobbs, A. E. A., Burgess, S. M., Srinivasan, M., and Jensen, R. E. (2004) Mmm2p, a mitochondrial outer membrane protein required for yeast mitochondrial shape and maintenance of mtDNA nucleoids. *Journal of Cell Biology*. **164**, 677–688

93. Reichert, A. S., and Neupert, W. (2002) Contact sites between the outer and inner membrane of mitochondria—role in protein transport. *Biochimica et Biophysica Acta (BBA) - Molecular Cell Research*. **1592**, 41–49

94. Tamura, Y., Onguka, O., Hobbs, A. E. A., Jensen, R. E., Iijima, M., Claypool, S. M., and Sesaki, H. (2012) Role for Two Conserved Intermembrane Space Proteins, Ups1p and Up2p, in Intra-mitochondrial Phospholipid Trafficking. *Journal of Biological Chemistry*. **287**, 15205–15218

95. Kemmerer, Z. A., Robinson, K. P., Schmitz, J. M., Manicki, M., Paulson, B. R., Jochem, A., Hutchins, P. D., Coon, J. J., and Pagliarini, D. J. (2021) UbiB proteins regulate cellular CoQ distribution in Saccharomyces cerevisiae. *Nat Commun*. **12**, 4769

96. Eisenberg-Bord, M., Shai, N., Schuldiner, M., and Bohnert, M. (2016) A Tether Is a Tether Is a Tether: Tethering at Membrane Contact Sites. *Developmental Cell*. **39**, 395–409

97. Wilson, E. L., and Metzakopian, E. (2021) ER-mitochondria contact sites in neurodegeneration: genetic screening approaches to investigate novel disease mechanisms. *Cell Death Differ*. **28**, 1804–1821

98. Mourier, A., Motori, E., Brandt, T., Lagouge, M., Atanassov, I., Galinier, A., Rappl, G., Brodesser, S., Hultenby, K., Dieterich, C., and Larsson, N.-G. (2015) Mitofusin 2 is required to maintain mitochondrial coenzyme Q levels. *Journal of Cell Biology*. **208**, 429–442

Chapter 2

Nonfunctional *coq10* mutants maintain the ERMES complex and reveal true phenotypes associated with the loss of the coenzyme Q chaperone protein Coq10

ABSTRACT

Coenzyme Q (CoQ) is a redox-active lipid molecule that acts as an electron carrier in the mitochondrial electron transport chain. In *Saccharomyces cerevisiae*, CoQ is synthesized in the mitochondrial matrix by a multi-subunit protein-lipid complex termed the CoQ synthome, the spatial positioning of which is coordinated by the Endoplasmic Reticulum-Mitochondria Encounter Structure (ERMES). The gene encoding the cytosolic subunit of ERMES, *MDM12*, is coexpressed with *COQ10*, which encodes the putative CoQ chaperone Coq10, via a shared bidirectional promoter. Deletion of *COQ10* results in respiratory deficiency, impaired CoQ biosynthesis, and reduced spatial coordination between ERMES and the CoQ Synthome. While deleting *MDM12* maintains Coq10 levels, we show that deletion of *COQ10* results in diminished Mdm12 protein content. Since deletion of individual ERMES subunits prevents ERMES formation, we asked whether some or all of the phenotypes associated with *COQ10* deletion are a consequence of ERMES dysfunction. To determine which phenotypes result solely due to the loss of Coq10, we constructed strains expressing a functionally impaired (Coq10-L96S) or truncated (Coq10-R147*) Coq10 isoform using CRISPR-Cas9. We show that both *coq10* mutants preserve Mdm12 protein content and exhibit impaired respiratory capacity like the *coq10*Δ mutant, indicating that Coq10's function is vital for respiration regardless of ERMES integrity. Moreover, the maintenance of CoQ synthome stability and efficient CoQ biosynthesis observed for the Coq10-R147* mutant suggests these deleterious phenotypes in the *coq10*Δ mutant are a consequence of ERMES disruption. Overall, this study clarifies the role of Coq10 in modulating the intricate relationship between CoQ biosynthesis and ERMES.

INTRODUCTION

Coenzyme Q (ubiquinone or CoQ) is an essential redox-active lipid molecule found in the plasma membranes and endomembranes of all eukaryotic species (1, 2). Proper localization of CoQ is dependent on its hydrophobic tail, which enables CoQ to anchor itself into the mid-plane of lipid bilayers and is comprised of a species-specific number of isoprene units (indicated by n in CoQ_n) (3). The fully substituted benzoquinone head group imparts its characteristic redox activity, enabling CoQ to perform its most well-known function as an electron and proton carrier within the mitochondrial electron transport chain (1, 2). Other processes that rely on CoQ's ability to act as electron acceptor include sulfide detoxification, proline catabolism, and choline degradation (1, 2). Additionally, the fully reduced form $CoQH_2$ (ubiquinol) serves as a vital lipid-soluble antioxidant capable of ameliorating peroxidation of lipids in cellular membranes (1, 4).

In *Saccharomyces cerevisiae* (yeast), biosynthesis of CoQ_6 (the CoQ isoform synthesized by yeast) requires fourteen nuclear-encoded proteins: Coq1-Coq11, Yah1, Arh1, and Hfd1 (2, 5). Of the Coq polypeptides, Coq1 synthesizes hexaprenyldiphosphate, which is subsequently attached to the C3 position of the ring precursor 4-hydroxyamino benzoic acid (4HB) or para-aminobenzoic acid (pABA), by Coq2 (2, 5). The remaining headgroup modifications are then carried out by several other Coq polypeptides to generate the final product, CoQ_6/CoQ_6H_2 (Fig. 1A). Efficient CoQ_6 biosynthesis requires many of the aforementioned Coq polypeptides (Coq3-Coq9 and Coq11) to localize to the matrix side of the inner mitochondrial membrane where they assemble into a high-molecular-weight complex termed the CoQ synthome (2, 5). Individual deletion of genes encoding Coq1-Coq9 results in abolished CoQ_6 biosynthesis and an inability to respire, as these Coq polypeptides are required for catalytic steps within the CoQ biosynthetic

pathway and/or structural stability of the CoQ synthome (6, 7).

Unlike most yeast *coq* mutants, the *coq10* delete (*coq10*Δ) mutant contains near wild-type amounts of CoQ_6 in the stationary phase, yet still displays a respiratory-deficient growth phenotype, impaired *de novo* CoQ_6 biosynthesis during log phase growth, and a destabilized CoQ synthome (8–12). The NMR structure of the *Caulobacter crescentus* Coq10 ortholog, CC1736, revealed the presence of a steroidogenic acute regulatory protein-related lipid transfer (START) domain (13), shown to be capable of binding CoQ and its late-stage quinone intermediates *in vitro* (12). Additionally, Coq10 isolated from either *S. cerevisiae* or the fission yeast, *Schizosaccharomyces pombe*, were shown to copurify with CoQ_6 or CoQ_{10}, respectively (9, 10). These studies have led to the hypothesis that Coq10 functions as a CoQ chaperone, directing CoQ from its sites of synthesis to its sites of function at the respiratory complexes (8). In several fungal species, Coq10 and Coq11 evolved as fusion proteins, suggesting a possible functional relationship between these two polypeptides (14). This hypothesis is supported by the observation that subsequent deletion of *COQ11* ameliorates many of the defects of the *coq10*Δ mutant, including restored respiratory growth and CoQ synthome formation (15). These data suggest the Coq11 polypeptide may act as a negative modulator of CoQ biosynthesis and the CoQ synthome (15).

Recent studies have suggested that proper assembly and stability of the yeast CoQ synthome also relies on the presence of the endoplasmic reticulum-mitochondria encounter structure (ERMES) in yeast (16, 17) (Fig. 1B). ERMES is a multisubunit complex composed of four main proteins (Mmm1, Mdm10, Mdm12, and Mdm34) that tethers the ER to the mitochondria and is essential for biosynthesis and transport of phospholipids between these organelles (18). In addition to its most well-studied role in shuttling phospholipids between the

ER and mitochondria, ERMES is proposed to act as a platform for recruiting proteins and other small molecules to the mitochondria based on the needs of the cell (18–20). Additionally, yeast lacking ERMES constituents (*ERMES*Δ) exhibit distorted mitochondrial morphology, increased loss of mitochondrial DNA, and respiratory deficiency (18, 21–23). Recently, members of the CoQ synthome were shown to selectively localize into puncta (termed "CoQ domains") that colocalize with ER-mitochondria contact sites marked by ERMES. Deletion or mutation of individual ERMES subunits results in a loss of puncta representative of the CoQ synthome, indicating destabilization (16, 17). In accordance with this observation, *ERMES*Δ mutants were found to accumulate steady-state and *de novo* synthesized CoQ_6 intermediates. These data demonstrate proper CoQ synthome assembly and efficient CoQ_6 production rely on ERMES complex formation.

In addition to the aforementioned defects attributed to the *coq10*Δ mutant, deletion of *COQ10* results in loss of the spatial relationship between the CoQ domains and ERMES (17). *MDM12*, which encodes the cytosolic subunit of ERMES, is coexpressed with *COQ10* via a bidirectional promoter, suggesting a functional relationship and/or physical interaction between their gene products (8, 24, 25). While a previous study confirmed that deletion of *MDM12* does not significantly diminish Coq10 protein content (17), it has yet to be determined whether deletion of *COQ10* negatively impacts *MDM12* expression.

In this study, we show that deletion of *COQ10* results in diminished Mdm12 protein content. To determine which phenotypes result from deletion of the *COQ10* open reading frame alone versus phenotypes that may be a consequence of disrupted *MDM12* expression and subsequent ERMES dysfunction, we constructed chromosomal *coq10* point mutants (Coq10-L96S and Coq10-R147*) in which Mdm12 protein content is preserved. While strains expressing

either of the *coq10* point mutants phenocopied the respiratory deficiency of the *coq10*Δ mutant, we found that the Coq10-R147* mutant, which encodes an unstable truncated Coq10 isoform, maintained a stable CoQ synthome and efficient CoQ_6 biosynthesis. Based on these data, we propose that the destabilized CoQ synthome and resultant defects in *de novo* CoQ_6 production observed for the *coq10*Δ mutant are the result of disrupted *MDM12* expression, and therefore ERMES dysfunction, rather than from the loss of the Coq10 polypeptide.

EXPERIMENTAL PROCEDURES

All reagents were obtained commercially from Thermo Fisher Scientific, unless specified otherwise.

Yeast strains and growth medium

Saccharomyces cerevisiae strains were derived from W303 (26) or S288C (27). Yeast strains used in this study are listed in Table 1. Growth media was prepared as described (28) and included YPD (1% yeast extract, 2% peptone, 2% dextrose), YPG (1% yeast extract, 2% peptone, 3% glycerol), and YPGal (1% yeast extract, 2% peptone, 2% galactose, 0.1% dextrose). Plate medium contained 2% bacto-agar.

Introduction of guide sequences into pCAS by polymerase chain reaction

Guide sequences for introduction of Coq10 point mutations via CRISPR-Cas9 genome editing were cloned into the pCAS sgRNA cassette as previously described (29, 30). Briefly, point mutations within 20 base pairs of a Protospace Adjacent Motif (PAM) site and that were located at least halfway in the *COQ10* open reading frame (ORF) to avoid disruption of the

endogenous *MDM12* promoter were selected for mutagenesis. Guide efficiency was evaluated using the CRISPR design tool in Benchling (Benchling, Inc). Primers for introduction of guide sequences into the pCAS plasmid (Addgene, plasmid #60847) via PCR were designed according to Armaleo et al. (30), including one mutagenic primer per guide sequence containing the 20-bp guide sequence flanked on either side by 20-bp sequences homologous to the parental pCAS plasmid and a short 20-bp primer whose 5′ end is immediately adjacent to the 5′ end of the mutagenic primer. All primers were 5′ phosphorylated according to standard protocols prior to use. PCR reactions for cloning the guide sequences into the pCAS plasmid were carried out according to the modified protocol described by Armaleo et al. (30) and the linear PCR products were blunt-end-ligated using a Quick Ligation™ Kit (NEB). The resultant plasmids were transformed into competent *E. coli* (NEB) and plated on LB + kanamycin (50 μg/mL) medium. Plasmids were isolated from transformants, and correct integration of the guide sequence was verified by Sanger sequencing (Table 2). All primers utilized in pCAS plasmid construction are listed in Table S1.

Use of CRISPR-Cas9 to generate Coq10-L96S and Coq10-R147*

Coq10 point mutations were introduced chromosomally using CRISPR-Cas9 as previously described (29, 30). Briefly, complementary 60-mer oligonucleotides containing the desired point mutation were designed to serve as the double-stranded DNA repair template (Table S1). The previously designed pCAS plasmids and their corresponding donor oligonucleotides were co-transformed into competent W303-1B or W303 *coq11*Δ yeast cells according to standard yeast transformation protocols (31). Competent yeast cells were prepared according to Ryan et al. (29). For each co-transformation, 90 μL competent cells were combined

with 1.0 µg pCAS plasmid and 5.0 µg of each complementary donor oligonucleotide. Transformants were selected on YPD + G148 (0.2 mg/mL) plates incubated at 37 °C. Successful transformants were isolated on fresh YPD + G418 plates incubated at 30 °C. Isolated strains were cultured in 5 mL YPD without G418 for 22 hours to confer loss of the pCAS plasmid. Cultures were subsequently plated for single colonies onto YPD medium. To confirm the desired mutations, genomic DNA was extracted using the Promega Wizard® Genomic DNA Purification Kit (Promega) and the *COQ10* open reading frame was amplified by PCR and verified by Sanger sequencing (Table 1 & Table S1).

Drop dilution plate assays

Yeast strains were grown overnight in 5 mL of YPD. The following day, cultures were diluted to an A_{600} = 0.2 with sterile phosphate-buffered saline and 2 µL of 5-fold serial dilutions were spotted onto YPD and YPG plate medium, corresponding to a final A_{600} = 0.2, 0.04, 0.008, 0.0016, and 0.00032. Plates were incubated at 30 °C and pictures were taken after two or three days.

Analysis of CoQ and CoQ-intermediates and stable isotope labeling

Cells were grown overnight in 5 mL of YPGal at 30 °C with shaking. The pre-cultures were then back diluted to an $A_{600} \sim 0.1$ in 25 mL of fresh YPGal and allowed to further expand to mid-log phase ($A_{600} \sim 0.6$). For analysis of *de novo* CoQ biosynthesis, cultures were treated with 8 µg/mL of $^{13}C_6$-pABA (Sigma-Aldrich) or ethanol as a vehicle control for 5 hours. All cultures were harvested by centrifugation and cell pellets were stored in –20 °C until use.

To prepare for lipid extraction, cell pellets were resuspended in phosphate-buffered

saline. An aliquot of each cell suspension was added to 2 mL of methanol and cells were lysed by vortexing in the presence of glass beads. Lipids were extracted twice in the presence of the internal standard CoQ_4 (Sigma-Aldrich) with the addition of 2 mL petroleum ether followed by vortexing each time. A standard curve was constructed by preparing and extracting standards with known amounts of CoQ_6 (Avanti Polar Lipids) and the internal standard CoQ_4 alongside the experimental samples. Extracted lipids were dried under N_2 gas and reconstituted prior to analysis.

Lipid content was analyzed by LC-MS/MS as previously described (8). Briefly, lipids were reconstituted in 200 µL of 1 mg/mL benzoquinone prepared in ethanol and 20 µL of each sample was injected into an API4000 linear MS/MS spectrometer (Applied Biosystems). The instrument's corresponding analysis software, Analyst version 1.4.2, was used for data acquisition and processing. CoQ_6 content was determined by normalizing the peak using the aforementioned standard curve. Relative levels of CoQ-intermediates are represented as peak areas normalized to the internal standard. A one-way analysis of variance with multiple comparisons corrected for using Dunnett's test was performed using GraphPad Prism 10.

Isolation of crude mitochondria

Yeast strains were cultured overnight in 30 or 50 mL of YPD at 30 °C with shaking. Pre-cultures were back diluted with YPGal and grown with shaking (30 °C, 250 rpm) until cell density reached an $A_{600} \sim 4$. Spheroplasts were prepared with Zymolyase-20T (MP Biomedicals) and subsequent fractionation steps were carried out as previously described (32). Briefly, spheroplasts were lysed using dounce homogenization and the resulting homogenate was subjected to centrifugation at 1,500 × *g* to pellet large cellular debris and membranes. The

supernatant was collected and centrifuged at 12,000 × *g* to pellet mitochondria. The mitochondrial pellet was washed and centrifuged again at 1,500 × *g* to remove unwanted impurities. The final centrifugation step was conducted at 12,500 × *g*, and the resultant crude mitochondrial pellet was resuspended in MES sorbitol buffer. Aliquots of crude mitochondria were flash-frozen in liquid nitrogen and stored at –80 °C until further use. All fractionation steps were completed in the presence of EDTA-free protease inhibitor cocktail tablets (Roche), phosphatase inhibitor cocktail set I (Sigma-Aldrich), phosphatase inhibitor cocktail set II (Sigma-Aldrich), and phenylmethylsulfonyl fluoride (Fisher Scientific), and all centrifugations were conducted at 4 °C. Protein concentration of crude extracts was determined by the bicinchoninic acid (BCA) assay (ThermoFisher Scientific). For strains lacking ERMES, crude mitochondria were prepared as described above with the exception that all culturing steps were performed in YPG to ensure retention of mitochondrial DNA.

SDS-PAGE and immunoblot analysis of steady-state protein expression

Crude mitochondria (12.5 or 25 μg) were resuspended in SDS sample buffer (50 mM Tris, pH 6.8, 10% glycerol, 2% SDS, 0.1% bromophenol blue, and 1.33% β-mercaptoethanol) and separated by gel electrophoresis on 10 or 12% Tris-glycine polyacrylamide gels. Proteins were transferred to 0.45 μm PVDF membranes (Millipore) and blocked with blocking buffer (5% milk and 0.1% Tween-20 in phosphate-buffered saline). Coq polypeptides, ERMES subunits, and mitochondrial protein loading control Mdh1 were detected using rabbit polyclonal antibodies prepared in 0.5% bovine serum albumin or 5% milk at the dilutions listed in Table 3. IRDye 680LT IgG secondary antibodies (LiCOR) were used at a dilution of 1:20,000. Proteins were visualized using the LiCOR Odyssey Infrared Scanner (LiCOR) and immunoblots were

quantified by hand using ImageJ software (National Institutes of Health, Bethesda, MD).

Two-dimensional Blue Native/SDS-PAGE of high molecular weight complexes

2D-BN/SDS-PAGE was performed as described previously (33, 34). Crude mitochondria (300 μg) were solubilized for one hour on ice with 16 mg/mL digitonin (Biosynth) in the presence of the protease and phosphatase inhibitors used during mitochondrial isolation. Solubilized protein was quantified using the BCA assay. 75 μg of solubilized mitochondria were separated on NativePAGE 4-16% Bis-Tris gels (Invitrogen) and cut into strips for the second-dimension separation. Gel strips were then further separated on 10% Tris-glycine polyacrylamide gels. Following the second-dimension separation, immunoblot analyses of the CoQ synthome was performed as described above using an antibody against Coq9. Lyophilized protein used for the native gel high molecular weight standards were obtained from GE Healthcare (Sigma-Aldrich).

RESULTS

Mdm12 protein levels are diminished in yeast lacking *COQ10*

Steady-state levels of the Coq10 polypeptide were previously ascertained in *ERMES*Δ mutants, including the *mdm12*Δ mutant, and were found to be similar to that of control cells, suggesting that deletion of *MDM12* does not disrupt the expression of *COQ10* despite their coexpression from a bidirectional promoter (17). However, relative protein content of each ERMES component in the *coq10*Δ mutant was not investigated, and it remained uncertain if deletion of *COQ10* impacted Mdm12 protein levels. To this end, we quantified the steady state levels of Mmm1, Mdm10, and Mdm12 in the *coq10*Δ, *coq11*Δ, and *coq10*Δ*coq11*Δ mutants. For

this analysis, we used crude mitochondria to retain the endogenous protein tethers, such as ERMES, that may be lost during the preparation of gradient-purified mitochondria.

Despite the preservation of Coq10 protein content previously observed for *ERMES*Δ mutants, yeast lacking *COQ10* had dramatically reduced amounts of Mdm12 and Mmm1 (Fig. 2). The reduction in Mmm1 protein levels is consistent with previous work that showed the presence of Mdm12 is required for stable expression of Mmm1, and vice versa (35). Mdm10 levels were preserved across all mutants, likely due to the involvement of Mdm10 in other mitochondrial import machinery, such as TOM and SAM complex biogenesis and function (36). Regardless, the depletion or loss of a single ERMES subunit results in an inability to form the ERMES complex (18), raising concern that some or all of the phenotypes ascribed to the *coq10*Δ mutant could be a consequence of ERMES dysfunction due to diminished *MDM12* expression.

Chromosomal mutations in the *COQ10* open reading frame preserve Mdm12 and Mmm1 protein levels

To distinguish phenotypes that result solely due to loss of Coq10 from those that could be the result of disrupted *MDM12* expression, two separate mutations were introduced into the yeast genome using CRISPR-Cas9 as described in *Experimental Procedures* (29, 30). The first mutation, L96S, is located within the hydrophobic tunnel formed by the Coq10 START domain and is predicted to disrupt ligand binding (Fig. 3A-B). Structural and biochemical evidence using Coq10 orthologs from *C. crescentus* (12, 13), *S. pombe* (9), and humans (8) have shown its START domain can directly bind CoQ and its late-stage quinone-containing intermediates. Moreover, expression of the Coq10-L96S mutant from an integrative locus or a high-copy plasmid in *coq10*Δ yeast fail to rescue respiratory defects, indicating L96 is an important residue

for Coq10 function (11). The second mutation, R147*/N149*, encodes a truncated isoform of Coq10 where two stop codons were introduced at residues 147 and 149 (hereafter referred to as Coq10-R147*) (Fig. 3A-B). We rationalized both mutations should be downstream enough from the portion of the *MDM12* promoter region located within the *COQ10* open reading frame to allow for preservation of *MDM12* expression (Fig. 3C).

Upon successful genomic integration of the Coq10-L96S and Coq10-R147* mutations, we examined the steady-state levels of Coq10 in addition to select ERMES subunits (Mmm1, Mdm10, and Mdm12) (Fig. 4). All ERMES components, including Mdm12, were present at levels similar to that of the wild-type control in strains harboring either the Coq10-L96S or Coq10-R147* mutation (Fig. 4A-D). This observation supports the conclusion that introduction of the selected mutations does not disrupt the promoter region, and therefore expression, of *MDM12*. Additionally, no band corresponding to the Coq10 polypeptide was detected in mitochondria isolated from strains expressing the Coq10-R147* mutant (Fig. 4E-F). While it is possible that the Coq10-R147* mutant no longer possesses the epitope recognized by the Coq10 antibody, we predict that the truncated mRNA is degraded through nonsense-mediated decay due to the presence of the premature stop codons. As such, we conclude that Coq10-R147* mutant is an excellent candidate for determining which *coq10*Δ phenotypes are solely due to loss of Coq10 as this mutant maintains protein levels of each ERMES component even in the absence of the Coq10 polypeptide.

It is of note that significantly reduced levels of the Coq10-L96S polypeptide were detected when compared with the wild-type control (Fig. 4E-F). The partial expression of Coq10-L96S may confound the assignment of phenotypes as ones that result solely from loss of Coq10 function. However, we decided to proceed with the characterization of both mutant

constructs given Mdm12 and Mmm1 are stably expressed in strains harboring either the Coq10-L96S or Coq10-R147* mutation, including those containing a subsequent deletion of *COQ11* (Fig. 4A-D).

The *coq10* point mutants display impaired respiratory growth similar to the *coq10*Δ mutant.

Given protein levels of ERMES constituents are preserved in strains harboring the Coq10-L96S or Coq10-R147* mutation, we proceeded to reassess phenotypes associated with loss of Coq10 function. The Coq10 polypeptide is required for respiration in yeast (9, 10). As such, yeast *coq10*Δ mutants display impaired growth on medium containing a nonfermentable carbon source, such as YPGlycerol (YPG). As expected, the *coq10*Δ mutant had poor growth on YPG that was phenocopied by the Coq10-R147* mutant across two different genetic backgrounds (Fig. 5). In line with a previous study, the Coq10-L96S mutant displayed anemic growth on nonfermentable medium that was only slightly improved when compared with the *coq10*Δ and Coq10-R147* mutants (11) (Fig. 5). The poor respiratory growth of both the Coq10-R147* and Coq10-L96S mutant indicates the lipid-binding function of Coq10 is necessary for viability on nonfermentable medium, thus supporting the previous conclusion that Coq10 is required for respiration in yeast.

As many defects associated with the deletion of *COQ10* were shown to be alleviated by subsequent deletion of *COQ11* (15), we also sought to reassess this phenotype in *coq11*Δ strains expressing each of the mutant Coq10 isoforms. Like the *coq10*Δ*coq11*Δ mutant, loss of *COQ11* rescued the respiratory growth defect of both the Coq10-R147* and Coq10-L96S mutant in two different genetic backgrounds (Fig. 5). This suggests that deletion of *COQ11* is capable of

rescuing the respiratory growth defect of the *coq10*Δ mutant irrespective of the presence of ERMES.

The Coq10-R147* mutant maintains efficient CoQ_6 biosynthesis

Like most *coq* mutants that display respiratory growth defects, the *coq10*Δ mutant exhibits impaired CoQ_6 biosynthesis during log phase growth (6–8, 12). To determine whether this defect in CoQ_6 biosynthesis can be solely attributed to loss of Coq10, we evaluated *de novo* CoQ_6 biosynthesis in yeast harboring the mutant Coq10 isoforms by treating yeast cultures of each strain with the isotopically labeled ring precursor, $^{13}C_6$-pABA, or ethanol as a vehicle control. Additionally, in accordance with previous work (8, 14, 15), we performed these analyses in both dextrose-containing medium and galactose-containing medium to determine carbon source-dependent changes in biosynthetic efficiency. It is important to note that despite the robust growth on nonfermentable medium (Fig. 5), only a small percentage (0.2-3%) of CoQ is required for efficient growth on nonfermentable plate medium (5). As such, growth on nonfermentable medium is not always indicative of CoQ biosynthetic efficiency.

Consistent with previous studies performed in YPGal medium (15), the *coq10*Δ mutant produced less *de novo* synthesized $^{13}C_6$-CoQ_6 and had decreased total CoQ_6 content (determined by the sum of $^{13}C_6$-CoQ_6 and unlabeled ^{12}C-CoQ_6) when compared with the W303 wild-type control (Fig. 6). The Coq10-L96S mutant produced similar amounts of *de novo* synthesized $^{13}C_6$-CoQ_6 but had decreased total CoQ_6 content in YPGal when compared with the *coq10*Δ mutant (Fig. 6). Further analyses of key CoQ_6-intermediates revealed the Coq10-L96S mutant accumulated the early-stage intermediate $^{13}C_6$-hexaprenylaminobenzoic acid ($^{13}C_6$-HAB) and had decreased amounts of the late-stage intermediate $^{13}C_6$-demethoxy-Q_6 ($^{13}C_6$-DMQ_6) when

compared with the *coq10*Δ mutant (Fig. S1). These data indicate that the CoQ biosynthetic pathway is less efficient in the Coq10-L96S mutant when compared to the *coq10*Δ mutant.

In contrast, the Coq10-R147* mutant produced elevated amounts of *de novo* synthesized $^{13}C_6$-CoQ_6 and total CoQ_6 relative to the *coq10*Δ mutant when cultured in YPGal (Fig. 6). As previously reported (15), changing the carbon source in the medium from galactose to dextrose decreased the CoQ_6 content across all the *coq10* single mutants, however the Coq10-R147* mutant still produced the highest amounts of ^{12}C-CoQ_6 and *de novo* synthesized $^{13}C_6$-CoQ_6 when compared to the *coq10*Δ mutant (Fig. S2). The elevated CoQ_6 content and slight decrease in the amount of *de novo* synthesized $^{13}C_6$-HAB as well as total HAB content in the Coq10-R147* mutant (Fig. S1) suggests that Coq10 is not required to observe efficient CoQ_6 biosynthesis.

Mutants lacking both *COQ10* and *COQ11* have decreased total CoQ_6 content similar to the *coq10*Δ mutant (15). In line with this observation, the Coq10-R147* and Coq10-L96S mutants harboring a subsequent deletion of *COQ11* had decreased amounts of ^{12}C-CoQ_6 and *de novo* synthesized $^{13}C_6$-CoQ_6 like the *coq10*D mutant (Fig. 6A-B). Similarly, both double mutants had elevated $^{13}C_6$-HAB and $^{13}C_6$-DMQ_6 content, suggesting CoQ biosynthesis is still impaired in the absence of Coq11 (Fig. S1). Taken together, these data support the conclusion that the status of ERMES does not influence the functional relationship between Coq10 and Coq11.

The Coq10-R147* mutant has diminished Coq protein content while still maintaining a stable CoQ synthome

To observe efficient CoQ_6 biosynthesis in yeast, several Coq polypeptides must assemble into a high-molecular weight complex termed the CoQ synthome (5). Loss of *COQ10* results in diminished levels of several Coq polypeptides and a destabilized CoQ synthome (6, 7). In line

with our previous findings, the Coq10-R147* mutant phenocopied the *coq10*Δ nutant with respect to having decreased amounts of Coq3, Coq4, Coq6, Coq7, and Coq9 when compared with the wild-type control (Fig. 7A-B). Notably, the Coq10-L96S mutant contained significantly less Coq7 and Coq9 than the *coq10*Δ mutant (Fig. 7A-B). Both the Coq10-R147* and Coq10-L96S mutant displayed elevated Coq11 protein content similar to the *coq10Δ* mutant (Fig. S3).

While deletion of ERMES subunits does not perturb steady state levels of the Coq polypeptides, CoQ synthome stability is abolished in the absence of ERMES (17). Given the diminished levels of Mdm12 and Mmm1 in the *coq10*Δ mutant, we assessed CoQ synthome stability by two-dimensional blue native/SDS-PAGE (2D-BN/SDS-PAGE) with Coq9 serving as an indicator for complex formation (6) in strains expressing Coq10-R147* or Coq10-L96S. The CoQ synthome in wild-type yeast can be observed as a large heterogeneous high molecular weight complex that spans ~ 100 kDa to >1 MDa. The Coq10-L96S mutant displayed only a very faint signal corresponding to a CoQ synthome (Fig. 8), likely due to its dramatically decreased abundance of several Coq polypeptides as compared with the *coq10*Δ mutant (Fig. 7A-B). This suggests that the presence of a nonfunctional Coq10 polypeptide is more detrimental to complex stability than its complete absence. Surprisingly, the truncated Coq10 isoform displayed a stable high-molecular-weight complex similar to the wild-type control (Fig. 8). This suggests that the preservation of Mdm12 levels in the Coq10-R147* mutant allows for proper ERMES formation and, subsequently, maintenance of a stable CoQ synthome. Overall, these observations support a model in which the destabilized CoQ synthome, and resultant inefficient CoQ_6 biosynthesis, observed in the *coq10*Δ mutant result from loss of ERMES rather than loss of the Coq10 polypeptide.

Subsequent deletion of *COQ11* from the *coq10*Δ mutant has been shown to rescue CoQ

synthome formation due to an increased abundance of several Coq polypeptides (15). Like the *coq10*Δ*coq11*Δ mutant, the Coq10-L96S *coq11*Δ and Coq10-R147* *coq11*Δ double mutants displayed restored levels of most Coq polypeptides and a stable CoQ synthome when compared with the wild-type control (Fig. 7C & Fig. 8). Notably, the rescued Coq protein levels observed for the Coq10-L96S *coq11*Δ double mutant likely explains its restored CoQ synthome formation, as indicated by the reappearance of a high-molecular-weight signal in the Coq10-L96S *coq11*Δ mutant (Fig. 8).

DISCUSSION

This work sought to re-evaluate phenotypes attributed to deletion of *COQ10* through introduction of chromosomal mutations within the *COQ10* open reading frame in *S. cerevisiae*. Previous studies identified *MDM12* as the top-ranked gene coexpressed with *COQ10* in *S. cerevisiae* (8, 24, 25) due to their head-to-head positioning within the yeast genome. *MDM12* encodes the cytosolic component of the ERMES complex, which acts as a bridge connecting the ER-residing subunit of ERMES, Mmm1, with its mitochondrial components, Mdm10 and Mdm34 (18). While the *mdm12*Δ mutant displays unperturbed steady state levels of the Coq10 polypeptide (17), we found that deletion of *COQ10* results in a significant decrease in Mdm12 protein content (Fig. 2). Prior work has shown deletion of *MDM12*, and consequently loss of ERMES complex formation, causes decreased respiration (18, 37) and inefficient CoQ_6 biosynthesis as a result of a destabilized CoQ synthome (17). Given these deleterious phenotypes are shared with yeast harboring a deletion of *COQ10* (10, 12), we sought to distinguish which of the *coq10*Δ phenotypes result solely from loss of the Coq10 polypeptide as opposed to those caused by ERMES defects. Using CRISPR-Cas9 genome editing, we introduced mutations

within the *COQ10* open reading frame that result in loss of Coq10 function (Coq10-L96S) or loss of the Coq10 polypeptide (Coq10-R147*) while still preserving Mdm12 protein content (Fig. 4D). Our characterization of these mutants demonstrates that while the Coq10 polypeptide is required for respiration (Fig. 5), it is not essential for efficient CoQ_6 biosynthesis or stable formation of the CoQ synthome (Fig. 6 & Fig. 8).

The function of Coq10 is widely conserved across several organisms, including *C. crescentus* (12, 13), *S. pombe* (9), and humans (8). Notably, the NMR structure of a Coq10 ortholog from *C. crescentus*, CC1736, revealed the presence of a START domain capable of binding CoQ with variable polyisoprenoid chain lengths and its late-stage quinone intermediates (12, 13). Additionally, Coq10 polypeptides from *S. cerevisiae* and *S. pombe* were found to copurify with CoQ_6 and CoQ_{10}, respectively, leading to the hypothesis that Coq10 functions as a CoQ chaperone (9, 10). This hypothesis is further supported by studies showing yeast Coq10 and its orthologs are required for respiration and efficient *de novo* CoQ biosynthesis (8). Surprisingly, the introduction of the L96S mutation within the START domain resulted in more pronounced defects in CoQ_6 biosynthetic efficiency, Coq polypeptide abundance, and CoQ synthome stability despite the slightly improved respiratory capacity of this mutant when compared to the *coq10*Δ control (Fig. 5, Fig. 6, Fig. 7, & Fig. 8). We posit that that the abrogated lipid-binding function of this mutant is compounded by its partial expression (Fig. 4E), resulting in a dominant negative effect. In contrast, the phenotypes displayed by the Coq10-R147* mutant manifest solely from loss of the Coq10 polypeptide as opposed to the unforeseen defects that resulted when we expressed the unstable, nonfunctional Coq10-L96S mutant. This conclusion is supported by the observation that the Coq10-R147* mutant did not exhibit augmented deleterious phenotypes when compared with the *coq10*Δ control.

Stable formation of the CoQ synthome requires the presence of both CoQ and prenylated CoQ-intermediates (7, 38, 39). Studies have shown that bypassing defective steps of the CoQ biosynthetic pathway with appropriate substrate analogs can restore the appearance of CoQ domains, indicating that the late-stage CoQ intermediates are required for CoQ synthome assembly (16, 40). In accordance with these observations, the *coq10*Δ mutant, which produces higher amounts of early-stage intermediates and lower amounts of late-stage intermediates, displays a destabilized CoQ synthome (8, 12, 15). Strikingly, we found that the Coq10-R147* mutant, which lacks the Coq10 polypeptide, retained the ability to synthesize CoQ_6 efficiently and could form a stable CoQ synthome (Fig. 6 & Fig. 8). Despite its elevated total CoQ_6 content, the Coq10-R147* mutant had defective respiratory growth similar to the *coq10*Δ mutant (Fig. 5). This suggests that the CoQ chaperone function of Coq10 is required only for respiration, and is not essential for CoQ biosynthesis and, subsequently, stable formation of the CoQ synthome. We attribute the clear demarcation between respiratory capacity and CoQ synthome stability observed for the Coq10-R147* mutant to the preservation of Mdm12 protein content (Fig. 4D), thus allowing us to separate phenotypes caused by loss of Coq10 from those that result due to ERMES dysfunction.

Humans possess two distinct Coq10 orthologs, COQ10A and COQ10B (8). Complementation of the yeast *coq10*Δ mutant with either human isoform was shown to rescue defects in respiratory growth on nonfermentable plate medium, supporting the hypothesis that the function of Coq10 as a CoQ chaperone is conserved across organisms. Our data corroborates this conclusion in that both *coq10* mutants constructed in this study had defective respiratory growth on medium containing a nonfermentable carbon source (Fig. 5). In contrast, complementation of the yeast *coq10*Δ mutant with either human Coq10 ortholog failed to fully

restore both efficient CoQ_6 biosynthesis and CoQ synthome formation (8). Our data suggests the negligible effect on CoQ synthome stabilization and CoQ_6 biosynthesis observed when expressing either COQ10A or COQ10B is a consequence of disrupted ERMES formation in the yeast *coq10*Δ mutant rather than an incompatibility between the human Coq10 orthologs and yeast CoQ biosynthesis.

Coq10 and Coq11 exist as a fusion protein in several *Ustilaginaceae* species, indicating the presence of a functional relationship between these two polypeptides (14). Previous studies have shown that while the *coq11*Δ mutant does not display defects in respiratory growth, it does have decreased *de novo* $^{13}C_6$-CoQ_6 production. Despite its impairment in CoQ_6 biosynthesis, the *coq11*Δ mutant displays a more stable CoQ synthome as a result of increased Coq polypeptide abundance (15, 16). As such, the Coq11 polypeptide is proposed to play a regulatory role in CoQ_6 biosynthesis through its function as a negative modulator of CoQ synthome formation (15). This hypothesized function of Coq11 is supported by the observation that deletion of *COQ11* in tandem with *COQ10* rescues the respiratory defect of the *coq10*Δ mutant as a result of increased protein content for several Coq polypeptides and subsequent stabilization of the CoQ synthome (15). Similarly, our *coq10* mutants that harbor a subsequent deletion of *COQ11* displayed restored growth on a nonfermentable medium when compared with the *coq10*Δ mutant (Fig. 5). Furthermore, the Coq10-R147* and -L96S *coq11*Δ double mutants also had decreased *de novo* CoQ_6 production and restored protein content for several Coq polypeptides like the *coq10*Δ*coq11*Δ mutant (Fig. 6 and Fig. 7). This suggests the mechanism by which deletion of *COQ11* rescues the sickly *coq10*Δ phenotypes is independent of ERMES. Elevated Coq11 protein content in all the *coq10* mutants regardless of the type of mutation or its effect on ERMES supports this conclusion (Fig. S3).

A fundamental feature of membrane contact sites is their ability to spatially coordinate cellular processes such that contact sites can serve as nucleation sites for specific pathways depending on the needs of the cell. Previous studies have shown the spatial positioning of the CoQ synthome is mediated by ER-mitochondrial contacts established by ERMES, as evidenced by colocalization of the CoQ domain marker, Coq9-yEGFP, with the ERMES marker, Mdm34-mCherry (17). Deletion of *COQ10* results in significantly less colocalization between the CoQ domains and ERMES (17), suggesting Coq10 may modulate the spatial coordination between ERMES and the CoQ domains. However, it is also possible that the disparity in colocalization in the *coq10*Δ mutant could be attributed to its destabilized CoQ synthome and, as we have shown, disrupted ERMES formation via attenuated Mdm12 and Mmm1 protein content (Fig. 2). While we were able to preserve ERMES protein content in our *coq10* mutants (Fig. 4A-D), it remains unclear if the spatial coordination between ERMES and the CoQ domains is maintained. It is possible that despite the formation of a stable CoQ synthome in the Coq10-R147* mutant (Fig. 8), the Coq10 polypeptide may still be required to mediate the localization of the CoQ synthome alongside ERMES.

Since the initial characterization of the ERMES complex (18), several other ER-mitochondrial contact sites have been discovered (41). The viability of yeast lacking individual ERMES constituents suggests that ERMES-related functions can be compensated for by auxiliary contact sites. In support of this, CoQ domains have been shown to also colocalize with puncta marked by Ltc1 (16), the ER-residing component of an auxiliary ER-mitochondrial tether (42). This suggests it is more important CoQ domains localize to any given ER-mitochondrial contact site rather than contact sites established specifically by ERMES. However, it is tempting to speculate that there is a unique regulatory relationship between Coq10 and ERMES given the

positioning of the *COQ10* and *MDM12* genes within the yeast genome (Fig. 3C). Commonly, bidirectional promoters couple two divergent protein-encoding genes involved in related processes to allow for their tight regulation (43, 44). It is possible coexpression of *COQ10* and *MDM12* via their shared bidirectional promoter allows for the coupling of CoQ biosynthesis with a transport mechanism capable of distributing CoQ to other cellular membranes. Three ERMES subunits (Mmm1, Mdm12, and Mdm34) possess a synaptotagmin-like mitochondrial lipid binding protein (SMP) domain shown to facilitate the transport of phospholipids between the ER and mitochondria (18, 19, 37). Structural characterization of ERMES using correlative light and electron cryo-microscopy (cryo-CLEM) has shown that these SMP domains align to form a channel for lipid transport (20). As such, ERMES could serve as a platform for the mitochondrial distribution of CoQ in yeast following its synthesis.

Despite the absence of a direct human homolog for ERMES, the prevalence of ER-mitochondrial contact sites in humans indicates that spatial regulation of mitochondrial processes via contact sites is conserved. For example, knockdown of the gene encoding the mitofusin-2 (MFN2) ortholog, *MFN2*, in mice results in CoQ deficiency and decreased respiratory capacity (45). MFN2 is most commonly known for its role in mitochondrial fusion, but its dual localization to ER and outer mitochondrial membranes enables it to form a physical tether between the two organelles via its homodimerization (46). In contrast, mitofusin-1 (MFN1) localizes solely to outer mitochondrial membranes where it can form a heterodimeric tether with ER-localized MFN2 (47). Notably, mice with knockdown of *Mfn1* retain the ability to synthesize CoQ (45). This suggests the CoQ deficiency observed in *Mfn2* knockdown mice is not due loss of MFN2 function in mitochondrial fusion, but rather results from the loss of MFN2-mediated tethering between the ER and mitochondria. Our work reinforces the finding that ER-

mitochondrial contacts can specifically regulate CoQ biosynthesis in that the preservation of ERMES in the Coq10-R147* mutant results in *de novo* CoQ production similar to the wild-type control (Fig. 6).

In summary, this work revealed that previously reported phenotypes attributed to deletion of *COQ10* in *S. cerevisiae* were conflated with those caused by significantly attenuated Mdm12 protein content in the *coq10*Δ mutant. To disentangle these phenotypes, we generated two separate *coq10* point mutants using CRISPR-Cas9 genome editing that maintain Mdm12 protein content and ERMES complex formation. Through our characterization of these mutants, we demonstrate that Coq10 is required for respiration but not efficient CoQ_6 biosynthesis or formation of a stable CoQ synthome. Taken together, these results support a model in which Coq10 functions solely as a CoQ chaperone responsible for directing CoQ from its sites of synthesis to its sites of function at the respiratory complexes.

Table 1. Genotype and source of yeast strains.

Strain	Genotype	Source
W303 1B	MAT α *leu2-3,-112; his3-11,-15; trp1-1; ura3-1; ade2-1; can1-100*	R. Rothstein[a]
BY4742	MAT α *his3Δ0 leu2Δ0 met15Δ0 ura3Δ0*	(27)
JM6	*MAT a his-4 ρ^0*	J. E. McEwen[b]
JM8	*MAT α ade-1 ρ^0*	J. E. McEwen[b]
W303a *coq2*Δ	*MAT a, ade2-1 can1-100 his3-11,15 leu2-3,112 trp1-1 ura3-1 coq2::HIS3*	(48)
W303 1B *coq3*Δ	MAT α *leu2-3,-112; his3-11,-15; trp1-1; ura3-1; ade2-1; can1-100 coq3::LEU2*	(49)
W303a *coq4*Δ	MAT a *leu2-3,-112; his3-11,-15; trp1-1; ura3-1; ade2-1; can1-100 coq4::TRP1*	(50)
W303 1B *coq5*Δ	MAT α *leu2-3,-112; his3-11,-15; trp1-1; ura3-1; ade2-1; can1-100 coq5::HIS3*	(51)
W303a *coq6*Δ	MAT a *leu2-3,-112; his3-11,-15; trp1-1; ura3-1; ade2-1; can1-100 coq6::LEU2*	(52)

Table 1. Genotype and source of yeast strains. (Cont.)

Strain	Genotype	Source
W303 1B *coq7*Δ	MAT α *leu2-3,-112; his3-11,-15; trp1-1; ura3-1; ade2-1; can1-100 coq7::LEU2*	(53)
W303a *coq8*Δ	MAT a *leu2-3,-112; his3-11,-15; trp1-1; ura3-1; ade2-1; can1-100 coq8::HIS3*	(50)
W303 1B *coq9*Δ	MAT α *leu2-3,-112; his3-11,-15; trp1-1; ura3-1; ade2-1; can1-100 coq9::URA3*	(54)
W303a *coq10*Δ	MAT a *leu2-3,-112; his3-11,-15; trp1-1; ura3-1; ade2-1; can1-100 coq10::HIS3*	(10)
W303 1B *coq11*Δ	MAT α *leu2-3,-112; his3-11,-15; trp1-1; ura3-1; ade2-1; can1-100 coq11::LEU2*	(15)
W303 1B *coq10*Δ*coq11*Δ	MAT α *leu2-3,-112; his3-11,-15; trp1-1; ura3-1; ade2-1; can1-100 coq10::HIS3 coq11::LEU2*	(15)
W303a *mmm1*Δ	MAT a *leu2-3,-112; his3-11,-15; trp1-1; ura3-1; ade2-1; can1-100 mmm1::KanMX*	(37)
W303a *mdm10*Δ	MAT a *leu2-3,-112; his3-11,-15; trp1-1; ura3-1; ade2-1; can1-100 mdm10::HIS3*	(37)

Table 1. Genotype and source of yeast strains. (Cont.)

Strain	Genotype	Source
W303a *mdm12*Δ	MAT a *leu2-3,-112; his3-11,-15; trp1-1; ura3-1; ade2-1; can1-100 mdm12::HIS3*	(37)
W303 1B Coq10-L96S	MAT α *leu2-3,-112; his3-11,-15; trp1-1; ura3-1; ade2-1; can1-100 coq10-L96S*	This work
W303 1B Coq10-L96S *coq11*Δ	MAT α *leu2-3,-112; his3-11,-15; trp1-1; ura3-1; ade2-1; can1-100 coq10-L96S coq11::LEU2*	This work
W303 1B Coq10-R147*	MAT α *leu2-3,-112; his3-11,-15; trp1-1; ura3-1; ade2-1; can1-100 coq10-R147**	This work
BY4741 *coq2*Δ	MAT a *his3Δ0 leu2Δ0 met15Δ0 ura3Δ0 coq2::KanMX4*	(55)
BY4742 *coq10*Δ	MAT α *his3Δ0 leu2Δ0 met15Δ0 ura3Δ0 coq10::KanMX4*	(55)
BY4742 *coq11*Δ	MAT α *his3Δ0 leu2Δ0 met15Δ0 ura3Δ0 coq11::LEU2*	(15)
BY4742 *coq10*Δ*coq11*Δ	MAT α *his3Δ0 leu2Δ0 met15Δ0 ura3Δ0 coq10::HIS3 coq11::LEU2*	(15)

Table 1. Genotype and source of yeast strains. (Cont.)

Strain	Genotype	Source
BY4742 Coq10-L96S	MAT α *his3Δ0 leu2Δ0 met15Δ0 ura3Δ0 coq10-L96S*	This work
BY4742 Coq10-L96S *coq11*Δ	MAT α *his3Δ0 leu2Δ0 met15Δ0 ura3Δ0 coq10-L96S coq11::LEU2*	This work
BY4742 Coq10-R147*	MAT α *his3Δ0 leu2Δ0 met15Δ0 ura3Δ0 coq10-R147**	This work
BY4742 Coq10-R147* *coq11*Δ	MAT α *his3Δ0 leu2Δ0 met15Δ0 ura3Δ0 coq10-R147* coq11::LEU2*	This work

[a] Dr. Rodney Rothstein, Department of Human Genetics, Columbia University

[b] Dr. Joan E. McEwen

Table 2. Plasmids used in this study.

Plasmid	*Construct Description*	*Source*
pCAS	Expresses *S. pyogenes* Cas9 plus an HDV ribozyme-sgRNA for genome editing in yeast	(29)
pCAS_C10-L96	pCAS backbone with modified sgRNA targeting L96 of yeast Coq10	This Work
pCAS_C10-R147	pCAS backbone with modified sgRNA targeting R147 of yeast Coq10	This Work

Table 3. Description and source of antibodies.

Antibody	*Working Dilution*	*Source*
Coq3	1:200	(56)
Coq4	1:2,000	(57)
Coq5	1:5,000	(58)
Coq6	1:200	(52)
Coq7	1:500	(59)
Coq8	Affinity purified, 1:30	(6)
Coq9	1:1,000	(6)
Coq10	Affinity purified, 1:400	(8)
Coq11	1:500	(8)
Mdh1	1:10,000	Lee McAlister-Henn[c]
Mdm10	1:250	(36)
Mdm12	1:200	(36)
Mmm1	1:500	(36)

[c] Dr. Lee McAlister-Henn, Department of Molecular Biophysics and Biochemistry, University of Texas Health Sciences Center

FIGURES

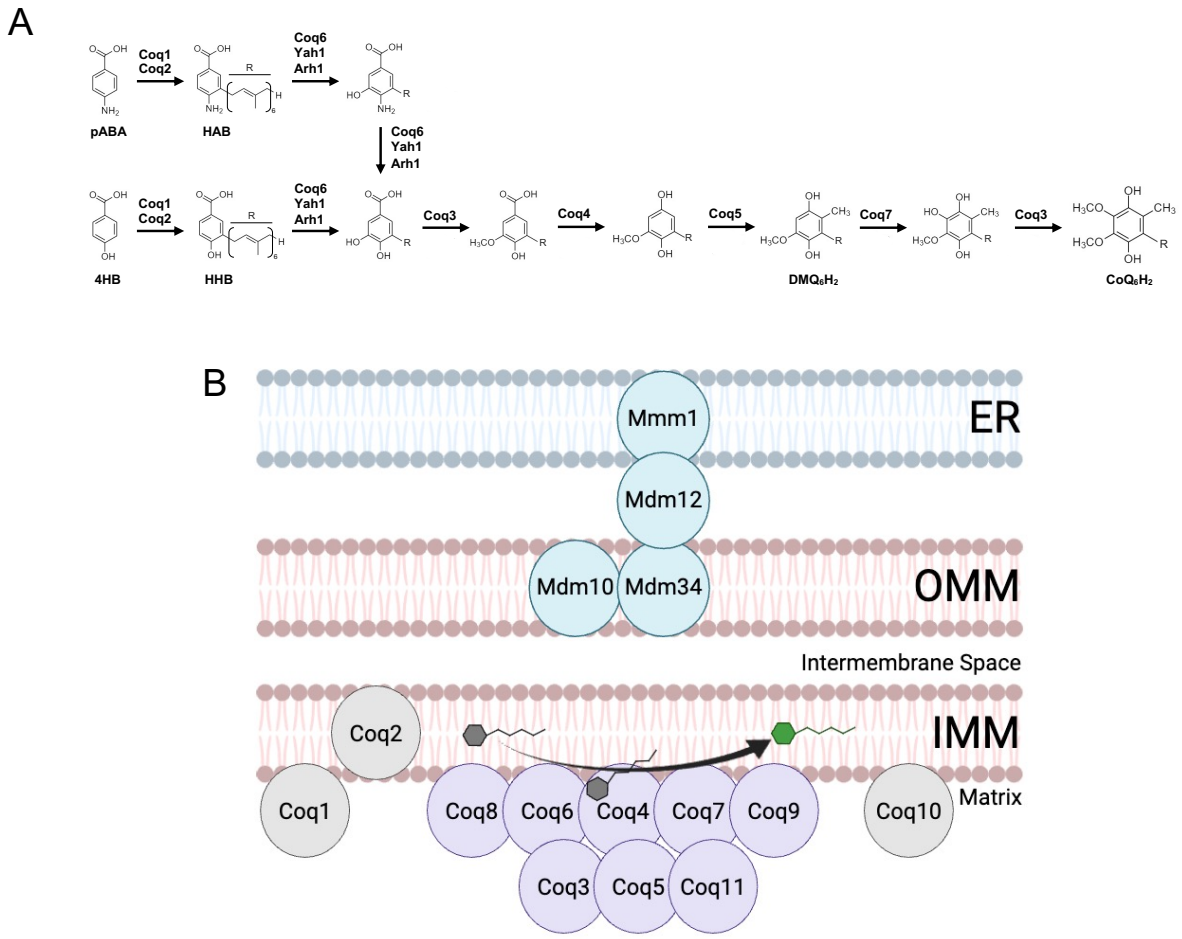

Figure 1. CoQ biosynthesis in yeast requires the CoQ synthome to assemble adjacent to ERMES contact sites. *A,* The proposed CoQ biosynthetic pathway in *Saccharomyces cerevisiae*. *B*, Schematic depicting the CoQ synthome positioned adjacent to the ERMES complex. CoQ synthome members are represented in purple and ERMES components are highlighted in turquoise. Coq1, Coq2, and Coq10 (gray) are not members of the CoQ synthome, but are still required to observe efficient CoQ_6 biosynthesis.

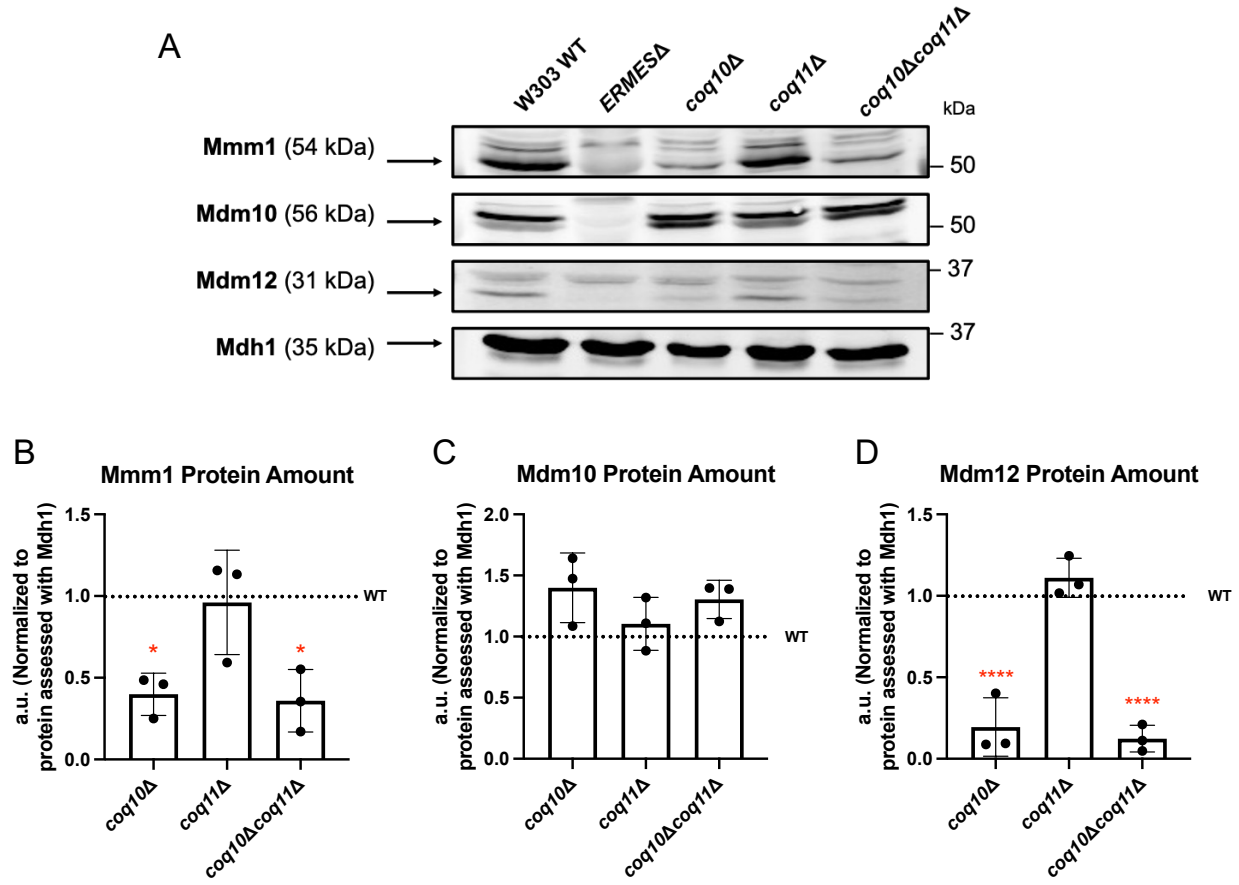

Figure 2. Mdm12 and Mmm1 polypeptides are depleted in yeast *coq10*Δ mutants. *A,* Aliquots of crude mitochondria (25 µg) from WT, *coq10*Δ, *coq11*Δ, and *coq10*Δ*coq11*Δ yeast strains were subjected to 10% Tris-glycine SDS-PAGE. Immunoblotting was performed with antisera against the indicated ERMES subunits (Mmm1, Mdm10, and Mdm12), and yeast harboring the corresponding deletions were used as negative controls (*ERMES*Δ). Malate dehydrogenase (Mdh1) was used as a loading control. Data are representative of three biological replicates. *B,* ImageJ was used to quantify triplicate band intensities of select ERMES subunits. Band intensities were normalized to Mdh1 and plotted as percentage of the wild-type (WT) control. The data depicts the mean ± SD of three biological replicates, and the statistical significance compared with WT is represented by *, $p < 0.05$, and ****, $p < 0.0001$.

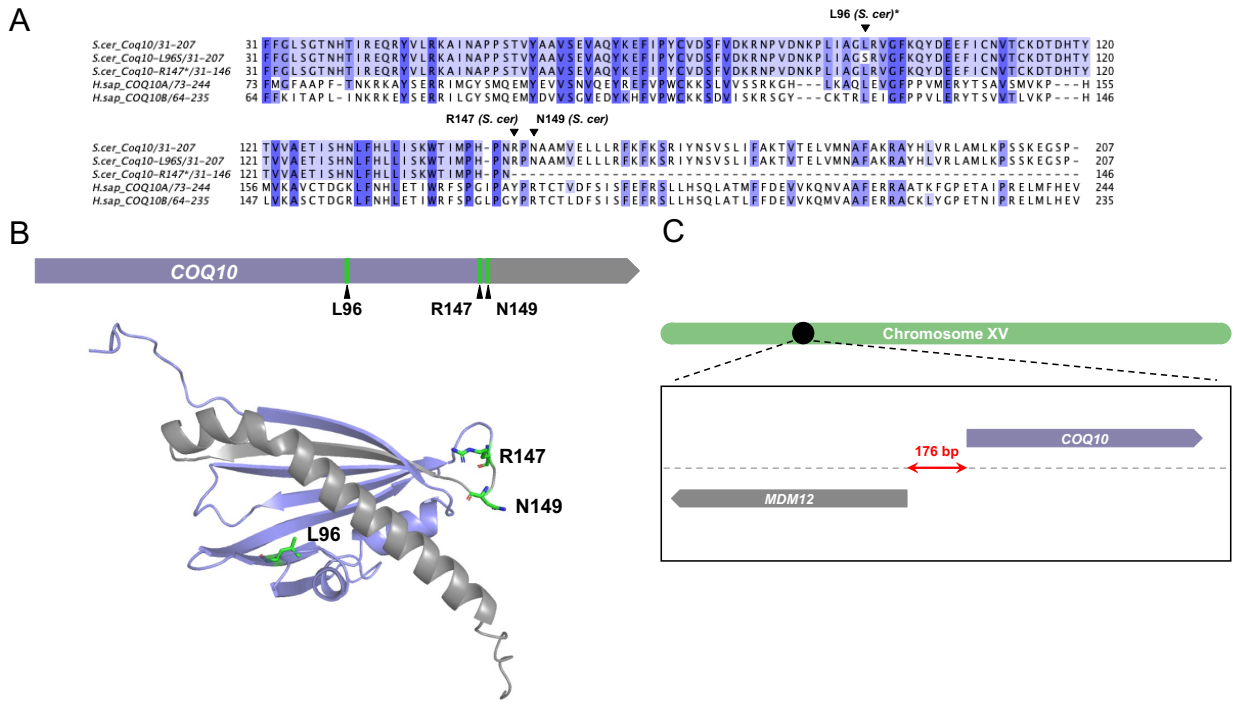

Figure 3. Structural prediction of *S. cerevisiae* Coq10 and sequence alignment with human orthologs highlight residues targeted for mutagenesis. *A,* Multiple sequence alignment of *S. cerevisiae* Coq10 (residues 31-207) with the Coq10-L96S and Coq10-R147* mutants constructed in this study and the human homologs COQ10A (residues 73-244)/COQ10B (residues 64-235). The yeast Coq10 polypeptide and orthologous human sequences were obtained from Universal Protein Knowledgebase (UniProtKB). The MSA was constructed using the ClustalW package of Clustal Omega and visualized in JalView2. Conservation of each residue is indicated by degree of shading, which represent 80%, 60% and 40% percent identity from darkest to lightest shade, respectively. Residues targeted for mutagenesis in this study are indicated with an inverted triangle, and asterisks indicate residues deemed critical for ligand binding in previous studies. *B,* Location of the Coq10 residues targeted for mutagenesis by CRISPR-Cas9 (shown in green) within the context of the *COQ10* open-reading frame (top) and the AlphaFold predicted structure for *S. cerevisiae* Coq10 (bottom, AF-Q08058-F1). The region

shown in gray represents the truncation that results from introducing the Coq10-R147*/N149* double mutation. *C,* Schematic depicting the head-to-head positioning of *COQ10* (purple) and *MDM12* (gray) within the context of *S. cerevisiae* Chromosome XV (green). Notably, these two genes are separated by only 176 base pairs (bp), suggesting deletion of gene one could impact the expression of the other and vice versa.

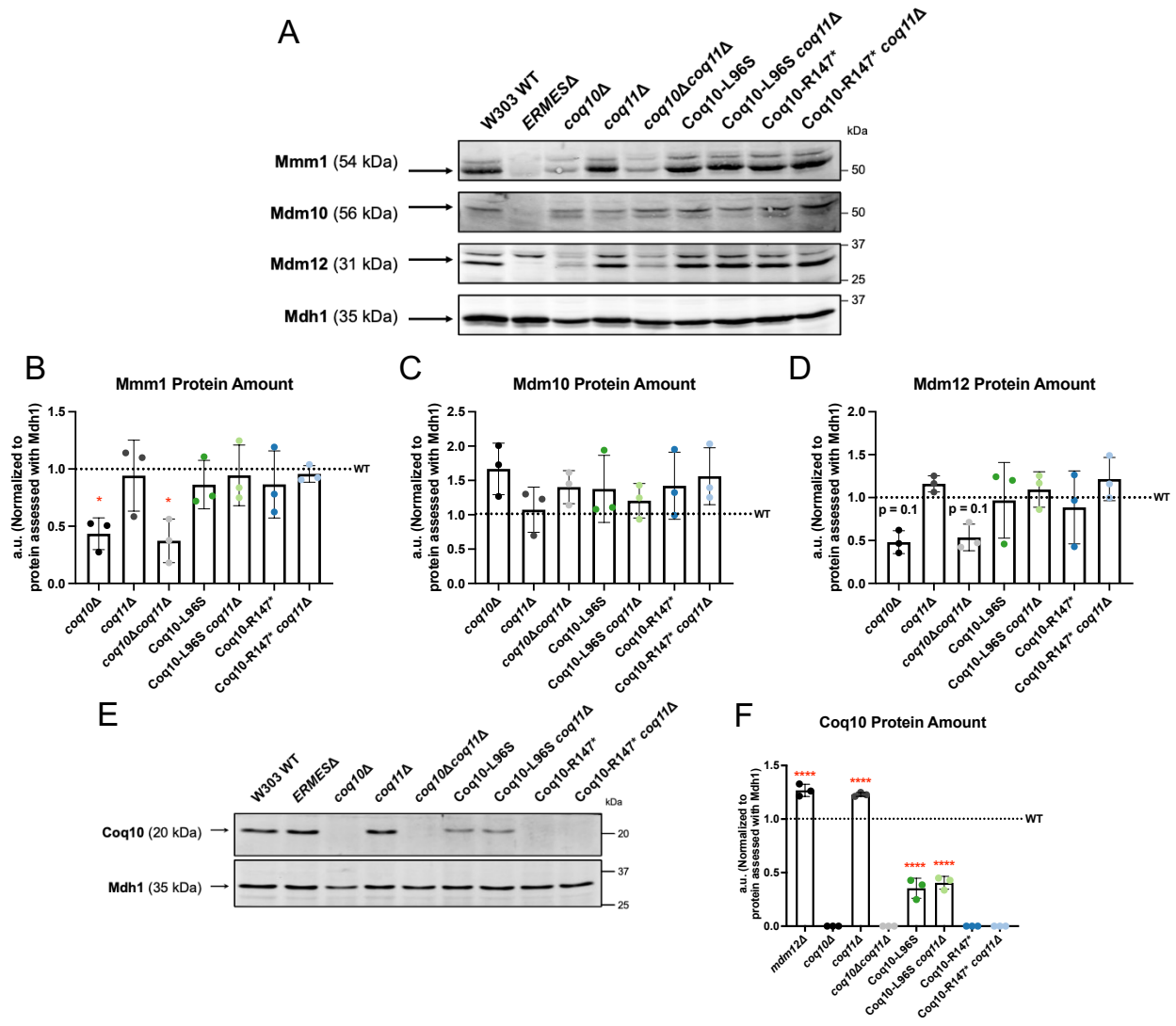

Figure 4. Mdm12 protein levels are preserved in strains expressing the Coq10-L96S or Coq10-R147* mutant. *A,* Aliquots of crude mitochondria (25 µg) from the indicated yeast strains were subjected to 10% Tris-glycine SDS-PAGE. Immunoblotting was performed with antisera against the indicated ERMES subunits (Mmm1, Mdm10, and Mdm12), and yeast harboring the corresponding deletions were used as negative controls (*ERMES*Δ). Malate dehydrogenase (Mdh1) was used as a loading control. Data are representative of three biological replicates. *B-D*, ImageJ was used to quantify triplicate band intensities of the indicated ERMES proteins. Band intensities were normalized to Mdh1 and plotted as percentage of the wild-type

control. The data depict mean ± SD of three biological replicates, and the statistical significance compared with WT is represented by *, $p < 0.05$. *E,* 12.5 µg of crude mitochondria were separated on 12% Tris-glycine SDS-PAGE and immunoblotting was performed using Coq10 antisera. An aliquot of mitochondria from the *coq10*Δ yeast was used as a negative control. *F,* ImageJ was used to quantify triplicate band intensities for the Coq10 polypeptide. Band intensities were normalized to Mdh1 and plotted as percentage of the wild-type control. The data depict the mean ± SD of three biological replicates, and the statistical significance compared with WT is represented by ****, $p < 0.0001$.

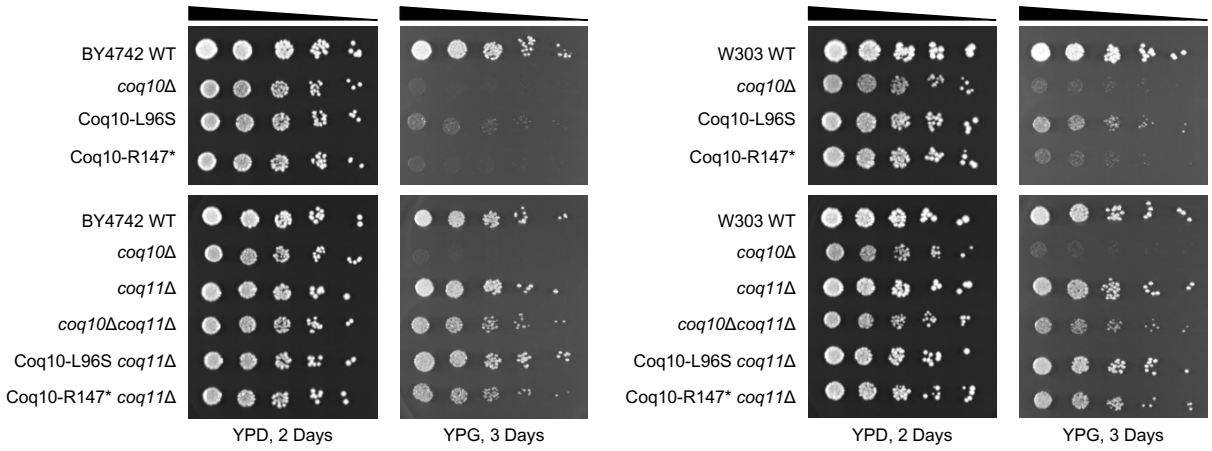

Figure 5. Strains expressing the Coq10-L96S or Coq10-R147* mutant display impaired respiratory growth similar to the *coq10*Δ mutant. Overnight cultures of the indicated yeast strains were diluted to an A_{600} = 0.2, and 2 µL of 5-fold serial dilutions were spotted onto fermentable (YPDextrose, YPD) or respiratory (YPGlycerol, YPG) medium. Plates were incubated at 30 ℃ for two or three days prior to imaging. Data are representative of three biological replicates.

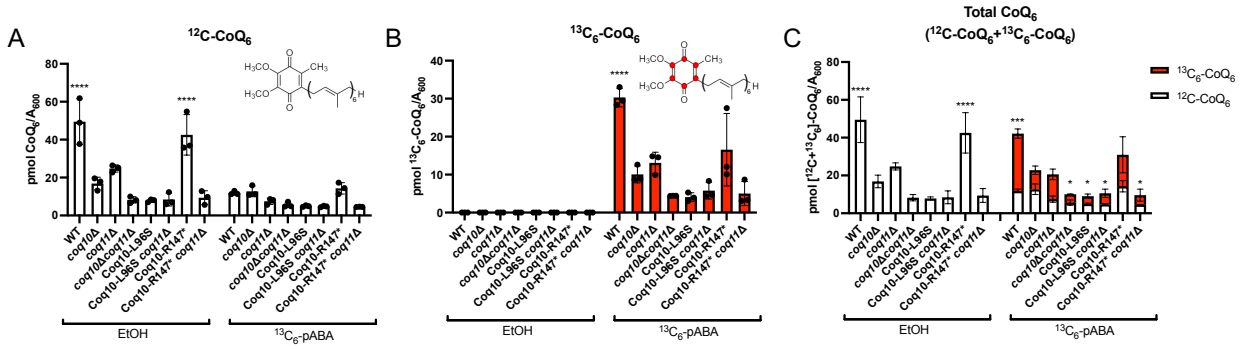

Figure 6. The Coq10-R147* mutant retains the ability to efficiently synthesize CoQ_6. Triplicates of yeast cultured in 25 mL YPGal were labeled at an $A_{600} \sim 0.6$ with 8 µg/mL $^{13}C_6$-pABA or ethanol as a vehicle control. 15 mL of each culture were harvested after 5 hours, lipid extracted, and analyzed by LC-MS/MS. *A*, unlabeled ^{12}C-CoQ_6; *B*, labeled $^{13}C_6$-CoQ_6; *C*, total amount of CoQ_6 determined from the sum of ^{12}C-CoQ_6 (white) and $^{13}C_6$-CoQ_6 (red). The data depict the mean ± SD, and the statistical significance as compared with the *coq10*Δ mutant is represented by *, $p < 0.05$; ***, $p < 0.001$; and ****, $p < 0.0001$.

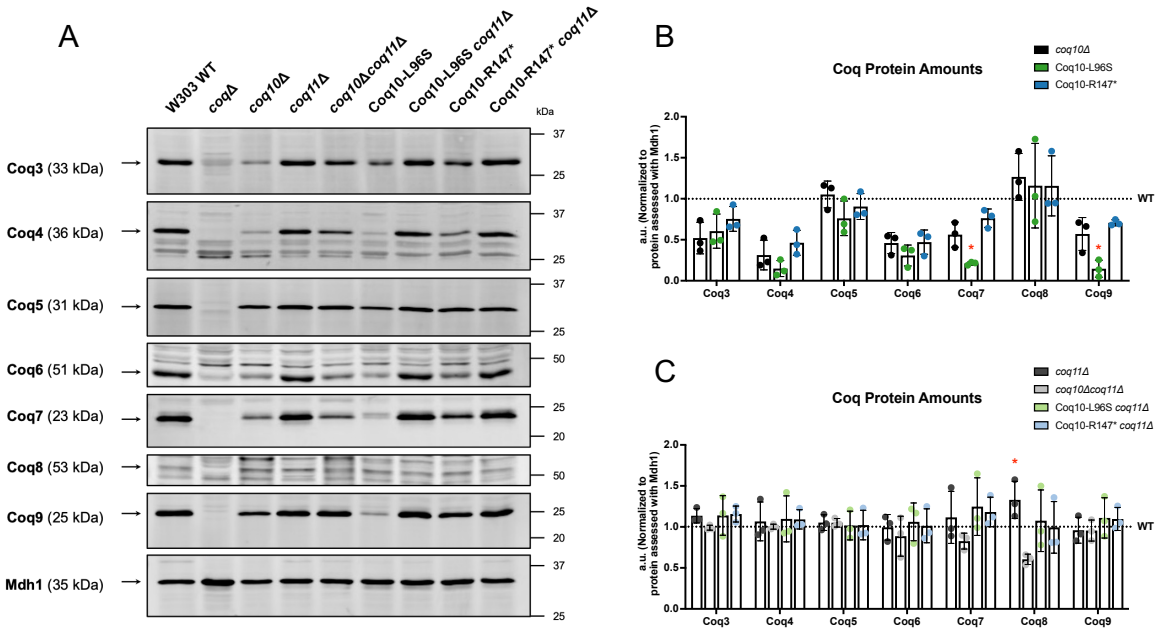

Figure 7. Lowered abundance of the Coq polypeptides in the *coq10* point mutants can be rescued by deletion of *COQ11* like the *coq10*Δ*coq11*Δ mutant. *A,* Aliquots of crude mitochondria (12.5 µg) from the indicated yeast strains were subjected to 10% or 12% Tris-glycine SDS-PAGE. Crude mitochondria from *coq3*Δ-*coq9*Δ mutants were included as negative controls for Western blotting using antisera against each of the Coq polypeptides. Mitochondrial malate dehydrogenase (Mdh1) was included as a loading control. Data are representative of three biological replicates. *B,* ImageJ was used to quantify triplicate band intensities for each of the Coq polypeptides. Band intensities were normalized to Mdh1 and plotted as percentage of the wild-type control. The data depict the mean ± SD of three biological replicates, and the statistical significance compared with the *coq10*Δ mutant is represented by *, $p < 0.05$. *C,* Blots were quantified as in *B*. The data depict the mean ± SD of three biological replicates, and the statistical significance compared with the *coq10*Δ*coq11*Δ mutant is represented by *, $p < 0.05$.

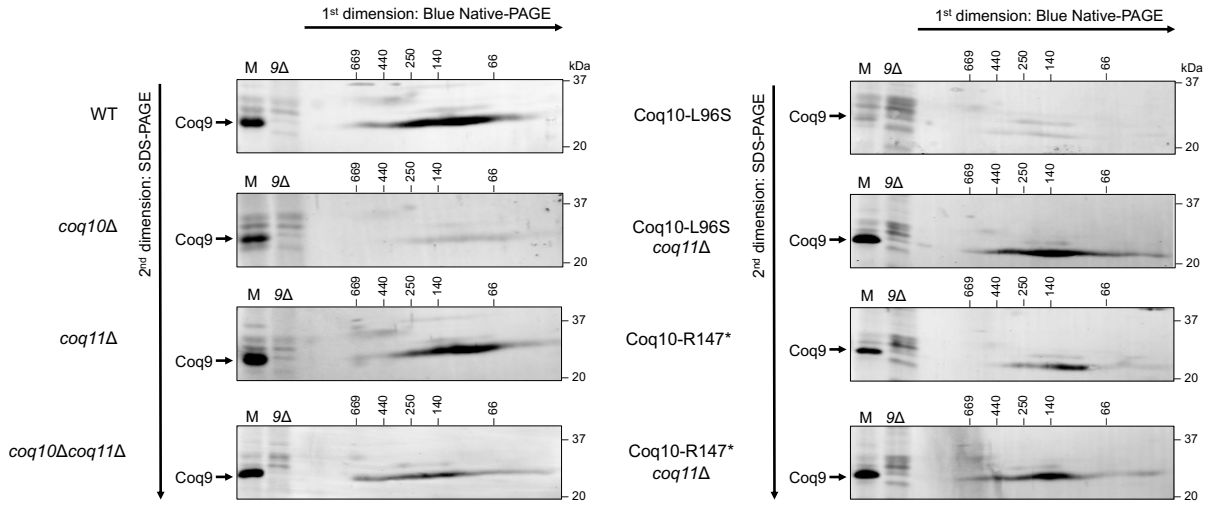

Figure 8. The destabilized CoQ synthome in the Coq10-L96S mutant is corrected by the deletion of *COQ11*, whereas strains harboring the R147* mutation exhibit no difference in CoQ synthome stability. Aliquots (75 µg) of crude mitochondria isolated from wild type, *coq10*Δ, *coq11*Δ, *coq10*Δ*coq11*Δ, Coq10-L96S, Coq10-L96S *coq11*Δ, Coq10-R147*, and Coq10-R147* *coq11*Δ yeast were solubilized with digitonin and separated by two-dimensional BN/SDS-PAGE. Proteins were transferred to PVDF membranes and the CoQ synthome was visualized using antisera against Coq9. Aliquots (25 µg) of intact crude mitochondria from each strain (*M*) and *coq9*Δ (*9*Δ) yeast were included as a loading control and negative control, respectively.

REFERENCES

1. Banerjee, R., Purhonen, J., and Kallijärvi, J. (2022) The mitochondrial coenzyme Q junction and complex III: biochemistry and pathophysiology. *The FEBS Journal*. **289**, 6936–6958
2. Guerra, R. M., and Pagliarini, D. J. (2023) Coenzyme Q biochemistry and biosynthesis. *Trends in Biochemical Sciences*. **48**, 463–476
3. Okada, K., Suzuki, K., Kamiya, Y., Zhu, X., Fujisaki, S., Nishimura, Y., Nishino, T., Nakagawad, T., Kawamukai, M., and Matsuda, H. (1996) Polyprenyl diphosphate synthase essentially defines the length of the side chain of ubiquinone. *Biochimica et Biophysica Acta (BBA) - Lipids and Lipid Metabolism*. **1302**, 217–223
4. Frei, B., Kim, M. C., and Ames, B. N. (1990) Ubiquinol-10 is an effective lipid-soluble antioxidant at physiological concentrations. *Proceedings of the National Academy of Sciences*. **87**, 4879–4883
5. Awad, A. M., Bradley, M. C., Fernández-del-Río, L., Nag, A., Tsui, H. S., and Clarke, C. F. (2018) Coenzyme Q10 deficiencies: pathways in yeast and humans. *Essays in Biochemistry*. **62**, 361–376
6. Hsieh, E. J., Gin, P., Gulmezian, M., Tran, U. C., Saiki, R., Marbois, B. N., and Clarke, C. F. (2007) Saccharomyces cerevisiae Coq9 polypeptide is a subunit of the mitochondrial coenzyme Q biosynthetic complex. *Archives of Biochemistry and Biophysics*. **463**, 19–26
7. He, C. H., Xie, L. X., Allan, C. M., Tran, U. C., and Clarke, C. F. (2014) Coenzyme Q supplementation or over-expression of the yeast Coq8 putative kinase stabilizes multi-subunit Coq polypeptide complexes in yeast coq null mutants. *Biochimica et Biophysica*

Acta (BBA) - Molecular and Cell Biology of Lipids. **1841**, 630–644

8. Tsui, H. S., Pham, NguyenV. B., Amer, B. R., Bradley, M. C., Gosschalk, J. E., Gallagher-Jones, M., Ibarra, H., Clubb, R. T., Blaby-Haas, C. E., and Clarke, C. F. (2019) Human COQ10A and COQ10B are distinct lipid-binding START domain proteins required for coenzyme Q function. *Journal of Lipid Research*. **60**, 1293–1310
9. Cui, T.-Z., and Kawamukai, M. (2009) Coq10, a mitochondrial coenzyme Q binding protein, is required for proper respiration in Schizosaccharomyces pombe: CoQ-binding protein in fission yeast. *FEBS Journal*. **276**, 748–759
10. Barros, M. H., Johnson, A., Gin, P., Marbois, B. N., Clarke, C. F., and Tzagoloff, A. (2005) The Saccharomyces cerevisiae COQ10 Gene Encodes a START Domain Protein Required for Function of Coenzyme Q in Respiration. *Journal of Biological Chemistry*. **280**, 42627–42635
11. Busso, C., Bleicher, L., Ferreira-Júnior, J. R., and Barros, M. H. (2010) Site-directed mutagenesis and structural modeling of Coq10p indicate the presence of a tunnel for coenzyme Q6 binding. *FEBS Letters*. **584**, 1609–1614
12. Allan, C. M., Hill, S., Morvaridi, S., Saiki, R., Johnson, J. S., Liau, W.-S., Hirano, K., Kawashima, T., Ji, Z., Loo, J. A., Shepherd, J. N., and Clarke, C. F. (2013) A conserved START domain coenzyme Q-binding polypeptide is required for efficient Q biosynthesis, respiratory electron transport, and antioxidant function in Saccharomyces cerevisiae. *Biochimica et Biophysica Acta (BBA) - Molecular and Cell Biology of Lipids*. **1831**, 776–791
13. Shen, Y., Goldsmith-Fischman, S., Atreya, H. S., Acton, T., Ma, L., Xiao, R., Honig, B., Montelione, G. T., and Szyperski, T. (2005) NMR structure of the 18 kDa protein

CC1736 from *Caulobacter crescentus* identifies a member of the "START" domain superfamily and suggests residues mediating substrate specificity. *Proteins*. **58**, 747–750

14. Allan, C. M., Awad, A. M., Johnson, J. S., Shirasaki, D. I., Wang, C., Blaby-Haas, C. E., Merchant, S. S., Loo, J. A., and Clarke, C. F. (2015) Identification of Coq11, a New Coenzyme Q Biosynthetic Protein in the CoQ-Synthome in Saccharomyces cerevisiae. *Journal of Biological Chemistry*. **290**, 7517–7534
15. Bradley, M. C., Yang, K., Fernández-del-Río, L., Ngo, J., Ayer, A., Tsui, H. S., Novales, N. A., Stocker, R., Shirihai, O. S., Barros, M. H., and Clarke, C. F. (2020) COQ11 deletion mitigates respiratory deficiency caused by mutations in the gene encoding the coenzyme Q chaperone protein Coq10. *Journal of Biological Chemistry*. **295**, 6023–6042
16. Subramanian, K., Jochem, A., Le Vasseur, M., Lewis, S., Paulson, B. R., Reddy, T. R., Russell, J. D., Coon, J. J., Pagliarini, D. J., and Nunnari, J. (2019) Coenzyme Q biosynthetic proteins assemble in a substrate-dependent manner into domains at ER–mitochondria contacts. *Journal of Cell Biology*. **218**, 1353–1369
17. Eisenberg-Bord, M., Tsui, H. S., Antunes, D., Fernández-del-Río, L., Bradley, M. C., Dunn, C. D., Nguyen, T. P. T., Rapaport, D., Clarke, C. F., and Schuldiner, M. (2019) The Endoplasmic Reticulum-Mitochondria Encounter Structure Complex Coordinates Coenzyme Q Biosynthesis. *Contact*. **2**, 2515256418825409
18. Kornmann, B., Currie, E., Collins, S. R., Schuldiner, M., Nunnari, J., Weissman, J., and Walter, P. (2009) An ER-Mitochondria Tethering Complex Revealed by a Synthetic Biology Screen. *Science*. **325**, 477–481
19. AhYoung, A. P., Jiang, J., Zhang, J., Khoi Dang, X., Loo, J. A., Zhou, Z. H., and Egea, P. F. (2015) Conserved SMP domains of the ERMES complex bind phospholipids and

mediate tether assembly. *Proc. Natl. Acad. Sci. U.S.A.* 10.1073/pnas.1422363112

20. Wozny, M. R., Di Luca, A., Morado, D. R., Picco, A., Khaddaj, R., Campomanes, P., Ivanović, L., Hoffmann, P. C., Miller, E. A., Vanni, S., and Kukulski, W. (2023) In situ architecture of the ER–mitochondria encounter structure. *Nature*. **618**, 188–192

21. Berger, K. H., Sogo, L. F., and Yaffe, M. P. (1997) Mdm12p, a Component Required for Mitochondrial Inheritance That Is Conserved between Budding and Fission Yeast. *Journal of Cell Biology*. **136**, 545–553

22. Hobbs, A. E. A., Srinivasan, M., McCaffery, J. M., and Jensen, R. E. (2001) Mmm1p, a Mitochondrial Outer Membrane Protein, Is Connected to Mitochondrial DNA (Mtdna) Nucleoids and Required for Mtdna Stability. *J Cell Biol*. **152**, 401–410

23. Youngman, M. J., Hobbs, A. E. A., Burgess, S. M., Srinivasan, M., and Jensen, R. E. (2004) Mmm2p, a mitochondrial outer membrane protein required for yeast mitochondrial shape and maintenance of mtDNA nucleoids. *Journal of Cell Biology*. **164**, 677–688

24. Okamura, Y., Aoki, Y., Obayashi, T., Tadaka, S., Ito, S., Narise, T., and Kinoshita, K. (2015) COXPRESdb in 2015: coexpression database for animal species by DNA-microarray and RNAseq-based expression data with multiple quality assessment systems. *Nucleic Acids Research*. **43**, D82–D86

25. Hibbs, M. A., Hess, D. C., Myers, C. L., Huttenhower, C., Li, K., and Troyanskaya, O. G. (2007) Exploring the functional landscape of gene expression: directed search of large microarray compendia. *Bioinformatics*. **23**, 2692–2699

26. Thomas, B. J., and Rothstein, R. (1989) Elevated recombination rates in transcriptionally active DNA. *Cell*. **56**, 619–630

27. Baker Brachmann, C., Davies, A., Cost, G. J., Caputo, E., Li, J., Hieter, P., and Boeke, J. D. (1998) Designer deletion strains derived from Saccharomyces cerevisiae S288C: A useful set of strains and plasmids for PCR-mediated gene disruption and other applications. *Yeast*. **14**, 115–132

28. Burke, D., Dawson, D., and Stearns, T. (2000) Methods in Yeast Genetics, pp. 177–186, Cold Spring Harbor Laboratory, Cold Spring Harbor, NY

29. Ryan, O. W., Poddar, S., and Cate, J. H. D. (2016) CRISPR–Cas9 Genome Engineering in *Saccharomyces cerevisiae* Cells. *Cold Spring Harb Protoc*

30. Armaleo, D., and Chiou, L. (2021) Modeling in yeast how rDNA introns slow growth and increase desiccation tolerance in lichens. *G3*. **11**, jkab279

31. Daniel Gietz, R., and Woods, R. A. (2002) Transformation of yeast by lithium acetate/single-stranded carrier DNA/polyethylene glycol method. *Methods in Enzymology*. **350**, 87–96

32. Xie, L. X., Hsieh, E. J., Watanabe, S., Allan, C. M., Chen, J. Y., Tran, U. C., and Clarke, C. F. (2011) Expression of the human atypical kinase ADCK3 rescues coenzyme Q biosynthesis and phosphorylation of Coq polypeptides in yeast coq8 mutants. *Biochimica et Biophysica Acta (BBA) - Molecular and Cell Biology of Lipids*. **1811**, 348–360

33. Schägger, H., Cramer, W. A., and von Jagow, G. (1994) Analysis of Molecular Masses and Oligomeric States of Protein complexes by Blue Native Electrophoresis and Isolation of Membrane Protein Complexes by Two-Dimensional Native Electrophoresis. *Analytical Biochemistry*. **217**, 220–230

34. Wittig, I., Braun, H.-P., and Schägger, H. (2006) Blue native PAGE. *Nat Protoc*. **1**, 418–428

35. Meisinger, C., Pfannschmidt, S., Rissler, M., Milenkovic, D., Becker, T., Stojanovski, D., Youngman, M. J., Jensen, R. E., Chacinska, A., Guiard, B., Pfanner, N., and Wiedemann, N. (2007) The morphology proteins Mdm12/Mmm1 function in the major β-barrel assembly pathway of mitochondria. *EMBO*. **26**, 2229–2239

36. Ellenrieder, L., Opaliński, Ł., Becker, L., Krüger, V., Mirus, O., Straub, S. P., Ebell, K., Flinner, N., Stiller, S. B., Guiard, B., Meisinger, C., Wiedemann, N., Schleiff, E., Wagner, R., Pfanner, N., and Becker, T. (2016) Separating mitochondrial protein assembly and endoplasmic reticulum tethering by selective coupling of Mdm10. *Nat Commun*. **7**, 13021

37. Tan, T., Özbalci, C., Brügger, B., Rapaport, D., and Dimmer, K. S. (2013) Mcp1 and Mcp2, two novel proteins involved in mitochondrial lipid homeostasis. *Journal of Cell Science*. 10.1242/jcs.121244

38. Tran, U. C., and Clarke, C. F. (2007) Endogenous synthesis of coenzyme Q in eukaryotes. *Mitochondrion*. **7**, S62–S71

39. Wang, Y., and Hekimi, S. (2019) The Complexity of Making Ubiquinone. *Trends in Endocrinology & Metabolism*. **30**, 929–943

40. Ozeir, M., Mühlenhoff, U., Webert, H., Lill, R., Fontecave, M., and Pierrel, F. (2011) Coenzyme Q Biosynthesis: Coq6 Is Required for the C5-Hydroxylation Reaction and Substrate Analogs Rescue Coq6 Deficiency. *Chemistry & Biology*. **18**, 1134–1142

41. Eisenberg-Bord, M., Shai, N., Schuldiner, M., and Bohnert, M. (2016) A Tether Is a Tether Is a Tether: Tethering at Membrane Contact Sites. *Developmental Cell*. **39**, 395–409

42. Murley, A., Sarsam, R. D., Toulmay, A., Yamada, J., Prinz, W. A., and Nunnari, J.

(2015) Ltc1 is an ER-localized sterol transporter and a component of ER–mitochondria and ER–vacuole contacts. *Journal of Cell Biology*. **209**, 539–548

43. Wei, W., Pelechano, V., Järvelin, A. I., and Steinmetz, L. M. (2011) Functional consequences of bidirectional promoters. *Trends in Genetics*. **27**, 267–276

44. Arnone, J. T., Robbins-Pianka, A., Arace, J. R., Kass-Gergi, S., and McAlear, M. A. (2012) The adjacent positioning of co-regulated gene pairs is widely conserved across eukaryotes. *BMC Genomics*. **13**, 546

45. Mourier, A., Motori, E., Brandt, T., Lagouge, M., Atanassov, I., Galinier, A., Rappl, G., Brodesser, S., Hultenby, K., Dieterich, C., and Larsson, N.-G. (2015) Mitofusin 2 is required to maintain mitochondrial coenzyme Q levels. *Journal of Cell Biology*. **208**, 429–442

46. Wilson, E. L., and Metzakopian, E. (2021) ER-mitochondria contact sites in neurodegeneration: genetic screening approaches to investigate novel disease mechanisms. *Cell Death Differ*. **28**, 1804–1821

47. Zung, N., and Schuldiner, M. (2020) New horizons in mitochondrial contact site research. *Biological Chemistry*. **401**, 793–809

48. Ashby, M. N., Kutsunai, S. Y., Ackerman, S., Tzagoloff, A., and Edwards, P. A. (1992) COQ2 is a candidate for the structural gene encoding para-hydroxybenzoate:polyprenyltransferase. *Journal of Biological Chemistry*. **267**, 4128–4136

49. Do, T. Q., Schultz, J. R., and Clarke, C. F. (1996) Enhanced sensitivity of ubiquinone-deficient mutants of Saccharomyces cerevisiae to products of autoxidized polyunsaturated fatty acids. *Proc Natl Acad Sci U S A*. **93**, 7534–7539

50. Hsu, A. Y., Do, T. Q., Lee, P. T., and Clarke, C. F. (2000) Genetic evidence for a multi-subunit complex in the O-methyltransferase steps of coenzyme Q biosynthesis. *Biochimica et Biophysica Acta (BBA) - Molecular and Cell Biology of Lipids*. **1484**, 287–297

51. Barkovich, R. J., Shtanko, A., Shepherd, J. A., Lee, P. T., Myles, D. C., Tzagoloff, A., and Clarke, C. F. (1997) Characterization of the COQ5 Gene from Saccharomyces cerevisiae EVIDENCE FOR A C-METHYLTRANSFERASE IN UBIQUINONE BIOSYNTHESIS. *Journal of Biological Chemistry*. **272**, 9182–9188

52. Gin, P., Hsu, A. Y., Rothman, S. C., Jonassen, T., Lee, P. T., Tzagoloff, A., and Clarke, C. F. (2003) The Saccharomyces cerevisiae COQ6 Gene Encodes a Mitochondrial Flavin-dependent Monooxygenase Required for Coenzyme Q Biosynthesis. *Journal of Biological Chemistry*. **278**, 25308–25316

53. Marbois, B. N., and Clarke, C. F. (1996) The COQ7 Gene Encodes a Protein in Saccharomyces cerevisiae Necessary for Ubiquinone Biosynthesis. *Journal of Biological Chemistry*. **271**, 2995–3004

54. Johnson, A., Gin, P., Marbois, B. N., Hsieh, E. J., Wu, M., Barros, M. H., Clarke, C. F., and Tzagoloff, A. (2005) COQ9, a New Gene Required for the Biosynthesis of Coenzyme Q in Saccharomyces cerevisiae. *Journal of Biological Chemistry*. **280**, 31397–31404

55. Winzeler, E. A., Shoemaker, D. D., Astromoff, A., Liang, H., Anderson, K., Andre, B., Bangham, R., Benito, R., Boeke, J. D., Bussey, H., Chu, A. M., Connelly, C., Davis, K., Dietrich, F., Dow, S. W., El Bakkoury, M., Foury, F., Friend, S. H., Gentalen, E., Giaever, G., Hegemann, J. H., Jones, T., Laub, M., Liao, H., Liebundguth, N., Lockhart,

D. J., Lucau-Danila, A., Lussier, M., M'Rabet, N., Menard, P., Mittmann, M., Pai, C., Rebischung, C., Revuelta, J. L., Riles, L., Roberts, C. J., Ross-MacDonald, P., Scherens, B., Snyder, M., Sookhai-Mahadeo, S., Storms, R. K., Véronneau, S., Voet, M., Volckaert, G., Ward, T. R., Wysocki, R., Yen, G. S., Yu, K., Zimmermann, K., Philippsen, P., Johnston, M., and Davis, R. W. (1999) Functional Characterization of the *S. cerevisiae* Genome by Gene Deletion and Parallel Analysis. *Science*. **285**, 901–906

56. Poon, W. W., Barkovich, R. J., Hsu, A. Y., Frankel, A., Lee, P. T., Shepherd, J. N., Myles, D. C., and Clarke, C. F. (1999) Yeast and Rat Coq3 and Escherichia coli UbiG Polypeptides Catalyze Both O-Methyltransferase Steps in Coenzyme Q Biosynthesis. *Journal of Biological Chemistry*. **274**, 21665–21672

57. Belogrudov, G. I., Lee, P. T., Jonassen, T., Hsu, A. Y., Gin, P., and Clarke, C. F. (2001) Yeast COQ4 Encodes a Mitochondrial Protein Required for Coenzyme Q Synthesis. *Archives of Biochemistry and Biophysics*. **392**, 48–58

58. Baba, S. W., Belogrudov, G. I., Lee, J. C., Lee, P. T., Strahan, J., Shepherd, J. N., and Clarke, C. F. (2004) Yeast Coq5 C-Methyltransferase Is Required for Stability of Other Polypeptides Involved in Coenzyme Q Biosynthesis. *Journal of Biological Chemistry*. **279**, 10052–10059

59. Tran, U. C., Marbois, B., Gin, P., Gulmezian, M., Jonassen, T., and Clarke, C. F. (2006) Complementation of Saccharomyces cerevisiae coq7 Mutants by Mitochondrial Targeting of the Escherichia coli UbiF Polypeptide. *Journal of Biological Chemistry*. **281**, 16401–16409

Chapter 3

Deletion of *COQ11* rescues the respiratory deficiency of yeast lacking *MMM1*, a component of the ERMES complex

ABSTRACT

Coenzyme Q (CoQ) is an essential redox-active lipid that plays a major role in the electron transport chain, driving mitochondrial ATP synthesis. In *Saccharomyces cerevisiae*, CoQ biosynthesis takes place exclusively in the mitochondrial matrix via a large molecular weight protein-lipid complex, the CoQ synthome, which is comprised of the polypeptides Coq3-Coq9 and Coq11. Formation of this complex is coordinated by the endoplasmic reticulum-mitochondria encounter structure (ERMES), as the CoQ synthome resides in specific membrane niches adjacent to ERMES. Loss of ERMES results in CoQ synthome destabilization, consequently impairing CoQ biosynthesis, which has been implicated in the common respiratory deficient phenotype exhibited by *ERMES* mutants. The *COQ11* gene product is suggested to act as a negative modulator of CoQ synthome assembly and CoQ synthesis, as its deletion results in an enlarged complex and enhanced *de novo* CoQ biosynthetic efficiency. In this work, we sought to determine if the subsequent deletion of *COQ11* can bypass the CoQ defects associated with *ERMES*Δ mutants. We show that select *ERMES* mutants regain the ability to grow on respiratory medium when *COQ11* is deleted, and that the stability of the CoQ synthome is also rescued in the *ERMES*Δ*coq11*Δ double mutant. Lastly, we utilize RNA sequencing data to identify pathway candidates that may detail the mechanism of rescue enabled by deletion of *COQ11*. Overall, this work identifies the deletion of *COQ11* as a novel bypass mechanism of phenotypes associated *ERMES* mutants, and characterizes the resultant effects on CoQ synthome assembly and CoQ production.

INTRODUCTION

Coenzyme Q (ubiquinone or CoQ) is an essential redox-active lipid molecule found in the plasma membranes and endomembranes of all eukaryotic species (1, 2). Its canonical function takes place in the mitochondrial electron transport chain, where it serves as a mobile electron carrier between respiratory complexes to drive ATP synthesis. Other functions of CoQ include pyrimidine biosynthesis, proline and sulfide catabolism, and choline degradation (1, 2). Additionally, the fully reduced $CoQH_2$ is able to serve as a lipid-soluble antioxidant to ameliorate peroxidation of lipids in cellular membranes (3).

Proper localization of CoQ is dependent on its hydrophobic tail, comprised of various lengths of isoprene units (denoted by *n* in CoQ_n) that is species dependent (4). The polyisoprenyl tail enables CoQ to anchor itself into the mid-plane of lipid bilayers, and the fully substituted benzoquinone head group affords its characteristic redox-active capabilities, permitting electron and proton transfer in a variety of biological pathways (1–3). Clinical phenotypes associated with diminished CoQ levels in humans can be treated with exogenous CoQ_{10} supplementation (5). Unfortunately, uptake of exogenous CoQ_{10} is often minimal because the hydrophobicity of CoQ with n=6-10 prevents its ability to traverse aqueous environments, and impairs its delivery to the inner mitochondrial membrane (5, 6). Thus, an understanding of regulatory elements directly associated with the CoQ biosynthetic machinery and putative transport mechanisms would provide a holistic view of how CoQ is produced and distributed within the cell.

In *Saccharomyces cerevisiae*, biosynthesis of CoQ_6 requires fourteen nuclear-encoded proteins (Coq1-Coq11, Yah1, Arh1, and Hfd1), located within the mitochondria (2, 7). The polypeptides Coq3-Coq9 and Coq11 assemble into a mega complex, the CoQ synthome; correct assembly of this metabolon is required for efficient CoQ_6 biosynthesis (8). The CoQ synthome

can be visualized as discrete puncta within mitochondria, termed CoQ domains, using select Coq polypeptides tagged with a fluorescent marker at their endogenous loci (9, 10) Individual deletions of the *COQ1-COQ9* genes halt CoQ_6 production, preventing respiratory growth on nonfermentable medium (7). Deletion of these essential genes also leads to the loss of the CoQ domains, and results in fluorescent signal that is dispersed throughout mitochondria (9). This is due to the loss of the late-stage polyprenylated intermediates, which have also been shown to be required for CoQ synthome formation and complex integrity (11, 12).

The genes encoding the Coq10 and Coq11 proteins are considered nonessential, as deletions of either open reading frame result in reduced production of *de novo* CoQ_6 (13, 14). However, it has been discovered that co-deletion of both *COQ10* and *COQ11* elevates CoQ_6 mitochondrial content relative to the *coq10*Δ (15). The *coq10*Δ*coq11*Δ double mutants are able to respire on nonfermentable carbon sources (15), rescuing the respiratory defect of the *coq10* single mutant (16, 17). Deletion of *COQ11* in *coq10*Δ yeast also rescues other CoQ_6-related functions, such as antioxidant protection against lipid peroxidative stress and oxygen consumption rates (15). The *coq11*Δ mutant possesses an enlarged CoQ synthome, as demonstrated by two-dimensional Blue Native/SDS-PAGE and fluorescence microscopy (9, 15), suggesting the Coq11 polypeptide may serve as a negative modulator of CoQ synthome assembly.

The endoplasmic reticulum-mitochondria encounter structure (ERMES) has been identified as a regulator of CoQ synthome assembly and efficient CoQ production (9, 10). ERMES is comprised of four proteins (Mmm1, Mdm10, Mdm12, and Mdm34) that tether the ER to the mitochondria and is essential for biosynthesis and transport of phospholipids between these organelles (18). Interestingly, both ERMES puncta and CoQ domains colocalize into

discrete puncta (10). Deletion of any of the ERMES subunits results in a destabilized CoQ synthome and loss of the puncta (10). Additionally, *ERMES*Δ mutants display inefficient CoQ_6 biosynthesis, as they accumulate significant amounts of CoQ_6-intermediates (10). Together, these data demonstrate a dependence on ERMES complex formation for proper CoQ Synthome assembly and efficient CoQ_6 production. Independently, ERMES is proposed to act as a platform to recruit proteins or other small molecules based on the need of the cell (19). These membrane contact sites allow ERMES to shuttle phospholipids between the ER and mitochondria (19). Three of the four ERMES subunits (Mmm1, Mdm12, and Mdm34) possess synaptotagmin-like mitochondrial lipid binding protein (SMP) domains that are arranged to form a hydrophobic tunnel poised for lipid transport (18–21). Given the localization of ERMES and the CoQ synthome, and the structural and biochemical evidence for lipid trafficking via ERMES, the ERMES complex is an attractive candidate for modulating intracellular CoQ distribution, however its ability to bind CoQ has not been evaluated.

The *COQ10* open reading frame is the neighboring gene to *MDM12*, which encodes the cytosolic subunit of ERMES; their close apposition within the genome suggests a putative functional relationship or physical interaction between their gene products (17, 22, 23). In fact, the deletion of *COQ10* results in the loss of spatial coordination between the CoQ synthome and ERMES contacts, as the percent of complex colocalization is significantly reduced in the *coq10*Δ mutant (10). While it has been previously shown that deletion of *MDM12* does not significantly impact Coq10 protein levels (10), recent evidence demonstrates that the *coq10*Δ mutant has severely attenuated Mdm12 polypeptide content (24). Loss, depletion, or mutations of ERMES components results in the inability to form the ERMES complex (18), and consequently, the phenotypes associated with ERMES dysfunction conflated with *coq10* mutant phenotypes (24).

Importantly, the engineered *coq10* truncation mutant (Coq10-R147*) preserved ERMES polypeptide levels (24). Although the Coq10-R147* mutant still showed impaired growth on nonfermentable medium, both CoQ biosynthesis and the CoQ synthome was preserved, indicating that these defects previously noted in the *coq10*Δ deletion mutant instead resulted from disruption of ERMES function (24).

Given that deletion of *COQ11* previously rescued *coq10*Δ phenotypes irrespective of ERMES integrity, we questioned if phenotypes associated with *ERMES* mutants can also be remedied by deletion of *COQ11*. We show that the respiratory growth of select *ERMES*Δ mutants can be mitigated by deletion of *COQ11*, which highlights the possibility of unique functions for individual ERMES subunits, despite residing in the same complex. Overall, we identify the deletion of *COQ11* as a novel suppressor of *ERMES* mutant phenotypes, offering a potential broader role to Coq11 as a modulator of CoQ synthesis as well as a potential modulator of mitochondrial function and mitochondrial-ER CoQ trafficking.

EXPERIMENTAL PROCEDURES

Yeast strains and growth medium

Saccharomyces cerevisiae strains used in this study are listed in Table 1. Yeast strains were derived from W303 (25) or BY4741 (26). Growth media included: YPG (1% yeast extract, 2% peptone, 3% glycerol), YPD (1% yeast extract, 2% peptone, 2% glucose), and YPGal (1% yeast extract, 2% peptone, 2% galactose, 0.1% dextrose). Synthetic dextrose/glycerol medium consisted of all components minus leucine. Plate medium contained 2% bacto-agar.

The *COQ11* open reading frame was disrupted using the one-step gene disruption method (27). The donor DNA fragment was amplified by polymerase chain reaction (PCR) from a bona

fide *coq11*Δ strain using the primers 5′AGTGTCTCCTCGTAATGCCATC3′ and 5′CAACCAAGAGGCATATCAGGC3′. PCR products were introduced into yeast cells using the lithium acetate method (28). Yeast strains harboring fluorescent tags were generated via sporulation and tetrad dissection; these constructs were gifted by Dr. Jodi Nunnari from the Bay Area Institute at Altos Labs. Prior to performing experiments, the *rho* status of cells was confirmed either by maintaining growth on glycerol, or using JM6 and JM8 as *rho*0 test trains for strains that are not viable on YPG, such as *coq*Δ mutants (29).

Drop dilution plate assays

Yeast cultures of W303 wild type, *mmm1*Δ, *coq11*Δ, and *mmm1*Δ*coq11*Δ were grown overnight in 5 mL of YPG to ensure mutants lacking ERMES retain mitochondrial DNA. The following day, cultures were diluted to an A_{600} ~ 0.25 in 15 mL of fresh YPG and expanded to a final A_{600} ~ 1.0. Cells were harvested by centrifugation, washed with sterile water, and diluted in phosphate-buffered saline (PBS) to an A_{600} = 0.2. 200 µL of the cell resuspension was transferred to a 96-well plate and serial dilutions were performed four times, where for each dilution 40 µL of the cell suspension was added to a subsequent well of 160 µL of PBS. 2 µL of each dilution were spotted on YPD and YPG plates, corresponding to a final A_{600} = 0.2, 0.04, 0.008, 0.0016, and 0.00032. All plates were incubated at 30 °C for 2-3 days.

Isolation of crude mitochondria

Yeast strains were cultured overnight in 50 mL of YPG at 30 °C with shaking. Pre-cultures were back-diluted with YPG and grown for 24 hours with shaking (30 °C, 250 rpm) until cell density reached an A_{600} ~ 4. Cells were harvested and subsequently treated with

Zymolyase-20T (MP Biomedicals) to produce spheroplasts. Spheroplasts were lysed using dounce homogenization and the resulting homogenate was subjected to centrifugation at 1,500 × *g* to pellet large debris including unlysed cells and nuclei. The supernatant was collected and subjected to centrifugation at 12,000 × *g* to pellet mitochondria. The resulting mitochondrial pellet was washed and centrifuged again at 1,500 × *g* to remove impurities. The final centrifugation was conducted at 12,500 × *g*, and the crude mitochondrial pellet was resuspended in MES sorbitol buffer, frozen in liquid nitrogen, and stored at –80 °C until further use. All fractionation steps were completed in the presence of EDTA-free protease inhibitor cocktail tablets (Roche), phosphatase inhibitor cocktail set I (Sigma-Aldrich), phosphatase inhibitor cocktail set II (Sigma-Aldrich), and PMSF (Fisher Scientific), and all centrifugations were conducted at 4 °C. Protein concentration of crude extracts was determined by the bicinchoninic acid (BCA) assay (ThermoFisher Scientific). Due to the inability of the *coq*Δ mutant control strains to grow in YPG, crude mitochondria were isolated using the same protocol, with the culturing step completed in YPGal instead of YPG.

Analysis of CoQ_6 and CoQ_6-intermediates and stable isotope labeling

Cells were grown overnight in 25 mL of YPG at 30 °C with shaking. The pre-cultures were then back-diluted to an A_{600} ~ 0.1 and allowed to further expand to mid-log phase (A_{600} ~ 0.6). For analysis of *de novo* biosynthesis, cells were treated with 8 µg/mL of $^{13}C_6$-pABA for 5 hours or ethanol as a vehicle control. Labelled pABA was obtained from Sigma-Aldrich. All cultures were harvested by centrifugation and cell pellets were stored at –20 °C until use. Cell pellets were resuspended in PBS and lysed in 2 mL of methanol with the addition of glass beads. The same amount of internal standard CoQ_4 was added to each sample, and lipids were extracted

with the addition of 2 mL petroleum ether twice. Extracted lipids were dried with N_2 and stored at –20 °C.

Lipid content was analyzed by LC-MS/MS as previously described (17). Briefly, lipids were reconstituted in 200 µL of ethanol containing 0.5 mg/mL benzoquinone and 20 µL of each sample was injected into an API4000 linear MS/MS spectrometer (Applied Biosystems). The instrument's corresponding analysis software, Analyst version 1.4.2, was used for data acquisition and processing. CoQ_6 content was determined by normalizing the peak area to a standard curve constructed with known amounts of CoQ_6 and the CoQ_4 internal standard. Standards of CoQ_6 were obtained from Avanti Polar Lipids, and CoQ_4 was obtained from Sigma-Aldrich. Relative levels of CoQ_6-intermediates are represented as peak areas normalized to the internal standard. A one-way analysis of variance with Dunnett's multiple comparisons test was performed using GraphPad Prism 10.

SDS-PAGE and immunoblot analysis of steady-state protein expression

Crude mitochondria (25 µg) were resuspended in SDS sample buffer and separated by gel electrophoresis on 10% Tris-glycine polyacrylamide gels. Proteins were transferred to 0.45 µm PVDF membranes (Millipore) and blocked with blocking buffer (5% milk and 0.1% Tween-20 in PBS). Coq proteins and mitochondrial protein loading control Mdh1 were probed with rabbit polyclonal antibodies prepared in 0.5% bovine serum albumin at dilutions listed in Table 2. IRDye 680LT IgG secondary antibodies (LiCOR) were used at a dilution of 1:20,000. Proteins were visualized using the LiCOR Odyssey Infrared Scanner (LiCOR). Immunoblots were quantified by hand using ImageJ software (National Institutes of Health, Bethesda, MD).

Two-dimensional Blue Native/SDS-PAGE of high molecular weight complexes

2D-BN/SDS-PAGE was performed as previously described (30, 31). Crude mitochondria (300 μg) were solubilized for one hour on ice with 16 mg/mL digitonin (Biosynth) in the presence of the same protease and phosphatase inhibitors from the mitochondrial isolation protocol. Solubilized protein was quantified using the BCA assay. 80 μg of solubilized mitochondria were separated on NativePAGE 4-16% Bis-Tris gels (Invitrogen) and cut into strips for the second-dimension separation. Gel strips were separated on 10% Tris-glycine polyacrylamide gels, followed by immunoblot analysis using an antibody against Coq9. Lyophilized protein used for the native gel high molecular weight standards were obtained from GE Healthcare (Sigma-Aldrich).

Manual fluorescence microscopy

Yeast cells were grown overnight in YEPGly (2% peptone, 1% yeast extract, 3% glycerol) liquid media. Stationary phase cells were diluted in fresh media and incubated for either 4 hours or overnight. Back-dilution was done either into YEPGly media or, when auxotrophic selection or microscopy imaging was required, synthetic minimal media (S; 0.67% [w/v] yeast nitrogen base (YNB) without amino acids and with ammonium sulphate, with 3% [w/v] glycerol, supplemented with required amino acids.

50 μL of cells in mid logarithmic growth phase from each well were transferred to a glass-bottomed 384-well microscopy plate (Azenta Life Sciences) coated with Concanavalin A (ConA). Following 20 minutes of incubation at 25 °C, wells were washed two times with the imaging medium and then imaged. Cells were imaged using a fluorescent microscopy system (Olympus) with Hamamatsu Orca Flash 4.0 camera and a Yokogawa confocal spinning disk unit

(CSUW1-T2) with a 50 μm pinhole disk and 100X oil lens (NA 1.3). Images were obtained with two channels: GFP (excitation wavelength 488 nm, emission filter set B525/50 nm) and mCherry (excitation 561 nm, emission filter set 617/73 nm). The imaging was performed by the scanR acquisition software (V3.2, Olympus). The cells from the microscopy images were segmented by scanR Analysis software (V3.2) using neural networks for recognition and measurement of their intensity. We are grateful to Dr. Timo Deikman (Olympus) for his help in building the neural networks.

RNA sequencing

Overnight cultures of wild type and *coq11*Δ yeast were back-diluted in 50 mL of YPG and allowed to expand to mid-log phase (A_{600} ~ 0.6). Cells were harvested by centrifugation and frozen until extraction. To frozen cell pellets, 500 μL of phenol-chloroform (phenol: chloroform: isoamyl alcohol 25:24:1, pH 8.0, ThermoFisher Scientific), 500 μL of RNA-SDS buffer (50 mM Tris-HCl, pH 7.5, 100 mM NaCl, 10 mM EDTA, 2% SDS w/v), and acid-washed glass beads were added and vortexed for one minute. Samples were heated at 65 °C for 6 minutes, vortexed for another minute, and subjected to centrifugation at 15,000 × *g* or 5 minutes to allow phase separation. The top aqueous layer was transferred to a new Eppendorf tube with 450 μL of fresh phenol-chloroform. before vortexing and subsequent centrifugation as before. The top aqueous layer was transferred again to a new tube with 1 mL of ethanol and 40 μL of 3 M sodium acetate, pH 5.2 and cooled to –80 °C to facilitate RNA precipitation. Samples were centrifuged as before, and the resulting RNA pellets were washed with 70% ethanol and treated with DNase I (New England Biomedicals) before the final resuspension in nuclease-free water. Preparation of RNA library and sequencing were conducted by Novogene (Beijing, China).

RNA sequencing reads for *Saccharomyces cerevisiae* strains were aligned to the R64-1-1 Ensembl annotated genome reference (https://useast.ensembl.org/), using the top-level annotation assembled with gffread (32). Raw sequencing reads were quality-controlled and trimmed using fastp (version 0.19.4) (33). Reads were then aligned using STAR (version 2.7.8a) (34). Transcript abundance was quantified using Cufflinks (version 2.2.1) (35), generating FPKM (Fragments Per Kilobase of transcript per Million mapped reads) values. An expression matrix was constructed for all strains and biological replicates. Differential gene expression analysis was conducted in a pairwise manner between strains. For each gene, $\log_2$ fold changes, mean expression differences, and z-scores were calculated between strains. *P*-values were determined using a two-sample t-test (assuming unequal variances) on FPKM values. A gene was considered differentially expressed if it met all the following criteria: a mean expression level (FPKM) in at least one strain above 1, an absolute $\log_2$ fold change above 1, an absolute expression difference above 1, an absolute z-score above 3, and a *p*-value less than 0.05. GO analyses was performed using GO Term Finder from the Saccharomyces Genome Database (36).

RESULTS

Deletion of *COQ11* rescues respiratory growth defect in select *ERMES*Δ mutants

Given the close relationship between the *COQ10* gene and the *MDM12* gene of ERMES, and that deletion of *COQ11* alleviates the ERMES-related phenotypes manifested by the *coq10*Δ mutant, we questioned if phenotypes associated with *ERMES*Δ mutants can also be mitigated by the subsequent deletion of *COQ11*. The *COQ11* open reading frame was successfully deleted in the *mmm1*Δ, *mdm10*Δ, and *mdm34*Δ mutants (Table 1); due to the inability to retain mitochondrial DNA, a common phenotype in ERMES mutants (18, 21, 37–39), the

*mdm12*Δ*coq11*Δ double mutant was not able to be generated for this study. Despite this, the remaining mutants generated still serve as promising targets, given ERMES complex formation is abolished when any of the subunits are absent (18).

The *mmm1*Δ and *mdm10*Δ strains regained the ability to grow on the nonfermentable medium YPGlycerol (YPG) upon subsequent deletion of *COQ11* (Fig. 1A & Fig. S1A). In contrast, the *mdm34*Δ*coq11*Δ mutant across two genetic backgrounds maintained the sickly growth on YPG (Fig. 1B & Fig. S1B). We found it particularly interesting that the *mdm10*Δ and *mdm34*Δ mutants exhibited opposite phenotypes, as their respective genes encode the two mitochondrial components of ERMES, and are direct interacting partners within the complex (40). However, it is not uncommon for suppressors of *ERMES* defects to rescue select mutants, or rescue the individual deletions to varying degrees (18, 21). Additionally, it was surprising to find that deletion of the gene encoding the ER-residing component, *MMM1*, was rescued by the *coq11* knockout (Fig. 1A). Considering Mdm12 protein stability is contingent upon stable expression of *MMM1* (41), and that Mmm1, Mdm12, and Mdm34 protein levels are not altered in *mdm10* mutants (40), we selected the *mmm1*Δ*coq11*Δ as the most representative *ERMES*Δ*coq11*Δ mutant to proceed with further analyses.

CoQ synthome stability is repaired in the *mmm1*Δ*coq11*Δ double mutant

Compared to the *coq10*Δ single mutant, which has diminished Coq polypeptide content (16, 17), the *coq10*Δ*coq11*Δ double mutant contained elevated levels of select Coq proteins (15). Considering *ERMES*Δ mutants contain Coq polypeptide levels similar to wild-type yeast (10), we were curious if the *mmm1*Δ*coq11*Δ mutant would have augmented Coq polypeptide content. Using isolated mitochondria, we performed immunoblot analyses against all the identified

members of the CoQ synthome, Coq3-Coq9 and Coq11, as well as Coq10, given its corresponding gene's relationship with *MDM12*. Unsurprisingly, the steady state expression of all Coq polypeptides remained unchanged in the *mmm1*Δ*coq11*Δ mutant (Fig. 2).

Despite the similar steady state Coq protein levels, yeast lacking ERMES exhibit a dramatically destabilized CoQ synthome, which was proposed to initiate a feedback loop to upregulate transcription of *COQ* genes (10). Using two-dimensional Blue Native/SDS-PAGE (2D BN/SDS-PAGE), a stable CoQ synthome can be visualized as a heterogeneous signal between ~66 kDa and ~669 kDa when using an anti-Coq9 probe (8). However, in all *ERMES*Δ mutants, the CoQ synthome instead migrates to ~440 kDa or less (10), which we have also replicated in our analyses for the *mmm1*Δ mutant (Fig. 3). Although all mutants possess similar levels of each Coq polypeptide, the signal representing the CoQ synthome in the *mmm1*Δ*coq11*Δ mutant migrates at a similar size to the wild type (Fig. 3), indicating that the CoQ synthome is restabilized upon deletion of the *COQ11* open reading frame.

CoQ domain formation is restored in the *mmm1*Δ*coq11*Δ mutant

Yeast lacking ERMES components are known to possess mitochondria with severe morphological defects (18, 37–39, 42). As such, it is tricky to discern whether CoQ synthome destabilization is attributed to loss of ERMES specifically, or rather the integrity of mitochondrial morphology. Regardless, the signal observed using 2D BN/SDS-PAGE suggests the complex is indeed unstable, such that the migration pattern represents several smaller and more stable subcomplexes corresponding to lower molecular weights. This interpretation of this biochemical analyses is supported by the stable reconstruction of a human COQ7:COQ9 subcomplex that is stably expressed in *E. coli* (43). The *coq10*Δ mutant also exhibits a migration

pattern representative of an unstable CoQ synthome (15, 17), however fluorescence microscopy experiments have demonstrated that the *coq10*Δ mutant is still able to form the complex, represented as "CoQ domains" marked by fluorescently tagged Coq polypeptides, but in fewer quantities than wild-type cells (9, 10). To evaluate for the presence of CoQ domains representative of biosynthetic complexes, we used an imaging-based approach using strains that possess a tagged Coq9 and aconitase (Aco2) as a mitochondrial marker, which were tagged at their endogenous loci. Mitochondrial function is not affected as demonstrated by the phenocopied growth of each tagged strain on YPG (Fig. S2). Our results corroborate the 2D BN/SDS-PAGE analyses in that the *mmm1*Δ*coq11*Δ double mutant indeed is able to rescue CoQ synthome complex formation, as represented by an increased number of cells that contain CoQ domains compared to the *mmm1*Δ mutant (Fig. 4). Upon closer examination of the mitochondria that contain CoQ domains, mitochondria from the *mmm1*Δ and *mmm1*Δ*coq11*Δ mutants harbor one puncta, whereas the wild type and *coq11*Δ mutants can possess more than one CoQ domain per mitochondrion (Fig. S3). This could suggest that the number of CoQ domains may be modulated by ERMES, such that when ERMES is absent, only few CoQ domains can form, even in the absence of the negative effector, Coq11.

Coq11 mutants accumulate lipid intermediates and exhibit inefficient CoQ_6 biosynthesis

To evaluate if the stabilization of the CoQ synthome mediated by deletion of *COQ11* influences CoQ_6 production, we measured *de novo* CoQ_6 biosynthesis *in vivo*. CoQ biosynthesis is the result of several pathways whose intermediates converge within the mitochondria to generate the essential lipid molecule (2). Namely, the components that generate the polyisoprenyl tail moiety are derived from the mevalonate pathway, while the head group, 4-

hydroxybenzoic acid (4HB), is derived predominantly from tyrosine in eukaryotes; yeast are able to utilize 4HB derived from the shikimate pathway but can also use para-aminobenzoic acid (pABA), derived from chorismate, as an alternative head group precursor. In yeast, prenylation of pABA and 4HB by the Coq2 polypeptide results in the early intermediates, hexaprenyl-aminobenzoic acid (HAB) and hexaprenyl-hydroxyamino benzoic acid (HHB), respectively. The essential Coq polypeptides that constitute the CoQ synthome, Coq3-Coq9, are then able to perform the remaining head group modifications that eventually lead to the final product, CoQ_6 (2) (Fig. 5A).

It has been shown previously that deletion of *ERMES* results in altered *de novo* CoQ_6 biosynthesis (10). Similarly, the *coq10*Δ*coq11*Δ double mutant displayed slightly improved *de novo* CoQ_6 biosynthesis with respect to the *coq10*Δ single mutant (15). To determine the effect on CoQ biosynthesis in the *mmm1*Δ*coq11*Δ double mutant, we treated yeast cultures with ^{13}C ring-labeled pABA and analyzed whole cell lipid extracts using liquid chromatography with tandem mass spectrometry (LC-MS/MS). While the total CoQ_6 content did not change between the *mmm1*Δ and *mmm1*Δ*coq11*Δ mutants, $^{13}C_6$-CoQ_6 was significantly decreased as compared to WT and the *mmm1*Δ mutant, respectively (Fig. 5B). We next analyzed key intermediates, HAB and demethoxy-Q_6 (DMQ_6), that are representative of early and late stages in the biosynthetic pathway, respectively. Consistent with previous literature (14), the *coq11*Δ mutant retained higher amounts of ^{12}C-HAB and $^{13}C_6$-HAB compared to the wild-type control, which the *mmm1*Δ*coq11*Δ mutant mirrors when compared to the *mmm1*Δ mutant (Fig. 5C). The *mmm1*Δ*coq11*Δ mutant possessed the highest total DMQ_6 content, despite the *de novo* DMQ_6 levels to be unchanged compared to the *mmm1*Δ mutant (Fig. 5D). The elevation in total DMQ_6 content in this mutant appears to be from the accumulation of unlabeled DMQ_6, which can also

be observed in the *coq11*Δ single mutant, albeit insignificant compared to the wild type (Fig. 5D). Taken together, the results indicate that CoQ_6 biosynthesis is attenuated in mutants harboring the *COQ11* deletion, when compared to either wild type or to the *mmm1*Δ mutant. Thus, the enhanced Coq polypeptide content and restoration of the CoQ synthome is not indicative of more efficient CoQ biosynthesis. It is possible that deletion of *COQ11* changes the state of the CoQ synthome and/or alters the redox state of CoQ.

*Coq11*Δ mutants have lower transcript levels of genes related to respiration

To identify candidate pathways that may be prompted by the deletion of *COQ11*, we performed RNA sequencing on wild type and *coq11*Δ yeast and quantified changes in transcript abundance (Fig. 6A). Gene ontology (GO) analysis of the downregulated genes in the *coq11*Δ mutant (174 genes total) indicate significant enrichment of genes associated with cellular respiration (Fig. 6B). The results of this analysis were surprising considering the robust growth on respiratory medium exhibited by mutants that lack *COQ11*. The Coq11 polypeptide has also been ascribed to function as part of the mitochondrial organization of gene expression (MIOREX) complex involved in the mitochondrial genetic expression system (44). Given its dual localization, it is possible that the loss of Coq11 results in decreased abundance of respiratory complexes, which may require less CoQ_6 to maintain respiratory function. In fact, transcript abundance of several genes that encode respiratory complex components, including complex V (ATP synthase) and the complex I equivalent in yeast (Ndi1), are significantly downregulated in the *coq11*Δ mutant (data not shown). In contrast, GO analysis of the upregulated genes indicate enrichment of genes associated with ribosomal biogenesis and rRNA processing (Fig. 6C). In yeast, transcriptional upregulation of ribosome biogenesis has been

tightly linked to maintenance of the proteome (45); a tentative model might suggest that the upregulation of ribosomal biogenesis is a consequence of not meeting energy demands required to maintain proteostasis, especially if mitochondrial ATP production is also downregulated (Fig. 6B). Additionally, another enriched upregulated cellular process is nucleic acid catabolism (Fig. 6B); nucleotide degradation and ribose salvage pathways have been implicated in mitigating oxidative stress, as fructose-6-phosphate derived from ribose sugars can be used to regenerate NAD(P)H, which can reduce glutathione to modulate cellular reactive oxygen species (46). One gene with significantly increased transcript abundance in the *coq11*Δ mutant that is not categorized with these gene ontology annotations is *GPX2* (data not shown). The *GPX2* gene product, glutathione peroxidase, is able to mitigate reactive oxygen species production and preserve mitochondrial respiration (47), which may provide a mechanism for how respiration persists despite the transcriptional consequence prompted by deletion of *COQ11*.

DISCUSSION

This work revealed the deletion of *COQ11* is a novel suppressor of *ERMES*Δ phenotypes. Deletion of *COQ11* was previously shown to rescue defects associated with *coq10*Δ yeast, such as impaired respiratory growth, destabilization of the CoQ synthome, and inefficient CoQ biosynthesis (15). It was later discovered that several *coq10*Δ phenotypes are attributed to ERMES dysfunction, as the deletion of *COQ10* attenuates Mdm12 protein content due to the close proximity of the *COQ10* and *MDM12* open reading frames within the yeast genome (24). Considering the rescued phenotypes in the *coq10*Δ*coq11*Δ double mutant were those caused by ERMES disruption, we sought to determine if *COQ11* deletion could also ameliorate *ERMES* mutant phenotypes. In this work, we have generated several *ERMES*Δ*coq11*Δ mutants, and show

that the respiratory growth defect of the *mmm1*Δ and *mdm10*Δ mutants can be rescued by deletion of *COQ11* (Fig. 1 and Fig. S1). The Coq11 polypeptide is proposed to be a negative modulator of CoQ synthome assembly, as *coq11*Δ yeast exhibit enhanced CoQ synthome formation via 2D BN/SDS-PAGE (15) and also higher intensity CoQ domains (9). Using the same biochemical and fluorescence-based approaches, we demonstrate that the *mmm1*Δ*coq11*Δ mutant possesses a more stable CoQ synthome (Fig. 3) and higher frequency of CoQ domains (Fig. 4) relative to the *mmm1*Δ single mutant. Our characterization of the *mmm1*Δ*coq11*Δ mutant further supports the notion that the Coq11 polypeptide modulates the assembly of the CoQ synthome, and spotlights a unique relationship between ERMES, the CoQ synthome, and CoQ biosynthesis.

The functional component of the Mmm1, Mdm12, and Mdm34 subunits is comprised of the SMP domain, a common lipid binding motif that, when aligned, can serve as a conduit for transporting lipids in and out of mitochondria (19, 20). Despite being unable to generate the *mdm12*Δ*coq11*Δ double mutant, we predict the *coq11* knockout would also rescue *mdm12*Δ yeast, as Mdm12 protein content relies on stable expression of *MMM1*, and vice versa (41). Intriguingly, Mmm1 protein content is also depleted in *mdm34*Δ mutants, but Mdm34 polypeptide is still detected in *mmm1*Δ yeast (38). This may suggest that the presence of Mdm34 is required for the *COQ11* deletion to rescue respiratory growth, as the *mdm34*Δ mutant was unable to be rescued across two genetic backgrounds (Fig. 1B & Fig. S1B).

The Mdm10 protein possesses a β-barrel core structure, similar to that of VDAC and Tom40 (40, 48). Instead of binding lipids, Mdm10 functions as part of the Sorting and Assembly Machinery (SAM) complex, facilitating in TOM complex biogenesis and subsequent mitochondrial protein import (49). Considering this additional role of Mdm10, we found it

surprising that the respiratory growth of the *mdm10*Δ mutant was able to be rescued robustly by the *COQ11* deletion (Fig. S1A). However, previous work has demonstrated that overexpression of Mcp1 and Mcp2 (Mdm10 Complementing Proteins 1 and 2) can suppress the respiratory growth defect of *mdm10*Δ mutants, and this rescue phenotype was attributed to changes in mitochondrial phospholipid content mediated by Mcp1 and Mcp2 (21). In a more recent study, Mcp2 was renamed Cqd2 (CoQ Distribution protein 2), as it was shown to mobilize CoQ_6 from the mitochondrial inner membrane to non-mitochondrial membranes (50). Given the role of Mcp2/Cqd2 in rescuing *mdm10*Δ respiratory growth and modulating CoQ distribution, it is tempting to speculate that CoQ has a unique role in this suppression mechanism, which can potentially be investigated further in our *mdm10*Δ*coq11*Δ mutant.

Deletion of *COQ11* results in less efficient CoQ_6 biosynthesis relative to wild-type cells (14, 15), which we have also reproduced in our analyses (Fig. 5B). Despite HAB and DMQ_6 being fixed points in the biosynthetic pathway, it is tempting to interpolate that flux throughout the pathway is also inefficient. The elevated levels of both the total HAB and total DMQ_6 could suggest that flux is impaired, consequently leading to high levels of remaining intermediates as well (outlined in Fig. 5A, however unable to be detected via LC-MS/MS). Given that late-stage lipid intermediates are also required to stabilize the CoQ synthome (11, 12), the deletion of *COQ11* may be rescuing CoQ synthome stability via retention of late-stage lipid intermediates, contributing to an inefficient production of CoQ_6 (Fig. 5B-D). This model is feasible considering the *mmm1*Δ and *mmm1*Δ*coq11*Δ mutants harbor Coq polypeptide content similar to WT (Fig. 2), yet only the *mmm1*Δ*coq11*Δ double mutant possesses a more stable CoQ synthome, which can also be readily detected via fluorescence microscopy (Fig. 3 & Fig. 4). Irrespective of the stability of the CoQ synthome, the number CoQ domains per mitochondrion in the strains

lacking *MMM1* suggests that ERMES may modulate the copy number or frequency of CoQ domains that can form per mitochondrion (Fig. S3). A fundamental role of membrane contact sites is to serve as recruitment sites that can help modulate interorganelle metabolite exchange. For this reason, it would make sense that fewer contact sites due to loss of ERMES would result in fewer CoQ domains, as there is no platform to facilitate in the potential distribution of CoQ.

We had hoped to identify candidates that may detail the mechanism of rescue that is prompted by the *COQ11* deletion using RNA sequencing data (Fig. 5A). Gene ontology analysis of the downregulated transcripts highlight that the most enriched pathways are involved in respiration (Fig. 5B). Considering Coq11 has dual localization with the MIOREX complex (44), which is responsible for mitochondrial gene expression, it is reasonable that the loss of Coq11 could affect transcript abundance of several respiratory complex genes. Given the canonical role of CoQ as a mobile electron carrier in the mitochondrial electron transport chain, it has been noted that CoQ deficiency, and consequently decreased electron transport, can contribute to increased oxidative stress (51). Notably, decreased respiration can cause complex V, ATP synthase, to run in reverse, which can alter the membrane potential due to extrusion of protons from the mitochondrial matrix (51). The decreased abundance of respiratory complexes could compensate for decreased CoQ, thereby maintaining forward electron transport and respiration even with reduced CoQ biosynthesis. For the enriched upregulated pathways (Fig. 6C), it is important to note that the significance of enrichment is of lesser magnitude than the downregulated pathways (Fig. 6B); this denotes that even if the upregulated pathways are likely stress responses, they are not as significant as those that are transcriptionally downregulated. The results from our sequencing further illuminate a unique role for Coq11 in mitochondrial respiration, akin to its closest human homolog, NDUFA9, a component of complex I (14).

Given previous work showed deletion of *COQ11* can rescue *coq10*Δ phenotypes (15) that were later revealed to be *ERMES* mutant phenotypes (24), we were not surprised to find that deletion of *COQ11* could ameliorate *ERMES*Δ defects. In accordance with previous work (9, 10) this study further supports a specific role for ERMES in modulating CoQ synthome stability and CoQ domain formation, but also highlights that individual subunits may fulfill unique roles, given that not all *ERMES* deletions are able to rescued. While the function of Coq11 remains unclear, its dual localization with MIOREX, the role of its human homolog, NDUFA9, in complex I, and the transcriptional consequence prompted by its deletion suggest it serves a specific role in regulating respiration, potentially through modulating the redox pool of $CoQ/CoQH_2$.

Table 1. Yeast strains used in study

Strain	Genotype	Source
W303 1B	*MAT α, ade2-1 can1-100 his3-11,15 leu2-3,112 trp1-1 ura3-1*	R. Rothstein[a]
BY4741	*MAT a his3Δ1 leu2Δ0 met15Δ0 ura3Δ0*	(26)
JM6	*MAT a his-4 ρ^0*	J. E. McEwen[b]
JM8	*MAT α ade-1 ρ^0*	J. E. McEwen[b]
W303a *coq2*Δ	*MAT a, ade2-1 can1-100 his3-11,15 leu2-3,112 trp1-1 ura3-1 coq2::HIS3*	(52)
W303 1B *coq3*Δ	*MAT α, ade2-1 can1-100 his3-11,15 leu2-3,112 trp1-1 ura3-1 coq3::LEU2*	(53)
W303a *coq4*Δ	*MAT a, ade2-1 can1-100 his3-11,15 leu2-3,112 trp1-1 ura3-1 coq4::TRP1*	(54)
W303 1B *coq5*Δ	*MAT α, ade2-1 can1-100 his3-11,15 leu2-3,112 trp1-1 ura3-1 coq5::HIS3*	(55)
W303a *coq6*Δ	*MAT a, ade2-1 can1-100 his3-11,15 leu2-3,112 trp1-1 ura3-1 coq6::LEU2*	(56)

Table 1. Yeast strains used in study (cont.)

Strain	Genotype	Source
W303 1B *coq7*Δ	*MAT α, ade2-1 can1-100 his3-11,15 leu2-3,112 trp1-1 ura3-1 coq7::LEU2*	(57)
W303a *coq8*Δ	*MAT a, ade2-1 can1-100 his3-11,15 leu2-3,112 trp1-1 ura3-1 coq8::HIS3*	(54)
W303 1B *coq9*Δ	*MAT α, ade2-1 can1-100 his3-11,15 leu2-3,112 trp1-1 ura3-1 coq9::URA3*	(58)
W303a *coq10*Δ	*MAT a, ade2-1 can1-100 his3-11,15 leu2-3,112 trp1-1 ura3-1 coq10::HIS3*	(13)
W303 1B *coq11*Δ	*MAT α ade2-1 his3-1,15 leu2-3,112trp1-1 ura3-1 coq11::LEU2*	(15)
W303a *mmm1*Δ	*MAT a, leu2-3,-112; his3-11,-15; trp1-1; ura3-1; ade2-1; can1-100 mmm1::KanMX*	(21)
W303a *mmm1*Δ*coq11*Δ	*MAT a, leu2-3,-112; his3-11,-15; trp1-1; ura3-1; ade2-1; can1-100 mmm1::KanMX coq11::LEU2*	This work
W303a *mdm10*Δ	*MAT a, leu2-3,-112; his3-11,-15; trp1-1; ura3-1; ade2-1; can1-100 mdm10::HIS3*	(21)

Table 1. Yeast strains used in study (cont.)

Strain	Genotype	Source
W303a *mdm12*Δ	*MAT a, leu2-3,-112; his3-11,-15; trp1-1; ura3-1; ade2-1; can1-100 mdm12::HIS3*	(21)
W303a *mdm34*Δ	*MAT a, leu2-3,-112; his3-11,-15; trp1-1; ura3-1; ade2-1; can1-100 mdm34::KanMX*	(21)
W303a *mdm34*Δ*coq11*Δ	*MAT a, leu2-3,-112; his3-11,-15; trp1-1; ura3-1; ade2-1; can1-100 mdm34::KanMX coq11::LEU2*	This work
W303a Coq9-yeGFP Aco2-mCherry	*MAT α, ade2-1 can1-100 his3-11,15 leu2-3,112 trp1-1 ura3-1 Coq9-yEGFP::Hygro Aco2-mCherry::HIS3*	This work
W303a Coq9-yeGFP Aco2-mCherry *mmm1*Δ	*MAT α, ade2-1 can1-100 his3-11,15 leu2-3,112 trp1-1 ura3-1 Coq9-yEGFP::Hygro Aco2-mCherry::HIS3 mmm1::KanMX*	This work
W303a Coq9-yeGFP Aco2-mCherry *coq11*Δ	*MAT α, ade2-1 can1-100 his3-11,15 leu2-3,112 trp1-1 ura3-1 Coq9-yEGFP::Hygro Aco2-mCherry::HIS3 coq11::LEU2*	This work

Table 1. Yeast strains used in study (cont.)

Strain	Genotype	Source
W303a Coq9-yeGFP Aco2-mCherry *mmm1*Δ *coq11*Δ	*MAT α, ade2-1 can1-100 his3-11,15 leu2-3,112 trp1-1 ura3-1 Coq9-yEGFP::Hygro Aco2-mCherry::HIS3 mmm1::KanMX coq11::LEU2*	This work
BY4741 *coq2*Δ	*MAT a his3Δ1 leu2Δ0 met15Δ0 ura3Δ0 coq2::KanMX4*	(59)
BY4742 *coq11*Δ	*MAT α his3Δ1 leu2Δ0 met15Δ0 ura3Δ0 coq11::LEU2*	(15)
BY4741 *mdm10*Δ	*MAT a his3Δ1 leu2Δ0 met15Δ0 ura3Δ0 mdm10::KanMX4*	(59)
BY4741 *mdm10*Δ*coq11*Δ	*MAT a his3Δ1 leu2Δ0 met15Δ0 ura3Δ0 mdm10::KanMX4 coq11::LEU2*	This work
BY4741 *mdm34*Δ	*MAT a his3Δ1 leu2Δ0 met15Δ0 ura3Δ0 mdm34::KanMX4*	(59)
BY4741 *mdm34*Δ*coq11*Δ	*MAT a his3Δ1 leu2Δ0 met15Δ0 ura3Δ0 mdm34::KanMX4 coq11::LEU2*	This work

[a] Dr. Rodney Rothstein, Department of Human Genetics, Columbia University

[b] Dr. Joan E. McEwen

Table 2. Description and source of antibodies

Antibody	Working Dilution	Source
Coq3	1:200	(60)
Coq4	1:2,000	(61)
Coq5	1:5,000	(62)
Coq6	1:200	(56)
Coq7	1:1,000	(63)
Coq8	Affinity purified, 1:30	(8)
Coq9	1:1,000	(8)
Coq10	Affinity purified, 1:400	(17)
Coq11	1:500	(17)
Mdh1	1:10,000	Lee McAlister-Henn[c]

[c] Dr. Lee McAlister-Henn, Department of Molecular Biophysics and Biochemistry, University of Texas Health Sciences Center

FIGURES

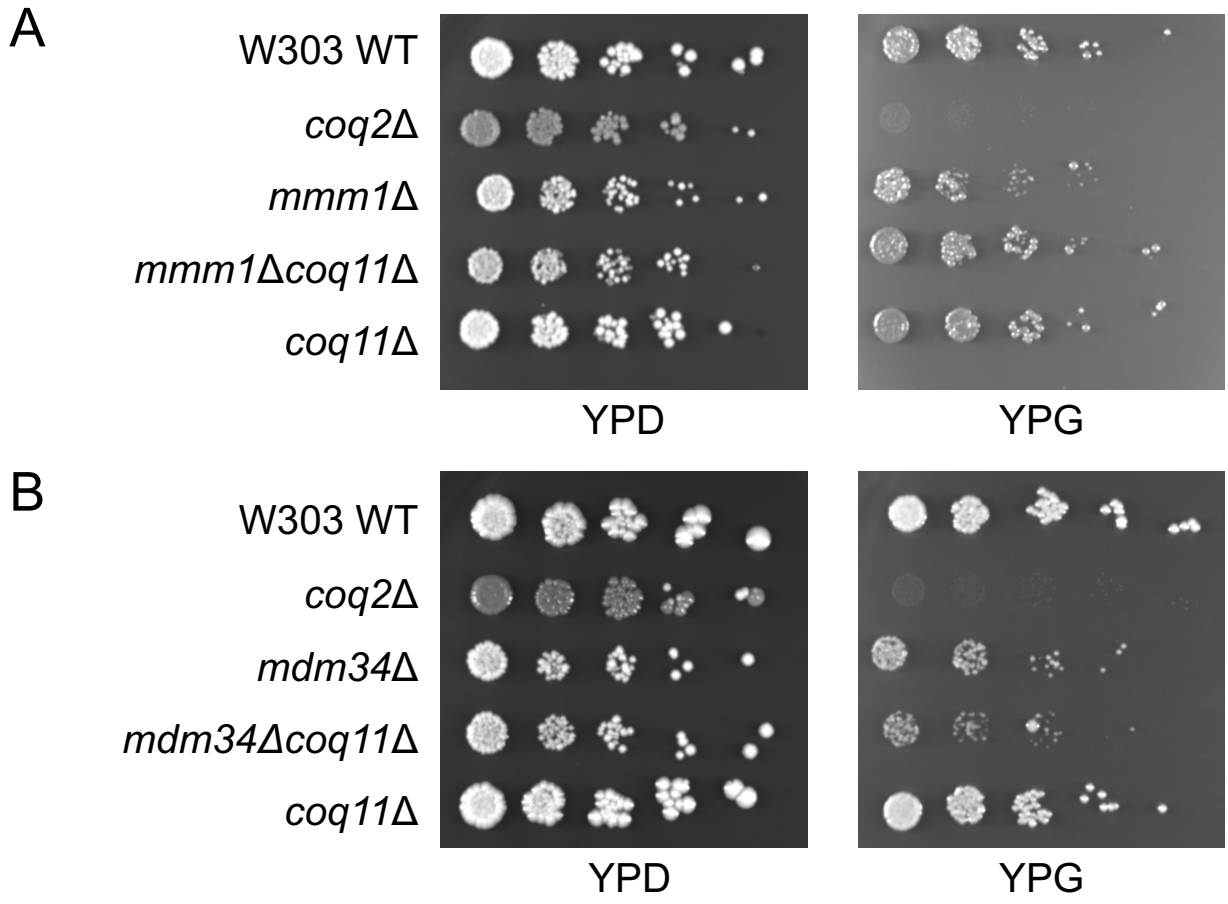

Figure 1. Deletion of *COQ11* rescues respiratory growth defect in the *mmm1*Δ mutant. Spot-dilution assays were performed to assess viability of *A*, the *mmm1*Δ*coq11*Δ and *B*, *mdm34*Δ*coq11*Δ mutants on fermentable (YPD) and nonfermentable (YPG) plate medium. Yeast cells were cultured in YPG to a final A_{600} ~1.0, harvested by centrifugation, and washed twice with sterile water. Isolated cells were resuspended and serial-diluted in sterile phosphate-buffered saline to a final A_{600} = 0.2, 0.04, 0.008, 0.0016, and 0.00032. 2 µL of each dilution were spotted on YPD and YPG plates, and plates were incubated at 30 °C for 2-3 days. Images are representative of at least three biological replicates.

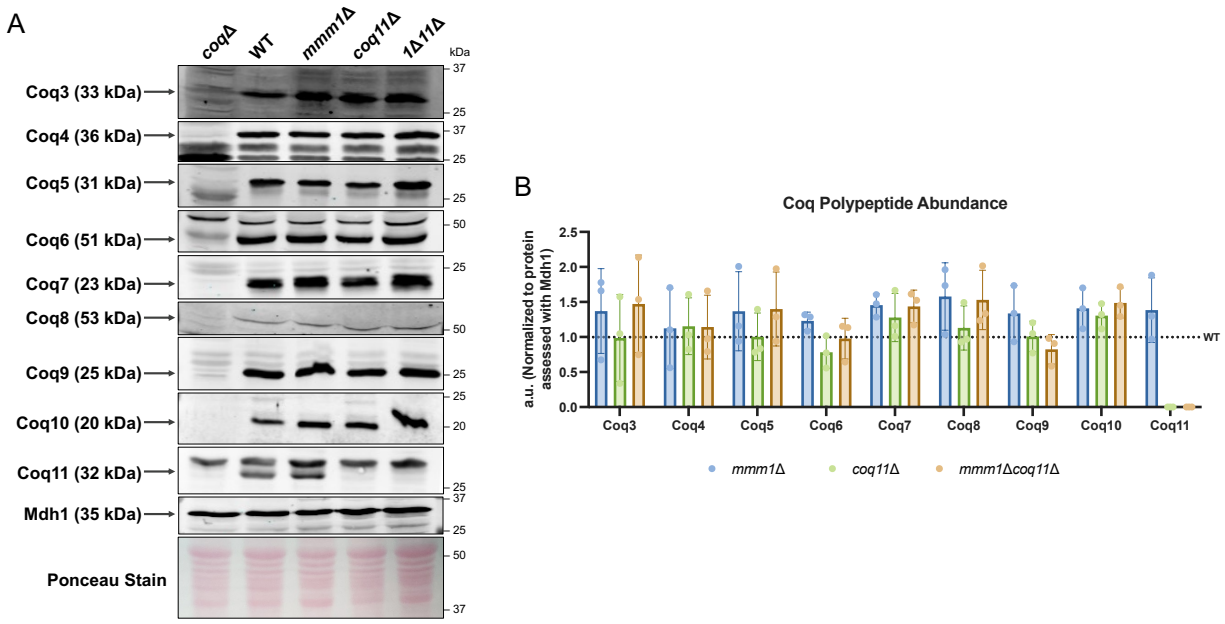

Figure 2. Coq polypeptide content is unaltered in the *mmm1*Δ, *coq11*Δ, and *mmm1*Δ*coq11*Δ mutants as compared to WT. *A*, Aliquots of crude mitochondria (25 µg) from WT, *mmm1*Δ, *coq11*Δ, and *mmm1*Δ*coq11*Δ yeast strains were subjected to 10% or 12% Tris-glycine SDS-PAGE. Proteins stained with Ponceau stain and mitochondrial malate dehydrogenase (Mdh1) were used as loading controls. Mitochondria isolated from *coq3*Δ–*coq11*Δ (*coq*Δ) strains were used as negative controls. Black arrows indicate the location of each protein on the membrane. *B*, Band intensities corresponding to the Coq proteins were quantified by hand using ImageJ, which were normalized to Mdh1 and plotted as a percentage of WT. The data show mean ± SD of three biological replicates. A one-way analysis of variance with Dunnett's multiple comparisons showed no statistical significance.

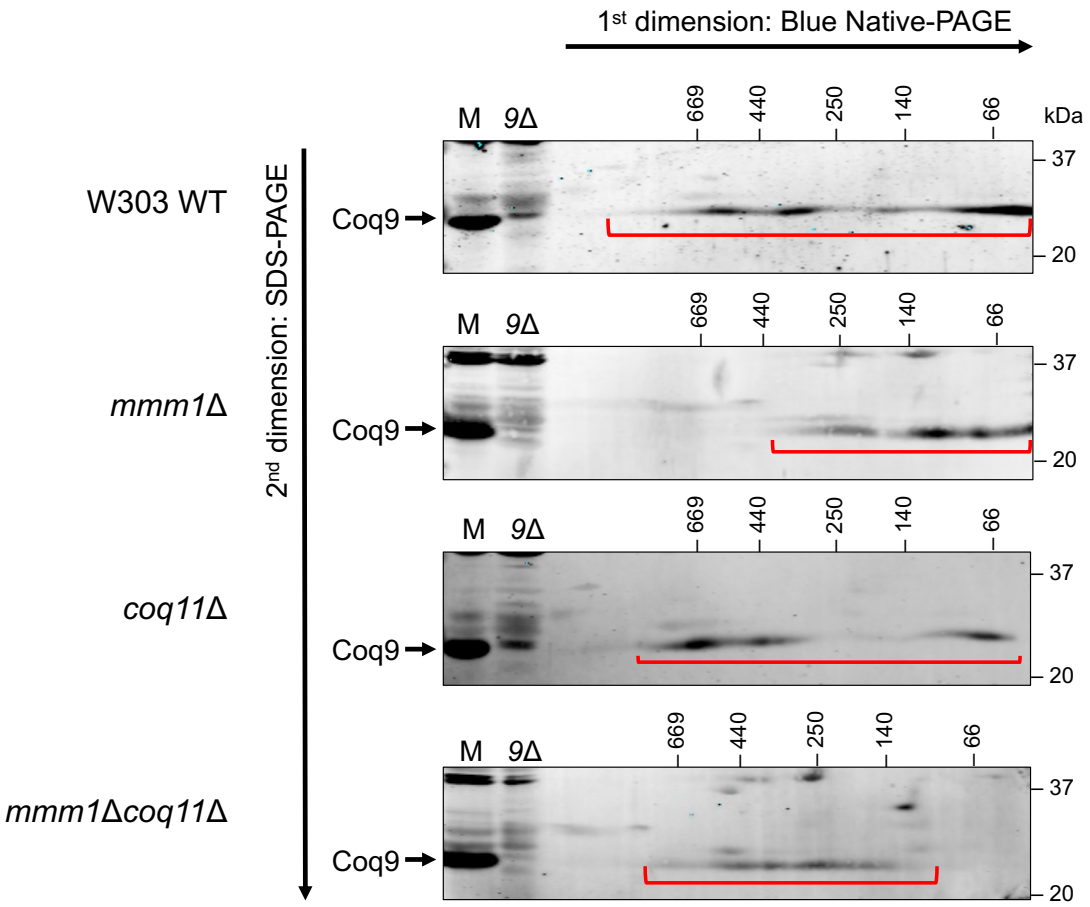

Figure 3. The *mmm1*Δ*coq11*Δ mutant has a more stabilized CoQ synthome relative to the *mmm1*Δ mutant. Digitonin-solubilized crude mitochondria from the indicated strains were subjected to two-dimensional Blue Native/SDS-PAGE (2D BN/SDS-PAGE). The CoQ synthome can be visualized in the W303 WT control as a heterogeneous signal between ~66 kDa and ~669 kDa when probed using an antibody against the Coq9 polypeptide. The signals corresponding to the CoQ synthome are indicated with the red bracket. 25 µg of intact mitochondria of the indicated strains (M) were included as a positive control, and mitochondria from *coq9*Δ yeast (*9*Δ) were included as a negative control. Data are representative of three biological replicates.

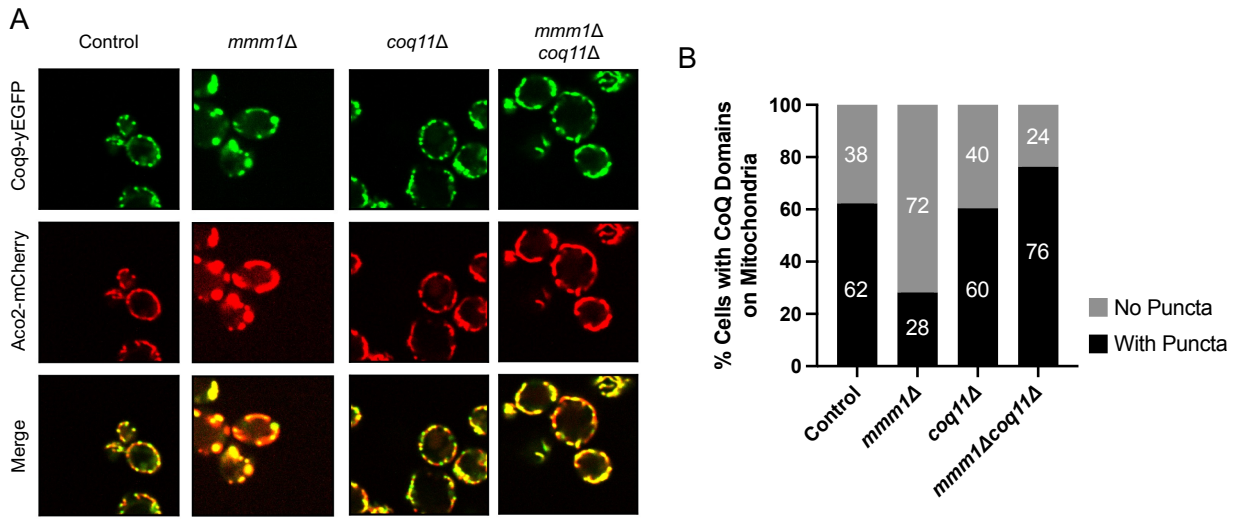

Figure 4. Frequency of CoQ domain formation is rescued in *mmm1*Δ*coq11*Δ mutant. *A*, Yeast expressing yEGFP-tagged Coq9 and Aco2 tagged with mCherry as a mitochondrial marker were imaged using fluorescence microscopy. *B*, Quantification of panel *A*: for each cell, Coq9-yEGFP foci were detected using a neural network, and plotted as percentage of cells containing CoQ domains. At least 500 cells were used for this analysis.

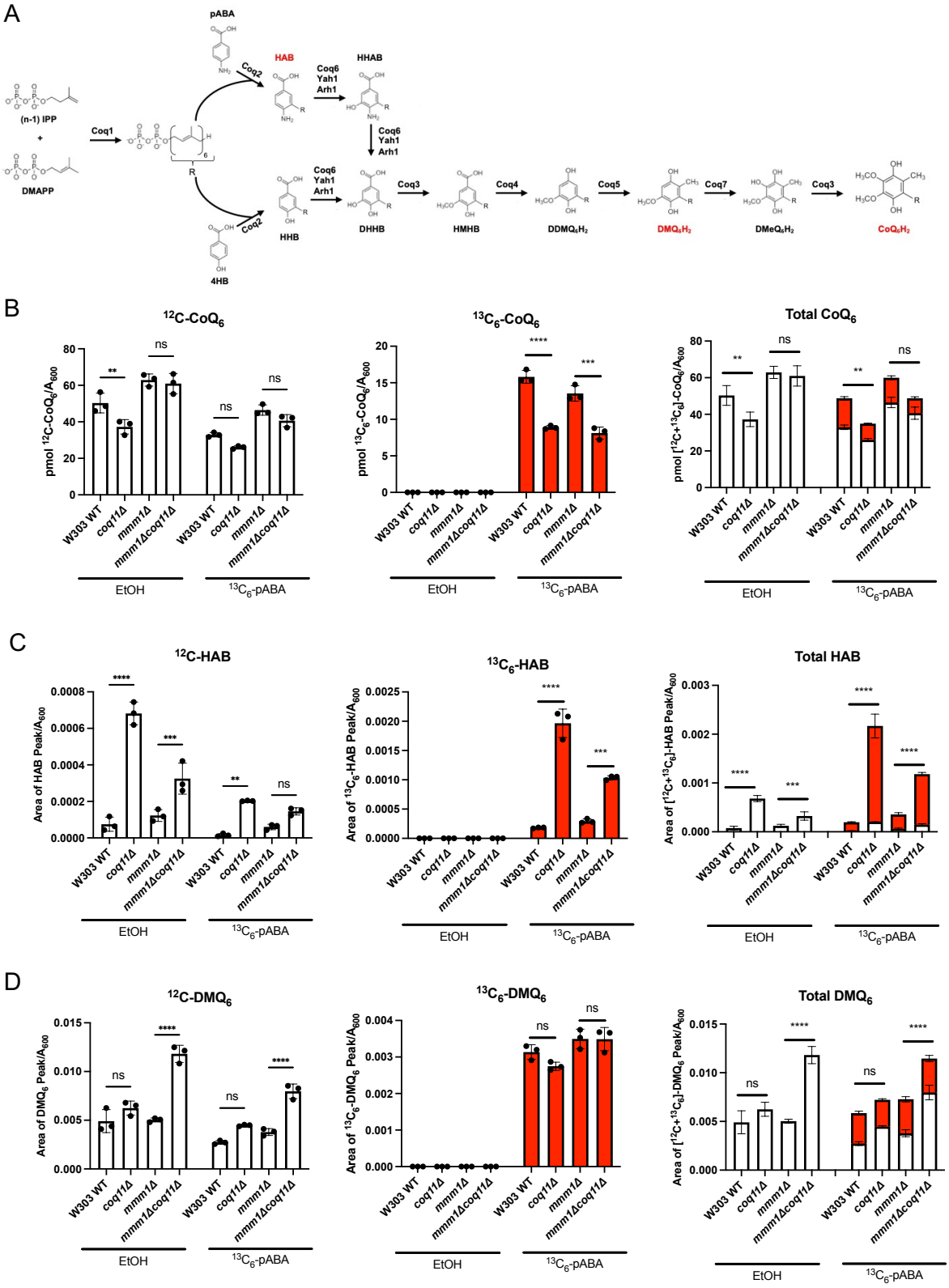
A
pABA
HAB
HHAB
(n-1) IPP
DMAPP
Coq1
Coq2
Coq6
Yah1
Arh1
HHB
4HB
DHHB
Coq3
HMHB
Coq4
DDMQ6H2
Coq5
DMQ6H2
Coq7
DMeQ6H2
CoQ6H2
B
12C-CoQ6
13C6-CoQ6
Total CoQ6
pmol 12C-CoQ6/A600
pmol 13C6-CoQ6/A600
pmol [12C+13C6]-CoQ6/A600
C
12C-HAB
13C6-HAB
Total HAB
Area of HAB Peak/A600
Area of 13C6-HAB Peak/A600
Area of [12C+13C6]-HAB Peak/A600
D
12C-DMQ6
13C6-DMQ6
Total DMQ6
Area of DMQ6 Peak/A600
Area of 13C6-DMQ6 Peak/A600
Area of [12C+13C6]-DMQ6 Peak/A600
W303 WT
coq11Δ
mmm1Δ
mmm1Δcoq11Δ
EtOH
13C6-pABA

Figure 5. The CoQ biosynthetic pathway is inefficient in the *mmm1*Δ*coq11*Δ mutant. *A*, Representation of the CoQ_6 biosynthetic pathway in yeast. Intermediates analyzed are indicated in red text. Triplicates of 25 mL cultures in YPG were labeled at A_{600} ~ 0.6 with 8 µg/mL $^{13}C_6$-para-aminobenzoic acid ($^{13}C_6$-pABA) or ethanol as a vehicle control. Labeled and unlabeled *B*, Hexaprenyl-aminobenzoic acid (HAB), *C*, demethoxy-Q_6 (DMQ_6), and *D*, CoQ_6 were analyzed from whole cell lipid extracts after 5 hours of labeling. Total content was determined using the sum of [^{12}C+$^{13}C_6$] of each analyte. The data depict mean ± SD of three biological replicates, and statistical significance is represented as **, $p < 0.01$; ***, $p < 0.001$; ****, $p < 0.0001$; and ns, no significance. Abbreviations: IPP, isopentenyl pyrophosphate; DMAPP, dimethylallyl pyrophosphate; 4HB, 4-hydroxybenzoic acid; HHB, 3-hexaprenyl-4-hydroxybenzoic acid; HHAB, 3-hexaprenyl-4-amino-5-hydroxybenzoic acid; DHHB, 4,5-dihydroxy-3-hexylbenzoic acid; HMHB, 4-hydroxy-5-methoxy-3-hexaprenylbenzoic acid; $DDMQ_6H_2$; 2-methoxy-6-hexaprenyl-1,4-benzohydroquinone; $DMeQ_6H_2$, 3-methyl-6-methoxy-2-hexaprenyl-1,4,5-benzenetriol.

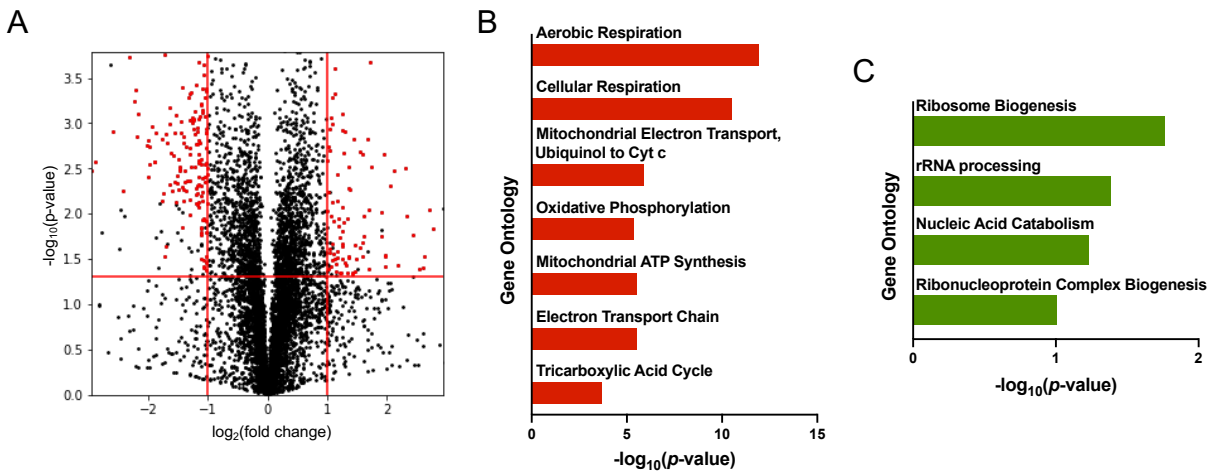

Figure 6. Deletion of *COQ11* downregulates cellular respiration. *A*, Fold changes in transcript abundances ($\log_2$(*coq11*Δ/WT), n = 3) versus statistical significance (–$\log_{10}$(*p*-value)) as quantified by RNA sequencing. Horizontal red line indicates significant *p*-value boundary and red dots indicate transcripts with absolute z-scores > 3. *B*, GO analysis of 174 downregulated genes in *coq11*Δ compared with WT. *C*, GO analysis of 113 upregulated genes in *coq11*Δ compared with WT. For gene ontology analyses, only genes with > 2-fold up- or downregulation were selected.

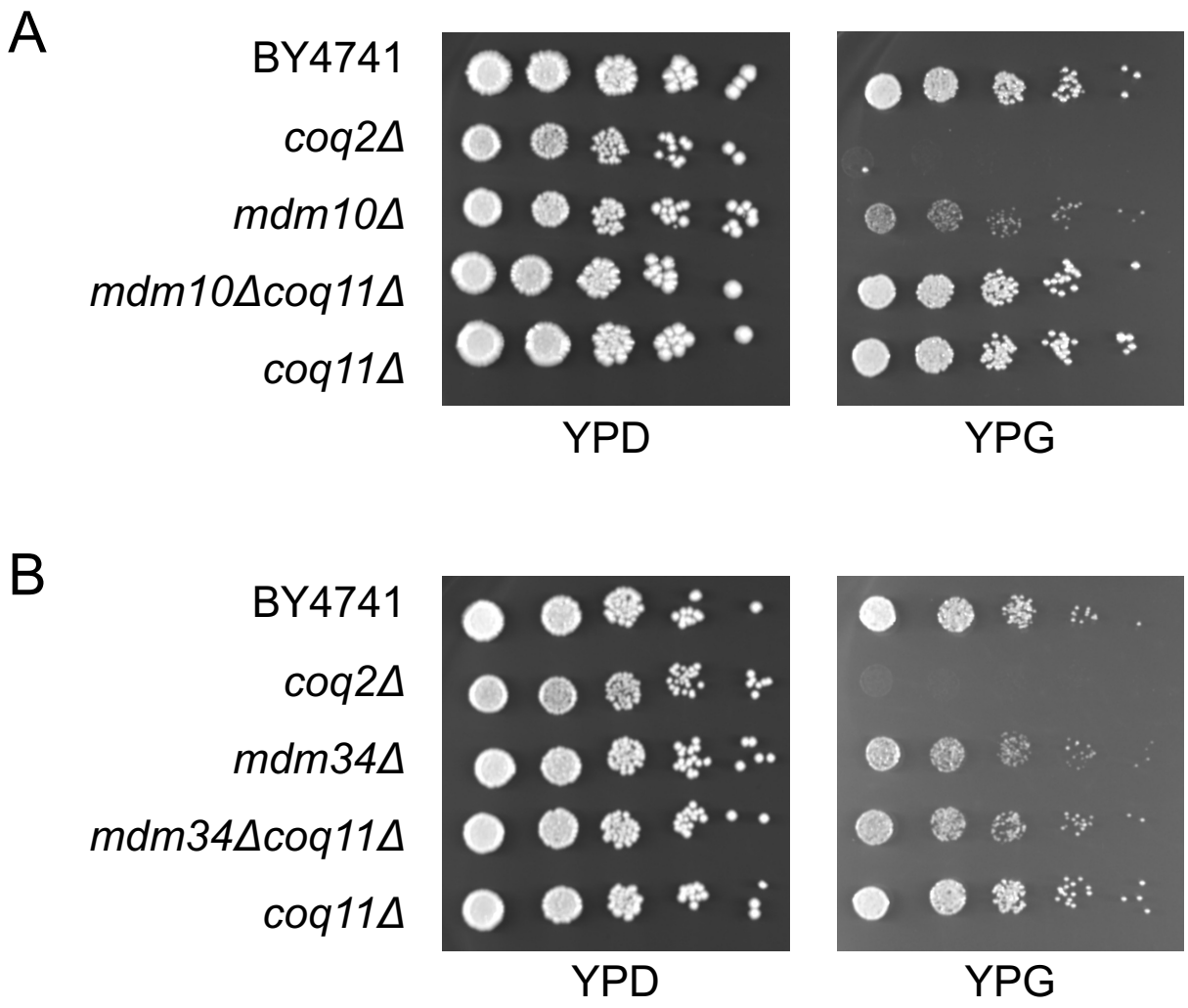

Figure S1. Deletion of *COQ11* rescues respiratory growth in select *ERMES*Δ mutants. Spot-dilution assays were performed as described for Fig. 1. *A*, The respiratory phenotype of the *mdm10*Δ mutant is robustly rescued by the deletion of *COQ11*. *B*, The inability to rescue the *mdm34*Δ mutant is conserved in the BY47471 genetic background. Images are representative of at least three biological replicates.

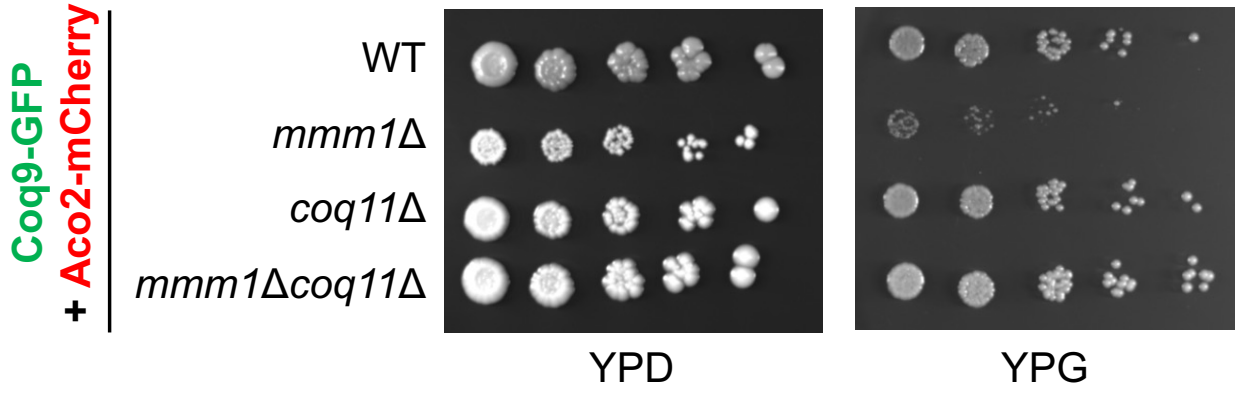

Figure S2. Tagged strains are functional and reproduce respiratory growth phenotype. Spot-dilution assays were performed as described for Fig. 1. Normal growth on respiratory medium from the WT strain expressing Coq9-GFP and Aco2-mCherry indicates the endogenously tagged proteins retain function. Images are representative of at least three biological replicates.

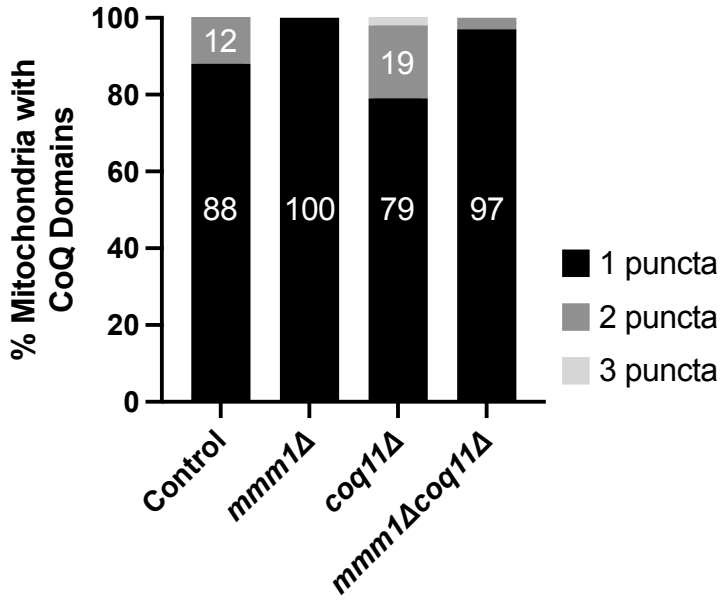

Figure S3. In strains lacking *MMM1*, mitochondria possess fewer CoQ domains. Using the fraction of cells that contained CoQ domains (Fig. 4 in the main text), the number of puncta per mitochondrion were detected using neural networks and plotted as a percentage of total mitochondria with CoQ domains.

REFERENCES

1. Banerjee, R., Purhonen, J., and Kallijärvi, J. (2022) The mitochondrial coenzyme Q junction and complex III: biochemistry and pathophysiology. *The FEBS Journal*. **289**, 6936–6958
2. Guerra, R. M., and Pagliarini, D. J. (2023) Coenzyme Q biochemistry and biosynthesis. *Trends in Biochemical Sciences*. **48**, 463–476
3. Frei, B., Kim, M. C., and Ames, B. N. (1990) Ubiquinol-10 is an effective lipid-soluble antioxidant at physiological concentrations. *Proceedings of the National Academy of Sciences*. **87**, 4879–4883
4. Okada, K., Suzuki, K., Kamiya, Y., Zhu, X., Fujisaki, S., Nishimura, Y., Nishino, T., Nakagawad, T., Kawamukai, M., and Matsuda, H. (1996) Polyprenyl diphosphate synthase essentially defines the length of the side chain of ubiquinone. *Biochimica et Biophysica Acta (BBA) - Lipids and Lipid Metabolism*. **1302**, 217–223
5. Garrido-Maraver, J., Cordero, M. D., Oropesa-Ávila, M., Fernández Vega, A., De La Mata, M., Delgado Pavón, A., De Miguel, M., Pérez Calero, C., Villanueva Paz, M., Cotán, D., and Sánchez-Alcázar, J. A. (2014) Coenzyme Q_{10} Therapy. *Mol Syndromol*. **5**, 187–197
6. Fernández-del-Río, L., Kelly, M. E., Contreras, J., Bradley, M. C., James, A. M., Murphy, M. P., Payne, G. S., and Clarke, C. F. (2020) Genes and lipids that impact uptake and assimilation of exogenous coenzyme Q in Saccharomyces cerevisiae. *Free Radical Biology and Medicine*. **154**, 105–118
7. Awad, A. M., Bradley, M. C., Fernández-del-Río, L., Nag, A., Tsui, H. S., and Clarke, C. F. (2018) Coenzyme Q10 deficiencies: pathways in yeast and humans. *Essays in*

Biochemistry. **62**, 361–376

8. Hsieh, E. J., Gin, P., Gulmezian, M., Tran, U. C., Saiki, R., Marbois, B. N., and Clarke, C. F. (2007) Saccharomyces cerevisiae Coq9 polypeptide is a subunit of the mitochondrial coenzyme Q biosynthetic complex. *Archives of Biochemistry and Biophysics*. **463**, 19–26
9. Subramanian, K., Jochem, A., Le Vasseur, M., Lewis, S., Paulson, B. R., Reddy, T. R., Russell, J. D., Coon, J. J., Pagliarini, D. J., and Nunnari, J. (2019) Coenzyme Q biosynthetic proteins assemble in a substrate-dependent manner into domains at ER–mitochondria contacts. *Journal of Cell Biology*. **218**, 1353–1369
10. Eisenberg-Bord, M., Tsui, H. S., Antunes, D., Fernández-del-Río, L., Bradley, M. C., Dunn, C. D., Nguyen, T. P. T., Rapaport, D., Clarke, C. F., and Schuldiner, M. (2019) The Endoplasmic Reticulum-Mitochondria Encounter Structure Complex Coordinates Coenzyme Q Biosynthesis. *Contact*. **2**, 2515256418825409
11. Wang, Y., and Hekimi, S. (2019) The Complexity of Making Ubiquinone. *Trends in Endocrinology & Metabolism*. **30**, 929–943
12. Tran, U. C., and Clarke, C. F. (2007) Endogenous synthesis of coenzyme Q in eukaryotes. *Mitochondrion*. **7**, S62–S71
13. Barros, M. H., Johnson, A., Gin, P., Marbois, B. N., Clarke, C. F., and Tzagoloff, A. (2005) The Saccharomyces cerevisiae COQ10 Gene Encodes a START Domain Protein Required for Function of Coenzyme Q in Respiration. *Journal of Biological Chemistry*. **280**, 42627–42635
14. Allan, C. M., Awad, A. M., Johnson, J. S., Shirasaki, D. I., Wang, C., Blaby-Haas, C. E., Merchant, S. S., Loo, J. A., and Clarke, C. F. (2015) Identification of Coq11, a New

Coenzyme Q Biosynthetic Protein in the CoQ-Synthome in Saccharomyces cerevisiae. *Journal of Biological Chemistry*. **290**, 7517–7534

15. Bradley, M. C., Yang, K., Fernández-del-Río, L., Ngo, J., Ayer, A., Tsui, H. S., Novales, N. A., Stocker, R., Shirihai, O. S., Barros, M. H., and Clarke, C. F. (2020) COQ11 deletion mitigates respiratory deficiency caused by mutations in the gene encoding the coenzyme Q chaperone protein Coq10. *Journal of Biological Chemistry*. **295**, 6023–6042
16. Allan, C. M., Hill, S., Morvaridi, S., Saiki, R., Johnson, J. S., Liau, W.-S., Hirano, K., Kawashima, T., Ji, Z., Loo, J. A., Shepherd, J. N., and Clarke, C. F. (2013) A conserved START domain coenzyme Q-binding polypeptide is required for efficient Q biosynthesis, respiratory electron transport, and antioxidant function in Saccharomyces cerevisiae. *Biochimica et Biophysica Acta (BBA) - Molecular and Cell Biology of Lipids*. **1831**, 776–791
17. Tsui, H. S., Pham, NguyenV. B., Amer, B. R., Bradley, M. C., Gosschalk, J. E., Gallagher-Jones, M., Ibarra, H., Clubb, R. T., Blaby-Haas, C. E., and Clarke, C. F. (2019) Human COQ10A and COQ10B are distinct lipid-binding START domain proteins required for coenzyme Q function. *Journal of Lipid Research*. **60**, 1293–1310
18. Kornmann, B., Currie, E., Collins, S. R., Schuldiner, M., Nunnari, J., Weissman, J., and Walter, P. (2009) An ER-Mitochondria Tethering Complex Revealed by a Synthetic Biology Screen. *Science*. **325**, 477–481
19. AhYoung, A. P., Jiang, J., Zhang, J., Khoi Dang, X., Loo, J. A., Zhou, Z. H., and Egea, P. F. (2015) Conserved SMP domains of the ERMES complex bind phospholipids and mediate tether assembly. *Proc. Natl. Acad. Sci. U.S.A.* 10.1073/pnas.1422363112
20. Wozny, M. R., Di Luca, A., Morado, D. R., Picco, A., Khaddaj, R., Campomanes, P.,

Ivanović, L., Hoffmann, P. C., Miller, E. A., Vanni, S., and Kukulski, W. (2023) In situ architecture of the ER–mitochondria encounter structure. *Nature*. **618**, 188–192

21. Tan, T., Özbalci, C., Brügger, B., Rapaport, D., and Dimmer, K. S. (2013) Mcp1 and Mcp2, two novel proteins involved in mitochondrial lipid homeostasis. *Journal of Cell Science*. 10.1242/jcs.121244

22. Okamura, Y., Aoki, Y., Obayashi, T., Tadaka, S., Ito, S., Narise, T., and Kinoshita, K. (2015) COXPRESdb in 2015: coexpression database for animal species by DNA-microarray and RNAseq-based expression data with multiple quality assessment systems. *Nucleic Acids Research*. **43**, D82–D86

23. Hibbs, M. A., Hess, D. C., Myers, C. L., Huttenhower, C., Li, K., and Troyanskaya, O. G. (2007) Exploring the functional landscape of gene expression: directed search of large microarray compendia. *Bioinformatics*. **23**, 2692–2699

24. Novales, N. A., Feustel, K. J., and Clarke, C. F. (2024) Nonfunctional coq10 mutants maintain the ERMES complex and reveal true phenotypes associated with the loss of the coenzyme Q chaperone protein Coq10. *Journal of Biological Chemistry, In Review*

25. Thomas, B. J., and Rothstein, R. (1989) Elevated recombination rates in transcriptionally active DNA. *Cell*. **56**, 619–630

26. Baker Brachmann, C., Davies, A., Cost, G. J., Caputo, E., Li, J., Hieter, P., and Boeke, J. D. (1998) Designer deletion strains derived from Saccharomyces cerevisiae S288C: A useful set of strains and plasmids for PCR-mediated gene disruption and other applications. *Yeast*. **14**, 115–132

27. Rothstein, R. (1983) One-Step Gene Disruption Method. *Methods in Enzymology*. **101**, 101–211

28. Daniel Gietz, R., and Woods, R. A. (2002) Transformation of yeast by lithium acetate/single-stranded carrier DNA/polyethylene glycol method. *Methods in Enzymology*. **350**, 87–96

29. Santos-Ocaña, C., Do, T. Q., Clarke, C. F., Padilla, S., and Navas, P. (2002) Uptake of Exogenous Coenzyme Q and Transport to Mitochondria Is Required for bc1 Complex Stability in Yeast coq Mutants. *Journal of Biological Chemistry*. **277**, 10973–10981

30. Schägger, H., Cramer, W. A., and von Jagow, G. (1994) Analysis of Molecular Masses and Oligomeric States of Protein complexes by Blue Native Electrophoresis and Isolation of Membrane Protein Complexes by Two-Dimensional Native Electrophoresis. *Analytical Biochemistry*. **217**, 220–230

31. Wittig, I., Braun, H.-P., and Schägger, H. (2006) Blue native PAGE. *Nat Protoc*. **1**, 418–428

32. Pertea, G., and Pertea, M. (2020) GFF Utilities:GffRead and GffCompare [version 2; peer review: 3 approved]. *F1000Research*. **9**, 304

33. Chen, S., Zhou, Y., Chen, Y., and Gu, J. (2018) fastp: an ultra-fast all-in-one FASTQ preprocessor. *Bioinformatics*. **34**, i884–i890

34. Dobin, A., Davis, C. A., Schlesinger, F., Drenkow, J., Zaleski, C., Jha, S., Batut, P., Chaisson, M., and Gingeras, T. R. (2013) STAR: ultrafast universal RNA-seq aligner. *Bioinformatics*. **29**, 15–21

35. Trapnell, C., Roberts, A., Goff, L., Pertea, G., Kim, D., Kelley, D. R., Pimentel, H., Salzberg, S. L., Rinn, J. L., and Pachter, L. (2012) Differential gene and transcript expression analysis of RNA-seq experiments with TopHat and Cufflinks. *Nat Protoc*. **7**, 562–578

36. Boyle, E. I., Weng, S., Gollub, J., Jin, H., Botstein, D., Cherry, J. M., and Sherlock, G. (2004) GO::TermFinder—open source software for accessing Gene Ontology information and finding significantly enriched Gene Ontology terms associated with a list of genes. *Bioinformatics*. **20**, 3710–3715

37. Berger, K. H., Sogo, L. F., and Yaffe, M. P. (1997) Mdm12p, a Component Required for Mitochondrial Inheritance That Is Conserved between Budding and Fission Yeast. *Journal of Cell Biology*. **136**, 545–553

38. Youngman, M. J., Hobbs, A. E. A., Burgess, S. M., Srinivasan, M., and Jensen, R. E. (2004) Mmm2p, a mitochondrial outer membrane protein required for yeast mitochondrial shape and maintenance of mtDNA nucleoids. *Journal of Cell Biology*. **164**, 677–688

39. Hobbs, A. E. A., Srinivasan, M., McCaffery, J. M., and Jensen, R. E. (2001) Mmm1p, a Mitochondrial Outer Membrane Protein, Is Connected to Mitochondrial DNA (Mtdna) Nucleoids and Required for Mtdna Stability. *J Cell Biol*. **152**, 401–410

40. Ellenrieder, L., Opaliński, Ł., Becker, L., Krüger, V., Mirus, O., Straub, S. P., Ebell, K., Flinner, N., Stiller, S. B., Guiard, B., Meisinger, C., Wiedemann, N., Schleiff, E., Wagner, R., Pfanner, N., and Becker, T. (2016) Separating mitochondrial protein assembly and endoplasmic reticulum tethering by selective coupling of Mdm10. *Nat Commun*. **7**, 13021

41. Meisinger, C., Pfannschmidt, S., Rissler, M., Milenkovic, D., Becker, T., Stojanovski, D., Youngman, M. J., Jensen, R. E., Chacinska, A., Guiard, B., Pfanner, N., and Wiedemann, N. (2007) The morphology proteins Mdm12/Mmm1 function in the major β-barrel assembly pathway of mitochondria. *EMBO*. **26**, 2229–2239

42. Meisinger, C., Wiedemann, N., Rissler, M., Strub, A., Milenkovic, D., Schönfisch, B., Müller, H., Kozjak, V., and Pfanner, N. (2006) Mitochondrial Protein Sorting. *Journal of Biological Chemistry*. **281**, 22819–22826

43. Manicki, M., Aydin, H., Abriata, L. A., Overmyer, K. A., Guerra, R. M., Coon, J. J., Dal Peraro, M., Frost, A., and Pagliarini, D. J. (2022) Structure and functionality of a multimeric human COQ7:COQ9 complex. *Molecular Cell*. **82**, 4307-4323.e10

44. Kehrein, K., Möller-Hergt, B. V., and Ott, M. (2015) The MIOREX complex - lean management of mitochondrial gene expression. *Oncotarget*. **6**, 16806–16807

45. Shore, D., Zencir, S., and Albert, B. (2021) Transcriptional control of ribosome biogenesis in yeast: links to growth and stress signals. *Biochemical Society Transactions*. **49**, 1589–1599

46. Xu, Y., Létisse, F., Absalan, F., Lu, W., Kuznetsova, E., Brown, G., Caudy, A. A., Yakunin, A. F., Broach, J. R., and Rabinowitz, J. D. (2013) Nucleotide degradation and ribose salvage in yeast. *Molecular Systems Biology*. **9**, 665

47. Canizal-García, M., Olmos-Orizaba, B. E., Moreno-Jiménez, M., Calderón-Cortés, E., Saavedra-Molina, A., and Cortés-Rojo, C. (2021) Glutathione peroxidase 2 (Gpx2) preserves mitochondrial function and decreases ROS levels in chronologically aged yeast. *Free Radical Research*. **55**, 165–175

48. Flinner, N., Ellenrieder, L., Stiller, S. B., Becker, T., Schleiff, E., and Mirus, O. (2013) Mdm10 is an ancient eukaryotic porin co-occurring with the ERMES complex. *Biochimica et Biophysica Acta (BBA) - Molecular Cell Research*. **1833**, 3314–3325

49. Becker, T., Vögtle, F.-N., Stojanovski, D., and Meisinger, C. (2008) Sorting and assembly of mitochondrial outer membrane proteins. *Biochimica et Biophysica Acta*

(BBA) - Bioenergetics. **1777**, 557–563

50. Kemmerer, Z. A., Robinson, K. P., Schmitz, J. M., Manicki, M., Paulson, B. R., Jochem, A., Hutchins, P. D., Coon, J. J., and Pagliarini, D. J. (2021) UbiB proteins regulate cellular CoQ distribution in Saccharomyces cerevisiae. *Nat Commun*. **12**, 4769

51. Valdebenito, G. E., Chacko, A. R., and Duchen, M. R. (2023) The mitochondrial ATP synthase as an ATP consumer—a surprising therapeutic target. *The EMBO Journal*. **42**, e114141

52. Ashby, M. N., Kutsunai, S. Y., Ackerman, S., Tzagoloff, A., and Edwards, P. A. (1992) COQ2 is a candidate for the structural gene encoding para-hydroxybenzoate:polyprenyltransferase. *Journal of Biological Chemistry*. **267**, 4128–4136

53. Do, T. Q., Schultz, J. R., and Clarke, C. F. (1996) Enhanced sensitivity of ubiquinone-deficient mutants of Saccharomyces cerevisiae to products of autoxidized polyunsaturated fatty acids. *Proc Natl Acad Sci U S A*. **93**, 7534–7539

54. Hsu, A. Y., Do, T. Q., Lee, P. T., and Clarke, C. F. (2000) Genetic evidence for a multi-subunit complex in the O-methyltransferase steps of coenzyme Q biosynthesis. *Biochimica et Biophysica Acta (BBA) - Molecular and Cell Biology of Lipids*. **1484**, 287–297

55. Barkovich, R. J., Shtanko, A., Shepherd, J. A., Lee, P. T., Myles, D. C., Tzagoloff, A., and Clarke, C. F. (1997) Characterization of the COQ5 Gene from Saccharomyces cerevisiae EVIDENCE FOR A C-METHYLTRANSFERASE IN UBIQUINONE BIOSYNTHESIS. *Journal of Biological Chemistry*. **272**, 9182–9188

56. Gin, P., Hsu, A. Y., Rothman, S. C., Jonassen, T., Lee, P. T., Tzagoloff, A., and Clarke,

C. F. (2003) The Saccharomyces cerevisiae COQ6 Gene Encodes a Mitochondrial Flavin-dependent Monooxygenase Required for Coenzyme Q Biosynthesis. *Journal of Biological Chemistry*. **278**, 25308–25316

57. Marbois, B. N., and Clarke, C. F. (1996) The COQ7 Gene Encodes a Protein in Saccharomyces cerevisiae Necessary for Ubiquinone Biosynthesis. *Journal of Biological Chemistry*. **271**, 2995–3004

58. Johnson, A., Gin, P., Marbois, B. N., Hsieh, E. J., Wu, M., Barros, M. H., Clarke, C. F., and Tzagoloff, A. (2005) COQ9, a New Gene Required for the Biosynthesis of Coenzyme Q in Saccharomyces cerevisiae. *Journal of Biological Chemistry*. **280**, 31397–31404

59. Winzeler, E. A., Shoemaker, D. D., Astromoff, A., Liang, H., Anderson, K., Andre, B., Bangham, R., Benito, R., Boeke, J. D., Bussey, H., Chu, A. M., Connelly, C., Davis, K., Dietrich, F., Dow, S. W., El Bakkoury, M., Foury, F., Friend, S. H., Gentalen, E., Giaever, G., Hegemann, J. H., Jones, T., Laub, M., Liao, H., Liebundguth, N., Lockhart, D. J., Lucau-Danila, A., Lussier, M., M'Rabet, N., Menard, P., Mittmann, M., Pai, C., Rebischung, C., Revuelta, J. L., Riles, L., Roberts, C. J., Ross-MacDonald, P., Scherens, B., Snyder, M., Sookhai-Mahadeo, S., Storms, R. K., Véronneau, S., Voet, M., Volckaert, G., Ward, T. R., Wysocki, R., Yen, G. S., Yu, K., Zimmermann, K., Philippsen, P., Johnston, M., and Davis, R. W. (1999) Functional Characterization of the *S. cerevisiae* Genome by Gene Deletion and Parallel Analysis. *Science*. **285**, 901–906

60. Poon, W. W., Barkovich, R. J., Hsu, A. Y., Frankel, A., Lee, P. T., Shepherd, J. N., Myles, D. C., and Clarke, C. F. (1999) Yeast and Rat Coq3 and Escherichia coli UbiG Polypeptides Catalyze Both O-Methyltransferase Steps in Coenzyme Q Biosynthesis.

Journal of Biological Chemistry. **274**, 21665–21672

61. Belogrudov, G. I., Lee, P. T., Jonassen, T., Hsu, A. Y., Gin, P., and Clarke, C. F. (2001) Yeast COQ4 Encodes a Mitochondrial Protein Required for Coenzyme Q Synthesis. *Archives of Biochemistry and Biophysics*. **392**, 48–58

62. Baba, S. W., Belogrudov, G. I., Lee, J. C., Lee, P. T., Strahan, J., Shepherd, J. N., and Clarke, C. F. (2004) Yeast Coq5 C-Methyltransferase Is Required for Stability of Other Polypeptides Involved in Coenzyme Q Biosynthesis. *Journal of Biological Chemistry*. **279**, 10052–10059

63. Tran, U. C., Marbois, B., Gin, P., Gulmezian, M., Jonassen, T., and Clarke, C. F. (2006) Complementation of Saccharomyces cerevisiae coq7 Mutants by Mitochondrial Targeting of the Escherichia coli UbiF Polypeptide. *Journal of Biological Chemistry*. **281**, 16401–16409

Chapter 4

Expression of an ER-mitochondrial artificial tether enhances the content of coenzyme Q

ABSTRACT

Early observations of close membrane apposition between separate organelles have suggested that organelles are not discrete entities, despite the well-known evolutionary advancement that is compartmentalization within eukaryotic cells. Indeed, organelles must engage in communication or crosstalk with one another to maintain homeostasis, enabled through proteinaceous membrane contact sites, or molecular tethers. Since the discovery of these tethers, membrane contact sites have been shown to serve as signaling platforms that can modulate cellular processes, such as lipid transport or metabolite exchange. Given the previous work that shows ER-mitochondrial contact sites coordinate coenzyme Q (CoQ) biosynthesis, we utilize an artificial tether in *S. cerevisiae* strains that contain the endogenous ER-mitochondria encounter structure (ERMES), the primary ER-mitochondrial tether in yeast, as well as yeast that lack ERMES via a deletion of *MDM34* to investigate the effect of tethers on CoQ biosynthesis. Overall, this work illuminates potential roles for general tethers in modulating lipid homeostasis, and further highlights a direct role of ERMES in modulating CoQ synthesis and distribution.

INTRODUCTION

The evolution of eukaryotic cells required the compartmentalization of functions into discrete organelles. The separation of cellular functions streamlined the efficiency of biochemical processes through the creation of chemical microenvironments tailored to such processes; for example, the acidic environment of lysosomes can help facilitate the degradation of biomolecules. However, the evolution of compartmentalization consequently created the need for organellular crosstalk, so that the designated compartments can communicate and together maintain cellular homeostasis. Some of the earliest evidence of interorganelle communication was observed using electron microscopy of rat liver cells, in which researchers noted the close apposition between mitochondria and endoplasmic reticulum (ER) membranes (1). The physical interaction between organelles was later discovered when yeast vacuolar protein Vac8 was shown to complex with the nuclear protein Nvj1, forming a physical nucleus-vacuole junction (NVJ) (2). These physical points of interaction were first identified as "novel interorganelle junction apparatuses," (2) which are now referred to as membrane contact sites or molecular tethers (3).

More recent research efforts have identified several membrane contact sites across various organelle pairs (4); the abundance of tethers illuminates the physiological relevance of membrane contact sites in health and onset of disease (5–7). The most commonly used tool to identify membrane contact sites is the use of artificial tethers composed of fluorophores to visualize the physical link between organelles (3, 8–10). *Saccharomyces cerevisiae* (yeast) are a powerful model organism to study membrane contact sites, given the relative ease of genetic manipulation compared to other organisms. Using these tools, the functions of specific protein tethers have been very well characterized, which includes the elucidation of their roles in lipid

transport, metabolite exchange, and modulating organelle dynamics (7, 11).

Within the realm of membrane contact sites, ER-mitochondrial contact sites have been extensively studied, and the most commonly known tether in yeast is the ER-mitochondria encounter structure (ERMES). ERMES was discovered using a synthetic biology screen that sought to explore a potential role for ER-mitochondrial contacts in respiration (8). The artificial tether in this work, the Construct helping in Mitochondrial ER Association (ChiMERA), was designed after a similar chimeric construct that was used to elucidate the role of ER-mitochondrial contacts in rat liver cells (9). The ChiMERA is comprised of a central GFP moiety flanked by the N-terminal mitochondrial targeting sequence and transmembrane domain from Tom70 and the C-terminal ER anchoring sequence from Ubc6, and was the first example of an artificial tether in yeast (8). The ChiMERA is considered a "static" artificial tether (3), in which the GFP moiety with this localization sequences create a fixed point of apposition between membranes. Further development of fluorescence-based tools led to the creation of reporters that better represent the dynamics of organelle interactions (12), such as the Split-Venus reporter. The Split-Venus reporter is designed such that the C-terminal half of the Venus fluorophore is conjugated to a protein on a candidate organelle, and the N-terminal half is conjugated to the proposed interacting organelle (4, 12). The ER-mitochondrial version, Split-MAM (Mitochondrial Associated Membrane; illustrated in Fig. 1), was shown to reinstate the ER and mitochondrial membrane apposition in the *mmm1*Δ and *mdm34*Δ mutants, demonstrating that the Split-MAM can be used to compensate for the loss of the ERMES tether (4).

In yeast, ER-mitochondrial membrane contact sites, and specifically ERMES, has been shown to modulate the efficiency of coenzyme Q (ubiquinone or CoQ_6) biosynthesis (13, 14). CoQ is an essential redox active lipid that is synthesized exclusively within the mitochondrial

matrix, yet present in all cellular membranes (15); the detailed mechanism of its distribution is presently unknown, but it is speculated that ERMES can serve as a platform or conduit to facilitate in CoQ transport out of the mitochondria. In this work, we sought to evaluate the role of molecular tethers in CoQ biosynthesis using the Split-MAM construct. Our results suggest that ER-mitochondrial tethers may influence the turnover and distribution of CoQ, and potentially other lipid molecules, highlighting the role of membrane contact sites in regulating lipid homeostasis.

EXPERIMENTAL PROCEDURES

Yeast strains and growth medium

Saccharomyces cerevisiae strains used in this study are listed in Table 1. Yeast strains were derived from BY4741 (16). Growth media included YPG (1% yeast extract, 2% peptone, 3% glycerol) and YPD (1% yeast extract, 2% peptone, 2% glucose). Plate medium contained 2% bacto-agar. Strains expressing the Split-MAM artificial tether were constructed by crossing yeast strains harboring the desired mutations and/or chromosomally integrated tethering constructs, followed by a series of plating on selection medium to obtain the final strains of interest (4, 17). We thank Dr. Maya Schuldiner from the Weizmann Institute for gifting us the strains containing the Split-MAM reporter.

Drop dilution plate assays

Yeast cultures of BY4741 wild type and *mdm34*Δ with and without the Split-MAM tether were grown overnight in 5 mL of YPG to ensure mitochondrial DNA retention. The following day, cultures were back-diluted in 15 mL of fresh YPG and expanded to a final A_{600} ~ 1.0. Cells

were harvested by centrifugation, washed with sterile water, and diluted in phosphate-buffered saline (PBS) to an A_{600} = 0.2. 2 µL of 5-fold serial dilutions were spotted on YPD and YPG plates, corresponding to a final A_{600} = 0.2, 0.04, 0.008, 0.0016, and 0.00032. All plates were incubated at 30 °C for 2-3 days.

Analysis of CoQ_6 and CoQ_6-intermediates and stable isotope labeling

Yeast cultures were grown overnight in 25 mL of YPG at 30 °C with shaking. The following day, cultures were back-diluted to an A_{600} ~ 0.1 in fresh medium and further cultured to mid-log phase (A_{600} ~ 0.6). To evaluate *de novo* biosynthesis, cultures were treated with 8 µg/mL of ^{13}C ring-labeled para-aminobenzoic acid ($^{13}C_6$-pABA) for 5 hours or ethanol as a vehicle control. Labeled pABA was obtained from Sigma-Aldrich. Following treatment, cultures were harvested by centrifugation and cell pellets were stored in –20 °C until use.

To prepare lipid extracts, cell pellets were resuspended in PBS, and 100 µL of the cell suspension were lysed by vortexing with glass beads in 2 mL of methanol. The same amount of internal standard CoQ_4 (Sigma-Aldrich) was added to each sample, and lipids were extracted with the addition of 2 mL of petroleum ether twice. A standard curve comprised of known amounts of CoQ_6 (Avanti Polar Lipids) and the CoQ_4 internal standard was also extracted as described. Extracts were dried with N_2 and stored at –20 °C.

Lipid content was analyzed by LC-MS/MS as previously described (18). Lipids were reconstituted in 200 µL of 0.5 mg/mL benzoquinone in ethanol. 20 µL of each sample was injected into an API4000 linear MS/MS spectrometer (Applied Biosystems). The instrument's corresponding analysis software, Analyst version 1.4.2, was used for data acquisition and processing. CoQ_6 content was determined by normalizing the corresponding peak area to the

standard curve, followed by correcting for the total amount of cells extracted, as represented by A_{600}. Relative levels of CoQ_6-intermediates are represented as peak areas also normalized to A_{600}. A one-way ANOVA with Dunnett's multiple comparisons test was performed using GraphPad Prism 10.

RESULTS

Respiratory growth is unchanged in yeast strains expressing Split-MAM artificial tether

Using wild-type and *mdm34*Δ cells, we first evaluated the ability to grow on nonfermentable medium, YPGlycerol (YPG), with and without the expression of the Split-MAM reporter. It is of note that the *mdm34*Δ mutant in the BY4741 background does not exhibit a dramatic respiratory growth defect (Fig. 2), but it was still of interest to determine if the addition of the artificial tether can bolster respiratory growth. The result of this plate viability assay show no differences in growth when the artificial tether is expressed (Fig. 2), however given only a small percentage of CoQ_6 is required to observed growth on respiratory medium (19), the growth phenotype may not be representative of CoQ_6 biosynthetic efficiency.

CoQ_6 content is altered in strains expressing Split-MAM

To assess the efficiency of CoQ_6 synthesis, we treated yeast cultures with isotopically labeled ring precursor, $^{13}C_6$-pABA, or ethanol as vehicle control. It has been previously reported that *ERMES*Δ mutants, including the *mdm34*Δ mutant, contain significantly increased content of CoQ_6 (13). However, in our analyses, we observe that the content of CoQ_6 is similar to that of the wild-type control (Fig. 3A). We attribute this difference in reproducibility to genetic background, as the former study was performed in W303 yeast, whereas our strains in this work

are in the BY4741 background.

In the ^{12}C-CoQ_6 analysis of the ethanol vehicle control group, which represents the steady state CoQ_6 content, we observe significantly elevated CoQ_6 levels in the strains with Split-MAM compared to without (Fig. 3A). This suggested to us that possibly the imposition of the artificial tether may be positively regulating CoQ_6 biosynthesis, such that the addition of the tether would promote *de novo* biosynthesis, even in WT. Interestingly, *de novo* $^{13}C_6$-CoQ_6 content remained unchanged regardless of the presence of the artificial tether (Fig. 3B), indicating that the tether does not enhance the *de novo* production of the final lipid molecule. Upon evaluating total CoQ_6 content, determined by the sum of unlabeled and labeled CoQ_6, we show that the accumulation of CoQ_6 is not due to the increase in *de novo* biosynthesis, but rather the content of unlabeled, or "pre-existing," CoQ_6 (Fig. 3C) Despite not observing any difference in *de novo* $^{13}C_6$-CoQ_6 content, the *mdm34*Δ mutant expressing Split-MAM exhibits augmented content of the early intermediate hexaprenyl-aminobenzoic acid ($^{13}C_6$-HAB) (Fig. 4A), and the late-stage intermediate demethoxy-Q_6 ($^{13}C_6$-DMQ_6) (Fig. 4B). This contrasts with the wild-type control, which does not contain elevated content of these intermediates with the additional tether (Fig. 4).

DISCUSSION

This work utilized a chromosomally integrated ER-mitochondrial contact site reporter, Split-MAM (Fig. 1), to evaluate the effects of tethers on CoQ_6 biosynthesis. We show that respiratory growth is not affected upon expression of the artificial tether (Fig. 2), even with the increased abundance of total CoQ_6 in strains expressing Split-MAM (Fig. 3). *De novo* Q_6 biosynthesis appears to be impaired in the *mdm34*Δ strain with the artificial tether, as determined via the accumulation of CoQ_6 intermediates, which is not observed in the wild-type control (Fig.

4).

The accumulation of intermediates despite unchanged amount of final product would suggest that the biosynthetic flux may be impaired with the addition of the tether. However, this model is not entirely sound as the wild-type control with the tether does not accumulate these intermediates (Fig. 4). It is possible that because WT still possesses the endogenous contact site, ERMES, that the addition of the Split-MAM tether is redundant and therefore does not provide additional function in concert with ERMES. This is mostly observed in *de novo* synthesis, as $^{13}C_6$-HAB, $^{13}C_6$-DMQ_6, and $^{13}C_6$-CoQ_6 are all unchanged in the WT irrespective of the expression of the Split-MAM tether (Fig. 3 & Fig. 4). However, in the absence of Mdm34 and ERMES, the catalytic efficiency of $^{13}C_6$-CoQ_6 biosynthesis is impaired, leading to the accumulation of both early- and late-stage biosynthetic $^{13}C_6$-labeled CoQ_6 intermediates (Fig. 4). This suggests that ERMES plays a more direct role in CoQ metabolon assembly, which has been reported to require proper assembly for appropriate substrate channeling and subsequent efficient lipid synthesis (20). This model is consistent with previous work that demonstrated that ERMES is required for the visualization of the CoQ synthome via biochemical analyses (13, 21).

On the other hand, the accumulation of unlabeled CoQ_6 in both the wild type and *mdm34*Δ mutant expressing the Split-MAM tether suggests that there is decreased turnover of "pre-existing" CoQ_6 (Fig. 3). We posit that the physical tether may alter the distribution of CoQ_6, which could modulate its stability. The architecture of ERMES is shown to possess a hydrophobic channel formed by the synaptotagmin-like mitochondrial lipid binding protein (SMP) domains of Mmm1, Mdm12, and Mdm34 (22, 23). The alignment of these domains poises ERMES, in tandem with the observed colocalization between ERMES and the CoQ metabolon (13), to be an excellent candidate to facilitate the trafficking of CoQ_6 out of the

mitochondria to the ER and to subsequent membranes, as ER membranes have been shown to form intricate networks with all other organelles as well (24). In the *mdm34*Δ mutants expressing Split-MAM, it is possible that without the lipid channel formed by ERMES, CoQ_6 is less able to be exported out of the mitochondria, and hence less susceptible to degradation, leading to elevated unlabeled (^{12}C-CoQ_6) content (Fig. 3).

This model becomes more complicated in the wild-type cells expressing Split-MAM, as the endogenous tether and putative export channel are still retained. Membrane contact sites in general are thought to be signaling platforms capable of recruiting proteins or metabolites depending on the need of the cell. Considering this, it is possible that the imposition of Split-MAM tether in addition to the endogenous ERMES tether introduces a degree of disorganization, resulting in decreased efficiency of CoQ_6 trafficking out of the mitochondria. The presence of ERMES would still provide a platform for efficient CoQ_6 synthesis and trafficking, yet the expression of the Split-MAM tethers imposes additional contact sites that lack a conduit for transporting CoQ_6 out of the mitochondria. This would indicate that while the membrane apposition between organelles is important, the presence of a molecular tether that is functional is required for the maintenance of cellular functions.

Table 1. Yeast strains used in study

Strain	Genotype	Source
BY4741	*MAT a his3Δ1 leu2Δ0 met15Δ0 ura3Δ0*	(16)
BY4741 *mdm34*Δ	*MAT a his3Δ1 leu2Δ0 met15Δ0 ura3Δ0 mdm34::KanMX4*	(25)
BY4741 + Split-MAM	*MAT α his3Δ1 leu2Δ0 lys2+/lys+ met15Δ0 ura3Δ0 can1Δ::STE2pr-sp HIS5 lyp1Δ::STE3pr-LEU2; Tom20-VC-His; Sec63-VN-Kan*	(4)
BY4741 *mdm34*Δ + Split-MAM	*MAT α his3Δ1 leu2Δ0 lys2+/lys+ met15Δ0 ura3Δ0 can1Δ::STE2pr-sp HIS5 lyp1Δ::STE3pr-LEU2; Tom20-VC-His; Sec63-VN-Kan; Δmdm34::Nat*	(4)
BY4741 *coq2*Δ	*MAT a his3Δ1 leu2Δ0 met15Δ0 ura3Δ0 coq2::KanMX4*	(25)

FIGURES

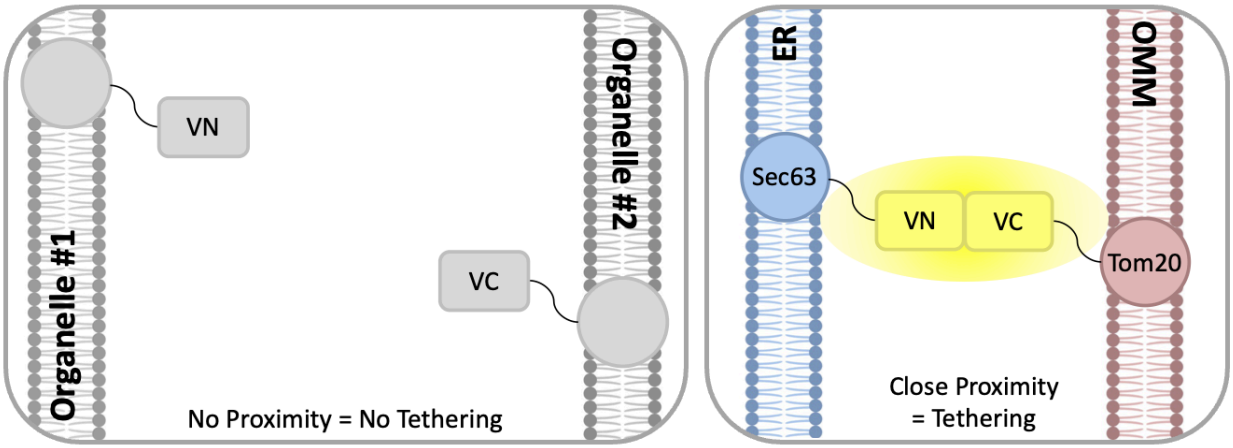

Figure 1. Schematic of artificial tether reporter. Split-Venus reporter was designed having the C-terminal (VC) and N-terminal (VN) halves of the Venus fluorophore each conjugated to a membrane protein on separate organelles proposed to form a contact site. The left panel shows the general scheme; organelles that do not have the natural tendency to form a contact site will not come into proximity for the two halves to rejoin and fluoresce. The right panel illustrates the Split-MAM reporter, comprised of the outer mitochondrial membrane protein, Tom20, with the N-terminal half of Venus and the C-terminal half conjugated to the ER protein, Sec63. Formation of the tether is permitted when the organelles come into close contact, allowing the two Venus halves to recombine and fluoresce. Figure based on Shai et al. (4)

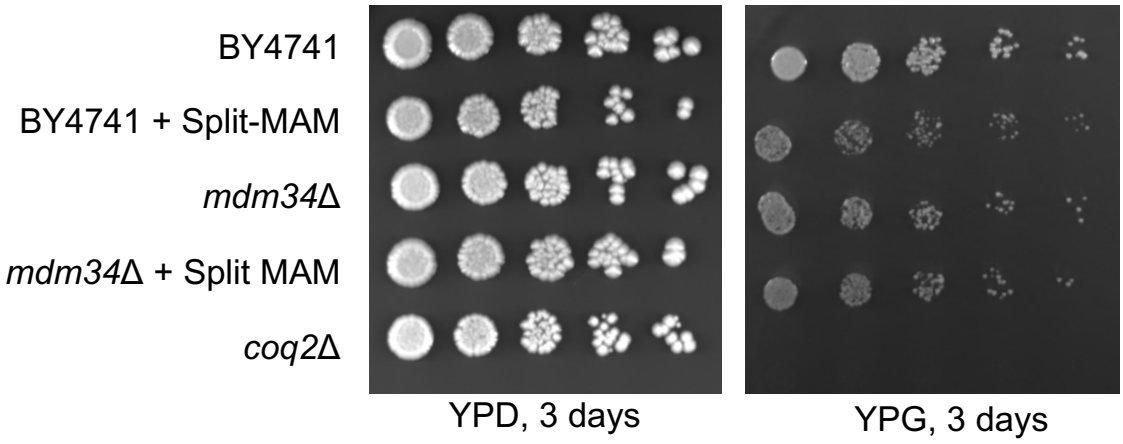

Figure 2. Growth on respiratory medium is unaltered in strains expressing Split-MAM compared to strains without the artificial tether. Drop dilution assay was performed as described in *Experimental Procedures*. The *coq2*Δ strain was included as a negative control, as it is unable to grow on the nonfermentable medium, YPGlycerol (YPG). Images are representative of three biological replicates.

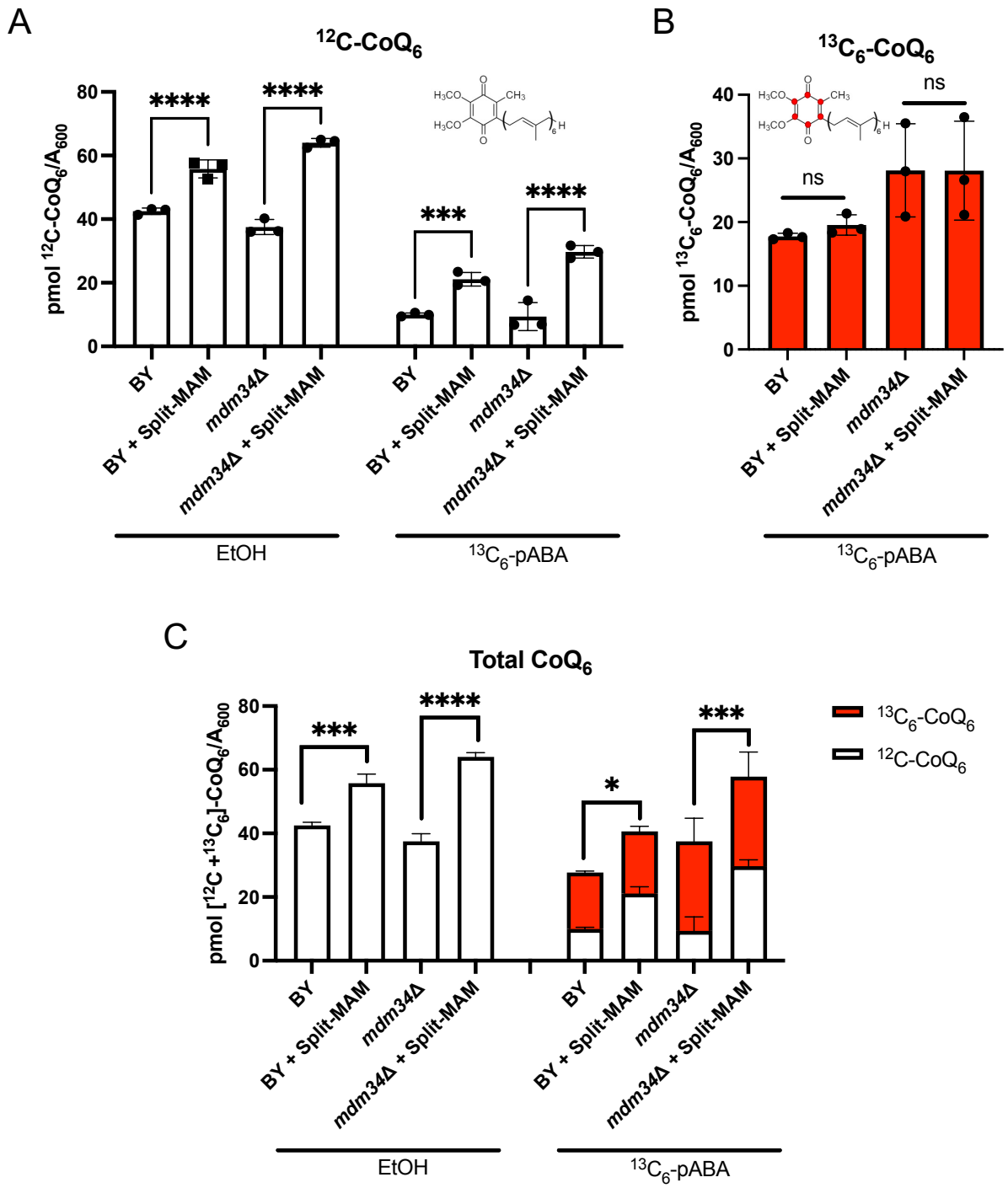

Figure 3. CoQ_6 content is augmented with the expression of Split-MAM, but *de novo* CoQ_6 content remains unchanged. Triplicate cultures of the indicated strains were grown in YPG and treated with either $^{13}C_6$-pABA or ethanol vehicle control. *A*, Unlabeled ^{12}C-CoQ_6 and *B*, labeled $^{13}C_6$-CoQ_6 were measured from whole cell lipid extracts. *C*, Total CoQ_6 was determined by

taking the sum of ^{12}C-CoQ_6 and $^{13}C_6$-CoQ_6. Data show mean ± SD of three biological replicates, where each data point is the average of three technical lipid extractions. Statistical significance is represented by *, $p < 0.05$; ***, $p < 0.001$; ****, $p < 0.0001$; or ns, no significance.

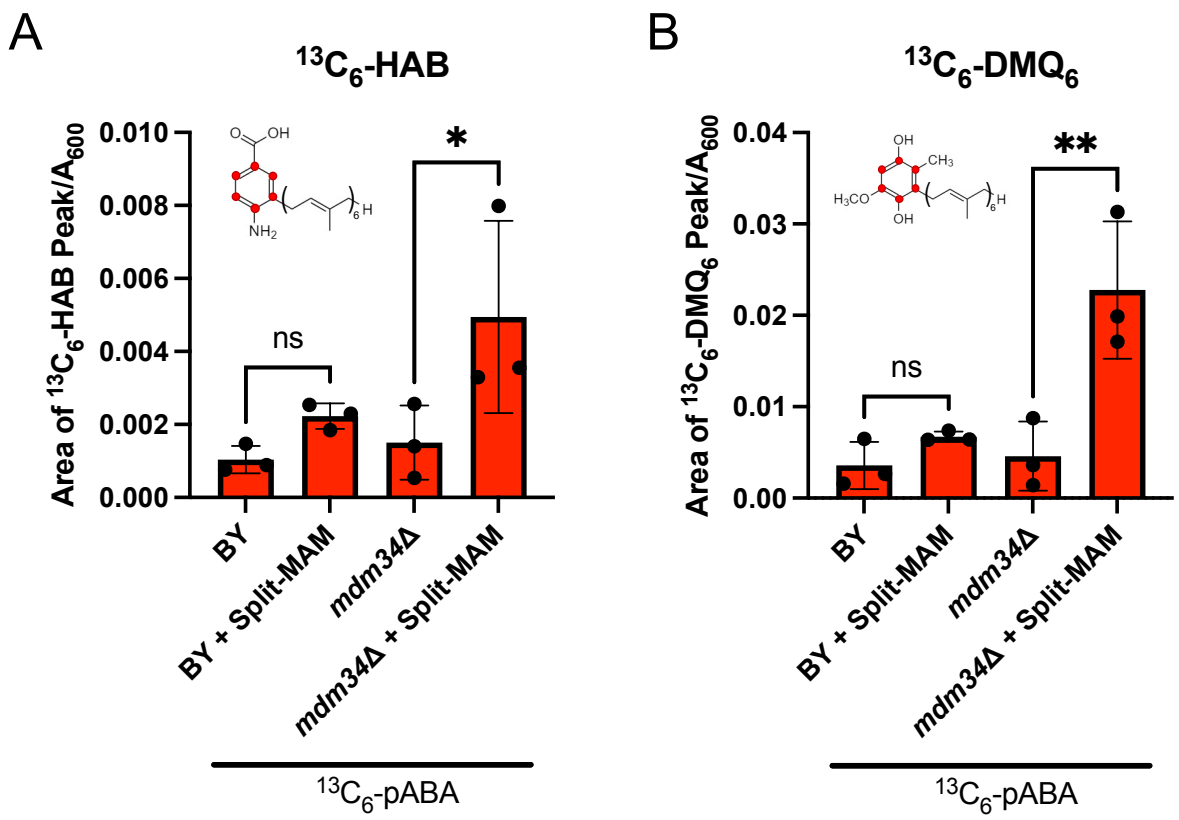

Figure 4. *De novo* synthesized intermediates are elevated in *mdm34*Δ mutant with Split-MAM. Triplicate cultures of the indicated strains were grown in YPG and treated with either $^{13}C_6$-pABA or ethanol vehicle control. Relative analyte levels are represented as peak area normalized to A_{600}. Intermediate levels of ^{13}C-ring labeled *A*, hexaprenyl-aminobenzoic acid (HAB) and *B*, demethoxy-Q$_6$ (DMQ$_6$, right) are only elevated in the *mdm34*Δ strain expressing Split-MAM relative to without the tether. Data show mean ± SD of three biological replicates, where each data point is the average of three technical lipid extractions. Statistical significance is represented by *, $p < 0.05$; **, $p < 0.01$; or ns, no significance.

REFERENCES

1. Bernhard, W., and Rouiller, C. (1956) Close topographical relationship between mitochondria and ergastoplasm of liver cells in a definite phase of cellular activity. *The Journal of Biophysical and Biochemical Cytology*. **2**, 73–78
2. Pan, X., Roberts, P., Chen, Y., Kvam, E., Shulga, N., Huang, K., Lemmon, S., and Goldfarb, D. S. (2000) Nucleus–Vacuole Junctions in *Saccharomyces cerevisiae* Are Formed Through the Direct Interaction of Vac8p with Nvj1p. *MBoC*. **11**, 2445–2457
3. Eisenberg-Bord, M., Shai, N., Schuldiner, M., and Bohnert, M. (2016) A Tether Is a Tether Is a Tether: Tethering at Membrane Contact Sites. *Developmental Cell*. **39**, 395–409
4. Shai, N., Yifrach, E., Van Roermund, C. W. T., Cohen, N., Bibi, C., IJlst, L., Cavellini, L., Meurisse, J., Schuster, R., Zada, L., Mari, M. C., Reggiori, F. M., Hughes, A. L., Escobar-Henriques, M., Cohen, M. M., Waterham, H. R., Wanders, R. J. A., Schuldiner, M., and Zalckvar, E. (2018) Systematic mapping of contact sites reveals tethers and a function for the peroxisome-mitochondria contact. *Nat Commun*. **9**, 1761
5. Zung, N., and Schuldiner, M. (2020) New horizons in mitochondrial contact site research. *Biological Chemistry*. **401**, 793–809
6. Veeresh, P., Kaur, H., Sarmah, D., Mounica, L., Verma, G., Kotian, V., Kesharwani, R., Kalia, K., Borah, A., Wang, X., Dave, K. R., Rodriguez, A.-M., Yavagal, D. R., and Bhattacharya, P. (2019) Endoplasmic reticulum–mitochondria crosstalk: from junction to function across neurological disorders. *Annals of the New York Academy of Sciences*. **1457**, 41–60
7. Wilson, E. L., and Metzakopian, E. (2021) ER-mitochondria contact sites in

neurodegeneration: genetic screening approaches to investigate novel disease mechanisms. *Cell Death Differ*. **28**, 1804–1821

8. Kornmann, B., Currie, E., Collins, S. R., Schuldiner, M., Nunnari, J., Weissman, J., and Walter, P. (2009) An ER-Mitochondria Tethering Complex Revealed by a Synthetic Biology Screen. *Science*. **325**, 477–481

9. Csordás, G., Renken, C., Várnai, P., Walter, L., Weaver, D., Buttle, K. F., Balla, T., Mannella, C. A., and Hajnóczky, G. (2006) Structural and functional features and significance of the physical linkage between ER and mitochondria. *The Journal of Cell Biology*. **174**, 915–921

10. Scorrano, L., De Matteis, M. A., Emr, S., Giordano, F., Hajnóczky, G., Kornmann, B., Lackner, L. L., Levine, T. P., Pellegrini, L., Reinisch, K., Rizzuto, R., Simmen, T., Stenmark, H., Ungermann, C., and Schuldiner, M. (2019) Coming together to define membrane contact sites. *Nat Commun*. **10**, 1287

11. Prinz, W. A., Toulmay, A., and Balla, T. (2020) The functional universe of membrane contact sites. *Nat Rev Mol Cell Biol*. **21**, 7–24

12. Kudla, J., and Bock, R. (2016) Lighting the Way to Protein-Protein Interactions: Recommendations on Best Practices for Bimolecular Fluorescence Complementation Analyses. *Plant Cell*. **28**, 1002–1008

13. Eisenberg-Bord, M., Tsui, H. S., Antunes, D., Fernández-del-Río, L., Bradley, M. C., Dunn, C. D., Nguyen, T. P. T., Rapaport, D., Clarke, C. F., and Schuldiner, M. (2019) The Endoplasmic Reticulum-Mitochondria Encounter Structure Complex Coordinates Coenzyme Q Biosynthesis. *Contact*. **2**, 2515256418825409

14. Subramanian, K., Jochem, A., Le Vasseur, M., Lewis, S., Paulson, B. R., Reddy, T. R.,

Russell, J. D., Coon, J. J., Pagliarini, D. J., and Nunnari, J. (2019) Coenzyme Q biosynthetic proteins assemble in a substrate-dependent manner into domains at ER–mitochondria contacts. *Journal of Cell Biology*. **218**, 1353–1369

15. Guerra, R. M., and Pagliarini, D. J. (2023) Coenzyme Q biochemistry and biosynthesis. *Trends in Biochemical Sciences*. **48**, 463–476

16. Baker Brachmann, C., Davies, A., Cost, G. J., Caputo, E., Li, J., Hieter, P., and Boeke, J. D. (1998) Designer deletion strains derived from Saccharomyces cerevisiae S288C: A useful set of strains and plasmids for PCR-mediated gene disruption and other applications. *Yeast*. **14**, 115–132

17. Yan Tong, A. H., and Boone, C. (2006) Synthetic Genetic Array Analysis in Saccharomyces cerevisiae. *Methods in Molecular Biology*. **313**, 171–192

18. Tsui, H. S., Pham, NguyenV. B., Amer, B. R., Bradley, M. C., Gosschalk, J. E., Gallagher-Jones, M., Ibarra, H., Clubb, R. T., Blaby-Haas, C. E., and Clarke, C. F. (2019) Human COQ10A and COQ10B are distinct lipid-binding START domain proteins required for coenzyme Q function. *Journal of Lipid Research*. **60**, 1293–1310

19. Awad, A. M., Bradley, M. C., Fernández-del-Río, L., Nag, A., Tsui, H. S., and Clarke, C. F. (2018) Coenzyme Q10 deficiencies: pathways in yeast and humans. *Essays in Biochemistry*. **62**, 361–376

20. Hsieh, E. J., Gin, P., Gulmezian, M., Tran, U. C., Saiki, R., Marbois, B. N., and Clarke, C. F. (2007) Saccharomyces cerevisiae Coq9 polypeptide is a subunit of the mitochondrial coenzyme Q biosynthetic complex. *Archives of Biochemistry and Biophysics*. **463**, 19–26

21. Novales, N. A., Feustel, K. J., and Clarke, C. F. (2024) Nonfunctional coq10 mutants

maintain the ERMES complex and reveal true phenotypes associated with the loss of the coenzyme Q chaperone protein Coq10. *Journal of Biological Chemistry, In Review*

22. AhYoung, A. P., Jiang, J., Zhang, J., Khoi Dang, X., Loo, J. A., Zhou, Z. H., and Egea, P. F. (2015) Conserved SMP domains of the ERMES complex bind phospholipids and mediate tether assembly. *Proc. Natl. Acad. Sci. U.S.A.* 10.1073/pnas.1422363112

23. Wozny, M. R., Di Luca, A., Morado, D. R., Picco, A., Khaddaj, R., Campomanes, P., Ivanović, L., Hoffmann, P. C., Miller, E. A., Vanni, S., and Kukulski, W. (2023) In situ architecture of the ER–mitochondria encounter structure. *Nature*. **618**, 188–192

24. Wu, H., Carvalho, P., and Voeltz, G. K. (2018) Here, there, and everywhere: The importance of ER membrane contact sites. *Science*. **361**, eaan5835

25. Winzeler, E. A., Shoemaker, D. D., Astromoff, A., Liang, H., Anderson, K., Andre, B., Bangham, R., Benito, R., Boeke, J. D., Bussey, H., Chu, A. M., Connelly, C., Davis, K., Dietrich, F., Dow, S. W., El Bakkoury, M., Foury, F., Friend, S. H., Gentalen, E., Giaever, G., Hegemann, J. H., Jones, T., Laub, M., Liao, H., Liebundguth, N., Lockhart, D. J., Lucau-Danila, A., Lussier, M., M'Rabet, N., Menard, P., Mittmann, M., Pai, C., Rebischung, C., Revuelta, J. L., Riles, L., Roberts, C. J., Ross-MacDonald, P., Scherens, B., Snyder, M., Sookhai-Mahadeo, S., Storms, R. K., Véronneau, S., Voet, M., Volckaert, G., Ward, T. R., Wysocki, R., Yen, G. S., Yu, K., Zimmermann, K., Philippsen, P., Johnston, M., and Davis, R. W. (1999) Functional Characterization of the *S. cerevisiae* Genome by Gene Deletion and Parallel Analysis. *Science*. **285**, 901–906

Chapter 5

Perspectives

This work explored the relationship between CoQ biosynthesis and membrane contact sites. ER-mitochondrial membrane contact sites, specifically those mediated by the ER-mitochondria encounter structure (ERMES), are able to modulate the assembly of the CoQ synthome, which can be represented by CoQ domains (1, 2). The spatial relationship between ERMES and the CoQ synthome was proposed to be coordinated by the Coq10 polypeptide, as deletion of *COQ10* results in reduced colocalization between the foci representative of each complex (1). Coq10 is not an essential polypeptide for CoQ synthesis, as *coq10*Δ yeast still produce CoQ, but in significantly reduced amounts compared to the wild type (3, 4). Instead, Coq10 is proposed to serve as a CoQ chaperone, enabled through its steroidogenic acute regulatory protein-related lipid transfer (START) domain that is capable of binding CoQ and CoQ-intermediates (5, 6). The *COQ10* open reading frame is positioned adjacent to the *MDM12* gene, which encodes the cytosolic subunit of ERMES, and the *COQ10* and *MDM12* genes are co-expressed via a shared bidirectional promoter (5, 7, 8). This arrangement within the yeast genome suggests a functional relationship between the respective gene products. In Chapter 2, we discover that deletion of *COQ10* impacts the expression of *MDM12*, as yeast lacking Coq10 contain severely attenuated Mdm12 protein levels. Using CRISPR-generated *coq10* point mutants, we separate the phenotypes resulting from the loss of Coq10 from those associated with ERMES disruption by impairing Coq10 and preserving ERMES protein content. We show that the CoQ biosynthetic defects previously observed in the *coq10*Δ deletion mutant are a consequence of ERMES dysfunction, as the CRISPR-engineered *coq10* point mutants retain the ability to synthesize CoQ and form a stable CoQ synthome. Rather, Coq10 uses its START domain to solely facilitate respiration, as both CRISPR-engineered *coq10* point mutants are unable to grow on nonfermentable medium. While this work clarified the role of Coq10, it

illuminated a more direct relationship between ERMES and CoQ synthesis, as the preservation of ERMES in the *coq10* point mutants maintained efficient CoQ biosynthesis and CoQ synthome assembly.

Previous work has demonstrated that *coq10*Δ deletion mutant phenotypes, including those attributed to loss of ERMES, can be mitigated by the deletion of the *COQ11* open reading frame (9) (Appendix I). The Coq11 polypeptide is also a nonessential Coq protein, as deletion of *COQ11* results in lowered CoQ content, however the *coq11*Δ deletion mutant maintains the ability to grow on respiratory medium (9, 10). The *coq11*Δ mutant possesses an enhanced CoQ synthome, which can be observed biochemically using two-dimensional Blue Native/SDS-PAGE (2D BN/SDS-PAGE) or via imaging analysis using a GFP-tagged Coq9 polypeptide as an indicator of CoQ domains (2, 9). From these analyses, the function of Coq11 is proposed to be a negative modulator of CoQ synthome assembly. We rationalized that if the deletion of *COQ11* rescues defects of the *coq10*Δ mutant, phenotypes that we now know are due to ERMES dysfunction (11), that the *coq11* mutation may also correct *ERMES*Δ defects (Chapter 3). Indeed, we show that the *mmm1*Δ*coq11*Δ double mutant regains the ability to grow on respiratory medium compared to the *mmm1*Δ mutant. Using 2D BN/SDS-PAGE and fluorescence microscopy, we show that the CoQ synthome and representative CoQ domains are also restored in the *mmm1*Δ*coq11*Δ mutant, but this enhanced assembly of the CoQ metabolon does not result in more efficient CoQ synthesis. Our results suggest that while the presence of ERMES is necessary for proper CoQ synthome stability, the reliance on ERMES for complex formation can be compensated by deletion of *COQ11*. Overall, this work further reinforced the notion that Coq11 modulates assembly of the CoQ synthome and is required for efficient CoQ biosynthesis, and identified the deletion of *COQ11* as a novel suppressor of *ERMES* defects.

The CoQ synthome resides exclusively in the mitochondrial matrix, and ERMES tethers the outer mitochondrial membrane to the ER. This arrangement prompts the question: how is CoQ trafficked across the intermembrane space (IMS)? Recently, two IMS-localized proteins have been implicated in facilitating the mobilization of CoQ from the mitochondrial matrix to non-mitochondrial membranes (12). These proteins, named CoQ distribution proteins 1 and 2 (Cqd1 and Cqd2), are homologs to the Coq8 polypeptide, and reciprocally regulate the distribution of CoQ in and out of the mitochondria. Specifically, deletion of *CQD1* results in excess export of CoQ out of the mitochondrial membranes, as determined by lipid analyses of subcellular fractions, and deletion of *CQD2* results in insufficient CoQ export out of the mitochondria, as indicated by sensitivity to lipid peroxidation via treatment with exogenous polyunsaturated fatty acids (12). It is of note that the Cqd proteins are peripherally associated to the inner mitochondrial membrane facing the IMS (12), so their mode of mobilizing CoQ would still require a mechanism to bring the inner and outer mitochondrial membranes in close proximity, or additional partner proteins may be required for this putative transport pathway. Interestingly, co-deletion of *CQD1* and *CQD2* resulted in normal intracellular CoQ distribution, indicating that there are redundant IMS-localized CoQ trafficking proteins that have yet to be identified.

Prior to being named Cqd2, the *YLR253W* gene product was named Mcp2, (Mdm10 complementing protein 2) (13). Overexpression of *MCP1* and *MCP2* resulted in altered phospholipid content in the *mdm10*Δ mutant, which may contribute to the rescued growth on nonfermentable medium (13). The Mcp1 protein, an integral outer mitochondrial membrane protein, colocalizes with Vps13, a protein that is commonly known to develop mutations that suppress *ERMES* mutant defects (14), which together recruit the vacuole and mitochondria patch

(vCLAMP) that tethers mitochondria to the vacuole. Overexpression of vCLAMP has been shown to cause the mitochondrial cristae organizing system (MICOS) to migrate from ERMES contact sites to vacuolar-mitochondrial contact sites (15), which is likely how *MCP1* overexpression compensates *ERMES* mutant defects. On the other hand, it remains unclear how lipid homeostasis modulated by Mcp2 was able to rescue *mdm10*Δ defects, as it resides in the IMS. Tan et al. note that they were unable to detect any physical interaction between Mcp2 and ERMES components using various pull-down assays, so they instead propose that Mcp2 may provide an alternate pathway for lipid flow that does not require ERMES (13). The CoQ domains were also found to colocalize with contact sites marked by a redundant ER-mitochondrial contact site, Ltc1 (lipid transfer at contact site 1), which could suggest that the coordination of CoQ synthome assembly is not specific to ERMES, but rather any membrane contact site (2). Additionally, the deletion of both *MDM34* and *LTC1* is synthetic lethal, indicating they likely fulfill similar roles and can compensate for the other when one is deleted (16). In this model, Ltc1 could serve as an auxiliary pathway for lipid transport, as *in vitro* lipid transfer assays using liposomes have demonstrated Ltc1 is capable of binding and transporting lipids, but preferentially sterols (16). Together, it is imperative to continue the pursuit of elucidating CoQ transport mechanisms, via the IMS-localized Cqd proteins, unidentified IMS trafficking proteins, or auxiliary mitochondrial membrane contact sites in general.

Akin to the deletion of *COQ11*, the overexpression of *COQ8* and its human homologs has also been shown to rescue CoQ synthome assembly and boost CoQ synthesis (17, 18). Given the homology with Cqd1 and Cqd2, and the ability for *CQD2* overexpression to complement *mdm10*Δ mutants (13), it may also be interesting to investigate if overexpression of *COQ8* can ameliorate *ERMES* mutant phenotypes. The ATPase activity required for Coq8 function is

stimulated by the presence of cardiolipin (19), and in an *in vitro* reconstitution of the CoQ metabolon, COQ8 is able to streamline CoQ biosynthesis in the presence of all other COQ metabolon members (20). These data suggest that Coq8 may promote CoQ synthome assembly and subsequent CoQ synthesis at sites enriched with cardiolipin. The enrichment of cardiolipin modulates membrane curvature (21), which could result in more membrane apposition of the inner and outer mitochondrial membranes. In this model, it may not be required to have a soluble lipid transporter to traverse the IMS as a direct pathway from the CoQ synthome to ERMES, which could be a feasible mechanism of rescue mediated by *COQ8* overexpression. It has been noted by Bradley et al. that rescue mediated by *COQ8* overexpression requires the presence of Coq11, as overexpression of *COQ8* was able to rescue the respiratory growth defect and markedly improve CoQ biosynthesis in the *coq10*Δ deletion mutant, yet was not able to bolster CoQ biosynthesis in either the *coq11*Δ or the *coq10*Δ*coq11*Δ mutants (9). Considering the phenotypes observed in the *coq10*Δ mutant are a result of *ERMES* dysfunction, we speculate that overexpression of *COQ8* could likely rescue *ERMES* mutant phenotypes, although via a different mechanism than the rescue mediated by *COQ11* deletion.

In Chapter 4, we explore the broad concept of molecular tethers and evaluate the effect on CoQ biosynthesis when an artificial tether is expressed. Our results suggest that contact sites may dictate the fate of CoQ, as the imposition of the Split-MAM artificial tether retains "pre-existing" CoQ that may accumulate due to the inability to be exported out of the mitochondria and subsequently degraded. The expression of the Split-MAM tether also does not enhance CoQ biosynthesis, even when expressed in *mdm34*Δ yeast, which has altered efficiency of CoQ synthesis compared to the wild type. In wild-type yeast, we suspect that the expression of the Split-MAM tether does not produce an additive effect with ERMES present, as ERMES is

considered the principal ER-mitochondrial tether in yeast (22). Considering efficient CoQ biosynthesis seems to rely specifically on the presence of ERMES (1, 11), it is likely that having the Split-MAM tether is negligible when ERMES is still intact. This model would also make sense for the *mdm34*Δ mutant expressing the Split-MAM tether, as the inefficiency of CoQ biosynthesis is further exacerbated in this strain, supporting the notion that Mdm34 and ERMES specifically have a direct role in CoQ biosynthesis, one that cannot be compensated by provision of an artificial tether. Overall, this chapter illuminates the power of synthetic biology tools in studying cellular processes, and highlights that in addition to the physical tethering function, membrane contact sites have dynamic roles to maintain cellular homeostasis.

While the arsenal of tools to study membrane contact sites that currently exist are largely imaging-based, it would be interesting to engineer artificial tethers that possess functions in addition to tethering. In other words, the existing artificial tethers, such as the ChiMERA (22) or Split-Venus reporters (23), solely fulfill the function of physical tethering, however several studies have demonstrated that membrane contact sites are far more dynamic (24–27). One may argue that the dynamic functions of membrane contact sites are more important than the ability to serve as a bridge between organelles, which we have alluded in Chapter 4 using the Split-MAM tether that was unable to rescue CoQ biosynthetic defects in the *mdm34*Δ mutant. With protein structure repositories and the emerging technology used for structural prediction tools, there is vast knowledge of how proteins function and how we can engineer proteins to possess certain functions, which may be implemented in future designs of artificial tethers. These more dynamic artificial tethers could help us better understand the specific functions of tethering complexes, which in turn can reveal more insight in how organelles communicate with one another.

REFERENCES

1. Eisenberg-Bord, M., Tsui, H. S., Antunes, D., Fernández-del-Río, L., Bradley, M. C., Dunn, C. D., Nguyen, T. P. T., Rapaport, D., Clarke, C. F., and Schuldiner, M. (2019) The Endoplasmic Reticulum-Mitochondria Encounter Structure Complex Coordinates Coenzyme Q Biosynthesis. *Contact*. **2**, 2515256418825409
2. Subramanian, K., Jochem, A., Le Vasseur, M., Lewis, S., Paulson, B. R., Reddy, T. R., Russell, J. D., Coon, J. J., Pagliarini, D. J., and Nunnari, J. (2019) Coenzyme Q biosynthetic proteins assemble in a substrate-dependent manner into domains at ER–mitochondria contacts. *Journal of Cell Biology*. **218**, 1353–1369
3. Barros, M. H., Johnson, A., Gin, P., Marbois, B. N., Clarke, C. F., and Tzagoloff, A. (2005) The Saccharomyces cerevisiae COQ10 Gene Encodes a START Domain Protein Required for Function of Coenzyme Q in Respiration. *Journal of Biological Chemistry*. **280**, 42627–42635
4. Allan, C. M., Hill, S., Morvaridi, S., Saiki, R., Johnson, J. S., Liau, W.-S., Hirano, K., Kawashima, T., Ji, Z., Loo, J. A., Shepherd, J. N., and Clarke, C. F. (2013) A conserved START domain coenzyme Q-binding polypeptide is required for efficient Q biosynthesis, respiratory electron transport, and antioxidant function in Saccharomyces cerevisiae. *Biochimica et Biophysica Acta (BBA) - Molecular and Cell Biology of Lipids*. **1831**, 776–791
5. Tsui, H. S., Pham, NguyenV. B., Amer, B. R., Bradley, M. C., Gosschalk, J. E., Gallagher-Jones, M., Ibarra, H., Clubb, R. T., Blaby-Haas, C. E., and Clarke, C. F. (2019) Human COQ10A and COQ10B are distinct lipid-binding START domain proteins required for coenzyme Q function. *Journal of Lipid Research*. **60**, 1293–1310

6. Cui, T.-Z., and Kawamukai, M. (2009) Coq10, a mitochondrial coenzyme Q binding protein, is required for proper respiration in Schizosaccharomyces pombe: CoQ-binding protein in fission yeast. *FEBS Journal*. **276**, 748–759

7. Okamura, Y., Aoki, Y., Obayashi, T., Tadaka, S., Ito, S., Narise, T., and Kinoshita, K. (2015) COXPRESdb in 2015: coexpression database for animal species by DNA-microarray and RNAseq-based expression data with multiple quality assessment systems. *Nucleic Acids Research*. **43**, D82–D86

8. Hibbs, M. A., Hess, D. C., Myers, C. L., Huttenhower, C., Li, K., and Troyanskaya, O. G. (2007) Exploring the functional landscape of gene expression: directed search of large microarray compendia. *Bioinformatics*. **23**, 2692–2699

9. Bradley, M. C., Yang, K., Fernández-del-Río, L., Ngo, J., Ayer, A., Tsui, H. S., Novales, N. A., Stocker, R., Shirihai, O. S., Barros, M. H., and Clarke, C. F. (2020) COQ11 deletion mitigates respiratory deficiency caused by mutations in the gene encoding the coenzyme Q chaperone protein Coq10. *Journal of Biological Chemistry*. **295**, 6023–6042

10. Allan, C. M., Awad, A. M., Johnson, J. S., Shirasaki, D. I., Wang, C., Blaby-Haas, C. E., Merchant, S. S., Loo, J. A., and Clarke, C. F. (2015) Identification of Coq11, a New Coenzyme Q Biosynthetic Protein in the CoQ-Synthome in Saccharomyces cerevisiae. *Journal of Biological Chemistry*. **290**, 7517–7534

11. Novales, N. A., Feustel, K. J., and Clarke, C. F. (2024) Nonfunctional coq10 mutants maintain the ERMES complex and reveal true phenotypes associated with the loss of the coenzyme Q chaperone protein Coq10. *Journal of Biological Chemistry, In Review*

12. Kemmerer, Z. A., Robinson, K. P., Schmitz, J. M., Manicki, M., Paulson, B. R., Jochem, A., Hutchins, P. D., Coon, J. J., and Pagliarini, D. J. (2021) UbiB proteins regulate

cellular CoQ distribution in Saccharomyces cerevisiae. *Nat Commun*. **12**, 4769

13. Tan, T., Özbalci, C., Brügger, B., Rapaport, D., and Dimmer, K. S. (2013) Mcp1 and Mcp2, two novel proteins involved in mitochondrial lipid homeostasis. *Journal of Cell Science*. 10.1242/jcs.121244

14. John Peter, A. T., Herrmann, B., Antunes, D., Rapaport, D., Dimmer, K. S., and Kornmann, B. (2017) Vps13-Mcp1 interact at vacuole–mitochondria interfaces and bypass ER–mitochondria contact sites. *Journal of Cell Biology*. **216**, 3219–3229

15. Tirrell, P. S., Nguyen, K. N., Luby-Phelps, K., and Friedman, J. R. (2020) MICOS subcomplexes assemble independently on the mitochondrial inner membrane in proximity to ER contact sites. *Journal of Cell Biology*. **219**, e202003024

16. Murley, A., Sarsam, R. D., Toulmay, A., Yamada, J., Prinz, W. A., and Nunnari, J. (2015) Ltc1 is an ER-localized sterol transporter and a component of ER–mitochondria and ER–vacuole contacts. *Journal of Cell Biology*. **209**, 539–548

17. He, C. H., Xie, L. X., Allan, C. M., Tran, U. C., and Clarke, C. F. (2014) Coenzyme Q supplementation or over-expression of the yeast Coq8 putative kinase stabilizes multi-subunit Coq polypeptide complexes in yeast coq null mutants. *Biochimica et Biophysica Acta (BBA) - Molecular and Cell Biology of Lipids*. **1841**, 630–644

18. Xie, L. X., Hsieh, E. J., Watanabe, S., Allan, C. M., Chen, J. Y., Tran, U. C., and Clarke, C. F. (2011) Expression of the human atypical kinase ADCK3 rescues coenzyme Q biosynthesis and phosphorylation of Coq polypeptides in yeast coq8 mutants. *Biochimica et Biophysica Acta (BBA) - Molecular and Cell Biology of Lipids*. **1811**, 348–360

19. Reidenbach, A. G., Kemmerer, Z. A., Aydin, D., Jochem, A., McDevitt, M. T., Hutchins, P. D., Stark, J. L., Stefely, J. A., Reddy, T., Hebert, A. S., Wilkerson, E. M., Johnson, I.

E., Bingman, C. A., Markley, J. L., Coon, J. J., Dal Peraro, M., and Pagliarini, D. J. (2018) Conserved Lipid and Small-Molecule Modulation of COQ8 Reveals Regulation of the Ancient Kinase-like UbiB Family. *Cell Chemical Biology*. **25**, 154-165.e11

20. Nicoll, C. R., Alvigini, L., Gottinger, A., Cecchini, D., Mannucci, B., Corana, F., Mascotti, M. L., and Mattevi, A. (2024) In vitro construction of the COQ metabolon unveils the molecular determinants of coenzyme Q biosynthesis. *Nat Catal*. **7**, 148–160
21. Ikon, N., and Ryan, R. O. (2017) Cardiolipin and mitochondrial cristae organization. *Biochimica et Biophysica Acta (BBA) - Biomembranes*. **1859**, 1156–1163
22. Kornmann, B., Currie, E., Collins, S. R., Schuldiner, M., Nunnari, J., Weissman, J., and Walter, P. (2009) An ER-Mitochondria Tethering Complex Revealed by a Synthetic Biology Screen. *Science*. **325**, 477–481
23. Shai, N., Yifrach, E., Van Roermund, C. W. T., Cohen, N., Bibi, C., IJlst, L., Cavellini, L., Meurisse, J., Schuster, R., Zada, L., Mari, M. C., Reggiori, F. M., Hughes, A. L., Escobar-Henriques, M., Cohen, M. M., Waterham, H. R., Wanders, R. J. A., Schuldiner, M., and Zalckvar, E. (2018) Systematic mapping of contact sites reveals tethers and a function for the peroxisome-mitochondria contact. *Nat Commun*. **9**, 1761
24. Zung, N., and Schuldiner, M. (2020) New horizons in mitochondrial contact site research. *Biological Chemistry*. **401**, 793–809
25. Prinz, W. A., Toulmay, A., and Balla, T. (2020) The functional universe of membrane contact sites. *Nat Rev Mol Cell Biol*. **21**, 7–24
26. Wu, H., Carvalho, P., and Voeltz, G. K. (2018) Here, there, and everywhere: The importance of ER membrane contact sites. *Science*. **361**, eaan5835
27. Scorrano, L., De Matteis, M. A., Emr, S., Giordano, F., Hajnóczky, G., Kornmann, B.,

Lackner, L. L., Levine, T. P., Pellegrini, L., Reinisch, K., Rizzuto, R., Simmen, T., Stenmark, H., Ungermann, C., and Schuldiner, M. (2019) Coming together to define membrane contact sites. *Nat Commun*. **10**, 1287

Appendix I

COQ11 deletion mitigates respiratory deficiency caused by mutations in the gene encoding the coenzyme Q chaperone protein Coq10

JBC ARTICLE

COQ11 deletion mitigates respiratory deficiency caused by mutations in the gene encoding the coenzyme Q chaperone protein Coq10

Received for publication, December 20, 2019, and in revised form, March 17, 2020 Published, Papers in Press, March 23, 2020, DOI 10.1074/jbc.RA119.012420

Michelle C. Bradley[‡], Krista Yang[‡], Lucía Fernández-del-Río[‡], Jennifer Ngo[‡§], Anita Ayer[¶‖], Hui S. Tsui[‡], Noelle Alexa Novales[‡], Roland Stocker[¶‖], Orian S. Shirihai[§], Mario H. Barros[**], and Catherine F. Clarke[‡1]

From the [‡]Department of Chemistry and Biochemistry, Molecular Biology Institute, UCLA, Los Angeles, California 90095-1569, the [§]Department of Molecular and Medical Pharmacology and Medicine, David Geffen School of Medicine, UCLA, Los Angeles, California 90095, the [¶]Vascular Biology Division, Victor Chang Cardiac Research Institute, Sydney, New South Wales 2010, Australia, the [‖]St. Vincent's Clinical School, University of New South Wales Medicine, Sydney, New South Wales 2050, Australia, and the [**]Departamento Microbiologia, Universidade de São Paulo, São Paulo 05508-900, Brazil

Edited by Dennis R. Voelker

Coenzyme Q (Q_n) is a vital lipid component of the electron transport chain that functions in cellular energy metabolism and as a membrane antioxidant. In the yeast *Saccharomyces cerevisiae*, *coq1–coq9* deletion mutants are respiratory-incompetent, sensitive to lipid peroxidation stress, and unable to synthesize Q_6. The yeast *coq10* deletion mutant is also respiratory-deficient and sensitive to lipid peroxidation, yet it continues to produce Q_6 at an impaired rate. Thus, Coq10 is required for the function of Q_6 in respiration and as an antioxidant and is believed to chaperone Q_6 from its site of synthesis to the respiratory complexes. In several fungi, Coq10 is encoded as a fusion polypeptide with Coq11, a recently identified protein of unknown function required for efficient Q_6 biosynthesis. Because "fused" proteins are often involved in similar biochemical pathways, here we examined the putative functional relationship between Coq10 and Coq11 in yeast. We used plate growth and Seahorse assays and LC-MS/MS analysis to show that *COQ11* deletion rescues respiratory deficiency, sensitivity to lipid peroxidation, and decreased Q_6 biosynthesis of the *coq10*Δ mutant. Additionally, immunoblotting indicated that yeast *coq11*Δ mutants accumulate increased amounts of certain Coq polypeptides and display a stabilized CoQ synthome. These effects suggest that Coq11 modulates Q_6 biosynthesis and that its absence increases mitochondrial Q_6 content in the *coq10*Δ*coq11*Δ double mutant. This augmented mitochondrial Q_6 content counteracts the respiratory deficiency and lipid peroxidation sensitivity phenotypes of the *coq10*Δ mutant. This study further clarifies the intricate connection between Q_6 biosynthesis, trafficking, and function in mitochondrial metabolism.

Coenzyme Q (ubiquinone or Q)[2] is a benzoquinone lipid that functions as an essential electron carrier within the electron transport chain (1). Because of its redox activities, Q is a versatile electron acceptor in biological pathways such as cellular respiration, oxidation of proline and sulfide, fatty acid β-oxidation, and pyrimidine biosynthesis (1–3). The reduced hydroquinone form of Q (ubiquinol or QH_2) also serves as an important chain-breaking antioxidant shown to alleviate lipid peroxidative damage in cellular membranes (4).

For proper functional localization, Q relies on its polyisoprenoid tail to remain anchored at the mid-plane of phospholipid bilayers. The number of isoprene units (*n*) that comprise the polyisoprenoid tail of Q_n depends on a species-specific polyprenyl diphosphate synthase (5), with Q_{10} representing the major isoform in humans (6). Patients unable to produce adequate levels of Q_{10} display a wide variety of health issues that stem from mitochondrial dysfunction across tissues (7). Attempts to ameliorate the consequences of primary Q_{10} deficiency by early Q_{10} supplementation have been partially successful in some cases (8); however, many patients fail to demonstrate full recovery, which is related to inefficient uptake of orally-supplied Q_{10}. Because of the striking homology between human *COQ* genes and those of *Saccharomyces cerevisiae* (7, 9), studies of Q_6 biosynthesis in *S. cerevisiae* may provide insight

This work was supported by National Science Foundation Grant MCB-1330803 (to C. F. C.), National Institutes of Health Grant T32 GM 007185 (to H. S. T. and M. C. B.) Ruth L. Kirschstein National Service (to M. C. B. and H. S. T.), the Whitcome Individual Predoctoral Fellowship (to M. C. B.), UCLA Summer Undergraduate Research Fellowship, Department of Chemistry and Biochemistry (to K. Y.), Fundação de Amparo a Pesquisa de São Paulo–FAPESP 2013/09482-8 and 2013/07937-8 (to M. H. B.), Gates Millennium Scholars Fellowship (to J. N.), and the Eugene V. Cota Robles Fellowship (to J. N.). The authors declare that they have no conflicts of interest with the contents of this article. The content is solely the responsibility of the authors and does not necessarily represent the official views of the National Institutes of Health.
This article contains Figs. S1–S3, Tables S1 and S2, and supporting Refs. 1–8.
[1] To whom correspondence should be addressed. Tel.: 310-825-0771; Fax: 310-206-5213; E-mail: cathy@chem.ucla.edu.

[2] The abbreviations used are: Q, ubiquinone; DMQ, demethoxy-Q; HHB, 3-hexaprenyl-4-hydroxybenzoic acid; Q_n, coenzyme Q_n (where *n* designates the number of isoprene units in the polyisoprenyl tail); QH_2, reduced coenzyme Q or ubiquinol; ORF, open reading frame; ER, endoplasmic reticulum; MIOREX complex, mitochondrial organization of gene expression complex; IMS, intermembrane space; OCR, oxygen consumption rate; FCCP, carbonyl cyanide *p*-trifluoromethoxyphenylhydrazone; PUFA, polyunsaturated fatty acid; qPCR, quantitative real-time PCR; ERMES, ER-mitochondrial encounter structure; START, steroidogenic acute regulatory protein–related lipid transfer; BisTris, 2-[bis(2-hydroxyethyl)amino]-2-(hydroxymethyl)propane-1,3-diol; SDR, short-chain dehydrogenase/reductase; 2D-BN/SDS-PAGE, two-dimensional blue native/SDS-PAGE; DOD, drop-out dextrose; SD, synthetic dextrose; lc*COQ11*, low-copy *COQ11*; RET, reverse electron transport; P, pellet; S, supernatant.

into human Q_{10} biosynthesis, leading to the discovery of potential therapeutic targets.

In *S. cerevisiae*, at least 14 nuclear-encoded mitochondrial proteins (Coq1–Coq11, Yah1, Arh1, and Hfd1) drive Q_6 biosynthesis (7, 9). Many Coq polypeptides (Coq3–Coq9, and Coq11) are localized to the matrix side of the mitochondrial inner membrane, where they organize into a high-molecular-weight multisubunit complex known as the "CoQ synthome" (7, 9). Several lines of evidence suggest that correct assembly of the CoQ synthome is necessary for efficient Q_6 biosynthesis (9–12). In fact, deletion of certain *COQ* genes results in decreased levels of other Coq polypeptides and contributes to a destabilized CoQ synthome in these mutants (12, 13). Recently, a protein of unknown function encoded by the ORF *YLR290C* was identified to associate with the CoQ synthome, via proteomic analysis of tandem affinity-purified tagged Coq proteins (14). YLR290C copurified with Coq5, Coq7, and Coq9, in addition to Q_6 and late-stage Q_6-intermediates (14). Furthermore, the *ylr290c*Δ mutant exhibited impaired *de novo* Q_6 biosynthesis, despite preserving growth on a nonfermentable carbon source (14). Given its effects on Q_6 biosynthesis and involvement with the CoQ synthome, YLR290C was renamed Coq11 (14).

In several fungi, Coq11 and Coq10 have evolved as fusion proteins (14), suggesting that Coq11 may have a functional relationship with Coq10 (15). High-throughput genetic analyses found *COQ11* to correlate with both *COQ2* and *COQ10* (16). Whereas the *coq* mutants generally lack Q_6, the *coq10*Δ mutant is different because it produces near WT amounts of Q_6 in stationary phase and only has decreased *de novo* Q_6 biosynthesis in log phase (17, 18). Although Q_6 biosynthesis is only minimally decreased in the absence of *COQ10*, the *coq10*Δ mutant has decreased NADH and succinate oxidase activity and displayed sickly growth on respiratory medium (18). The *coq10*Δ mutant is sensitive to lipid peroxidation initiated by exogenously supplemented polyunsaturated fatty acids (PUFAs), indicating that the Coq10 polypeptide is also required for antioxidant protection by Q_6 (17, 19).

The NMR structure of a Coq10 ortholog in *Caulobacter crescentus* was shown to possess a steroidogenic acute regulatory protein–related lipid transfer (START) domain (20) that can directly bind Q and late-stage Q-intermediates (17). Purified Coq10 from either *S. cerevisiae* or *Schizosaccharomyces pombe* eluted with the respective species' Q isoform (18, 21). This observation has prompted speculation that Coq10 acts as a Q_6 chaperone protein required for delivery of Q_6 from its synthesis site to sites where Q_6 functions as an antioxidant and to the respiratory complexes, thereby bridging efficient *de novo* Q_6 biosynthesis with respiration (17). Recent studies have shown a spatial compartmentalization of the mitochondrial inner membrane with the identification of different sites, such as the inner boundary membrane, the cristae membrane, and the ER-mitochondrial contact sites (22–25). Thus, for optimal respiratory competence, newly-synthesized Q_6 must move from its site of synthesis (*i.e.* the ER-mitochondrial contact sites (23, 24)) to the cristae membrane where the respiratory complexes are concentrated (22). The presence of Coq10–Coq11 fusions in fungal species indicates that Coq11 may have a functional association with the Coq10 chaperone to facilitate or regulate Q_6 transport for respiration in yeast.

In this work, the functional relationship between Coq10 and Coq11 was investigated using a series of single- and double-knockout mutants. Deletion of *COQ11* alleviated the *coq10*Δ respiratory defect, increased Coq polypeptides and CoQ synthome stability, and partially rescued Q_6 production. Based on this evidence, we propose a novel function for Coq11 as a negative modulator of Q_6 biosynthesis in the mitochondria.

Results

Coq10 and Coq11 reside in similar compartments within the mitochondria

Previous phylogenetic analyses of numerous fungi revealed that Coq11-like proteins are fused to Coq10 (14). Protein fusions often indicate a functional relationship between corresponding homologs in other organisms, such as direct protein–protein interaction or operation within the same biological pathway (15). Although Coq10 and Coq11 are not physically fused in yeast (Fig. 1*A*), we sought to investigate whether there is a functional link between the two proteins. Because protein localization is often associated with function, we first performed mitochondrial fractionation to localize both Coq10 and Coq11. Coq10 has been localized previously (18), but fractionation was re-performed here in the context of Coq11.

S. cerevisiae mitochondria were fractionated as described under "Experimental procedures." Purified mitochondria were incubated in hypotonic buffer to disrupt the outer membrane and release soluble components of the intermembrane space (IMS). The inner membrane was kept intact following hypotonic buffer treatment, protecting inner membrane and matrix proteins. Analysis of the fractions via immunoblot suggested that both Coq10 and Coq11 remained associated with the mitoplast fraction as opposed to colocalizing with the IMS marker cytochrome b_2. Mitoplasts were further fractionated after sonication to separate soluble matrix components (supernatant, S) from membrane components (pellet, P). The soluble matrix marker Hsp60 was partially released into the supernatant by sonication as demonstrated in earlier work (26). Although Coq11 remained associated with the membrane fraction, Coq10 was partially dissociated in a similar manner to Hsp60 (Fig. 1*B*). Previous Coq10 colocalization following sonication demonstrated that Coq10 was solely associated with the membrane fraction (18). The detection of Coq10 in the supernatant shown in Fig. 1*B* may be due to increased sensitivity of the polyclonal antisera used in this study.

Alternatively, mitoplasts were subjected to alkaline carbonate extraction to separate peripheral membrane components (supernatant, S) from integral membrane and matrix components (pellet, P) (27). Coq10 and Coq11 were released into the supernatant following alkaline treatment (Fig. 1*B*), matching the peripheral inner membrane marker Atp2 (28). There was no colocalization with the pellet fraction, marked by the integral membrane protein Cyt_1 (29). These results indicate that Coq10 and Coq11 are both peripheral inner membrane proteins, and Coq10 has additional localization to the matrix. The localization of Coq10 to the inner membrane is consistent with

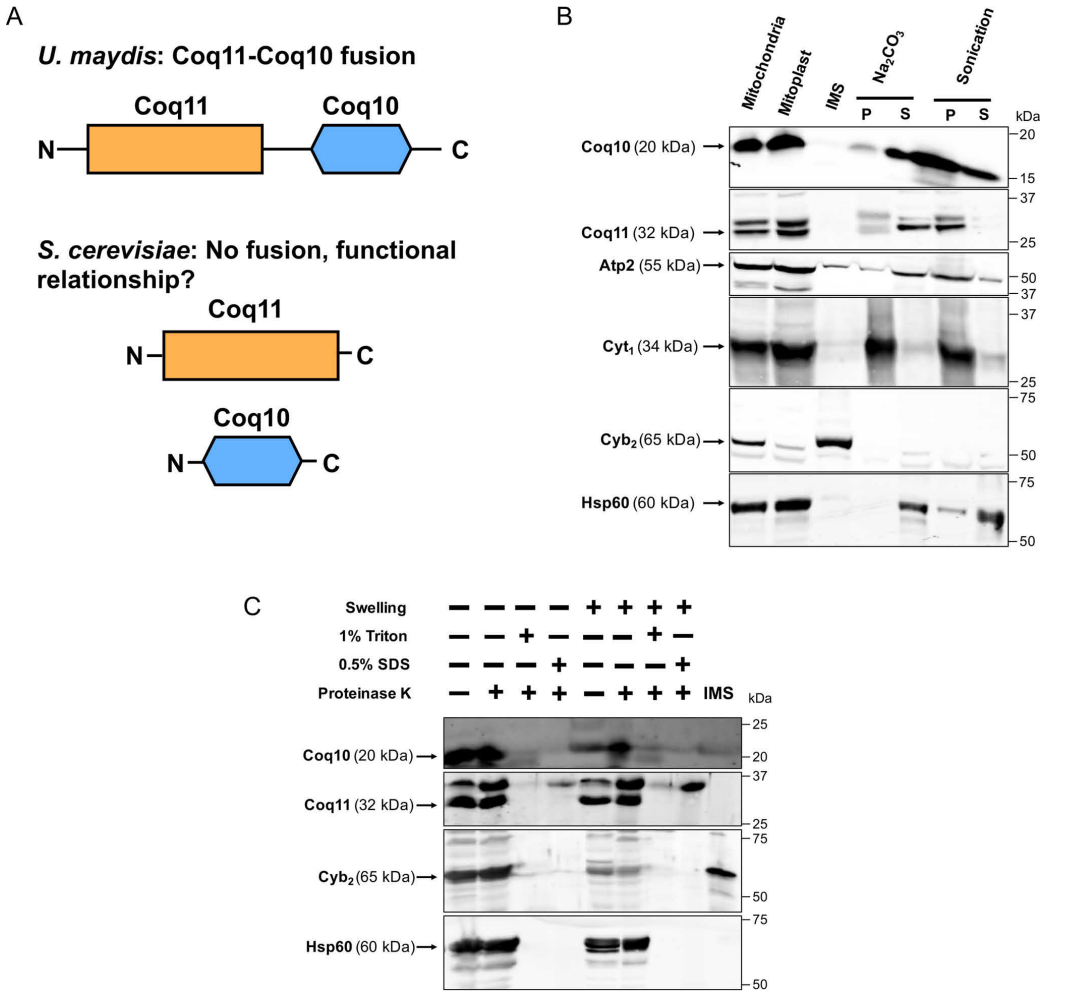

Figure 1. Coq11 and Coq10 are peripherally associated with the mitochondrial inner membrane facing the matrix, and Coq10 is additionally found in the mitochondrial matrix. *A*, Coq10 and Coq11 are fused in multiple fungi, suggesting an evolutionarily functional relationship between these proteins, although they are not found fused in *S. cerevisiae*. *B*, *S. cerevisiae* mitochondria purified from yeast strains cultured on YPGal medium were subjected to hypotonic swelling and centrifugation to separate the IMS proteins from mitoplasts. The mitoplasts were alkaline-treated (Na_2CO_3; pH 11.5) or sonicated and then separated by centrifugation (100,000 × *g* for 1 h) into supernatant (S) or pellet (P) fractions. *C*, intact mitochondria or mitoplasts were treated with 100 μg/ml proteinase K for 30 min on ice, with or without detergent. Mitochondrial polypeptide markers are as follows: *Atp2*, peripheral inner membrane protein; *Cyb*$_2$, intermembrane space protein; *Cyt*$_1$, integral inner membrane protein; and *Hsp60*, soluble matrix protein. Results are representative of two experiments.

its putative role as a START domain protein possessing a hydrophobic cavity to bind and chaperone Q_6 from its site of synthesis to complex III for respiration (17, 18). We hypothesize that dual mitochondrial matrix localization occurs when Coq10 is tightly bound to protein partners to decrease its hydrophobicity.

For better insight into the membrane association of Coq10 and Coq11, intact mitochondria or mitoplasts were treated with proteinase K in the absence or presence of two individual detergents (1% Triton X-100 or 0.5% SDS). Coq10 and Coq11 were both protected from protease treatment in purified mitochondria and mitoplasts, as was the matrix marker Hsp60 (Fig. 1*C*). When protease was used in the presence of either detergent in mitochondria or mitoplasts, all proteins became sensitive to the protease and were degraded. Expanding on the subfractionation results, these data indicate that Coq10 and Coq11 polypeptides are peripherally associated with the inner membrane facing the matrix side in yeast mitochondria, and Coq10 is also found in the mitochondrial matrix itself. The mitochondrial peripheral membrane association of these two proteins is also in agreement with their submitochondrial localization previously identified in a study of the yeast mitochondrial proteome (30).

Table 1
Genotype and source of yeast strains

Strain	Genotype	Source
W303-1B	MAT α *ade2-1 his3-1,15 leu2-,112trp1-1 ura3-1*	R. Rothstein[a]
BY4742	MAT α *his3Δ0 leu2Δ0 met15Δ0 ura3Δ0*	53
JM6	*MAT a his-4* ρ^0	68
JM8	*MAT* α *ade-1* ρ^0	68
BY4742 *coq1*Δ	MAT α *his3Δ0 leu2Δ0 met15Δ0 ura3Δ0 coq1::KanMX4*	69
BY4741 *coq2*Δ	MAT **a** *his3Δ0 leu2Δ0 met15Δ0 ura3Δ0 coq2::KanMX4*	69
BY4742 *coq3*Δ	MAT α *his3Δ0 leu2Δ0 met15Δ0 ura3Δ0 coq3::KanMX4*	69
BY4742 *coq4*Δ	MAT α *his3Δ0 leu2Δ0 met15Δ0 ura3Δ0 coq4::KanMX4*	69
BY4742 *coq5*Δ	MAT α *his3Δ0 leu2Δ0 met15Δ0 ura3Δ0 coq5:: KanMX4*	69
BY4741 *coq6*Δ	MAT **a** *his3Δ0 leu2Δ0 met15Δ0 ura3Δ0 coq6::KanMX4*	Dharmacon, Inc.
BY4742 *coq7*Δ	MAT α *his3Δ0 leu2Δ0 met15Δ0 ura3Δ0 coq7::KanMX4*	69
BY4742 *coq8*Δ	MAT α *his3Δ0 leu2Δ0 met15Δ0 ura3Δ0 coq8::KanMX4*	69
BY4742 *coq9*Δ	MAT α*his3Δ0 leu2Δ0 met15Δ0 ura3Δ0 coq9::KanMX4*	69
BY4742 *coq10*Δ	MAT α *his3Δ0 leu2Δ0 met15Δ0 ura3Δ0 coq10::KanMX4*	69
BY4742 *coq11*Δ	MAT α *his3Δ0 leu2Δ0 met15Δ0 ura3Δ0 coq11::LEU2*	This work
BY4742 *coq10*Δ*coq11*Δ	MAT α *his3Δ0 leu2Δ0 met15Δ0 ura3Δ0 coq10::HIS3 coq11::LEU2*	This work
W303 *coq10*Δ	MAT α *ade2-1 his3-1,15 leu2-3,112trp1-1 ura3-1 coq10::HIS3*	18
W303 *coq10*Δ	MAT **a** *ade2-1 his3-1,15 leu2-3,112trp1-1 ura3-1 coq10::HIS3*	18
W303 *coq10*rev	MAT α *ade2-1 his3-1,15 leu2-3,112trp1-1 ura3-1 coq10::HIS3 sup*	This work
MB-10	Diploid produced from W303 **a** *coq10*Δ x W303 α *coq10*Δrev	This work
W303 *coq11*Δ	MAT α *ade2-1 his3-1,15 leu2-3,112trp1-1 ura3-1 coq11::LEU2*	This work
W303 *coq10*Δ*coq11*Δ	MAT α *ade2-1 his3-1,15 leu2-3,112trp1-1 ura3-1 coq10::HIS3 coq11::LEU2*	This work
BY4741 *cor1*Δ	MAT **a** *his3Δ0 leu2Δ0 met15Δ0 ura3Δ0 cor1::KanMX4*	69

[a] Gift from Dr. Rodney Rothstein Department of Human Genetics, Columbia University.

coq10Δ respiratory defect is alleviated by deletion of COQ11

Based on similar mitochondria localization and genetic evolutionary evidence, a putative functional relationship between Coq10 and Coq11 was further probed using a series of *coq10* and *coq11* single- and double-knockout mutants. Strain descriptions are listed in Table 1. The Coq10 polypeptide is required for respiration in yeast, and mutants lacking *coq10* have poor growth on nonfermentable carbon sources, including YPGlycerol, hereafter referred to as "YPG" (18). Unlike deletion of *COQ10*, *coq11*Δ mutants are respiratory-capable and have comparable growth to WT on nonfermentable carbon sources (14). When *COQ11* was deleted in a *coq10*Δ mutant in two different yeast genetic backgrounds, the sickly growth of *coq10*Δ on nonfermentable YPG was rescued (Fig. 2*A*).

Quantitative respiratory capacity of each mutant was evaluated with an XF96 Extracellular Flux Analyzer (Fig. 2, *B* and *C*). Representative and normalized traces of oxygen consumption rates (OCR) of four independent experiments performed in nonrepressive medium (YPGal) are shown in Fig. 2*B*. Basal rates of OCR were measured prior to the addition of any small molecule inhibitors. Consistent with its slow growth on nonfermentable medium, the *coq10*Δ mutant had a low rate of basal oxygen consumption compared with WT ($p = 0.052$) (Fig. 2*C*). Basal OCR was rescued in the *coq10*Δ*coq11*Δ double mutant (Fig. 2*C*). Following the addition of two sequential injections of FCCP, a mitochondrial oxidative phosphorylation uncoupler, maximal respiration was also quantified. The maximal respiration of *coq10*Δ*coq11*Δ was rescued to that of WT (Fig. 2*C*). These results show that the deletion of *COQ11* in a *coq10*Δ mutant confers a beneficial effect, such that both growth on respiratory medium and OCR are rescued to WT.

Deletion of COQ11 rescues PUFA sensitivity of the coq10Δ mutant

PUFA autoxidation is initiated by the radical-mediated abstraction of vulnerable hydrogen atoms at bis-allylic positions (31). The ensuing carbon-centered radical adds to molecular oxygen to form a lipid peroxyl radical that propagates lipid peroxidation, with the resulting lipid hydroperoxides ultimately driving cellular toxicity (32). The *coq10*Δ mutant is sensitive to treatment with exogenous PUFAs (Fig. 2*D*) (17, 19), likely because the Q_6 chaperone function of Coq10 is required for the antioxidant function of Q_6. Attenuated respiration in *coq10*Δ is rescued in the *coq10*Δ*coq11*Δ double knockout (Fig. 2, *A–C*), presumably through regained function of Q_6 in the electron transport chain. To test whether the antioxidant capability of Q_6 is also restored in the *coq10*Δ*coq11*Δ mutant, yeast strains were evaluated for sensitivity to added PUFAs (Fig. 2*D*). As anticipated, all strains were resistant to treatment with the monounsaturated oleic acid (Fig. 2*D*). Q_6-less *coq9*Δ was sensitive to α-linolenic acid due to the lack of Q_6 antioxidant protection (Fig. 2*D*). Conversely, the Q_6-replete yet respiratory-deficient *cor1*Δ remained resistant to α-linolenic acid (Fig. 2*D*). Deletion of *COQ11* rescued the α-linolenic acid sensitivity of the *coq10*Δ mutant, suggesting that the double knockout has restored Q_6 antioxidant protection (Fig. 2*D*) despite the absence of Coq10 as a Q_6 chaperone.

Independent coq10 revertant with rescued growth on respiratory medium harbors a mutation within COQ11

Although the *coq10*Δ mutant is unable to grow robustly on nonfermentable medium, an earlier study identified a spontaneous *coq10* revertant (*coq10*rev) that arose when *coq10*Δ yeast was cultured for several weeks on nonfermentable medium containing ethanol and glycerol as carbon sources (18). Characterization of this revertant revealed a suppressor mutation within the *COQ11* ORF, resulting in a truncated Coq11 protein that is predicted to be nonfunctional (Fig. 3*A*). This mutation was further assessed for dominance to determine whether it was sufficient to explain the respiratory competence of *coq10*rev. A haploid *coq10*Δ mutant crossed with haploid *coq10*rev produced diploid MB-10 (Table 1), which was capable of growth on respiratory medium (Fig. 3*B*). Illustrated growth

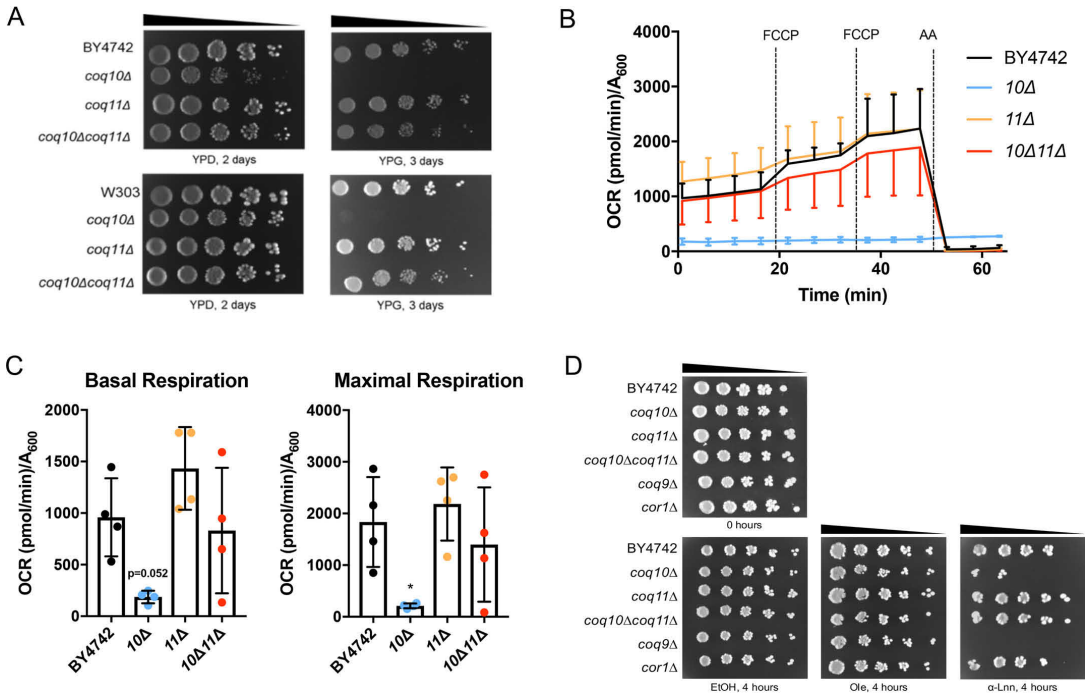

Figure 2. *COQ11* deletion rescues the lack of growth on YPG, low-oxygen consumption rates, and lost Q_6 antioxidant protection in the *coq10Δ* mutant. *A*, strains were grown overnight in 5 ml of YPD, diluted to an A_{600} = 0.2 with sterile PBS, and 2 μl of 5-fold serial dilutions were spotted onto fermentable (YPDextrose, *YPD*) or respiratory (YPGlycerol, *YPG*) medium, corresponding to a final A_{600} = 0.2, 0.04, 0.008, 0.0016, and 0.00032. Plates were incubated at 30 °C, and growth was captured after 2 or 3 days. *B* and *C*, quadruplicates of 25-ml cultures of WT, *coq10Δ*, *coq11Δ*, and *coq10Δcoq11Δ* yeast were grown in YPGal until they reached A_{600} ~4. Yeast were diluted to an A_{600} = 0.1 in fresh YPGal and collected by centrifugation on poly-D-lysine-coated Seahorse XF96 microplates to assess oxygen consumption. *B*, representative traces of OCR of yeast strains with the XF96 extracellular flux analyzer. FCCP and antimycin A (*AA*) were sequentially added to evaluate mitochondrial respiratory states. Measurements were taken approximately every 4 min, as represented by *points* and their respective *error bars*. Four independent experiments were performed (Fig. S1), and each group of average traces represents 8–10 technical replicates. *C*, quantification of basal and maximal (maximal electron transport activity induced by the uncoupler FCCP) OCR as obtained from four independent experiments (Fig. S1). The data show the mean ± S.D., and the statistical significance as compared with WT is represented by *, $p < 0.05$. *D*, deletion of *COQ11* in the *coq10Δ* rescues PUFA sensitivity. Results are representative of three experiments.

patterns suggest that the *coq11* truncated allele present in *coq10*rev is a dominant-negative mutation. Because the dominant mutation in *coq10*rev restores growth on respiratory medium via a functionally suppressive Coq11 truncation mutation, this mutant effectively validates the *coq10Δcoq11Δ* phenotype in an independent system.

Deletion of COQ11 fails to fully restore coq10Δ Q_6 biosynthesis in whole cells

When a *coq* mutant displays anemic growth on respiratory medium, it is often indicative of inefficient Q_6 biosynthesis (7, 9); yeast lacking *COQ10* exhibit both poor growth on respiratory medium and decreased Q_6 biosynthesis in log phase whole cells (17, 19). Although the *coq11Δ* mutant retains the ability to grow on nonfermentable medium, it is also characterized by impaired Q_6 biosynthesis (14). Only a small amount of Q_6 is required for growth on respiratory medium, ~0.2–3% of the total Q_6 found in WT (9, 33, 34). Because the *coq10Δcoq11Δ* double mutant has rescued respiration, we wanted to assess whether recovered growth was accompanied by increased Q_6 biosynthesis. Whole-cell *de novo*–synthesized $[^{13}C_6]Q_6$ and $[^{12}C]Q_6$ were measured in yeast by feeding the quinone ring-labeled precursor, $[^{13}C_6]$4HB, or EtOH vehicle control (Fig. 4). These analyses were performed in the fermentable, nonrepressive YPGal medium (35) to match the conditions of experiments involving purified mitochondria.

Consistent with previous results (14, 17), *coq10Δ* and *coq11Δ* had significantly decreased *de novo*-synthesized $[^{13}C_6]Q_6$ and $[^{12}C]Q_6$ compared with WT (Fig. 4*A*). The *coq10Δ* mutant had a lower total Q_6 content ($[^{13}C_6]Q_6$ + $[^{12}C]Q_6$) than WT and also a lower total Q_6 than *coq11Δ* (Fig. 4*B*). Deletion of *COQ11* in *coq10Δ* yeast led to a slight increase in *de novo*-synthesized $[^{13}C_6]Q_6$ and unchanged $[^{12}C]Q_6$ compared with *coq10Δ* (Fig. 4*A*). Therefore, the *coq10Δcoq11Δ* double mutant presented total Q_6 contents that were significantly lower than either WT or *coq11Δ* (Fig. 4*B*). Given the robust growth of the *coq10Δcoq11Δ* double mutant on YPG, restored respiration, and resistance to PUFA treatment, the low Q_6 concentrations observed are surprising.

Next, we quantified the concentrations of key Q_6-intermediates in the same whole-cell yeast pellets. As shown previously

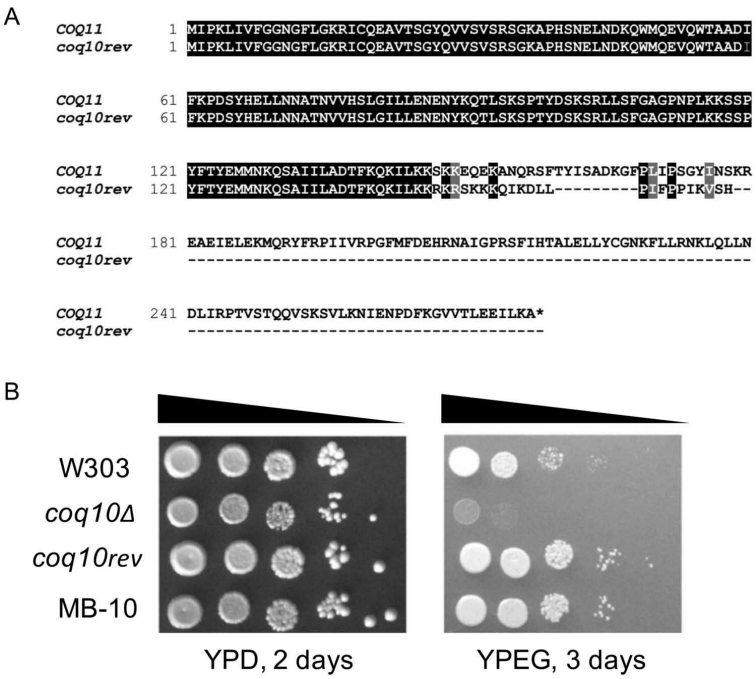

Figure 3. Spontaneous *coq10* revertant with rescued respiratory capacity was identified to possess a base-pair deletion in *COQ11*, encoding a truncated Coq11 protein. *A*, alignment of the amino acid sequence of WT *COQ11* ORF with the *coq11* allele (*coq10rev*) present in the *coq10* revertant. *B*, growth properties of WT were compared with *coq10* mutants and diploid MB-10 (defined in Table 1). Strains were grown overnight in 8 ml of YPDextrose (*YPD*), diluted to an $A_{600} = 0.2$ with sterile PBS, and 2 μl of 5-fold serial dilutions were spotted onto fermentable YPD or respiratory (YPEGlycerol (*YPEG*)) medium, corresponding to a final $A_{600} = 0.2$, 0.04, 0.008, 0.0016, and 0.00032. Plates were incubated at 30 °C, and growth was captured after 2 or 3 days. Results are representative of three experiments.

(17, 19), the *coq10*Δ mutant contained lower amounts of the late-stage intermediate [$^{13}C_6$]DMQ$_6$ and [^{12}C]DMQ$_6$ (Fig. 4*C*) than WT, and it accumulated the early-stage intermediate [$^{13}C_6$]HHB and [^{12}C]HHB (Fig. 4*D*). In contrast to *coq10*Δ, the *coq11*Δ mutant mirrored WT production of both *de novo*-synthesized and unlabeled early- and late-stage intermediates (Fig. 4, *C* and *D*), as shown previously (14). Q$_6$-intermediate trends in *coq10*Δ*coq11*Δ matched those of the *coq10*Δ mutant rather than *coq11*Δ (Fig. 4, *C* and *D*). The low Q$_6$ content and accumulation of early-stage Q$_6$-intermediates in the *coq10*Δ*coq11*Δ double knockout suggest the absence of *COQ10* still produces a notable effect on Q$_6$ biosynthesis, although respiratory capacity is rescued.

*coq10*Δ*coq11*Δ *double mutant has increased mitochondrial Q$_6$ compared with the coq10*Δ *single mutant*

Although Q$_6$ biosynthesis solely occurs within mitochondria, it is found in all cellular membranes (9). Therefore, Q$_6$ was quantified in both whole cells and purified mitochondria from mutant and WT cells cultured under the same conditions (36). Whole-cell Q$_6$ determined under mitochondrial purification conditions matched those determined in Figs. 4 and 5*A*. The *coq10*Δ*coq11*Δ double mutant made slightly more Q$_6$ than the *coq10*Δ single mutant, but overall less Q$_6$ compared with the *coq11*Δ single mutant. All mutants had lower whole-cell Q$_6$ amounts than WT (Fig. 5*A*).

Similarly, mitochondrial Q$_6$ content per microgram of mitochondrial protein was lower in *coq11*Δ than WT (Fig. 5*B*). However, deletion of *COQ11* in the *coq10*Δ mutant increased the mitochondrial Q$_6$ 5-fold (Fig. 5*B*). Despite these profound differences in mitochondrial Q$_6$ content, mitochondrial mass was consistent between strains as determined by three distinct assays (Fig. 5, *C–E*). Increased mitochondrial Q$_6$ in the *coq10*Δ*coq11*Δ double mutant compared with *coq10*Δ indicates that the absence of *COQ11* in part rescues defective Q$_6$ synthesis in the *coq10*Δ mutant.

*Low Coq protein content and destabilized CoQ synthome of the coq10*Δ *mutant are restored in the coq10*Δ*coq11*Δ *double mutant*

Proper formation of the CoQ synthome from component Coq polypeptides is required for efficient Q$_6$ biosynthesis in yeast (9, 12, 13). Deletion of *COQ10* causes a decrease in several other Coq polypeptides, including Coq3–Coq7, Coq9, as well as overall CoQ synthome destabilization (12, 13, 19). These results were confirmed when purified mitochondria from *coq10*Δ yeast were analyzed for each Coq polypeptide (Fig. 6*A*). The *coq10*Δ mutant had significantly decreased amounts of Coq3,

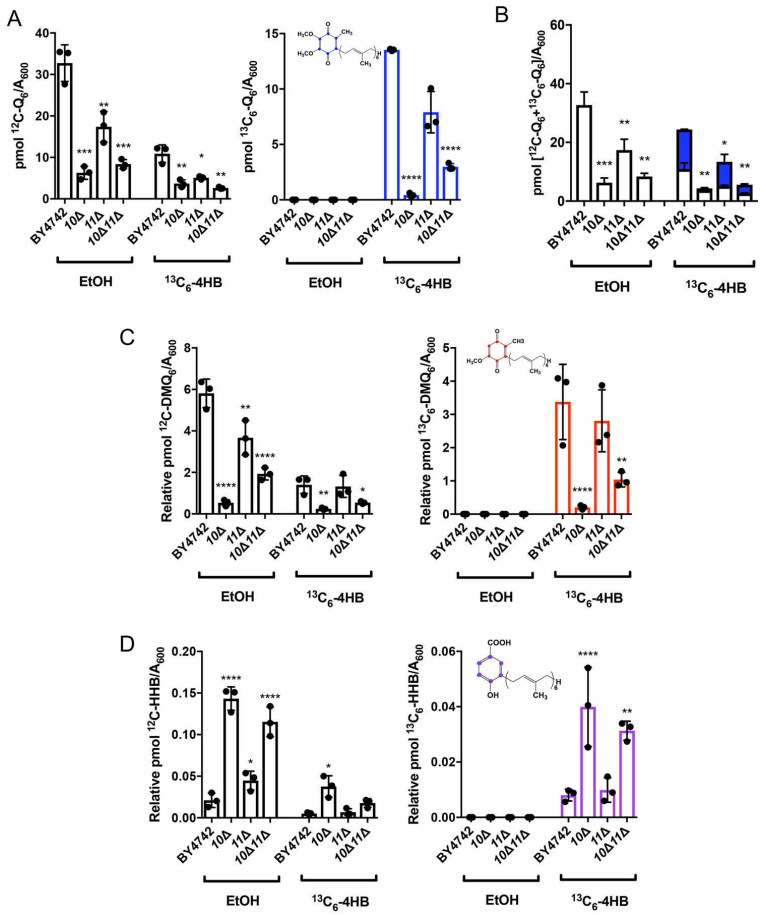

Figure 4. Low amounts of *de novo* [$^{13}C_6$]Q_6 in whole-cell lipid extracts of the *coq10*Δ mutant are only partially restored by deletion of *COQ11*. Triplicates of 6-ml cultures in YPGal were labeled at A_{600} ~1 with 5 μg/ml [$^{13}C_6$]4HB or EtOH vehicle control, and 5 ml of each culture were collected after 4 h, lipid-extracted, and analyzed by LC-MS/MS. *A*, unlabeled [^{12}C]Q_6 and *de novo*–synthesized [$^{13}C_6$]Q_6 (*blue*); *B*, total amount of Q_6 determined from the sum of [$^{13}C_6$]Q_6 and [^{12}C]Q_6; *C*, [^{12}C]DMQ$_6$ and [$^{13}C_6$]DMQ$_6$ (*red*); and *D*, [^{12}C]HHB and [$^{13}C_6$]HHB (*purple*) were measured from the whole-cell lipid extracts of WT and the *coq10*Δ, *coq11*Δ, and *coq10*Δ*coq11*Δ mutants. Values are the mean of three replicates. The data show mean ± S.D., and the statistical significance as compared with WT is represented by *, $p < 0.05$; ***, $p < 0.001$; and ****, $p < 0.0001$.

Coq4, Coq7, and Coq9 compared to and plotted as a percentage of WT (Fig. 6*B*).

In contrast to *coq10*Δ, the *coq11*Δ single mutant had elevated Coq4, Coq6, Coq7, and Coq9 (Fig. 6*A*), with protein quantification shown in Fig. 6*B*. Furthermore, the *coq10*Δ*coq11*Δ double mutant also had raised amounts of Coq4, Coq7, and Coq9 polypeptides compared with WT (Fig. 6, *A* and *B*). This increase in Coq proteins could not be explained by enhanced *COQ* transcription as there was no corresponding change in the concentration of the respective mRNAs, (Fig. 6*C*), although *COQ4* mRNA was not detected.

CoQ synthome formation was probed using two-dimensional blue native/SDS-PAGE (2D-BN/SDS-PAGE) with Coq4 and Coq9 serving as sensitive indicators of a high-molecular-weight complex (13). As expected, the CoQ synthome in WT yeast presented as a heterogeneous high-molecular-weight complex, spanning a range of ~140 kDa to >1 MDa for Coq4 (Fig. 7*A*) and from ~100 kDa to >1 MDa for Coq9 (Fig. 7*B*). Consistent with prior results (13, 19), the *coq10*Δ mutant displayed a highly-destabilized CoQ synthome, with a disappearance of large complexes that were replaced by lower-molecular-weight subcomplexes less than ~440 kDa for Coq4 (Fig. 7*A*) and less than ~232 kDa for Coq9 (Fig. 7*B*). The *coq11*Δ mutant had a stabilized CoQ synthome compared with WT, with high-molecular-weight complexes shifting to the left and collapsing into a more homogeneous complex spanning ~900 kDa to >1 MDa for both Coq4 (Fig. 7*A*) and Coq9 (Fig. 7*B*). When *COQ11* was deleted in combination with *COQ10*, there was a substantial rescue of high-molecular-weight complex formation compared with the *coq10*Δ single mutant (Fig. 7, *A* and *B*). The CoQ

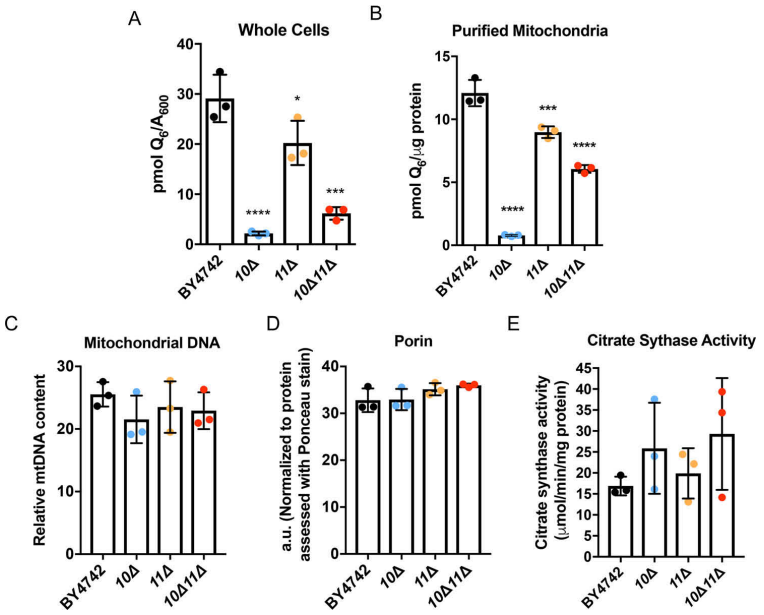

Figure 5. Deletion of *COQ11* in the *coq10*Δ mutant enhances mitochondrial Q_6 content. Triplicates of 30-ml cultures of WT, *coq10*Δ, *coq11*Δ, and *coq10*Δ*coq11*Δ yeast were grown in YPGal until they reached A_{600} ~4. *A*, 5 ml of whole cells from each culture were harvested, lipid-extracted, and analyzed by LC-MS/MS for Q_6 content. Alternatively, WT, *coq10*Δ, *coq11*Δ, and *coq10*Δ*coq11*Δ yeasts were grown in YPGal until they reached A_{600} ~4 and were subjected to mitochondrial preparation. *B*, lipids from triplicates of purified mitochondria (100 μg) were analyzed by LC-MS/MS for Q_6 content. *C–E*, mitochondrial mass was estimated using three distinct methods. *C*, relative mitochondrial DNA to actin was quantified by qPCR. *D*, porin protein amounts were quantified by hand using ImageStudioLite following immunoblot and normalized to total protein levels evaluated by Ponceau stain. *E*, citrate synthase activity was determined using a colorimetric assay as outlined under "Experimental procedures." Values are the mean of three replicates. The data show the mean ± S.D., and the statistical significance as compared with WT is represented by *, $p < 0.05$; ***, $p < 0.001$; and ****, $p < 0.0001$.

synthome of the *coq10*Δ*coq11*Δ double mutant appeared similar to that of *coq11*Δ complexes spanning ~66 kDa to > 1 MDa for Coq4 (Fig. 7*A*) and from ~66 kDa to > 1 MDa for Coq9 (Fig. 7*B*). However, the deletion of *COQ11* in *coq10*Δ does not negate the effect from the *COQ10* deletion, as it does not restore small subcomplexes <140 kDa to higher molecular weights (Fig. 7, *A* and *B*). These CoQ synthome signals for *coq11* mutants were complementary to the observed increased Coq polypeptides, indicating that the absence of *COQ11* enhanced the Q_6 biosynthetic machinery.

High-copy COQ8 does not restore Q_6 content in the coq10Δcoq11Δ single mutant

The Coq8 polypeptide is a member of an ancient atypical kinase family (37), with several conserved kinase motifs that are essential for Q biosynthesis (13, 38). Prior studies have demonstrated that overexpression of Coq8 in a *coq10*Δ mutant increased the otherwise low amounts of several key Coq polypeptides and stabilized CoQ synthome formation (13). This is similar to the phenotype observed when *COQ11* was deleted in the *coq10*Δ mutant. Furthermore, Coq8 overexpression has also been shown to influence Q_6 biosynthesis, including the restoration of late-stage Q_6-intermediates in *coq5–coq9* null mutants (39). Although the CoQ synthome of the *coq10*Δ mutant was stabilized by deletion of *COQ11*, Q_6 and late-stage Q_6-intermediates remained lower compared with WT and the *coq11*Δ single mutant (Fig. 4*C*). We hypothesized that the overexpression of Coq8 in the *coq10*Δ and *coq10*Δ*coq11*Δ mutant may restore Q_6 content in both mutants.

WT, *coq10*Δ, *coq11*Δ, and *coq10*Δ*coq11*Δ were analyzed for growth on nonfermentable medium and Q_6 biosynthesis upon transformation with high-copy *COQ8* (hc*COQ8*, Table 2) or empty vector control (Fig. 8). Similar to previous observations in a different yeast genetic background (18), *coq10*Δ-expressing hc*COQ8* regained the ability to grow on respiratory medium (Fig. 8*A*). This growth phenotype may be explained by a stabilized CoQ synthome in the *coq10*Δ mutant harboring hc*COQ8* (13). However, hc*COQ8* had no material effect on the growth properties of WT, *coq11*Δ, or *coq10*Δ*coq11*Δ strains on YPG (Fig. 8*A*).

Each strain was grown in minimal selection medium to maintain plasmid expression and was analyzed for Q_6 biosynthesis following metabolic labeling with the ring-labeled Q_6 precursor, [$^{13}C_6$]HB (Fig. 8, *B* and *C*). Changing the growth medium from rich (*i.e.* YPGal) to minimal synthetic (*i.e.* SD and dropout dextrose media (DOD)) changed the relative amounts of Q_6 content among the mutants (Figs. 4*B versus* 8*C*). Although WT [$^{13}C_6$]Q_6 and total Q_6 content is similar in Figs. 4*B* and 8*C*, the values for *coq11*Δ and the double mutant are quite different. When grown in YPGal, *coq10*Δ had the lowest Q_6 content, followed by the double mutant *coq10*Δ*coq11*Δ, with *coq11*Δ hav-

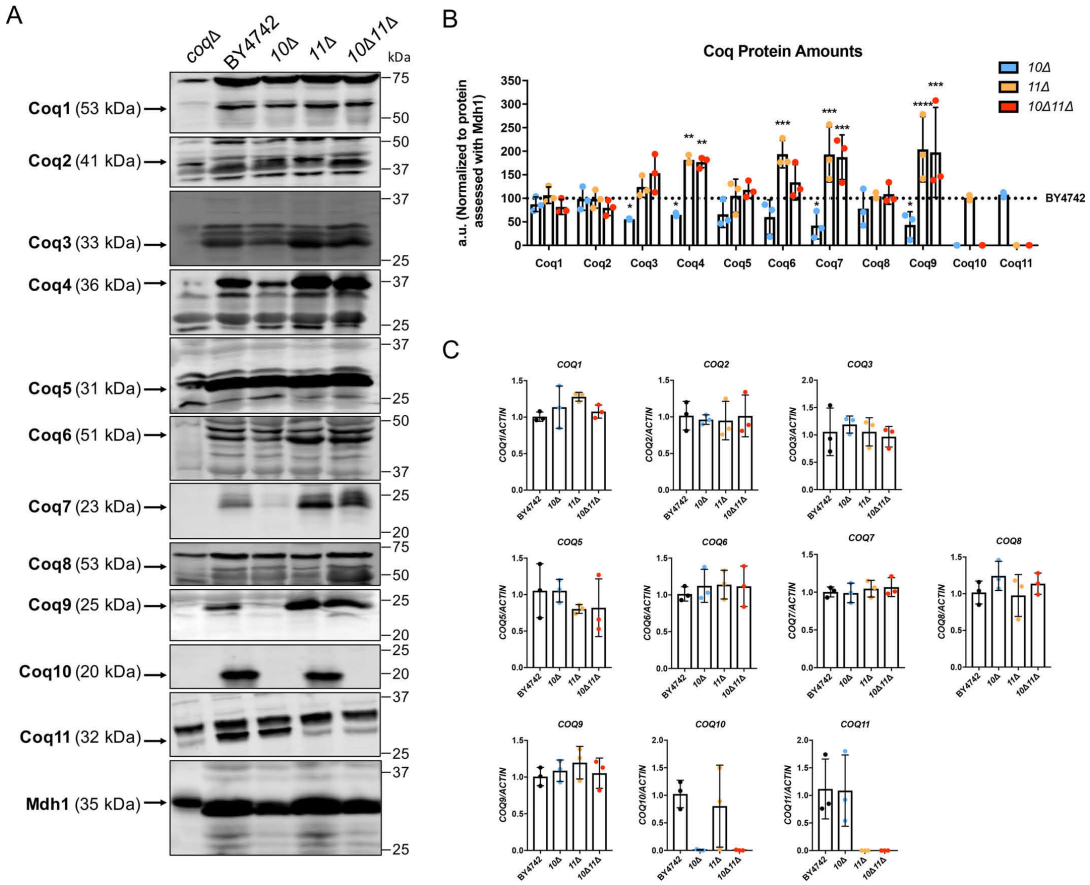

Figure 6. Several Coq polypeptides have increased abundance in *coq11*Δ and *coq10*Δ*coq11*Δ mutants compared with WT. *A*, aliquots of purified mitochondria (25 μg) from WT, *coq10*Δ, *coq11*Δ, and *coq10*Δ*coq11*Δ yeasts were subjected to 10 or 12% Tris-glycine SDS-PAGE. Mitochondrial malate dehydrogenase (Mdh1) was included as a loading control, with a representative blot shown. The Coq5 protein also serves as a qualitative loading control, because the Coq5 polypeptide amounts remain unchanged across the panel of *coq1*–*coq4* and *coq6*–*coq10* deletion mutants (12). Aliquots of purified *coq*Δ mitochondria (*coq1*Δ–*coq11*Δ) were included as negative controls for immunoblotting with antisera to each of the Coq polypeptides. *Black arrows* highlight the location of each protein on the membrane. *B*, ImageStudioLite was used to quantify triplicates of each Coq protein band's intensity by hand, which were normalized to Mdh1 and plotted as a percentage of WT. The data show mean ± S.D., and the statistical significance is as compared with WT is represented by *, $p < 0.05$; **, $p < 0.01$; ***, $p < 0.001$; and ****, $p < 0.0001$. *C*, qPCR was used to determine *COQ* gene expression from whole-cell cultures of WT, *coq10*Δ, *coq11*Δ, or *coq10*Δ*coq11*Δ, and data were normalized to actin. *COQ* RNA levels remain unchanged in the *coq10*Δ, *coq11*Δ, or *coq10*Δ*coq11*Δ mutants as compared with WT.

ing the closest Q_6 content to WT (Figs. 4, *A* and *B*, and 5*A* and Fig. S2, *A* and *B*). In contrast, when these strains are cultured in SD−Ura (Fig. 8, *B* and *C*), the double mutant *coq10*Δ*coq11*Δ had the lowest Q_6 content, as compared with either the *coq10*Δ or *coq11*Δ single mutant strains. Growth on minimal dextrose medium in the absence of plasmid selection produced similar trends (Fig. S2, *C* and *D*, and Fig. S3, *A* and *B*).

Upon Coq8 overexpression, *coq10*Δ had increased *de novo*-synthesized $[^{13}C_6]Q_6$ and $[^{12}C]Q_6$ (Fig. 8*B*), and total Q_6 concentrations ($[^{13}C_6]Q_6 + [^{12}C]Q_6$) were restored to those of WT (Fig. 8*C*). This finding is consistent with previous results, which also indicated that hc*COQ8* restored Q biosynthesis and amounts of Coq polypeptides and the CoQ synthome in the *coq10*Δ mutant (13, 17, 18). Intriguingly, expression of hc*COQ8* had no effect on *de novo* or unlabeled Q_6 content in either the *coq11*Δ single mutant or the *coq10*Δ*coq11*Δ double mutant (Fig. 8*B*). Total Q_6 contents of both *coq11*Δ and *coq10*Δ*coq11*Δ remained significantly decreased compared with WT (Fig. 8*C*). Together, these results show that the rescue of the *coq10*Δ mutant mediated by Coq8 overexpression requires Coq11.

*Expression of low-copy COQ11 rescues only some of the phenotypes of the coq10*Δ*coq11*Δ *mutant*

The functional complementation of *coq11*Δ single and *coq10*Δ*coq11*Δ double mutants with low-copy *COQ11* was assessed (lc*COQ11*, Table 2). As expected, the *coq10*Δ mutant, *coq10*Δ with empty vector, and *coq10*Δ complemented with lc*COQ11* showed slow growth on the nonfermentable carbon

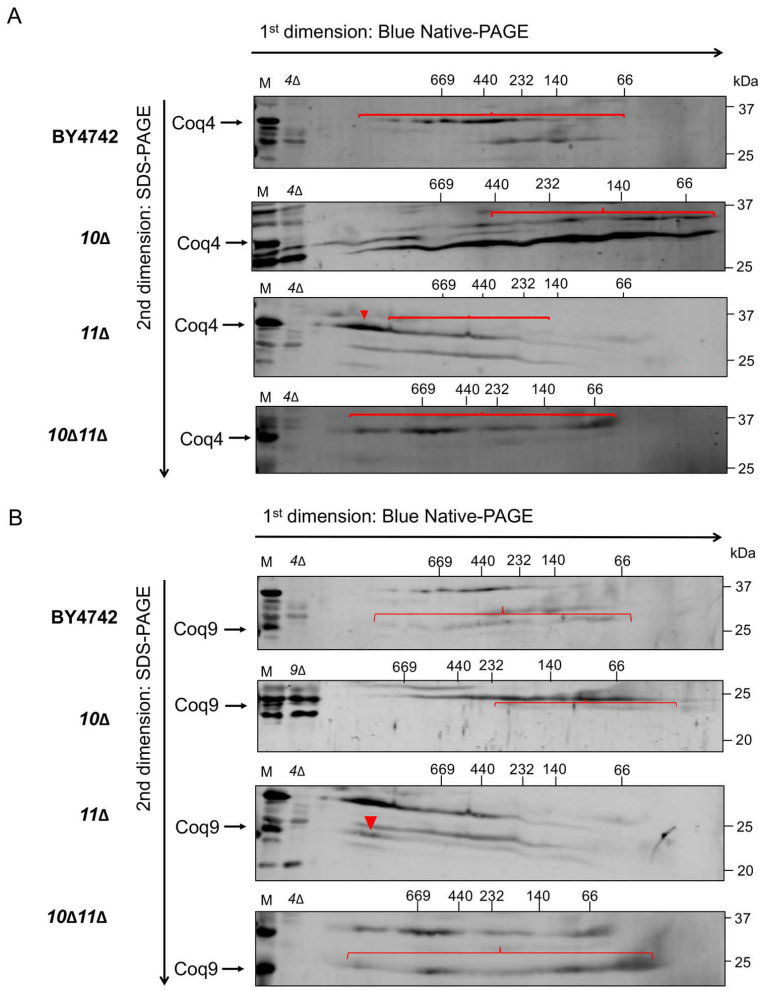

Figure 7. Deletion of *COQ11* in the *coq10*Δ mutant restores the CoQ synthome. Aliquots (100 μg) of purified mitochondria from WT, *coq10*Δ, *coq11*Δ, and *coq10*Δ*coq11*Δ yeasts cultured in YPGal were solubilized with digitonin and separated with two-dimensional BN/SDS-PAGE. Following transfer of proteins to membranes, the CoQ synthome was visualized as a heterogeneous signal from ~66 to ~669 kDa in WT control with antibodies to *A*, Coq4, or *B*, Coq9. Intact mitochondria (25 μg) from each designated strain was included as a loading control (*M*). Aliquots of *coq4*Δ- or *coq9*Δ-purified mitochondria (25 μg) were included as a negative control for the antisera to Coq4 and Coq9, as the Coq9 polypeptide is absent from the *coq4*Δ mutant. *Red arrowheads* and *brackets* indicate distinct complexes.

Table 2
Yeast expression vectors

Plasmid	Relevant genes/markers	Source
pRS305	Yeast vector with *LEU2* marker	70
pRS313	Yeast vector with *HIS3* marker	70
pRS316	Yeast shuttle vector; low-copy	70
lc*COQ11*	pRS316 with yeast *COQ11*; low-copy	This work
pRS426	Yeast shuttle vector; multi-copy	71
p4HN4	pRS426 with yeast *COQ8*; multi-copy	12

source YPGlycerol (Fig. 9*A*). Because yeast lacking *COQ11* retain respiratory capacity (Fig. 2) (14), *coq11*Δ complemented with lc*COQ11* had no detectable change in growth phenotype compared with either the *coq11*Δ mutant or *coq11*Δ with empty vector (Fig. 9*A*). Intriguingly, when lc*COQ11* was expressed in the *coq10*Δ*coq11*Δ double mutant, there was no repression of growth on YPG compared with that of the *coq10*Δ mutant (Fig. 9*A*).

This observation suggests that Q_6 biosynthesis in *coq10*Δ *coq11*Δ may not be affected by lc*COQ11*. To determine the effect of lc*COQ11* expression on mutant Q_6 biosynthesis, yeast was grown in selection medium to maintain plasmid expression. We tested whether lc*COQ11* expression rescued Q_6 content in the *coq11*Δ mutant. Expression of lc*COQ11* in *coq11*Δ efficiently rescued total Q_6 ($[^{13}C_6]Q_6$ + $[^{12}C]Q_6$) to WT amounts (Fig. 9*B*).

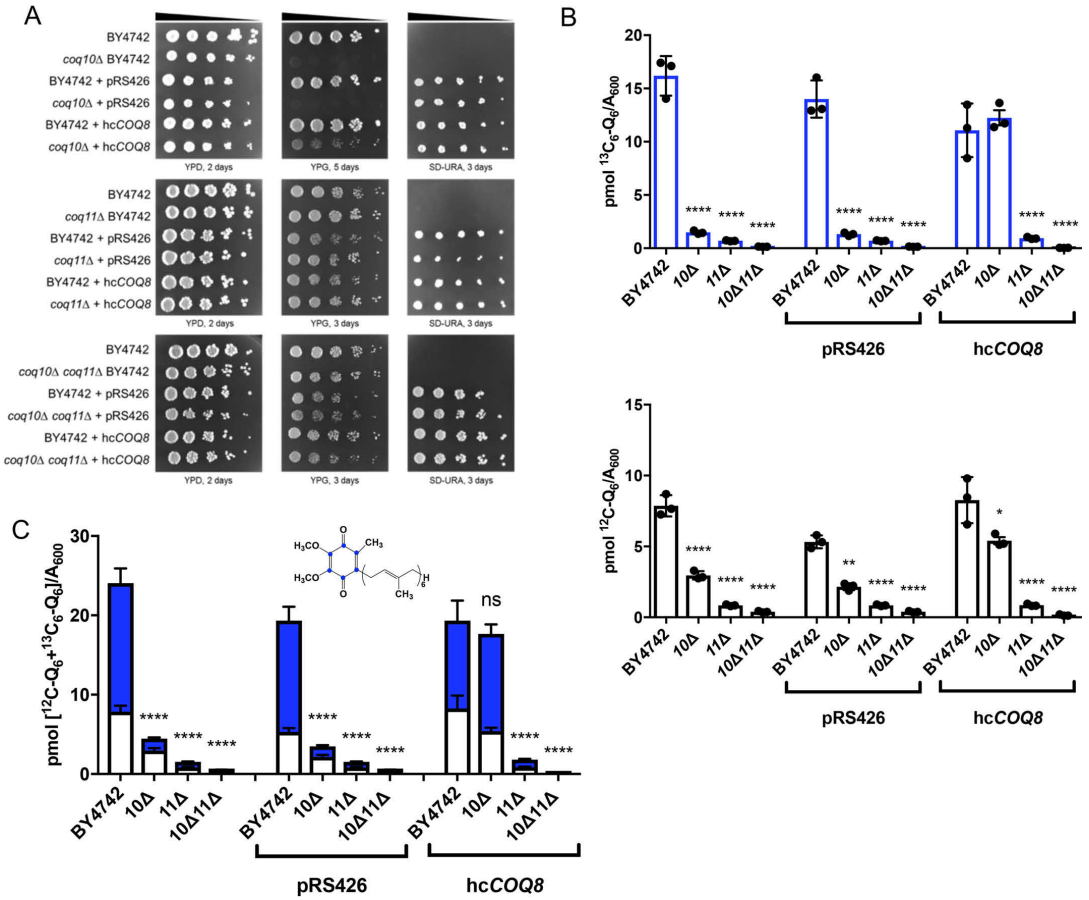

Figure 8. Overexpression of the CoQ synthome stabilizer, *COQ8*, has no effect on Q_6 synthesis in the *coq10Δcoq11Δ* mutant. WT, *coq10Δ*, *coq11Δ*, and *coq10Δcoq11Δ* mutants were transformed with high-copy *COQ8* (hc*COQ8*) or empty vector (pRS426) plasmids. *A*, strains were grown overnight in 5 ml of selection medium, diluted to an $A_{600} = 0.2$ with sterile PBS, and 2 μl of 5-fold serial dilutions were spotted onto YPD, YPG, or selection medium (SD−Ura), corresponding to a final $A_{600} = 0.2$, 0.04, 0.008, 0.0016, and 0.00032. Plates were incubated at 30 °C, and growth was captured after 2 or 3 days. Triplicates of 5 ml of culture in selection medium were labeled with 5 μg/ml [$^{13}C_6$]4HB, collected after 4 h, lipid-extracted, and analyzed by LC-MS/MS. *B*, [^{12}C]Q_6 (*white*) and *de novo* [$^{13}C_6$]Q_6 (*blue*). *C*, total amount of Q_6 was also plotted from the sum of [$^{13}C_6$]Q_6 and [^{12}C]Q_6. The values are the means of three replicates. The data show mean ± S.D., and the statistical significance as compared with WT is represented by *, $p < 0.05$; **, $p < 0.01$; ***, $p < 0.001$; and ****, $p < 0.0001$. The *ns* signifies that values are not significantly different from WT.

Finally, whole-cell steady-state Q_6 concentrations were evaluated in all mutants. Even though lc*COQ11* complementation did not suppress *coq10Δcoq11Δ* growth on YPGlycerol (Fig. 9*A*), Q_6 concentrations were increased in *coq10Δcoq11Δ* to a level comparable with that of *coq10Δ* (Fig. 9*C*). This implies that Coq11's role in Q_6 biosynthesis is not effective when the *COQ11* ORF is expressed on a single-copy plasmid in the absence of *COQ10*. Perhaps Coq11 expression from a plasmid does not account for multiple levels of regulation that occur through endogenous expression. Alternatively, the *coq10Δcoq11Δ* double mutant may have slightly lower amounts of the Coq11 polypeptide compared with *coq11Δ* when both are complemented by lc*COQ11* (Fig. 9*D*), and these lower levels may not be sufficient to suppress respiration (Fig. 9*A*).

Discussion

This work investigated a putative functional relationship between Coq10 and Coq11 within the *S. cerevisiae* Q_6 biosynthetic pathway. The presence of Coq10–Coq11 fusions in several Ustilaginaceae species suggests that these proteins may directly interact or participate in the same biological pathway in yeast (Fig. 1*A*) (14). Yeast Coq10 and its orthologs were previously shown to be required for efficient *de novo* Q biosynthesis and respiration (17, 18). We were surprised to discover that the yeast *coq10Δ* growth defect on nonfermentable medium and oxygen consumption rates were rescued upon deletion of *COQ11* (Fig. 2). Moreover, spontaneous revertants isolated from *coq10Δ* yeast were previously found to exhibit growth on

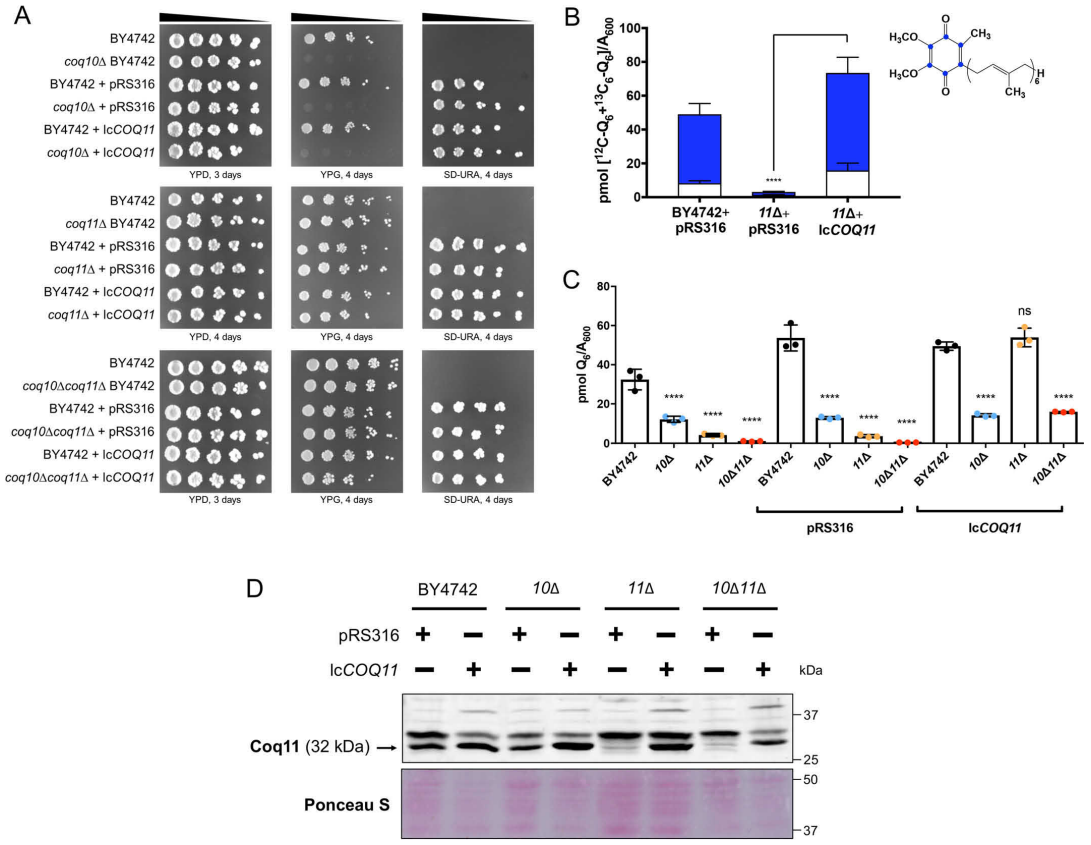

Figure 9. Low-copy *COQ11* rescues only some of the phenotypes of the *coq10Δcoq11Δ* double mutant. A low-copy plasmid expressing *COQ11* (*lcCOQ11*) and an empty vector control (pRS316) were transformed into WT, *coq10Δ*, *coq11Δ*, and *coq10Δcoq11Δ*. *A*, strains were grown overnight in 5 ml of YPDextrose (*YPD*) and diluted to an A_{600} = 0.2 with sterile PBS, and 2 μl of 5-fold serial dilutions were spotted onto YPDextrose, YPGlycerol (*YPG*), or selection medium (SD−Ura), corresponding to a final A_{600} = 0.2, 0.04, 0.008, 0.0016, and 0.00032. Plates were incubated at 30 °C, and growth was captured after 3 or 4 days. *B*, rescue of mutant *de novo* and unlabeled Q_6 production was initially demonstrated in *coq11Δ*. Triplicates of 6-ml cultures in selection medium were labeled with 5 μg/ml [$^{13}C_6$]4HB, and 5 ml of each culture was collected after 4 h, lipid-extracted, and analyzed by LC-MS/MS. Total amount of Q_6 was plotted from the sum of *de novo* [$^{13}C_6$]Q_6 (*blue*) and unlabeled [^{12}C]Q_6. Values are the mean of three replicates. *C*, rescue of mutant Q_6 content was evaluated in each mutant strain. Triplicates of 6-ml cultures in selection medium were grown until A_{600} ~4. Lipid extracts from 5 ml of each culture were analyzed by LC-MS/MS. The data show the means ± S.D., and the statistical significance as compared with WT is represented by *, $p < 0.05$; **, $p < 0.01$; ***, $p < 0.001$; and ****, $p < 0.0001$. *ns* signifies that values are not significantly different from WT. *D*, aliquots of purified mitochondria (25 μg) from WT and mutant yeast containing empty vector or lc*COQ11* were isolated in YPGal medium and were separated on 10% Tris-glycine SDS-polyacrylamide gels to determine Coq11 protein expression. Proteins stained with Ponceau stain were used as loading control.

nonfermentable medium (18). We have shown that this reversion is due to a dominant base pair deletion within the *COQ11* gene, likely resulting in a nonfunctional, truncated Coq11 protein (Fig. 3). Mutants lacking both *COQ10* and *COQ11* when cultured on YPGal have increased *de novo* Q_6 production (Fig. 4*A*) in addition to a 5-fold increase in mitochondrial Q_6 content compared with the *coq10*Δ single knockout (Fig. 5*B*). Therefore, we have demonstrated that deletion of the Coq11 polypeptide in a *coq10*Δ mutant confers a beneficial effect on both respiration and Q_6 biosynthesis (Fig. 10).

Enhanced Q_6 content in the *coq10*Δ*coq11*Δ double mutant compared with the *coq10*Δ single mutant may be partially due to increased amounts of several key Coq polypeptides (Fig. 6) and CoQ synthome stabilization (Fig. 7). The ring-modifying enzymes within the Q_6 biosynthetic pathway colocalize to numerous distinct "CoQ domains" *in vivo*, and proper assembly of the CoQ synthome components is required for the presence of these CoQ domains (23). Two recent studies demonstrated that mitochondria isolated from yeast lacking *COQ10* have a reduced number of CoQ domain puncta (23, 24). This is likely due to lower levels of certain Coq polypeptides and partial CoQ synthome destabilization in the *coq10*Δ mutant (17, 19), which was confirmed in this work (Figs. 6 and 7). In contrast, *coq11*Δ yeast displayed significantly higher amounts of Coq4, Coq6, Coq7, and Coq9 polypeptides (Fig. 6). The CoQ synthome was likewise shifted to a higher molecular weight in *coq11*Δ mitochondria compared with WT (Fig. 7). When Coq9 –yEGFP was used as a marker for CoQ domains, *coq11*Δ had increased CoQ

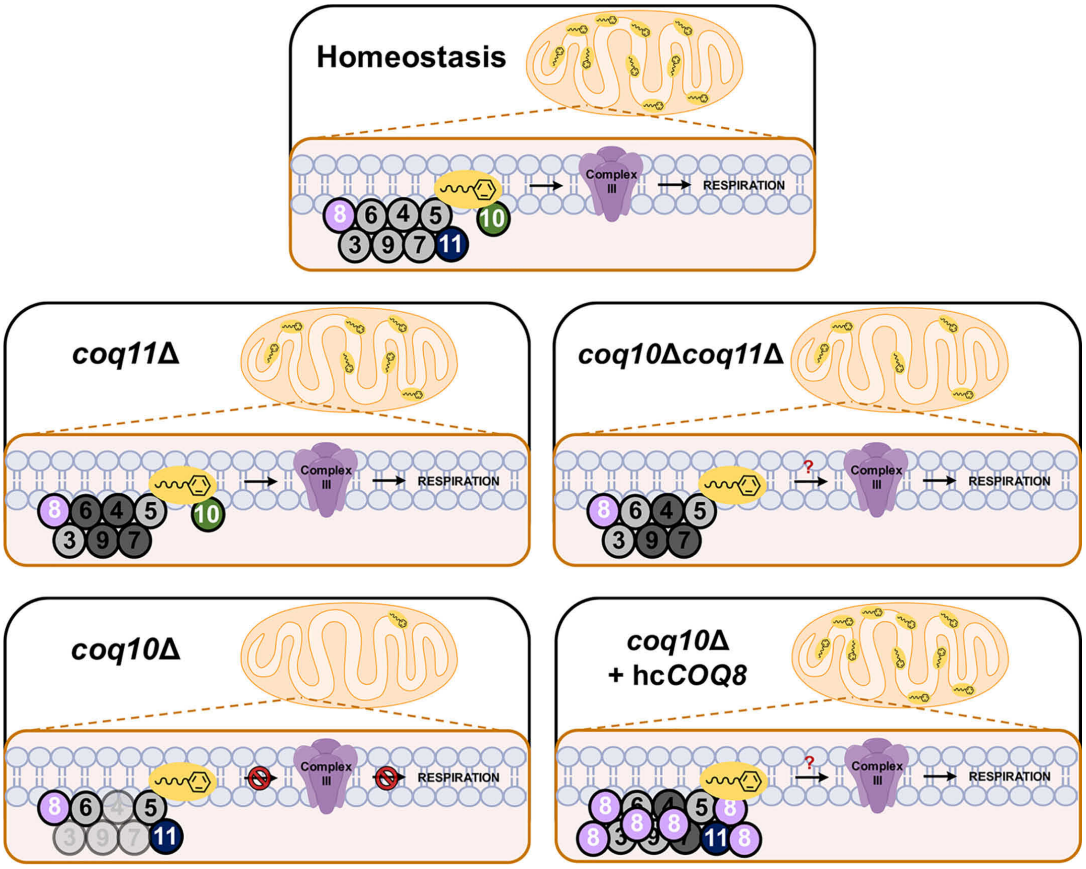

Figure 10. Scheme postulating Coq11 as a modulator of Q_6 synthesis in mitochondria. Under homeostasis, Coq11 associates with the CoQ synthome and acts as a modest negative regulator of Q_6 synthesis via Coq10. In the absence of *COQ11*, several Coq polypeptides are increased (*dark shading*), and the CoQ synthome is stabilized compared with WT cells, despite a slight decrease in Q_6 content. In contrast, the *coq10*Δ mutant is missing the Q_6 chaperone protein, resulting in a decreased amount (*light shading*) of Coq3, Coq4, Coq7, and Coq9, a destabilized CoQ synthome, substantially decreased Q_6 concentrations, and a lack of respiration. The deletion of *COQ11* in the *coq10*Δ mutant counterbalances the destabilized CoQ synthome and decreased Q_6 content phenotype of the *coq10*Δ mutant, allowing the *coq10*Δ*coq11*Δ double mutant to grow on YPG and respire. Expression of hc*COQ8* in the *coq10*Δ mutant produces many similar phenotypes to *COQ11* deletion in *coq10*Δ cells, including increased Coq polypeptides and a stabilized CoQ synthome (13), resulting in restored growth on YPG. Unlike the *coq10*Δ*coq11*Δ double mutant, *coq10*Δ + hc*COQ8* has rescued Q_6 content pointing to an additional role of Coq11 in Q_6 biosynthesis, redox regulation, or transportation.

domain intensity that stemmed from amplified expression of Coq9–yEGFP, although the number of domains was similar to WT. Mutants lacking essential Coq polypeptides *coq1*–*coq9*, or *coq10*, displayed significantly less Coq9-labeled domains (24). The CoQ synthome stabilization seen in *coq11*Δ via 2D-BN/SDS-PAGE analyses performed in this work (Fig. 7) agrees with the observation of increased CoQ domains and argues that the CoQ synthome is truly stabilized upon deletion of *COQ11*, as opposed to inducing a greater number of domains.

These observations are consistent with the biochemical data that led to the notion of a CoQ synthome whose formation relies on the presence of prenylated Q-intermediates (13, 40, 41). The *coq10*Δ mutant produced more early-stage intermediates (HHB) and had less late-stage intermediates (DMQ_6) compared with WT (Fig. 4, *C* and *D*), resulting in less CoQ synthome formation (Fig. 7). Because *coq11*Δ yeast displayed comparable amounts of early- and late-stage Q_6-intermediates to WT (Fig. 4, *C* and *D*), this mutant retained the ability to fully form the CoQ synthome (Fig. 7). The double knockout synthesized varying amounts of early- and late-stage Q_6-intermediates that were largely in-between those of the single knockouts (Fig. 4, *C* and *D*). The CoQ synthome is thus able to form in *coq10*Δ*coq11*Δ yeast, albeit not to the efficiency of the *coq11*Δ single mutant (Fig. 7). We suspect that the accumulation of Coq polypeptides and restoration of the CoQ synthome in the *coq10*Δ*coq11*Δ double mutant are sufficient to allow for Q_6 to escape its site of synthesis and reach the respiratory complexes, despite an absence of the Coq10 Q_6 chaperone protein and lower Q_6 in this strain (Fig. 10). How this occurs is presently not known. One possible explanation could be that Coq11 inhibits

a currently unidentified Q_6 chaperone with lower efficiency than Coq10 that is able to rescue respiration only in the absence of both Coq10 and Coq11.

Overexpression of the Q_6-biosynthetic protein Coq8 also rescued *coq10*Δ mutant growth on nonfermentable medium (Fig. 8*A*) and *de novo* Q_6 biosynthesis (Fig. 8, *B* and *C*) (17). Coq8 has been implicated in the partial extraction of Q_6-intermediates out of the mitochondrial inner membrane for enzymatic modification by other Coq proteins, allowing for appropriate Q_6 biosynthesis (25). Prior investigations also revealed that Coq8 overexpression in *coq10*Δ yeast increased Coq4 and Coq9 polypeptides and stabilized the CoQ synthome (13, 24). Despite the substantial benefit of Coq8 overexpression in a *coq10*Δ single mutant, Coq8 overexpression failed to enhance Q_6 biosynthesis in the *coq10*Δ*coq11*Δ double knockout (Figs. 8, *B* and *C,* and 10). The absence of *COQ11* in the double mutant is sufficient to restore Coq polypeptides and CoQ synthome formation (Figs. 6, *A* and *B,* 7, and 10). Coq11 and Coq8 may therefore work by different mechanisms to serve opposing functions for CoQ synthome and Coq polypeptide stabilization. Furthermore, it is clear that Coq11 is required to perform an additional function to Coq8, as hc*COQ8* requires the presence of Coq11 to restore Q_6 biosynthesis (Figs. 8, *B* and *C,* and 10).

Proper CoQ synthome formation is not only required for efficient Q_6 biosynthesis, but it is also vital for the establishment of ER-mitochondrial contact sites mediated by the ER-mitochondrial encounter structure (ERMES) complex (23, 24). The ERMES complex is essential for lipid exchange between the ER and mitochondria (42). Specifically, *ERMES* null mutants have irregular Q_6 cellular distribution and a destabilized CoQ synthome (23). When *COQ10* was deleted in yeast expressing Coq6–GFP, there was a significant decrease in Coq6–GFP puncta colocalization with Mdm34–mCherry, a component of the ERMES complex (23). These results indicate that CoQ synthome positioning next to the ERMES complex, and subsequent Q_6 distribution from the mitochondria, depends on Coq10. Because *COQ11* deletion stabilizes the CoQ synthome (Figs. 6, *A* and *B,* and 7), it is possible that *coq11*Δ mutants have more ER-mitochondrial contacts through the ERMES complex and improved transfer of lipids between these organelles. Therefore, one possible role of Coq11 may be an auxiliary protein mediating lipid transport between the ER and mitochondria.

In a recent study, Coq11 was named Mrx2, as part of the mitochondrial organization of gene expression (MIOREX) complex involved in the mitochondrial genetic expression system (43). Considering the proposed regulatory function of Coq11 in CoQ synthome assembly, it is tempting to speculate that Coq11 offers a mechanism to couple Q_6 synthesis with the assembly of the respiratory complexes. When the synthesis of the respiratory complexes is more active, Coq11 is associated to the MIOREX complex, and Q_6 synthesis at ER junctions is stimulated. Coq11 dual localization in the mitochondrial inner membrane, to the MIOREX complex and the CoQ synthome, would also explain the sensitivity of yeast cells to the number of *COQ11* copies, as well as present another example of a loop system control for balanced expression of mitochondrial products (44).

Another potential explanation for the phenotypes induced by the knockout of Coq11 relates to its structural connection with the short-chain dehydrogenase/reductase (SDR) superfamily of NAD(P)(H)-dependent oxidoreductases (14, 45). These enzymes catalyze an assortment of reactions, including isomerization, decarboxylation, epimerization, imine reduction, and carbonyl–alcohol oxidoreduction (45). SDR superfamily proteins contain a conserved protein structural motif known as a Rossmann fold, a feature used in the binding of nucleotide cofactors such as FAD, FMN, and NAD(P) (46). The crystal structure of the *Pseudomonas aeruginosa* gene UbiX, which catalyzes the decarboxylation step in Q_9 biosynthesis, revealed a Rossmann fold with a bound FMN (47). Thus, Coq11 may use its Rossmann fold in conjunction with a nucleotide cofactor to perform similar redox chemistry in *S. cerevisiae* Q_6 biosynthesis. The ratio of QH_2/Q serves as a metabolic sensor for electron transport chain efficiency (48). High QH_2/Q ratios induce respiratory complex I-mediated reverse electron transport (RET) under physiological conditions in both *Drosophila* and mammalian cell lines (48, 49). Superoxide and secondary reactive species produced specifically through complex I RET extended *Drosophila* lifespan and improved mitochondrial function in a model of Parkinson's disease (49). RET induced by over-reduction of the Q pool presumably generates a superoxide-dependent signal essential for homeostasis, such that manipulation of the Q redox state is beneficial for mitochondrial function (48, 49). Mitochondrial phenotypes in the absence of *COQ11*, including restored respiration in *coq10*Δ *coq11*Δ and up-regulated Q_6 machinery (Figs. 2, *A–C,* 6, and 7), seem to correlate well with the aforementioned effects of Q_6H_2 accumulation. Yeast *coq11*Δ and *coq10*Δ*coq11*Δ mutants retain antioxidant protection by Q_6H_2, demonstrated by their resistance to treatment with exogenously-added PUFAs (Fig. 2*D*). Because cells lacking the Coq11 polypeptide maintain Q_6H_2 as an antioxidant, it follows that Coq11 could be involved in the oxidation of Q_6H_2 to Q_6.

The phenotypes of Coq10 and Coq11 seen in this work are similar to those in both fungi and mammalian hosts. Several fungi use Coq11 or Coq11-like proteins as NAD-dependent epimerases/dehydratases, NADH-ubiquinone oxidoreductases, and NADH dehydrogenase subunits (14). Coq11 orthologs are commonly found in plant and algae genomes, including the chloroplast-localized flavin reductase protein At1g32220 from the land plant *Arabidopsis thaliana*, which is thought to be involved in plastoquinone biosynthesis and storage (14, 50). The closest but distinct higher eukaryotic Coq11-like protein is the SDR subfamily protein NDUFA9 (14), an auxiliary subunit of complex I in humans (51). Patients with decreased NDUFA9 expression are unable to properly assemble complex I and may develop a degenerative infancy respiratory disorder known as Leigh syndrome (52). Although yeast cells do not possess complex I, this evidence indicates that Coq11 may play a crucial role in respiratory regulation or function, supporting the observations of this study.

The function of Coq10 is widely conserved across different organisms. Expression of the Coq10 homolog from *C. crescentus* (CC1736) rescues the impaired respiration and antioxidant function of Q_6 in *coq10* yeast mutants (17). The NMR structure

of CC1736 reveals a START domain, which is known to bind lipids via a hydrophobic tunnel (20). Studies of *S. pombe* Coq10 demonstrate that it is able to bind Q_{10} (21). One proposed function of Q binding by CC1736 and Coq10 from *S. pombe* may be to regulate Q delivery to its proper sites in the respiratory complexes. Humans have two distinct homologs of yeast Coq10: COQ10A and COQ10B. Expression of either human protein rescues the *coq10*Δ respiratory deficiency and sensitivity to oxidative stress, and it restores the amounts of Coq polypeptides to WT (19). The conserved function of yeast Coq10 with human COQ10A and COQ10B suggests that the findings of this work will shed light on the role of Coq10 as a chaperone in humans, leading to a better understanding of the pathobiology of Q_{10} diseases.

In summary, this work reveals that Coq11 plays a regulatory role to maintain Q_6 homeostasis in concert with Coq10 in *S. cerevisiae* (Fig. 10). The absence of *COQ11* caused an augmentation of Q_6 production and respiration in the *coq10*Δ mutant, indicating that Coq11 confers a negative effect on the CoQ synthome. Coq11 may be crucial for Q_6 function in addition to Q_6 biosynthesis, as total whole-cell and mitochondrial Q_6 content remained lower than WT in *coq11*Δ and *coq10*Δ*coq11*Δ mutants.

Experimental procedures

All reagents were obtained commercially from Thermo Fisher Scientific unless otherwise specified

Yeast strains and growth medium

S. cerevisiae strains used in this study are described in Table 1. Yeast strains were derived from S288C (BY4742 (53)) or W303 (54). Growth media were prepared as described previously (55), and plate medium contained 2% bacto-agar. Growth media included the following: YPD (2% glucose, 1% yeast extract, and 2% peptone), YPGal (2% galactose, 1% yeast extract, 2% peptone, and 0.1% dextrose), YPG (3% glycerol, 1% yeast extract, and 2% peptone), and YPEG (3% glycerol, 2% ethanol, 1% yeast extract, and 2% peptone). Synthetic dextrose/selection media (SD–Complete, SD−Ura, SD-Leu, SD-His, SD-His–Leu, SD−Ura–Leu) were prepared as described previously (55) and consisted of all components minus uracil, leucine, histidine, or both uracil and leucine. Drop-out dextrose (DOD) medium was prepared as described previously (14).

COQ11 was disrupted by the one-step gene replacement method (56). The *LEU2* gene from pRS305 was amplified by polymerase chain reaction (PCR), with *COQ11* upstream and downstream flanking sequences 5′-GGGAAATATGTATCGTATACAAAAATACAGCTAAAGCTTGAACTG and 3′-GTACTTAACTATATACAGCTTGGTATAATTTTAAAATGGTAATAAC. Transformations of PCR products into yeast cells were performed using the Li-acetate method (57). The double *coq10*Δ*coq11*Δ mutant was constructed via disruption of *COQ10* within the *coq11*Δ strain. The *HIS3* gene from pRS313 was amplified by PCR with *COQ10* upstream and downstream flanking sequences 5′-GGATAAGGAGCCAAACAATAAACGGCTAAAGATACCGTGG and 3′-CAGATAACAAAGATCATGCCATCCAGGATAAGCGTATGCA, and transformation was performed as for the *COQ11* disruption. Primers were designed using SnapGene (GSL Biotech, LLC, Chicago, IL).

Mitochondria isolation from BY4742 WT and mutant yeast

Yeast cultures of BY4742, *coq10*Δ, *coq11*Δ, and *coq10*Δ *coq11*Δ were grown overnight in 5 ml of YPD. Yeast-containing plasmids were grown overnight in 5 ml of selection medium (SD−Ura). All pre-cultures were back-diluted with YPGal and grown overnight with shaking (30 °C, 250 rpm) until cell density reached an A_{600} ~4. Spheroplasts were prepared with Zymolyase-20T (MP Biomedicals) and fractionated as described previously (36), in the presence of cOmplete™ EDTA-free protease inhibitor mixture tablets (Roche Applied Science), phosphatase inhibitor mixture set I (Sigma-Aldrich), phosphatase inhibitor mixture set II (Sigma-Aldrich), and phenylmethylsulfonyl fluoride (Thermo Fisher Scientific). Nycodenz (Sigma-Aldrich) density gradient purified mitochondria were frozen in liquid nitrogen, aliquoted, and stored at −80 °C until further use. Protein concentration of mitochondria was measured by the bicinchoninic acid (BCA) assay (Thermo Fisher Scientific).

Submitochondrial localization of Coq10 and Coq11 polypeptides

Purified mitochondria from BY4742 yeast (3 mg of protein, 150 μl) were subfractionated, as described previously (13). Proteinase K treatment of purified BY4742 mitochondria was also performed as described previously (13). Proteinase K-treated mitoplasts and control samples were resuspended in SDS sample buffer (50 mM Tris, pH 6.8, 10% glycerol, 2% SDS, 0.1% bromphenol blue, and 1.33% β-mercaptoethanol); equal aliquots were separated by SDS-gel electrophoresis on 10 or 12% Tris-glycine polyacrylamide gels as detailed below. Several mitochondrial compartment markers and proteins of interest, Coq10 and Coq11, were detected with rabbit polyclonal antibodies prepared in blocking buffer at dilutions listed in Table S1.

Oxygen consumption evaluation by Seahorse

Mitochondrial function was assessed using the XF96 extracellular flux analyzer (Seahorse Bioscience, Agilent Technologies). Seahorse plates were coated with 50 μg/ml poly-D-lysine (Sigma-Aldrich), diluted 1:1 in UltraPure distilled water (Thermo Fisher Scientific). Volumes of 25 μl were added to each well for 30 min at room temperature and then aspirated before plates were dried overnight at room temperature. The Seahorse XF96 sensor cartridge was hydrated with Seahorse XF calibrant solution (Agilent) and was incubated overnight at room temperature.

Yeast cultures of BY4742, *coq10*Δ, *coq11*Δ, and *coq10*Δ*coq11*Δ were grown overnight in 25 ml of YPGal medium. On the day of measurement, all cultures were diluted to seed an A_{600} = 0.1 cells/well of BY4742, *coq10*Δ, *coq11*Δ, and *coq10*Δ*coq11*Δ into a Seahorse XF96 microplate in a total volume of 175 μl YPGal. Four wells containing only medium were included for background measurement. The loaded plate was centrifuged at 500 × *g* for 3 min at room temperature (with no brakes). Following centrifugation, the loaded plate was incubated for 30

min at 37 °C with no CO_2 to aid in the transitioning of the plate into the Seahorse machine's temperature. Cells were stimulated sequentially with two injections of 4 μM FCCP in ports A and B (optimized for maximum oxygen consumption rate) (Enzo Life Sciences) and 2.5 μM antimycin A in port C (Enzo Life Sciences), delivered in YPGal. Mix, wait, and measure times were 2 min, 30 s, and 2 min, respectively. Basal respiration included four measurements, and then following each injection three measurements were made. All OCR were subtracted for nonmitochondrial respiration and normalized to A_{600} = 0.1. Basal respiration was calculated as an average of OCR prior to the first FCCP addition. Maximal respiration was calculated as an average of OCR following the second FCCP addition. Nonmitochondrial respiration was measured as average OCR following antimycin A addition.

Fatty acid sensitivity assay

Sensitivity of yeast cells to PUFA-induced oxidative stress was performed as described previously (19, 58, 59), with some modifications. Briefly, BY4742 WT, *cor1*Δ, *coq9*Δ, *coq10*Δ, *coq11*Δ, and *coq10*Δ*coq11*Δ were inoculated in 5 ml of YPD medium and incubated overnight at 30 °C, 250 rpm. Cultures were subinoculated to an A_{600} = 0.25 in 15 ml of fresh YPD medium and incubated at 30 °C, 250 rpm until they reached an A_{600} ~1. Cells were harvested, washed twice with 10 ml of sterile H_2O, and diluted in 0.1 M phosphate buffer with 0.2% dextrose, pH 6.2, to an A_{600} = 0.2. This cell suspension was divided into 5-ml aliquots and treated with an ethanol vehicle control (final concentration 0.1% v/v), ethanol-diluted oleic acid (Nu-Check Prep), or α-linolenic acid (Nu-Check Prep) to a final concentration of 200 μM. Fatty acid-treated cultures were incubated for 4 h at 30 °C, 250 rpm, after which cell viability was assessed via plate dilutions. Cell viability prior to the addition of fatty acids was determined via plate dilutions, represented in the 0-h plate.

Analysis of Q_6 and Q_6-intermediates

Standards of Q_6 were obtained from Avanti Polar Lipids, and Q_4 was from Sigma-Aldrich. Yeast cultures were grown overnight in 30 ml of YPGal, or selection medium (SD-complete or SD−Ura) for strains harboring plasmids. Cultures were diluted into triplicates of 6 ml of fresh medium to A_{600} = 0.5, and 5 ml of medium was harvested by centrifugation once they reached A_{600} ~4. Cell pellets were stored at −20 °C. Following collection, frozen cell pellets were lipid-extracted in the presence of internal standard Q_4 and analyzed for Q_6 and Q_6-intermediates by LC-MS/MS as described previously (19).

Stable isotope labeling for determination of de novo Q_6 and Q_6-intermediates

Yeast cultures were grown overnight in 30 ml of YPGal and diluted in triplicates of 6 ml of fresh medium to an A_{600} = 0.1. Cultures were incubated until they reached an A_{600} ~1, at which point ethanol vehicle control (0.1% v/v) or 5 μg/ml of the stable isotope [$^{13}C_6$]4HB (Cambridge Isotope Laboratories, Inc.) was added. Cultures were allowed to grow for an additional 4 h when 5 ml of each culture was harvested by centrifugation and stored at −20 °C. Cell pellets were lipid extracted and analyzed by LC-MS/MS as described previously (19).

Mitochondrial DNA determination by qPCR analysis

DNA was extracted from yeast cells as follows. Yeast pellets (10 ml) grown in YPGal were collected at an A_{600} ~4 by centrifugation at 3000 × *g* for 5 min, washed with 5 ml of H_2O, and transferred to 2-ml screw-cap tubes. Pellets were frozen at −80 °C until DNA extraction was carried out. Cell pellets were resuspended in 200 μl of lysis buffer (10 mM Tris-Cl, pH 8.0, 2% (v/v) Triton X-100, 1 mM EDTA, 100 mM NaCl, 1% SDS), and 200 μl of acid-washed glass beads with 200 μl of phenol/chloroform/isoamyl alcohol (25:24:1) were added to the cell suspension. Cells were lysed using a bead-beater (Precellys 24; Bertin Technologies) three times for 10 s at 6500 rpm with a 45-s break between rounds at 4 °C. Tris-EDTA (TE, 200 μl) was added, and the cell suspension was centrifuged at 13,000 × *g* for 5 min at room temperature. The aqueous layer was removed to a new tube containing 200 μl of chloroform, mixed by inversion, and centrifuged at 13,000 × *g* for 5 min at room temperature. This was repeated once more. The aqueous layer was then transferred to a 2-ml screw-cap tube containing 1 ml of 95% EtOH, mixed by inversion, and centrifuged at 13,000 × *g* for 2 min at room temperature. The resulting pellet was resuspended in 400 μl of TE containing 30 μg of RNase A and incubated at 37 °C for 30 min. Then, 10 μl of 3 M sodium acetate and 1 ml of 95% EtOH was added, mixed by inversion, and incubated at −20 °C for 1 h. After 1 h at −20 °C, the suspension was centrifuged at 13,000 × *g* for 5 min, and the pellet was washed twice with 70% EtOH and air-dried. The dried pellet was resuspended in 25 μl of TE; concentration was measured by Nanodrop (Thermo Fisher Scientific), and the pellet was stored at −20 °C until use.

qPCR was performed on a CFX384 instrument (Bio-Rad) using the SensiFAST™SYBR® NO ROX kit (Bioline) as per the manufacturer's instructions. Each sample was run in duplicate with 150 ng of total DNA used per reaction using the following thermocycling protocol (95 °C for 2 min, 95 °C for 5 s, 60 °C for 10 s, and 72 °C for 20 s, plate read and cycle repeated ×40, melt curve 40–92 °C with plate read and 40 °C for 10 s). Melting-curve analysis confirmed that all PCRs produced a single product. mtDNA-specific primers (forward (13,999), 5′-GTG CGT ATA TTT CGT TGA TGC GT-3′; reverse (14,297), 5′-TTC ACA CTG CCT GTG CTA TCT AA-3′ (60) and actin-specific primers (forward, 5′-GAA TTG AGA GTT GCC CCA GA-3′; reverse, 5′-ATC ACC GGA ATC CAA AAC AA-3) were used. The relative level of gene expression of mitochondrial DNA was normalized to the expression level of actin as described previously (61).

Citrate synthase activity

The measurement of citrate synthase activity in cells was carried out as described previously (62). Briefly, yeast pellets (10 ml) grown in YPGal were collected at an A_{600} ~4 by centrifugation at 3000 × *g* for 5 min, washed with 5 ml of H_2O, and transferred to 2-ml screw-cap tubes. Cell pellets were resuspended in 200 μl of lysis buffer (100 mM Tris-Cl, pH 7.4, 1% (v/v) Triton X-100, 1 mM EDTA, 1 mM phenylmethylsulfonyl fluoride, 1× cOmplete™ Protease Inhibitor Mixture (Roche

Applied Science)), and then 200 μl of acid-washed glass beads were added. Cells were lysed using a bead-beater (Precellys 24; Bertin Technologies) three times for 10 s at 6500 rpm with a 45-s break between rounds at 4 °C. The clarified cell lysate was collected after centrifugation at 16,000 × *g* for 10 min at 4 °C. The concentration of protein was determined with the BCA assay (Thermo Fisher Scientific). Cell lysates were normalized to 0.05 μg/μl protein. The colorimetric citrate synthase assay was carried out using a VersaMax plate reader (Molecular Devices) and a flat-bottom 96-well plate. First, 40 μl of 500 mM Tris-Cl, pH 7.4, 2 μl of 30 mM acetyl-CoA, 8 μl of 2.5 mM 5,5′-dithiobis(2-nitrobenzoic acid), 90 μl of H_2O, and 50 μl cell lysate (2.5 μg total protein) were added into each well. Then, 10 μl of 10 mM oxaloacetic acid were added per well and mixed by pipetting up and down. A_{412} was measured every 30 s at 25 °C. The initial slope was calculated by using data from the first 10 min and used to determine the enzyme reaction rate using the extinction coefficient for 2-nitro-5-thiobenzoate of 14.15 mM^{-1} cm^{-1} (63).

Porin quantification

Porin content was quantified via immunoblot of yeast WT and mutant whole cells. Protein extraction from whole cells was performed (64), and 25 μg of each sample was separated by SDS-gel electrophoresis as described below. Three replicates of the immunoblots were performed and quantified by hand using ImageStudioLite software normalized to Ponceau total protein staining.

Quantitative real-time PCR (qRT-PCR)

Total RNA was isolated from yeast cells using TRIzol reagent (Invitrogen). DNA contamination from the resulting RNA was removed using the DNase TURBO kit as per the manufacturer's instructions (Invitrogen). RNA concentration was measured by Nanodrop (Thermo Fisher Scientific), and RNA was stored at −20 °C. Reverse transcription was carried out using the Superscript III first strand synthesis system using random hexamer primers (Invitrogen). cDNA was stored at −20 °C until qPCR analyses were carried out. Quantitative real-time PCR was performed on a CFX384 instrument (Bio-Rad) using the SensiFAST™SYBR® NO-ROX kit (Bioline) in duplicate. The relative levels of gene expression were normalized to the expression level of actin. Melting curve analysis confirmed that all PCRs produced a single product. The primers (forward/reverse) used in real-time PCR were designed using Primer3 on line (RRID: SCR_003139). Primers used are given in Table S2.

SDS-PAGE and immunoblot analysis

Purified mitochondria (25 μg) were resuspended in SDS sample buffer and separated by SDS-gel electrophoresis on 10 or 12% Tris-glycine polyacrylamide gels. Proteins were transferred to a 0.45-μm polyvinylidene difluoride membrane (Millipore) and blocked with blocking buffer (0.5% BSA, 0.1% Tween 20, 0.02% SDS in PBS). Representative Coq polypeptides and loading control mitochondrial malate dehydrogenase (Mdh1) were probed with rabbit polyclonal antibodies prepared in blocking buffer at dilutions listed in Table S1. IRDye 680LT goat anti-rabbit IgG secondary antibody (LiCOR) was used at a dilution of 1:10,000. Proteins were visualized using a LiCOR Odyssey IR Scanner (LiCOR). Immunoblots are representative of three replicates and were quantified by hand using ImageStudioLite software normalized to Mdh1.

Two-dimensional Blue Native/SDS-PAGE immunoblot analysis of high-molecular-weight complexes

2D-BN/SDS-PAGE was performed as described previously (13, 65, 66). Briefly, 200 μg of purified mitochondria were solubilized at 4 mg/ml for 1 h on ice with 16 mg/ml digitonin (Biosynth) in the presence of the protease and phosphatase inhibitors used during mitochondrial isolation. Protein concentration of solubilized mitochondria was determined by BCA assay. NativePAGE 5% G-250 sample additive (Thermo Fisher Scientific) was added to a final concentration of 0.25%. Solubilized mitochondria (100 μg) were separated on NativePAGE 4–16% BisTris gels (Thermo Fisher Scientific) in the first dimension, and native gel slices were further separated on 12% Tris-glycine polyacrylamide gel in the second dimension. Following the second-dimension separation, immunoblot analyses were performed as described above, using antibodies against Coq4 and Coq9 at the dilutions indicated in Table S1. Molecular weight standards for BN gel electrophoresis and SDS gel electrophoresis were obtained from GE Healthcare (Sigma-Aldrich) and Bio-Rad, respectively.

Construction of low-copy COQ11 yeast expression vectors

Plasmids used in this study are described in Table 2. A low-copy *COQ11*-containing plasmid was constructed using the pRS316 low-copy empty vector. The *COQ11* ORF and regions corresponding to 842 bp upstream and 256 bp downstream were cloned into pRS316 using Gibson Assembly (New England Biolabs). Clones were sequenced by Laragen, and successful clones were transformed into WT and mutant yeast, along with the corresponding empty vector (pRS316) control as described above.

Revertant isolation

As reported previously, *coq10* mutant growth deficiency on nonfermentable carbon sources (YPEG) spontaneously revert due to nuclear suppression mutations (18). Here, W303 *coq10*Δ yeast was grown on glucose to stationary phase, and ~10 million cells were plated on YPEG. After several weeks, a colony began to appear on this medium. The colony was purified, and its genome was sequenced.

Genome sequencing

The Wizard® genomic purification kit (Promega) was used to extract total DNA from the parental respiratory-deficient mutant W303 *coq10*Δ and from the spontaneous revertant W303 *coq10*rev. The DNA was quantified using the QUBIT DNA™ high-sensitivity assay, and 1 ng of the normalized DNA was tagged by the Nextera XTTM (Illumina) protocol. The libraries were amplified and pooled as described (67). The pooled libraries were subjected to sequencing with the NextSeq™ (Illumina) equipment in the Genome Investigation and Analysis Laboratory of the Institute of Biomedical Sciences at the University of Sao Paulo. The BWA Aligner tool,

version 1.1.4 (Base Space Labs-Illumina), was used to align ~23,000,000 reads obtained from each strain with the reference genomes of *S. cerevisiae*. The alignments were compared using the Integrative Genomics Viewer (Base Space Labs Illumina).

Statistical analyses

All data sets were tested for normality using GraphPad Prism 7 with the Shapiro-Wilk normality test. Because a majority of sets passed the normality test ($\alpha = 0.5$), statistical analyses were performed using GraphPad Prism 7 with parametric one-way analysis of variance correcting for multiple comparisons using Tukey's test, comparing the mean of each sample to the mean of its corresponding WT or empty vector control. The data show the means ± S.D., and the statistical significance as compared with WT or empty vector control is represented by the following: *, $p < 0.05$; **, $p < 0.01$; ***, $p < 0.001$; and ****, $p < 0.0001$. The denotation *ns* indicates values with "not significant" differences from the corresponding control.

Data availability

The MS source data for determination of Q_6 and Q_6 intermediates will be shared upon request. Please contact Catherine Clarke at cathy@chem.ucla.edu. All remaining data are contained within the article.

Author contributions—M. C. B., M. H. B., and C. F. C. conceptualization; M. C. B., J. N., A. A., H. S. T., O. S. S., M. H. B., and C. F. C. resources; M. C. B., K. Y., L. F.-dR., J. N., A. A., H. S. T., N. A. N., M. H. B., and C. F. C. data curation; M. C. B., J. N., A. A., and M. H. B. software; M. C. B., K. Y., L. F.-dR., J. N., A. A., H. S. T., N. A. N., R. S., M. H. B., and C. F. C. formal analysis; M. C. B., R. S., O. S. S., M. H. B., and C. F. C. supervision; M. C. B., J. N., H. S. T., M. H. B., and C. F. C. funding acquisition; M. C. B., K. Y., L. F.-dR., J. N., A. A., H. S. T., R. S., and M. H. B. validation; M. C. B., K. Y., L. F.-dR., J. N., A. A., H. S. T., N. A. N., R. S., M. H. B., and C. F. C. investigation; M. C. B., K. Y., L. F.-dR., J. N., A. A., H. S. T., N. A. N., M. H. B., and C. F. C. visualization; M. C. B., K. Y., L. F.-dR., J. N., A. A., H. S. T., N. A. N., R. S., M. H. B., and C. F. C. methodology; M. C. B. and C. F. C. writing-original draft; M. C. B., R. S., M. H. B., and C. F. C. project administration; M. C. B., K. Y., L. F.-dR., J. N., A. A., H. S. T., N. A. N., R. S., O. S. S., M. H. B., and C. F. C. writing-review and editing.

Acknowledgments—We thank the UCLA Molecular Instrumentation Core proteomics facility and Dr. Yu Chen for the use of the QTRAP4000 for lipid analysis. We thank undergraduate UCLA researcher Hope Ibarra for her contributions in assisting with experiments.

References

1. Turunen, M., Olsson, J., and Dallner, G. (2004) Metabolism and function of coenzyme Q. *Biochim. Biophys. Acta* **1660,** 171–199 CrossRef Medline
2. Alcázar-Fabra, M., Trevisson, E., and Brea-Calvo, G. (2018) Clinical syndromes associated with coenzyme Q_{10} deficiency. *Essays Biochem.* **62,** 377–398 CrossRef Medline
3. Desbats, M. A., Lunardi, G., Doimo, M., Trevisson, E., and Salviati, L. (2015) Genetic bases and clinical manifestations of coenzyme Q_{10} (CoQ 10) deficiency. *J. Inherit. Metab. Dis.* **38,** 145–156 CrossRef Medline
4. Frei, B., Kim, M. C., and Ames, B. N. (1990) Ubiquinol-10 is an effective lipid-soluble antioxidant at physiological concentrations. *Proc. Natl. Acad. Sci. U.S.A.* **87,** 4879–4883 CrossRef Medline
5. Okada, K., Suzuki, K., Kamiya, Y., Zhu, X., Fujisaki, S., Nishimura, Y., Nishino, T., Nakagawa, T., Kawamukai, M., and Matsuda, H. (1996) Polyprenyl diphosphate synthase essentially defines the length of the side chain of ubiquinone. *Biochim. Biophys. Acta* **1302,** 217–223 CrossRef Medline
6. Kawamukai, M. (2016) Biosynthesis of coenzyme Q in eukaryotes. *Biosci. Biotechnol. Biochem.* **80,** 23–33 CrossRef Medline
7. Stefely, J. A., and Pagliarini, D. J. (2017) Biochemistry of mitochondrial coenzyme Q biosynthesis. *Trends Biochem. Sci.* **42,** 824–843 CrossRef Medline
8. Montini, G., Malaventura, C., and Salviati, L. (2008) Early coenzyme Q_{10} supplementation in primary coenzyme Q_{10} deficiency. *N. Engl. J. Med.* **358,** 2849–2850 CrossRef Medline
9. Awad, A. M., Bradley, M. C., Fernández-Del-Río, L., Nag, A., Tsui, H. S., and Clarke, C. F. (2018) Coenzyme Q_{10} deficiencies: pathways in yeast and humans. *Essays Biochem* **62,** 361–376 CrossRef Medline
10. Tran, U. C., Marbois, B., Gin, P., Gulmezian, M., Jonassen, T., and Clarke, C. F. (2006) Complementation of *Saccharomyces cerevisiae coq7* mutants by mitochondrial targeting of the *Escherichia coli* UbiF polypeptide: two functions of yeast Coq7 polypeptide in coenzyme Q biosynthesis. *J. Biol. Chem.* **281,** 16401–16409 CrossRef Medline
11. Marbois, B., Gin, P., Faull, K. F., Poon, W. W., Lee, P. T., Strahan, J., Shepherd, J. N., and Clarke, C. F. (2005) Coq3 and Coq4 define a polypeptide complex in yeast mitochondria for the biosynthesis of coenzyme Q. *J. Biol. Chem.* **280,** 20231–20238 CrossRef Medline
12. Hsieh, E. J., Gin, P., Gulmezian, M., Tran, U. C., Saiki, R., Marbois, B. N., and Clarke, C. F. (2007) *Saccharomyces cerevisiae* Coq9 polypeptide is a subunit of the mitochondrial coenzyme Q biosynthetic complex. *Arch. Biochem. Biophys.* **463,** 19–26 CrossRef Medline
13. He, C. H., Xie, L. X., Allan, C. M., Tran, U. C., and Clarke, C. F. (2014) Coenzyme Q supplementation or overexpression of the yeast Coq8 putative kinase stabilizes multi-subunit Coq polypeptide complexes in yeast *coq* null mutants. *Biochim. Biophys. Acta* **1841,** 630–644 CrossRef Medline
14. Allan, C. M., Awad, A. M., Johnson, J. S., Shirasaki, D. I., Wang, C., Blaby-Haas, C. E., Merchant, S. S., Loo, J. A., and Clarke, C. F. (2015) Identification of Coq11, a new coenzyme Q biosynthetic protein in the CoQ-synthome in *Saccharomyces cerevisiae*. *J. Biol. Chem.* **290,** 7517–7534 CrossRef Medline
15. Marcotte, E. M., Pellegrini, M., Ng, H. L., Rice, D. W., Yeates, T. O., and Eisenberg, D. (1999) Detecting protein function and protein–protein interactions from genome sequences. *Science* **285,** 751–753 CrossRef Medline
16. Perocchi, F., Jensen, L. J., Gagneur, J., Ahting, U., von Mering, C., Bork, P., Prokisch, H., and Steinmetz, L. M. (2006) Assessing systems properties of yeast mitochondria through an interaction map of the organelle. *PLoS Genet.* **2,** e170 CrossRef Medline
17. Allan, C. M., Hill, S., Morvaridi, S., Saiki, R., Johnson, J. S., Liau, W. S., Hirano, K., Kawashima, T., Ji, Z., Loo, J. A., Shepherd, J. N., and Clarke, C. F. (2013) A conserved START domain coenzyme Q-binding polypeptide is required for efficient Q biosynthesis, respiratory electron transport, and antioxidant function in *Saccharomyces cerevisiae*. *Biochim. Biophys. Acta* **1831,** 776–791 CrossRef Medline
18. Barros, M. H., Johnson, A., Gin, P., Marbois, B. N., Clarke, C. F., and Tzagoloff, A. (2005) The *Saccharomyces cerevisiae COQ10* gene encodes a START domain protein required for function of coenzyme Q in respiration. *J. Biol. Chem.* **280,** 42627–42635 CrossRef Medline
19. Tsui, H. S., Pham, N. V. B., Amer, B. R., Bradley, M. C., Gosschalk, J. E., Gallagher-Jones, M., Ibarra, H., Clubb, R. T., Blaby-Haas, C. E., and Clarke, C. F. (2019) Human COQ10A and COQ10B are distinct lipid-binding START domain proteins required for coenzyme Q function. *J. Lipid Res.* **60,** 1293–1310 CrossRef Medline
20. Shen, Y., Goldsmith-Fischman, S., Atreya, H. S., Acton, T., Ma, L., Xiao, R., Honig, B., Montelione, G. T., and Szyperski, T. (2005) NMR structure of the 18 kDa protein CC1736 from *Caulobacter crescentus* identifies a member of the START domain superfamily and suggests residues mediating substrate specificity. *Proteins* **58,** 747–750 CrossRef Medline

21. Cui, T. Z., and Kawamukai, M. (2009) Coq10, a mitochondrial coenzyme Q binding protein, is required for proper respiration in *Schizosaccharomyces pombe*. *FEBS J.* **276,** 748–759 CrossRef Medline
22. Stoldt, S., Wenzel, D., Kehrein, K., Riedel, D., Ott, M., and Jakobs, S. (2018) Spatial orchestration of mitochondrial translation and OXPHOS complex assembly. *Nat. Cell Biol.* **20,** 528–534 CrossRef Medline
23. Eisenberg-Bord, M., Tsui, H. S., Antunes, D., Fernández-Del-Río, L., Bradley, M. C., Dunn, C. D., Nguyen, T. P. T., Rapaport, D., Clarke, C. F., and Schuldiner, M. (2019) The endoplasmic reticulum–mitochondria encounter structure complex coordinates coenzyme Q biosynthesis. *Contact* **2,** 2515256418825409 CrossRef Medline
24. Subramanian, K., Jochem, A., Le Vasseur, M., Lewis, S., Paulson, B. R., Reddy, T. R., Russell, J. D., Coon, J. J., Pagliarini, D. J., and Nunnari, J. (2019) Coenzyme Q biosynthetic proteins assemble in a substrate-dependent manner into domains at ER-mitochondria contacts. *J. Cell Biol.* **218,** 1353–1369 CrossRef Medline
25. Reidenbach, A. G., Kemmerer, Z. A., Aydin, D., Jochem, A., McDevitt, M. T., Hutchins, P. D., Stark, J. L., Stefely, J. A., Reddy, T., Hebert, A. S., Wilkerson, E. M., Johnson, I. E., Bingman, C. A., Markley, J. L., Coon, J. J., *et al.* (2018) Conserved lipid and small-molecule modulation of *COQ8* reveals regulation of the ancient kinase-like UbiB family. *Cell Chem. Biol.* **25,** 154–165.e11 CrossRef Medline
26. Reading, D. S., Hallberg, R. L., and Myers, A. M. (1989) Characterization of the yeast *HSP60* gene coding for a mitochondrial assembly factor. *Nature* **337,** 655–659 CrossRef Medline
27. Fujiki, Y., Hubbard, A. L., Fowler, S., and Lazarow, P. B. (1982) Isolation of intracellular membranes by means of sodium carbonate treatment: application to endoplasmic reticulum. *J. Cell Biol.* **93,** 97–102 CrossRef Medline
28. Chen, W. J., and Douglas, M. G. (1987) Phosphodiester bond cleavage outside mitochondria is required for the completion of protein import into the mitochondrial matrix. *Cell* **49,** 651–658 CrossRef Medline
29. Ohashi, A., Gibson, J., Gregor, I., and Schatz, G. (1982) Import of proteins into mitochondria. The precursor of cytochrome c_1 is processed in two steps, one of them heme-dependent. *J. Biol. Chem.* **257,** 13042–13047 Medline
30. Vögtle, F. N., Burkhart, J. M., Gonczarowska-Jorge, H., Kücükköse, C., Taskin, A. A., Kopczynski, D., Ahrends, R., Mossmann, D., Sickmann, A., Zahedi, R. P., and Meisinger, C. (2017) Landscape of submitochondrial protein distribution. *Nat. Commun.* **8,** 290 CrossRef Medline
31. Yin, H., Xu, L., and Porter, N. A. (2011) Free radical lipid peroxidation: mechanisms and analysis. *Chem. Rev.* **111,** 5944–5972 CrossRef Medline
32. Pryor, W. A., and Porter, N. A. (1990) Suggested mechanisms for the production of 4-hydroxy-2-nonenal from the autoxidation of polyunsaturated fatty acids. *Free Radic. Biol. Med.* **8,** 541–543 CrossRef Medline
33. Heeringa, S. F., Chernin, G., Chaki, M., Zhou, W., Sloan, A. J., Ji, Z., Xie, L. X., Salviati, L., Hurd, T. W., Vega-Warner, V., Killen, P. D., Raphael, Y., Ashraf, S., Ovunc, B., Schoeb, D. S., *et al.* (2011) COQ6 mutations in human patients produce nephrotic syndrome with sensorineural deafness. *J. Clin. Invest.* **121,** 2013–2024 CrossRef Medline
34. Nguyen, T. P., Casarin, A., Desbats, M. A., Doimo, M., Trevisson, E., Santos-Ocaña, C., Navas, P., Clarke, C. F., and Salviati, L. (2014) Molecular characterization of the human COQ5 *C*-methyltransferase in coenzyme Q_{10} biosynthesis. *Biochim. Biophys. Acta* **1841,** 1628–1638 CrossRef Medline
35. Conrad, M., Schothorst, J., Kankipati, H. N., Van Zeebroeck, G., Rubio-Texeira, M., and Thevelein, J. M. (2014) Nutrient sensing and signaling in the yeast *Saccharomyces cerevisiae*. *FEMS Microbiol. Rev.* **38,** 254–299 CrossRef Medline
36. Glick, B. S., and Pon, L. A. (1995) Isolation of highly purified mitochondria from *Saccharomyces cerevisiae*. *Methods Enzymol.* **260,** 213–223 CrossRef Medline
37. Stefely, J. A., Reidenbach, A. G., Ulbrich, A., Oruganty, K., Floyd, B. J., Jochem, A., Saunders, J. M., Johnson, I. E., Minogue, C. E., Wrobel, R. L., Barber, G. E., Lee, D., Li, S., Kannan, N., Coon, J. J., *et al.* (2015) Mitochondrial ADCK3 employs an atypical protein kinase-like fold to enable coenzyme Q biosynthesis. *Mol. Cell* **57,** 83–94 CrossRef Medline
38. Xie, L. X., Hsieh, E. J., Watanabe, S., Allan, C. M., Chen, J. Y., Tran, U. C., and Clarke, C. F. (2011) Expression of the human atypical kinase ADCK3 rescues coenzyme Q biosynthesis and phosphorylation of Coq polypeptides in yeast *coq8* mutants. *Biochim. Biophys. Acta* **1811,** 348–360 CrossRef Medline
39. Xie, L. X., Ozeir, M., Tang, J. Y., Chen, J. Y., Jaquinod, S. K., Fontecave, M., Clarke, C. F., and Pierrel, F. (2012) Overexpression of the Coq8 kinase in *Saccharomyces cerevisiae coq* null mutants allows for accumulation of diagnostic intermediates of the coenzyme Q_6 biosynthetic pathway. *J. Biol. Chem.* **287,** 23571–23581 CrossRef Medline
40. Tran, U. C., and Clarke, C. F. (2007) Endogenous synthesis of coenzyme Q in eukaryotes. *Mitochondrion* **7,** Suppl., S62–S71 CrossRef Medline
41. Wang, Y., and Hekimi, S. (2019) The complexity of making ubiquinone. *Trends Endocrinol. Metab.* **30,** 929–943 CrossRef Medline
42. Murley, A., and Nunnari, J. (2016) The emerging network of mitochondria-organelle contacts. *Mol. Cell* **61,** 648–653 CrossRef Medline
43. Kehrein, K., Möller-Hergt, B. V., and Ott, M. (2015) The MIOREX complex–lean management of mitochondrial gene expression. *Oncotarget* **6,** 16806–16807 CrossRef Medline
44. Fontanesi, F. (2013) Mechanisms of mitochondrial translational regulation. *IUBMB Life* **65,** 397–408 CrossRef Medline
45. Marchler-Bauer, A., Zheng, C., Chitsaz, F., Derbyshire, M. K., Geer, L. Y., Geer, R. C., Gonzales, N. R., Gwadz, M., Hurwitz, D. I., Lanczycki, C. J., Lu, F., Lu, S., Marchler, G. H., Song, J. S., Thanki, N., *et al.* (2013) CDD: conserved domains and protein three-dimensional structure. *Nucleic Acids Res.* **41,** D348–D352 CrossRef Medline
46. Rossmann, M. G., Moras, D., and Olsen, K. W. (1974) Chemical and biological evolution of nucleotide-binding protein. *Nature* **250,** 194–199 CrossRef Medline
47. Kopec, J., Schnell, R., and Schneider, G. (2011) Structure of PA4019, a putative aromatic acid decarboxylase from *Pseudomonas aeruginosa*. *Acta Crystallogr. Sect. F Struct. Biol. Cryst. Commun.* **67,** 1184–1188 CrossRef Medline
48. Guarás, A., Perales-Clemente, E., Calvo, E., Acín-Pérez, R., Loureiro-Lopez, M., Pujol, C., Martínez-Carrascoso, I., Nuñez, E., García-Marqués, F., Rodríguez-Hernández, M. A., Cortés, A., Diaz, F., Pérez-Martos, A., Moraes, C. T., Fernández-Silva, P., *et al.* (2016) The $CoQH_2$/CoQ ratio serves as a sensor of respiratory chain efficiency. *Cell Rep.* **15,** 197–209 CrossRef Medline
49. Scialò, F., Sriram, A., Fernández-Ayala, D., Gubina, N., Lõhmus, M., Nelson, G., Logan, A., Cooper, H. M., Navas, P., Enríquez, J. A., Murphy, M. P., and Sanz, A. (2016) Mitochondrial ROS produced via reverse electron transport extend animal lifespan. *Cell Metab.* **23,** 725–734 CrossRef Medline
50. UniProt Consortium (2018) UniProt: the universal protein knowledgebase. *Nucleic Acids Res.* **46,** 2699 CrossRef Medline
51. Pagliarini, D. J., Calvo, S. E., Chang, B., Sheth, S. A., Vafai, S. B., Ong, S. E., Walford, G. A., Sugiana, C., Boneh, A., Chen, W. K., Hill, D. E., Vidal, M., Evans, J. G., Thorburn, D. R., Carr, S. A., and Mootha, V. K. (2008) A mitochondrial protein compendium elucidates complex I disease biology. *Cell* **134,** 112–123 CrossRef Medline
52. van den Bosch, B. J., Gerards, M., Sluiter, W., Stegmann, A. P., Jongen, E. L., Hellebrekers, D. M., Oegema, R., Lambrichs, E. H., Prokisch, H., Danhauser, K., Schoonderwoerd, K., de Coo, I. F., and Smeets, H. J. (2012) Defective NDUFA9 as a novel cause of neonatally fatal complex I disease. *J. Med. Genet.* **49,** 10–15 CrossRef Medline
53. Brachmann, C. B., Davies, A., Cost, G. J., Caputo, E., Li, J., Hieter, P., and Boeke, J. D. (1998) Designer deletion strains derived from *Saccharomyces cerevisiae* S288C: a useful set of strains and plasmids for PCR-mediated gene disruption and other applications. *Yeast* **14,** 115–132 CrossRef Medline
54. Thomas, B. J., and Rothstein, R. (1989) Elevated recombination rates in transcriptionally active DNA. *Cell* **56,** 619–630 CrossRef Medline
55. Barkovich, R. J., Shtanko, A., Shepherd, J. A., Lee, P. T., Myles, D. C., Tzagoloff, A., and Clarke, C. F. (1997) Characterization of the *COQ5* gene from *Saccharomyces cerevisiae*. Evidence for a *C*-methyltransferase in ubiquinone biosynthesis. *J. Biol. Chem.* **272,** 9182–9188 CrossRef Medline

56. Rothstein, R. J. (1983) One-step gene disruption in yeast. *Methods Enzymol.* **101,** 202–211 CrossRef Medline
57. Gietz, R. D., and Woods, R. A. (2002) Transformation of yeast by lithium acetate/single-stranded carrier DNA/polyethylene glycol method. *Methods Enzymol.* **350,** 87–96 CrossRef Medline
58. Hill, S., Hirano, K., Shmanai, V. V., Marbois, B. N., Vidovic, D., Bekish, A. V., Kay, B., Tse, V., Fine, J., Clarke, C. F., and Shchepinov, M. S. (2011) Isotope-reinforced polyunsaturated fatty acids protect yeast cells from oxidative stress. *Free Radic. Biol. Med.* **50,** 130–138 CrossRef Medline
59. Hill, S., Lamberson, C. R., Xu, L., To, R., Tsui, H. S., Shmanai, V. V., Bekish, A. V., Awad, A. M., Marbois, B. N., Cantor, C. R., Porter, N. A., Clarke, C. F., and Shchepinov, M. S. (2012) Small amounts of isotope-reinforced polyunsaturated fatty acids suppress lipid autoxidation. *Free Radic. Biol. Med.* **53,** 893–906 CrossRef Medline
60. Santos, J. H., Mandavilli, B. S., and Van Houten, B. (2002) Measuring oxidative mtDNA damage and repair using quantitative PCR. *Methods Mol. Biol.* **197,** 159–176 CrossRef Medline
61. Gonzalez-Hunt, C. P., Rooney, J. P., Ryde, I. T., Anbalagan, C., Joglekar, R., and Meyer, J. N. (2016) PCR-based analysis of mitochondrial DNA copy number, mitochondrial DNA damage, and nuclear DNA damage. *Curr. Protoc. Toxicol.* **67,** 20.11.1–20.11.25 CrossRef Medline
62. Guo, X., Niemi, N. M., Hutchins, P. D., Condon, S. G. F., Jochem, A., Ulbrich, A., Higbee, A. J., Russell, J. D., Senes, A., Coon, J. J., and Pagliarini, D. J. (2017) Ptc7p dephosphorylates select mitochondrial proteins to enhance metabolic function. *Cell Rep.* **18,** 307–313 CrossRef Medline
63. Eyer, P., Worek, F., Kiderlen, D., Sinko, G., Stuglin, A., Simeon-Rudolf, V., and Reiner, E. (2003) Molar absorption coefficients for the reduced Ellman reagent: reassessment. *Anal. Biochem.* **312,** 224–227 CrossRef Medline
64. Zhang, T., Lei, J., Yang, H., Xu, K., Wang, R., and Zhang, Z. (2011) An improved method for whole protein extraction from yeast *Saccharomyces cerevisiae*. *Yeast* **28,** 795–798 CrossRef Medline
65. Schägger, H., Cramer, W. A., and von Jagow, G. (1994) Analysis of molecular masses and oligomeric states of protein complexes by blue native electrophoresis and isolation of membrane protein complexes by two-dimensional native electrophoresis. *Anal. Biochem.* **217,** 220–230 CrossRef Medline
66. Wittig, I., Braun, H. P., and Schägger, H. (2006) Blue NativePAGE. *Nat. Protoc.* **1,** 418–428 CrossRef Medline
67. Barros, M. H., and Tzagoloff, A. (2017) Aep3p-dependent translation of yeast mitochondrial *ATP8*. *Mol. Biol. Cell* **28,** 1426–1434 CrossRef Medline
68. Santos-Ocaña, C., Do, T. Q., Padilla, S., Navas, P., and Clarke, C. F. (2002) Uptake of exogenous coenzyme Q and transport to mitochondria is required for bc_1 complex stability in yeast *coq* mutants. *J. Biol. Chem.* **277,** 10973–10981 CrossRef Medline
69. Winzeler, E. A., Shoemaker, D. D., Astromoff, A., Liang, H., Anderson, K., Andre, B., Bangham, R., Benito, R., Boeke, J. D., Bussey, H., Chu, A. M., Connelly, C., Davis, K., Dietrich, F., Dow, S. W., *et al.* (1999) Functional characterization of the *S. cerevisiae* genome by gene deletion and parallel analysis. *Science* **285,** 901–906 CrossRef Medline
70. Sikorski, R. S., and Hieter, P. (1989) A system of shuttle vectors and yeast host strains designed for efficient manipulation of DNA in *Saccharomyces cerevisiae*. *Genetics* **122,** 19–27 Medline
71. Christianson, T. W., Sikorski, R. S., Dante, M., Shero, J. H., and Hieter, P. (1992) Multifunctional yeast high-copy-number shuttle vectors. *Gene* **110,** 119–122 CrossRef Medline

Appendix II

Comparing the effects of organic cosolvents on acetylcholinesterase and butyrylcholinesterase activity

Analytical Biochemistry 654 (2022) 114796

Contents lists available at ScienceDirect

Analytical Biochemistry

journal homepage: www.elsevier.com/locate/yabio

Comparing the effects of organic cosolvents on acetylcholinesterase and butyrylcholinesterase activity

Noelle A. Novales [1], Jason P. Schwans [*]

Department of Chemistry and Biochemistry, California State University, Long Beach, 1250 Bellflower Boulevard, California, 90840-9507, Long Beach, USA

ARTICLE INFO

Keywords:
Alzheimer's disease
Butyrylcholinesterase
Acetylcholinesterase
Cosolvent
Enzyme inhibition

ABSTRACT

The use of cosolvents to solubilize compounds under investigation while having minimal effects on enzyme activity is an important component in many biochemical studies. Predicting the effects of cosolvents on enzyme activity can be complicated, as enzymes with similar overall structures might exhibit different behaviors in different cosolvents. In this study, the effects of several commonly used cosolvents: Methanol, acetonitrile, acetone, and dimethyl sulfoxide (DMSO), on two cholinesterases, acetylcholinesterase (AChE) and butyrylcholinesterase (BChE), were evaluated. Although the overall structures are highly similar, AChE activity was more sensitive to the organic cosolvents tested compared to BChE. Effects of the cosolvents on activity did not vary over time and activity was restored upon dilution of the cosolvent. Michaelis-Menten kinetics experiments showed that V_{max} values were not substantially affected, while K_M values increased up to ~20-fold for AChE and ~4-fold for BChE in the presence of 5% DMSO or acetone. The results suggest that BChE demonstrates more robustness to its cosolvent environment compared to AChE, and that cosolvents effects may arise from the molecules acting as inhibitors. The results may aid decisions of cosolvents used in enzyme assays and may help guide experimental conditions and design when conducting experiments comparing different enzymes.

1. Introduction

The limited aqueous solubility of many organic compounds often presents a challenge in conducting biochemical studies. For example, small organic molecules designed as potential enzyme inhibitors often have limited solubility in water and this limitation can affect the scope of compounds investigated and/or conditions evaluated, e.g., Refs. [1–4]. To overcome this limitation, organic cosolvents, e.g., dimethyl sulfoxide (DMSO), methanol (MeOH), or acetonitrile (ACN), are often included in biochemical assays [5–9]. While organic cosolvents may help solubilize compounds, the cosolvents can affect enzyme activity and these changes can complicate comparing results from different studies when different cosolvents or cosolvent concentrations are used [6–10].

Herein, the effects for a series of cosolvents on cholinesterase activity were evaluated with a goal of assisting in the design of biochemical analyses. Cholinesterases were selected due to their proposed role in neurodegenerative diseases such as Alzheimer's disease (AD), and the development of potent and specific inhibitors of these enzymes is an active area of research, e.g., Refs. [8,9,11,12]. Indeed, multiple studies have evaluated the effect of small molecules on the activity of the two main types of cholinesterases: Acetylcholinesterase (AChE) and butyrylcholinesterase (BChE), and in these studies, several cosolvents have been used including acetone, acetonitrile, DMSO, and methanol [13–18]. While DMSO is an organic solvent commonly used in enzymatic studies, Kumar and Darreh-Shorri recently reported that DMSO was a mixed-competitive inhibitor of AChE [15]. In contrast to AChE, the authors also noted that the DMSO concentrations tested did not affect the activity of BChE. Building on the observations and noting the different cosolvents used in the literature for cholinesterase inhibition studies, we systematically evaluated and compared the effects of a series of organic cosolvents on AChE and BChE activity. Although the two cholinesterases share highly similar structures (~50% identity and a higher similarity; Fig. 1) [19–22] the results identified differences in the sensitivity of the enzymes to a series of cosolvents. The study may help guide the use of organic cosolvents in evaluating potential enzyme inhibitors and serve as the foundation for future investigations regarding the use of organic cosolvents in studying protein structure and function.

* Corresponding author.
E-mail address: Jason.schwans@csulb.edu (J.P. Schwans).
[1] Present Address: Department of Chemistry and Biochemistry and the Molecular Biology Institute, University of California, California, 90095–1569, Los Angeles.

https://doi.org/10.1016/j.ab.2022.114796
Received 1 February 2022; Received in revised form 15 June 2022; Accepted 16 June 2022
Available online 27 June 2022

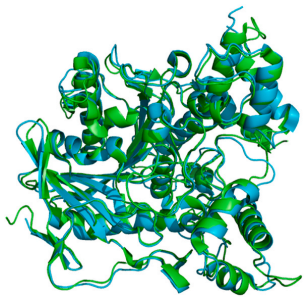

Fig. 1. Superposition of AChE (green) and BChE (cyan) x-ray structures (PDB IDs: AChE 1C2B; BChE 1P0I). (For interpretation of the references to color in this figure legend, the reader is referred to the Web version of this article.)

2. Materials and methods

2.1. Materials

All reagents were of the highest grade that could be obtained commercially (≥97%). Water (18.2 MΩ cm) was generated using a Barnstead Millipore Milli-Q water system and was used to prepare all buffers and aqueous solutions. Methanol, acetonitrile, acetone, and DMSO were from Fisher Scientific or Alfa Aesar and used without further purification. Acetylcholinesterase from *Electrophorus electricus* (AChE, E. C. 3.1.1.7) and butyrylcholinesterase (BChE, E.C. 3.1.1.8) from equine serum were obtained from Sigma-Aldrich (Catalog numbers: AChE: C3389; BChE: C7512).

2.2. Determining the extinction coefficient in water-organic cosolvent mixtures

The chromophoric indicator, 5,5′-dithiobis-(2-nitrobenzoic acid) (DTNB), was used to monitor enzyme activity [23]. The extinction coefficient of 5-thio-2-nitrobenzoic acid (TNB) in each water-organic cosolvent mixture was measured by determining the absorbance change upon adding a known concentration of reduced glutathione to DTNB. The reactions were conducted at 25 °C in 100 mM sodium phosphate, pH 7.5, 1 mM $MgCl_2$, 0.2 mM DTNB, 1.2 μg/μL BSA, and varying concentrations of organic cosolvent. Reduced glutathione was added in varying concentrations leading to measured absorbance values at 412 nm of 0.1–0.8 upon quantitative reaction of glutathione with DTNB. The known concentrations of glutathione in the assay were then used to calculate the extinction coefficients using Beer's law.

2.3. Stock enzyme solution preparation

Stock enzyme solutions were prepared to 7 mg/mL in double-distilled water and further diluted 40-400-fold immediately prior to assay. The varying dilutions were used to prepare starting enzyme solutions of different concentrations. Active enzyme concentrations were estimated as described by Carletti et al. [18] using the previously reported k_{cat} values of 8.2×10^5 min^{-1} for AChE [24] and of 1.7×10^5 min^{-1} for BChE [25]. Enzyme concentrations used in assays in the absent of cosolvents typically gave ΔAbs_{412} values of 0.4–1.0 min^{-1}.

2.4. Determining the relative effect of cosolvents on enzyme activity

Activity measurements were performed based on the method of Ellman [23]. Reactions were conducted at 25 °C in 100 mM sodium phosphate, pH 7.5, 1 mM $MgCl_2$, 0.2 mM DTNB, 1.2 μg/μL BSA, 100 μM butyrylthiocholine or 100 μM acetylthiocholine, and varying the cosolvent concentration. Reactions were initiated by adding enzyme (final concentrations of approximately 0.2–20 nM) and initial rates were determined by monitoring continuously at 412 nm. Relative activity was measured using a range of approximate enzyme concentrations to evaluate if the concentration affected the relative observed activity. As the molar absorptivity did not vary substantially under the cosolvent conditions tested, a molar absorptivity of 14,150 $M^{-1}cm^{-1}$ was used to calculate product formation without cosolvents and this value agreed with the molar absorptivity calculated using the method described above [26]. Relative activity was determined by dividing the initial rate for reaction in the presence of each cosolvent condition relative to the reaction without cosolvent. To evaluate if enzyme quantity affected relative activity measurements for the cosolvents, enzyme solutions of different concentrations were prepared immediately prior to the assays (dilutions over two orders of magnitude). Initial rates were determined by the recording absorbance change over 30–60 s with longer recording times for the lower enzyme concentrations. The absorbance changes remained linear over the length of the measurements and the relative activities in the presence of each cosolvent compared to reactions without cosolvents were indistinguishable for the different enzyme quantities.

2.5. Determining if cosolvent effects are time dependent

Measurements to evaluate if the cosolvent effects were time dependent were conducted similar to the relative activity measurements. The enzyme was incubated in the presence of cosolvent using the same conditions as in section 2.4 except DTNB and the substrate was omitted (25 °C in 100 mM sodium phosphate, pH 7.5, 1 mM $MgCl_2$, 1.2 μg/μL BSA and varying cosolvent concentrations). After the incubation time, an aliquot was removed and added to a solution containing DTNB, substrate, and 5% cosolvent. The final concentrations of DTNB and substrate were 0.2 mM and 0.1 mM, respectively. Initial rates were determined by continuously monitoring absorbance at 412 nm for 30–60 s. The cosolvent concentration was maintained at 5% throughout the incubation and activity measurement. Relative activity was determined by plotting the activity in the presence of each cosolvent after the incubation time versus a control reaction incubated without cosolvent. The activity of the control reaction was unchanged over the time evaluated. A minimum of three determinations from independent experiments were used to calculate the averages and standard deviations.

2.6. Determining if cosolvent effects are reversible

The enzyme was incubated in the presence of cosolvent using the same conditions as in section 2.4 except DTNB and the substrate was omitted (25 °C in 100 mM sodium phosphate, pH 7.5, 1 mM $MgCl_2$, 1.2 μg/μL BSA and 5% cosolvent). The samples were incubated at 25 °C for 10 min before dilution to evaluate reversibility. Similar results were observed upon a 30-min incubation time. For the dilution, a solution containing 100 mM sodium phosphate, pH 7.5, 1 mM $MgCl_2$, 1.2 μg/μL BSA, 0.2 mM DTNB, and 0.1 mM substrate was added. The final volume of the dilution was ~4 mL leading to a final concentration of ~0.02% cosolvent. After mixing, 1 mL was transferred to a cuvette, and the initial rates were determined by continuously monitoring absorbance at 412 nm for 30–60 s. Relative activity was determined by the ratio of activity between a sample undergoing the incubation and dilution with cosolvent present compared to sample undergoing the same protocol in the absence of cosolvent. A minimum of three determinations from independent experiments were used to calculate the averages and standard deviations.

2.7. Determining V_{max}, K_M, and estimating K_I values using Michaelis-Menten kinetics

Michaelis-Menten kinetics measurements were performed based on

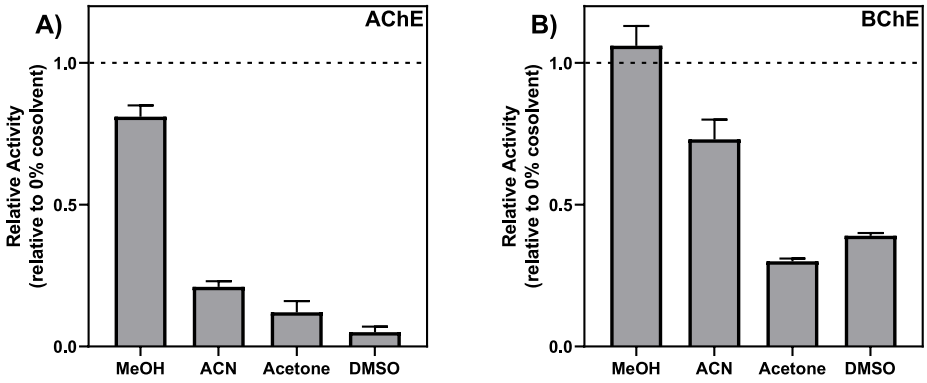

Fig. 2. Effect of 5% cosolvents on A) AChE and B) BChE activity. The values are from Table S2.

the method of Ellman [23]. Reactions were conducted at 25 °C in 100 mM sodium phosphate, pH 7.5, 1 mM $MgCl_2$, 0.2 mM DTNB, 1.2 μg/μL BSA, and varying the substrate concentration, *S*-acetylthiocholine and *S*-butyrylthiocholine for reactions with AChE and BChE, respectively. As noted in section 2.4, observed inhibition from the cosolvents were unaffected by the enzyme concentrations tested. Michaelis-Menten kinetics were conducted using an enzyme concentration to give an absorbance change of 0.4–0.8 min^{-1}. The V_{max} values were linear with the enzyme concentrations tested and were reproducible from different enzyme solution preparations. The values of V_{max} and K_M were determined by fitting the initial rates of product formation as a function of substrate concentration to the Michaelis-Menten equation using KaleidaGraph (Synergy Software). A minimum of three determinations from independent experiments were used to calculate the averages and standard deviations. A one-way ANOVA with Dunnett's multiple comparisons test was performed using GraphPad Prism 8. K_I values were estimated from the kinetics data using GraphPad Prism 8.

2.8. Determining IC_{50} values

Experiments to determine IC_{50} values were conducted similar to the Michaelis-Menten assays. A series of cosolvent dilutions in water was first generated. For each substrate concentration tested, reactions were conducted at 25 °C in 100 mM sodium phosphate, pH 7.5, 1 mM $MgCl_2$, 0.2 mM DTNB, 1.2 μg/μL BSA, and varying the cosolvent concentration. *S*-acetylthiocholine and *S*-butyrylthiocholine were the substrates for reactions with AChE and BChE, respectively. The initial rate of product formation was determined by monitoring the change in absorbance (412 nm) upon enzyme addition. The percent relative activity was determined by dividing the absorbance change slope for the reaction at each cosolvent concentration versus the reaction with the lowest cosolvent concentration. The activity at the lowest cosolvent concentrations were indistinguishable from reactions without cosolvent (a sample using a dilution of the cosolvent as the lowest concentration was used so the log of the cosolvent concentration could be plotted as the x-axis). The IC_{50} values were determined by plotting the relative activity versus the log of the cosolvent concentration and fitting the data using KaleidaGraph (Synergy Software). A minimum of three determinations from independent experiments were used to calculate the averages and standard deviations.

3. Results and discussion

3.1. Surveying the effect of 5% (vol/vol) organic cosolvent on AChE and BChE activity

Cholinesterase activity is often assayed via a colorimetric assay using Ellman's reagent [23,26]. In this experiment, enzymatic hydrolysis of a thiol-containing substrate such as *S*-acetylthiocholine or *S*-butyrylthiocholine generates a thiolate that undergoes a disulfide exchange reaction with 5, 5′-dithiobis-(2-nitrobenzoic acid) (Ellman's reagent; DTNB) generating 5-thio-2-nitrobenzoic acid (TNB). The change in absorbance at 412 nm due to TNB formation is monitored by absorbance spectroscopy and used to quantitate thiol concentration. As extinction coefficients are solvent dependent, changes in the TNB extinction coefficient in the presence of different cosolvents could complicate comparisons between reactions in different solvents [27].

To evaluate the magnitude of variation in the TNB extinction coefficient under the conditions tested, an experiment was first conducted to compare the observed absorbance and calculated extinction coefficients for reaction of Ellman's reagent with a thiol compound in the presence of different cosolvents. Glutathione was used as the thiol source, as the reagent is readily available and provided easy access to preparing thiol-containing solutions. The absorbance change for reaction of an excess of Ellman's reagent with glutathione was determined in the absence or presence of 5% of a cosolvent. As summarized in Supplementary Material Table S1, the absorbance values varied <1% for samples with or without organic cosolvent (leading to variation in the calculated extinction coefficients of <1%). The results suggested that the same extinction coefficient can be used to determine relative enzyme activity in the presence of different cosolvents.

With the ability to directly compare the absorbance change in presence of 5% cosolvent, enzyme activity was next evaluated with the inclusion of methanol, acetonitrile, acetone or DMSO. The cosolvents were selected, as they were previously used in cholinesterase assays [14–18]. All cosolvent concentrations are presented as vol/vol ratios in the cosolvent/water mixtures.

As shown in Fig. 2, all cosolvents tested decreased AChE activity with methanol (MeOH) having the smallest effect and DMSO leading to the largest effect decreasing enzyme to ~10% of the activity in the absence of cosolvent. For BChE, no decrease in activity was observed in 5% methanol, but activity was reduced in the presence of the other cosolvents tested. To test if the concentration of the enzyme in the assay affected the results, the estimated enzyme concentration was varied over two orders of magnitude. Similar results were obtained suggesting that the observations are independent of the concentration of enzyme in the

Table 1
Relative activity measurements over time in 5% cosolvent.

Cosolvent	AChE					
	Time (min)					
	1	2	5	10	30	60
MeOH	0.74 ± 0.02	0.75 ± 0.03	0.76 ± 0.02	0.73 ± 0.03	0.80 ± 0.01	0.71 ± 0.08
ACN	0.25 ± 0.05	0.25 ± 0.05	0.25 ± 0.03	0.24 ± 0.03	0.26 ± 0.04	0.26 ± 0.05
Acetone	0.10 ± 0.01	0.09 ± 0.01	0.09 ± 0.01	0.09 ± 0.01	0.10 ± 0.02	0.13 ± 0.04
DMSO	0.06 ± 0.01	0.06 ± 0.01	0.06 ± 0.01	0.06 ± 0.01	0.06 ± 0.01	0.06 ± 0.01
	BCHE					
Cosolvent	Time (min) 1	2	5	10	30	60
MeOH	1.08 ± 0.04	1.09 ± 0.08	1.11 ± 0.10	1.13 ± 0.06	1.11 ± 0.07	1.15 ± 0.07
ACN	0.78 ± 0.07	0.79 ± 0.06	0.78 ± 0.06	0.81 ± 0.09	0.77 ± 0.05	0.79 ± 0.11
Acetone	0.34 ± 0.03	0.34 ± 0.03	0.36 ± 0.03	0.36 ± 0.02	0.36 ± 0.04	0.37 ± 0.03
DMSO	0.42 ± 0.01	0.38 ± 0.04	0.44 ± 0.01	0.39 ± 0.09	0.45 ± 0.02	0.45 ± 0.01

experiment. While a recent study using a pooled sample of human plasma BChE report 1–5% DMSO did not affect BChE activity [15], herein activity was reduced to ~40% of the activity in the absence of a cosolvent. Acetonitrile (ACN) and acetone also led to a decrease in BChE activity. Overall, while the effect of the cosolvents on BChE activity was less than AChE, except for methanol in the BChE reaction, each of the cosolvents tested affected enzyme activity.

The greater sensitivity of AChE relative to BChE to organic cosolvents paralleled the results of Kumar and Darreh-Shorri where they tested enzyme activity in the presence of methanol, DMSO, acetonitrile, or acetone, but in this study a decrease in BChE activity was observed with most 5% cosolvent assays [15]. Several sources could account for the observation. In this study AChE from *Electrophorus electricus* and BChE from equine serum were used. The sources used herein were selected, as previous structural and functional studies have shown the enzymes are highly similar to the human forms, the enzyme sources have been used in previous biochemical studies, and the enzymes are commercially available at a substantially lower cost compared to the human enzymes. Differences in the sensitivity of BChE to organic cosolvents could be due to the enzyme source, preparation, or experimental conditions. Nevertheless, in agreement with the literature the results suggest that AChE activity is more sensitive to organic cosolvents.

3.2. Evaluating the effect of lower concentrations of organic cosolvents, 1–2% (vol/vol), on AChE and BChE activity

While a final cosolvent concentration of 5% generally reduces enzyme activity for AChE and BChE, studies have reported using lower concentrations of 1–2% cosolvent to solubilize the compounds analyzed. It is possible that the lower cosolvent concentrations have little effect on enzyme activity, thereby allowing ready comparison of results determined in the presence of different cosolvents. To test this possibility, the activity experiment was repeated with final cosolvent concentrations of 1% or 2% (Table S2). The effects of the cosolvents on activity were less than shown in Fig. 2, but even with 1% DMSO AChE activity was decreased by 75% and BChE activity decreased by approximately 20%. Acetonitrile had a smaller effect on activity, as while AChE activity was decreased in the presence of the cosolvent, BChE activity was not affected by 1–2% acetonitrile. In contrast, acetone reduced activity by 60% and 15% for AChE and BChE, respectively, even in the presence of 1% cosolvent. Together, the results further support that AChE is more sensitive to organic cosolvents relative to BChE.

Table 2
Evaluating reversibility of cosolvent effects.

AChE	Rel. Activity After Dilution	BChE	Rel. Activity After Dilution
No Cosolvent	(1)	No Cosolvent	(1)
MeOH	0.96 ± 0.04	MeOH	0.96 ± 0.02
ACN	1.00 ± 0.04	ACN	0.93 ± 0.09
Acetone	0.94 ± 0.08	Acetone	1.06 ± 0.10
DMSO	0.96 ± 0.04	DMSO	0.98 ± 0.06

3.3. Evaluating if cosolvent effects on activity vary over time for AChE and BChE

Next, assays were conducted to evaluate if the effect of the cosolvent on activity changes over time, potentially complicating time-dependent enzyme inhibition experiments. The enzyme was incubated in the presence of 5% cosolvent without substrate or DTNB present. Aliquots were removed at varying timepoints, and activity was measured maintaining 5% cosolvent in the assay. Control reactions without cosolvent present were performed concurrently and the reactions did not show a change in enzyme activity over the time course tested. The results are reported as relative activity (activity with cosolvent versus the absence of cosolvent). As shown in Table 1, the relative activity was unchanged for AChE and BChE in the presence of the cosolvents over the 1-h time course. The relative activity for the initial, 1-min timepoint was similar to experiments without preincubation, suggesting the enzyme activity was unchanged over the shortest incubation time relative to experiments without a preincubation period. As cholinesterase activity measurements are often completed in 30–60 s and no change was observed up to 1-h, longer time courses were not pursued. The time dependence was examined, as denaturation of the enzyme in the presence of the cosolvent or other physical changes could be time dependent. However, the results suggest that activity effects from the cosolvents do not have different time dependencies within the timeframe of many cholinesterase inhibition assays.

3.4. Evaluating if cosolvent effects on activity are reversible for AChE and BChE

The reversibility of the effects of cosolvents on activity was next tested. If the organic cosolvents change the protein conformation and/or denature the enzyme, then it is possible that activity will not be restored upon removal of the cosolvent [10]. If the organic cosolvent interacts with the enzyme such as acting as an inhibitor, then removal of the cosolvent might restore enzyme activity. To evaluate these possibilities, the enzymes were incubated in the presence of a cosolvent and then diluted to reduce the concentration of the cosolvent in the reaction medium. The results summarized in Table 2 show that upon dilution the relative enzyme activity was similar for samples incubated in the presence of a cosolvent compared to a control reaction undergoing the same dilution protocol without cosolvent present. Similar results were obtained for AChE and BChE suggesting that the cosolvent effects for the conditions tested were reversible. If the reduction in activity due to cosolvent results from partial denaturation of the enzyme, then the restoration of enzyme upon dilution suggests that the denaturation may be reversible. Another possibility is that the cosolvent is interacting as an inhibitor and the dilution reduces the concentration of this inhibitor. To test these possibilities and potential type of inhibition, Michaelis-Menten kinetics experiments were next conducted.

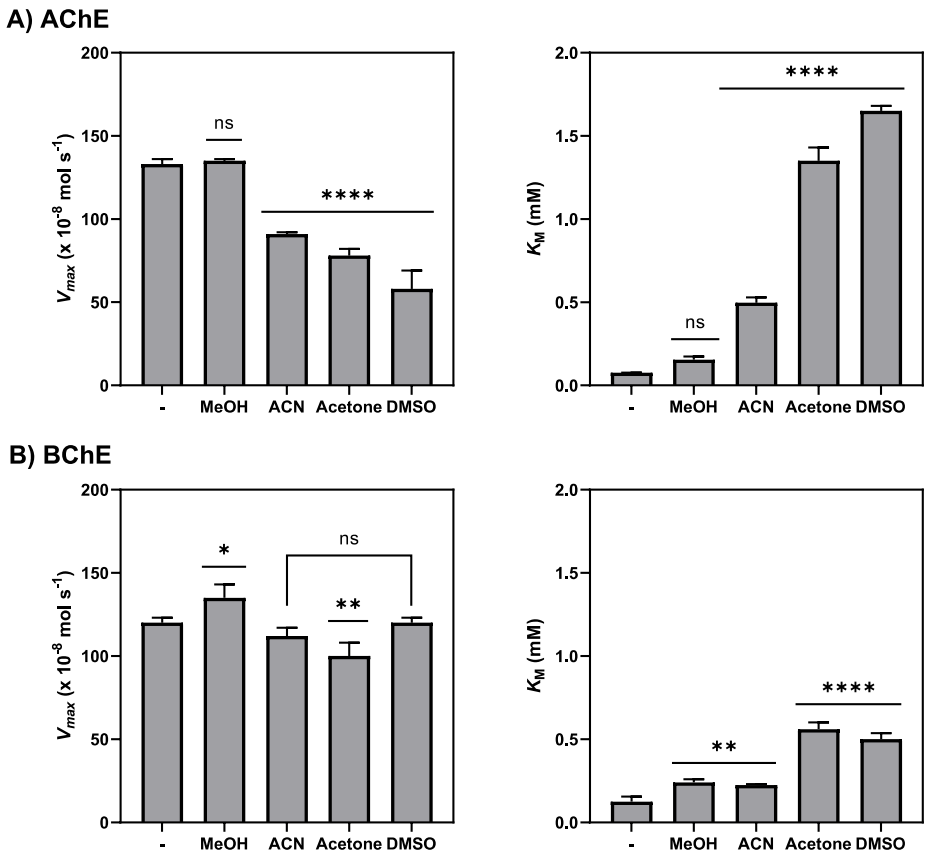

Fig. 3. Michaelis-Menten results for A) AChE and B) BChE in 5% cosolvent. Reaction with no cosolvent is noted with the dash (−). MeOH = methanol; ACN = acetonitrile. Values are from Table S3. The data show mean ± S.D., and the statistical significance as compared to reactions with no cosolvent is represented by *, $p < 0.05$; **, $p < 0.001$; and ****, $p < 0.0001$.

3.5. Evaluating the effect of organic cosolvents on V_{max} and K_M for AChE and BChE

If a cosolvent is acting as a competitive inhibitor with the substrate, then in the simplest case the cosolvent is predicted to increase the K_M value for the substrate without affecting V_{max}. However, as noted above, Kumar and Darreh-Shori reported that DMSO is a mixed competitive inhibitor for human AChE [15]. To evaluate the type of inhibition and compare AChE and BChE for the different cosolvents, the values for V_{max} and K_M were determined in the presence of each organic cosolvent for the two enzymes. While k_{cat} values can be useful for comparing enzyme activity between different studies, errors in concentration determination affect the calculated k_{cat} values. Herein, the values are reported as V_{max}, as although commercially available cholinesterases were used, potential impurities in the enzyme samples can affect concentration determinations and calculations of k_{cat} values. Nevertheless, comparing V_{max} values provides the information needed to evaluate the type of inhibition and relative activity.

The results from the kinetics measurements at 5% cosolvent are summarized in Fig. 3. This concentration was chosen as a change in the relative activity was observable in the presence of 5% cosolvent but the enzymes were active enough to allow reproducible kinetics measurements. Experiments were also conducted with 2% cosolvent and the results are summarized in Table S3.

Methanol had little effect on the V_{max} value for AChE, while acetonitrile, acetone, and DMSO decreased V_{max}. All the organic cosolvents tested had no observable or little effect on the V_{max} values for BChE. In contrast, the K_M values were increased in the presence of organic cosolvents. Acetone and DMSO had the largest effects on the K_M values for AChE with an increase of approximately ten-fold. Although the changes were smaller for BChE compared to AChE, the K_M value was approximately two-fold higher in the presence of acetonitrile, and approximately four-fold higher in the presence of acetone or DMSO. Smaller effects were observed if the cosolvent concentration was lower (2% versus 5%, Table S3).

One model to account for changes in K_M values upon cosolvent addition is that the cosolvent competes with the substrate as an inhibitor [28–30]. In the absence of substrate, water is expected to occupy the enzyme active site, and this water is likely displaced or reorganized upon substrate binding. Structures show the active sites of both AChE and BChE are lined with multiple hydrophobic residues and these residues could interact favorably with the hydrophobic portions of organic cosolvents [19–21]. Substrate binding occupies space in the active site likely displacing hydrophobic organic cosolvent. As the partitioning of

Table 3
Estimated K_I values from Michaelis-Menten experiments.

Cosolvent	AChE ~K_I (mM)	BChE ~K_I (mM)
MeOH	4500	>4500
ACN	420	3400
Acetone	145	1100
DMSO	80	1650

the substrate between bulk solvent and active site could be affected by competition between the substrate and solvent for the active site, the presence of different cosolvents could lead to the behavior observed like a competitive inhibitor. However, the changes in V_{max} for the different cosolvents suggest that more complicated mixed competitive inhibition may be occurring. DMSO is the most polar cosolvent tested and had the largest effect, leading to a suggestion that less polar cosolvents may show a smaller effect. However, methanol and acetone have a similar polarity index and the enzymes were more sensitive to acetone. Additional studies beyond on the scope of this work are needed to further dissect the molecular basis for the cosolvent effects. Nevertheless, the results show greater effects on the K_M value for the substrate compared to changes in V_{max}, and larger effects for AChE compared to BChE.

3.6. Comparing inhibition constant (K_I) values and dose-response inhibition curves for organic cosolvents on AChE and BChE activity

The kinetics data in the previous section allowed for estimation of the inhibition constant (K_I) values. Kumar and Darreh-Shorri conducted a similar study for human recombinant AChE and reported estimated K_I values of 4200, 360, 177, an 81 mM for methanol, acetonitrile, acetone, and DMSO [15]. The results for AChE from *Electrophorus electricus* AChE in this study summarized in Table 3 and Fig. S1 show similar estimated K_I values compared to human recombinant AChE. Comparison to BChE shows that the BChE K_I values are approximately 10-fold higher for acetonitrile and acetone and approximately 20-fold higher for DMSO as the cosolvent. The methanol K_I value for BChE is shown as a limit due to the activity being unchanged across the methanol concentrations tested.

IC_{50} values offer a useful approach to compare the relative inhibition for compounds under investigation. However, a potential complication when using IC_{50} values to evaluate inhibitors is that the values are dependent on substrate concentration. For the cholinesterases, Kumar and Darreh-Shorri reported IC_{50} values for DMSO inhibition of human recombinant AChE varied by ~2.5-fold across a 30-fold range of substrate concentrations (0.3–1.0 mM) [15]. To test if a similar variation was observed for eel AChE and to compare to equine BChE, IC_{50} values were determined at several substrate concentrations. For this dose-response experiment, the substrate concentration was held constant, and the percent inhibition was calculated using a series of cosolvent concentrations. The percent inhibition for each condition was then plotted versus the log of the cosolvent concentration to determine the IC_{50} value.

The results summarized in Tables 4 and SI Figs. 2-3s how that for AChE the IC_{50} values generally increased ~2.5-3-fold over the substrate ranges tested. A similar trend might be observed for methanol, but as >50% enzyme activity was observed at the highest cosolvent concentration tested (~5 mM) the value is represented as a limit. The IC_{50} values for BChE showed a similar 3-4-increase in IC_{50} values from the lowest to the highest substrate concentration. Methanol IC_{50} values reported as limits result from conditions where >50% activity remaining at the highest cosolvent concentration tested.

As cosolvent concentrations in experiments are often reported in percentages (vol/vol) and not molarity, to provide a more ready comparison the average IC_{50} concentrations were converted to percentages cosolvent (Tables 4 and SI Figs. 2–3). The results show that even with 1 mM substrate, ≤1% DMSO reduced AChE activity by 50% or greater. Acetonitrile and acetone also had pronounced effects on AChE activity with the lowest IC_{50} percentages of 1.6 and 0.5%, for acetonitrile and acetone, respectively. In contrast, the lowest methanol IC_{50} value was ~8%, a value below the 1–2% cosolvent often used in inhibition studies.

The cosolvent IC_{50} values for BChE were higher than those for AChE. However, at the lower substrate concentrations tested, ~2% cosolvent for acetone and DMSO reduced enzyme activity by ~50%. BChE was less sensitive to acetonitrile concentrations, and BChE activity was largely unaffected by the methanol concentrations tested. Overall, the results parallel the relative activity measurements summarized in Fig. 2. AChE is more sensitive to cosolvents than BChE. When comparing the same concentration of cosolvent, DMSO has the largest effect followed by acetone, acetonitrile, and methanol.

4. Conclusions

The effects of organic cosolvents on enzyme activity have been an important experimental consideration in biochemical studies and has been of long-standing interest in studying enzyme activity [5]. Organic cosolvents in enzymatic reactions have also received attention in the application of biocatalytic reactions where enzymes can be used in synthetic organic chemistry [31–34]. This widespread interest has led to the investigation of the effects of numerous organic cosolvents on different enzymes and with varying techniques. Here, a primary goal of

Table 4
IC_{50} values at different substrate concentrations.

AChE								
Substrate conc. (mM)	**MeOH**		**ACN**		**Acetone**		**DMSO**	
	IC_{50} (mM)	**(%)**	**IC_{50} (mM)**	**(%)**	**IC_{50} (mM)**	**(%)**	**IC_{50} (mM)**	**(%)**
0.03	1910 ± 113	7.7	309 ± 64	1.6	68 ± 8	0.5	35 ± 3	0.2
0.06	2130 ± 161	8.6	308 ± 47	1.6	67 ± 7	0.5	44 ± 3	0.3
0.12	2580 ± 223	10.4	342 ± 50	1.8	75 ± 7	0.6	48 ± 3	0.3
0.25	3460 ± 273	14.0	418 ± 66	2.2	98 ± 8	0.7	66 ± 3	0.5
0.5	5300 ± 242	21.4	549 ± 90	2.9	151 ± 1	1.1	87 ± 6	0.6
1.0	>5000	>20	730 ± 110	3.8	229 ± 20	1.7	133 ± 9	0.9
BChE								
Substrate conc. (mM)	**MeOH**		**ACN**		**Acetone**		**DMSO**	
	IC_{50} (mM)	**(%)**	**IC_{50} (mM)**	**(%)**	**IC_{50} (mM)**	**(%)**	**IC_{50} (mM)**	**(%)**
0.03	>5000	>20	618 ± 161	3.2	197 ± 37	1.5	229 ± 17	1.6
0.06	>5000	>20	706 ± 215	3.7	239 ± 50	1.8	274 ± 33	1.9
0.12	>5000	>20	1350 ± 513	7.1	305 ± 53	2.3	404 ± 38	2.9
0.25	>5000	>20	1580 ± 643	8.3	426 ± 94	3.2	594 ± 66	4.2
0.5	>5000	>20	1820 ± 678	9.5	606 ± 132	4.5	860 ± 54	6.1
1.0	>5000	>20	1900 ± 797	9.9	789 ± 114	5.8	752 ± 97	5.3

this study was to evaluate and compare cosolvent effects for two enzymes of similar structures to aid in developing experimental protocols.

Overall, the results suggest that while the two enzymes have similar structures, AChE is more sensitive to organic cosolvents relative to BChE. As noted in the Introduction, AChE and BChE share ~50% identity. Building on this structural comparison, a structural similarity search showed that other esterases such as cholesterol esterase and cocaine esterase share ~30–40% structural identity with the cholinesterases [35,36]. A potential future direction may be to evaluate the effects of organic cosolvents on other esterases with similar structure and cholinesterase activity to determine if their behavior is similar to AChE or BChE [37].

While raising potential complications in assaying inhibitors, the results may also help guide future experiments in evaluating the effects of cosolvents on enzyme activity. As noted above, DMSO was the most polar cosolvent tested and had the largest effect. However, solvents suggested to have similar polarities such as acetone and methanol had different effects on enzyme activity. Evaluating a series of structurally similar compounds such as a series of alcohols may help to better determine the contribution of polarity on inhibition.

Overall, the results highlight potential complexity in identifying conditions for screening of potential therapeutics across different enzymes and note that the organic cosolvent of interest may have differing effects of enzymes of similar structure. As organic cosolvents are often an important and necessary component of enzyme characterization and inhibition studies, their effects on activity can be accounted for by control experiments to account for different effects on enzymes even with nearly superimposable structures.

CRediT authorship contribution statement

Noelle A. Novales: Conceptualization, Methodology, Investigation, Writing – original draft, Writing – review & editing. **Jason P. Schwans:** Conceptualization, Methodology, Investigation, Writing – original draft, Writing – review & editing, Supervision.

Declaration of competing interest

None.

Acknowledgements

This work was supported in part by the National Institute of General Medical Sciences of the National Institutes of Health under Award Numbers and R25GM071638, UL1GM118979, TL4GM118980, and RL5GM118978. The content is solely the responsibility of the authors and does not necessarily represent the official views of the National Institutes of Health.

Appendix A. Supplementary data

Supplementary data to this article can be found online at https://doi.org/10.1016/j.ab.2022.114796.

References

[1] L. Di, E.H. Kerns, Biological assay challenges from compound solubility: strategies for bioassay optimization, Drug Discov. Today 11 (2006) 446–451, https://doi.org/10.1016/j.drudis.2006.03.004.
[2] M.V.G. De la Rosa, R. Santiago, J.M. Romero, J. Duconge, J.-C. Monbaliu, V. López-Mejías, T. Stelzer, Solubility determination and correlation of warfarin sodium 2-propanol solvate in pure, binary, and ternary solvent mixtures, J. Chem. Eng. Data 64 (2019) 1399–1413, https://doi.org/10.1021/acs.jced.8b00977.
[3] S. Mallick, S. Pattnaik, K. Swain, P.K. De, Current perspectives of solubilization: potential for improved bioavailability, Drug Dev. Ind. Pharm. 33 (2007) 865–873, https://doi.org/10.1080/03639040701429333.
[4] K. Kawakami, N. Oda, K. Miyoshi, T. Funaki, Y. Ida, Solubilization behavior of a poorly soluble drug under combined use of surfactants and cosolvents, Eur. J. Pharm. Sci. Off. J. Eur. Fed. Pharm. Sci. 28 (2006) 7–14, https://doi.org/10.1016/j.ejps.2005.11.012.
[5] T. Ke, A.M. Klibanov, On enzymatic activity in organic solvents as a function of enzyme history, Biotechnol. Bioeng. 57 (1998) 746–750, https://doi.org/10.1002/(sici)1097-0290(19980320)57:6<746::aid-bit12>3.0.co;2-5.
[6] E. Ruckenstein, I.L. Shulgin, Effect of salts and organic additives on the solubility of proteins in aqueous solutions, Adv. Colloid Interface Sci. (2006) 123–126, https://doi.org/10.1016/j.cis.2006.05.018, 97–103.
[7] T. Magsumov, L. Ziying, I. Sedov, Comparative study of the protein denaturing ability of different organic cosolvents, Int. J. Biol. Macromol. 160 (2020) 880–888, https://doi.org/10.1016/j.ijbiomac.2020.05.260.
[8] S. Zhou, G. Huang, The biological activities of butyrylcholinesterase inhibitors, Biomed. Pharmacother. 146 (2022), 112556, https://doi.org/10.1016/j.biopha.2021.112556.
[9] S. Zhou, G. Huang, Synthesis and inhibitory activities of inhibitors for the treatment of Alzheimer's disease, Chem. Biol. Drug Des. 99 (2022) 727–735, https://doi.org/10.1111/cbdd.14016.
[10] D.R. Canchi, A.E. García, Cosolvent effects on protein stability, Annu. Rev. Phys. Chem. 64 (2013) 273–293, https://doi.org/10.1146/annurev-physchem-040412-110156.
[11] K. Sharma, Cholinesterase inhibitors as Alzheimer's therapeutics (Review), Mol. Med. Rep. 20 (2019) 1479–1487, https://doi.org/10.3892/mmr.2019.10374.
[12] R. Singh, N.M. Sadiq, Cholinesterase inhibitors, in: Treasure Island (FL), 2022.
[13] C.D. Andersson, N. Forsgren, C. Akfur, A. Allgardsson, L. Berg, C. Engdahl, W. Qian, F. Ekström, A. Linusson, Divergent structure-activity relationships of structurally similar acetylcholinesterase inhibitors, J. Med. Chem. 56 (2013) 7615–7624, https://doi.org/10.1021/jm400990p.
[14] J.A. Doorn, T.T. Talley, C.M. Thompson, R.J. Richardson, Probing the active sites of butyrylcholinesterase and cholesterol esterase with isomalathion: conserved stereoselective inactivation of serine hydrolases structurally related to acetylcholinesterase, Chem. Res. Toxicol. 14 (2001) 807–813, https://doi.org/10.1021/tx015501s.
[15] A. Kumar, T. Darreh-Shori, DMSO: a mixed-competitive inhibitor of human acetylcholinesterase, ACS Chem. Neurosci. 8 (2017) 2618–2625, https://doi.org/10.1021/acschemneuro.7b00344.
[16] K. Nakayama, J.P. Schwans, E.J. Sorin, T. Tran, J. Gonzalez, E. Arteaga, S. McCoy, W. Alvarado, Synthesis, biochemical evaluation, and molecular modeling studies of aryl and arylalkyl di-n-butyl phosphates, effective butyrylcholinesterase inhibitors, Bioorg. Med. Chem. 25 (2017) 3171–3181, https://doi.org/10.1016/j.bmc.2017.04.002.
[17] N.H. Barakat, X. Zheng, C.B. Gilley, M. MacDonald, K. Okolotowicz, J.R. Cashman, S. Vyas, J.M. Beck, C.M. Hadad, J. Zhang, Chemical synthesis of two series of nerve agent model compounds and their stereoselective interaction with human acetylcholinesterase and human butyrylcholinesterase, Chem. Res. Toxicol. 22 (2009) 1669–1679, https://doi.org/10.1021/tx900096j.
[18] E. Carletti, L.M. Schopfer, J.-P. Colletier, M.-T. Froment, F. Nachon, M. Weik, O. Lockridge, P. Masson, Reaction of cresyl saligenin phosphate, the organophosphorus agent implicated in aerotoxic syndrome, with human cholinesterases: mechanistic studies employing kinetics, mass spectrometry, and X-ray structure analysis, Chem. Res. Toxicol. 24 (2011) 797–808, https://doi.org/10.1021/tx100447k.
[19] I. Silman, J.L. Sussman, Recent developments in structural studies on acetylcholinesterase, J. Neurochem. 142 (Suppl) (2017) 19–25, https://doi.org/10.1111/jnc.13992.
[20] Y. Nicolet, O. Lockridge, P. Masson, J.C. Fontecilla-Camps, F. Nachon, Crystal structure of human butyrylcholinesterase and of its complexes with substrate and products, J. Biol. Chem. 278 (2003) 41141–41147, https://doi.org/10.1074/jbc.M210241200.
[21] T.L. Rosenberry, X. Brazzolotto, I.R. Macdonald, M. Wandhammer, M. Trovaslet-Leroy, S. Darvesh, F. Nachon, Comparison of the binding of reversible inhibitors to human butyrylcholinesterase and acetylcholinesterase: a crystallographic, kinetic and calorimetric study, Molecules 22 (2017), https://doi.org/10.3390/molecules22122098.
[22] A. Chatonnet, O. Lockridge, Comparison of butyrylcholinesterase and acetylcholinesterase, Biochem. J. 260 (1989) 625–634, https://doi.org/10.1042/bj2600625.
[23] G.L. Ellman, K.D. Courtney, V. Andres, R.M. Featherstone, A new and rapid colorimetric determination of acetylcholinesterase activity, Biochem. Pharmacol. 7 (1961) 88–90, https://doi.org/10.1016/0006-2952(61)90145-9.
[24] T.L. Rosenberry, Acetylcholinesterase, Adv. Enzymol. Relat. Area Mol. Biol. 43 (1975) 103–218, https://doi.org/10.1002/9780470122884.ch3.
[25] A.R. Main, E. Tarkan, J.L. Aull, W.G. Soucie, Purification of horse serum cholinesterase by preparative polyacrylamide gel electrophoresis, J. Biol. Chem. 247 (1972) 566–571.
[26] P.W. Riddles, R.L. Blakeley, B. Zerner, Reassessment of Ellman's reagent, Methods Enzymol. 91 (1983) 49–60, https://doi.org/10.1016/s0076-6879(83)91010-8.
[27] X. Liu, J.M. Cole, K.S. Low, Solvent effects on the UV–vis absorption and emission of optoelectronic coumarins: a comparison of three empirical solvatochromic models, J. Phys. Chem. C 117 (2013) 14731–14741, https://doi.org/10.1021/jp310397z.
[28] D. Huang, E. Rossini, S. Steiner, A. Caflisch, Structured water molecules in the binding site of bromodomains can be displaced by cosolvent, ChemMedChem 9 (2014) 573–579, https://doi.org/10.1002/cmdc.201300156.
[29] A. Wangler, A. Hüser, G. Sadowski, C. Held, Simultaneous prediction of cosolvent influence on reaction equilibrium and Michaelis constants of enzyme-catalyzed

ketone reductions, ACS Omega 4 (2019) 6264–6272, https://doi.org/10.1021/acsomega.8b03159.
[30] A. Wangler, R. Canales, C. Held, T.Q. Luong, R. Winter, D.H. Zaitsau, S.P. Verevkin, G. Sadowski, Co-solvent effects on reaction rate and reaction equilibrium of an enzymatic peptide hydrolysis, Phys. Chem. Chem. Phys. 20 (2018) 11317–11326, https://doi.org/10.1039/c7cp07346a.
[31] A.S. Bommarius, M.F. Paye, Stabilizing biocatalysts, Chem. Soc. Rev. 42 (2013) 6534–6565, https://doi.org/10.1039/c3cs60137d.
[32] Y.-R. Liang, Q. Wu, X.-F. Lin, Effect of additives on the selectivity and reactivity of enzymes, Chem. Rec. 17 (2017) 90–121, https://doi.org/10.1002/tcr.201600016.
[33] B. Schulze, M.G. Wubbolts, Biocatalysis for industrial production of fine chemicals, Curr. Opin. Biotechnol. 10 (1999) 609–615, https://doi.org/10.1016/s0958-1669(99)00042-7.
[34] G. Carrea, S. Riva, Properties and synthetic applications of enzymes in organic solvents, Angew. Chem., Int. Ed. Engl. 39 (2000) 2226–2254.
[35] E. Krissinel, K. Henrick, Secondary-structure matching (SSM), a new tool for fast protein structure alignment in three dimensions, Acta Crystallogr. D. Biol. Crystallogr. 60 (2004) 2256–2268, https://doi.org/10.1107/S0907444904026460.
[36] L. Holm, Using dali for protein structure comparison, Methods Mol. Biol. 2112 (2020) 29–42, https://doi.org/10.1007/978-1-0716-0270-6_3.
[37] C.J. Rogers, L.M. Eubanks, T.J. Dickerson, K.D. Janda, Unexpected acetylcholinesterase activity of cocaine esterases, J. Am. Chem. Soc. 128 (2006) 15364–15365, https://doi.org/10.1021/ja066241+.

Appendix III

Predicting and Understanding the Pathology of Single Nucleotide Variants in Human *COQ* Genes

antioxidants

MDPI

Article

Predicting and Understanding the Pathology of Single Nucleotide Variants in Human *COQ* Genes

Sining Wang †, Akash Jain †, Noelle Alexa Novales, Audrey N. Nashner, Fiona Tran and Catherine F. Clarke *

Department of Chemistry & Biochemistry, The Molecular Biology Institute, UCLA, Los Angeles, CA 90095, USA
* Correspondence: cathy@chem.ucla.edu; Tel.: +1-(310)-825-0771
† The authors contributed equally to this work.

Abstract: Coenzyme Q (CoQ) is a vital lipid that functions as an electron carrier in the mitochondrial electron transport chain and as a membrane-soluble antioxidant. Deficiencies in CoQ lead to metabolic diseases with a wide range of clinical manifestations. There are currently few treatments that can slow or stop disease progression. Primary CoQ_{10} deficiency can arise from mutations in any of the *COQ* genes responsible for CoQ biosynthesis. While many mutations in these genes have been identified, the clinical significance of most of them remains unclear. Here we analyzed the structural and functional impact of 429 human missense single nucleotide variants (SNVs) that give rise to amino acid substitutions in the conserved and functional regions of human genes encoding a high molecular weight complex known as the CoQ synthome (or Complex Q), consisting of the *COQ3–COQ7* and *COQ9* gene products. Using structures of COQ polypeptides, close homologs, and AlphaFold models, we identified 115 SNVs that are potentially pathogenic. Further biochemical characterizations in model organisms such as *Saccharomyces cerevisiae* are required to validate the pathogenicity of the identified SNVs. Collectively, our results will provide a resource for clinicians during patient diagnosis and guide therapeutic efforts toward combating primary CoQ_{10} deficiency.

Keywords: coenzyme Q; ubiquinone; primary CoQ deficiency; mitochondrial disease; single nucleotide variants; Missense3D; *COQ* genes

Citation: Wang, S.; Jain, A.; Novales, N.A.; Nashner, A.N.; Tran, F.; Clarke, C.F. Predicting and Understanding the Pathology of Single Nucleotide Variants in Human *COQ* Genes. *Antioxidants* **2022**, *11*, 2308. https://doi.org/10.3390/antiox11122308

Academic Editor: Rafael Artuch

Received: 25 October 2022
Accepted: 14 November 2022
Published: 22 November 2022

1. Introduction

Coenzyme Q (CoQ), also known as ubiquinone, is a redox-active lipophilic molecule required for cellular respiration. Its structure consists of a tetra-substituted benzoquinone ring and includes a lipid-anchoring polyisoprenyl tail of variable unit-length (CoQn, n = ten isoprene units in humans, CoQ_{10}) [1]. In the mitochondria, CoQ functions as an electron carrier in metabolic processes, such as oxidative phosphorylation, fatty acid β-oxidation, and choline metabolism [1,2]. In its oxidized form, CoQ accepts electrons from Complex I, Complex II, and many other mitochondrial dehydrogenases, producing its reduced form, ubiquinol ($CoQH_2$), which donates electrons and protons to Complex III [1–3]. In addition, $CoQH_2$ serves as a general lipophilic antioxidant [4–6] that has been implicated in protection from lipid autoxidation [7,8], and regeneration of vitamin E [9], another small molecule antioxidant. More recently, $CoQH_2$ has also been identified as having a role in ferroptosis suppression [10,11].

In humans, the biosynthesis of CoQ begins with 4-hydroxybenzoic acid (4-HB), a tyrosine derivative [12] (Figure 1A). The bulk of CoQ biosynthesis occurs in the mitochondrial matrix, where at least thirteen nuclear-encoded COQ polypeptides (PDSS1, PDSS2, COQ2-COQ7, COQ8A (ADCK3), COQ8B (ADCK4), COQ9, COQ10A, and COQ10B) reside in or are peripherally associated with the inner mitochondrial membrane (IMM) [13] (Figure 1B). In addition, ferredoxin Yah1 (human homolog FDX1 and FDX2) and ferredoxin reductase Arh1 (human homolog FDXR) from *Saccharomyces cerevisiae* have been shown

to be important for CoQ biosynthesis through the monooxygenation step performed by Coq6, although the involvement of their human homologs in CoQ biosynthesis has not been demonstrated [14]. The PDSS1 and PDSS2 polypeptides catalyze the formation of the decaprenyl diphosphate tail characteristic of CoQ_{10}, and COQ2 attaches the tail to 4-HB [15]. The PDSS1/PDSS2 complex and the COQ2 polypeptides appear to work independently. Polypeptides COQ3–COQ7 and COQ9 assemble into a high molecular weight complex, termed the CoQ synthome (or complex Q), which has been confirmed by mass spectrometry [16] and co-purification methods [17–20]. COQ8A and COQ8B are reported to have dynamic interactions with the remaining protein components [16]. Similarly in yeast, while the Coq8 polypeptide is necessary for CoQ synthome assembly [21,22] and co-purified with the Coq6 polypeptide [23], fluorescence microscopy of yEGFP-tagged Coq8 reveals the protein is dispersed throughout the mitochondria, forming few domain-like patterns, unlike the remaining polypeptides in the core complex that specifically reside in discrete puncta [24]. In addition to protein components, this CoQ synthome in yeast and complex Q in human cells also contains lipid intermediates and small molecule ligands [23–27].

Mutations in the genes encoding COQ polypeptides lead to primary CoQ_{10} deficiency, as they directly affect the biosynthesis of CoQ. This rare condition is typically caused by autosomal recessive mutations and often results in highly variable clinical manifestations, ranging from isolated pathologies, such as in the kidneys or central nervous system (CNS), to a fatal multi-system disorder [28–30]. The high variability may be attributed to discrepancies in genetic backgrounds, variable tissue-specific expression levels, and a varying degree of pathogenicity for each mutation. Systems and tissues generally impacted by primary CoQ_{10} deficiencies include the CNS, heart, peripheral nervous system (PNS), kidneys, and muscles. Some rarer manifestations can involve the lungs, liver, thyroid, and more general metabolic or cardiovascular disorders [28,29]. To date, there are approximately 200 patients with primary CoQ_{10} deficiency described in the literature, spanning mutations in ten of fourteen genes encoding COQ polypeptides [28,29]. Additionally, secondary CoQ_{10} deficiencies can result from aging or treatment with statins and have also been linked to mutations in genes such as *APTX* (aprataxin), *BRAF* (B-Raf), *ETFDH* (mitochondrial electron transfer flavoprotein-ubiquinone oxidoreductase), and *MUT* (methylmalonyl-CoA mutase), that are not directly linked to the biosynthesis of CoQ_{10} [1]. Currently, the only treatment for CoQ_{10} deficiency is exogenous CoQ_{10} supplementation. However, therapeutic benefits of exogenous supplementation are limited due to the extreme hydrophobicity and low bioavailability of CoQ_{10} [31]. Supplementation with CoQ_{10} may slow or stop the progression of disease but cannot reverse the damage already incurred in the patient [30]. In cases of early intervention in patients diagnosed with CoQ_{10} deficiency-associated nephropathy, CoQ_{10} supplementation has been shown to be remarkably effective in resolving the nephrotic syndrome, underscoring the significance of prompt intervention [32].

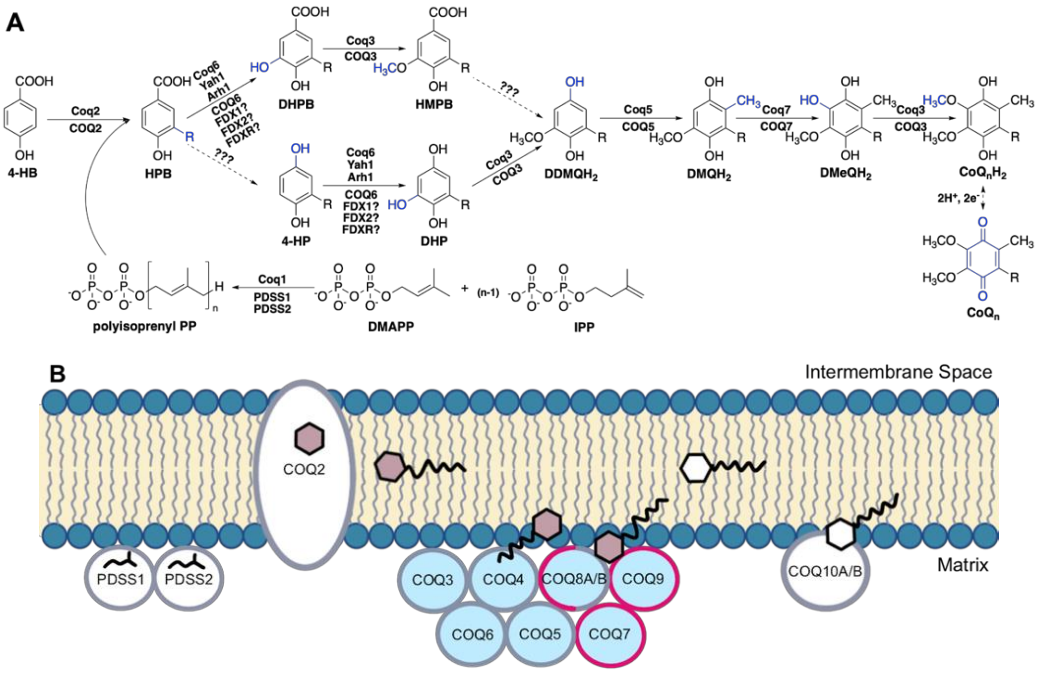

Figure 1. Biosynthesis of coenzyme Q. (**A**) The CoQ biosynthetic pathway is largely homologous between *S. cerevisiae* (polypeptide names above arrows) and humans (polypeptide names below arrows). In humans, at least seven nuclear-encoded catalytic proteins are directly responsible for the biosynthesis of CoQ from 4-hydroxybenzoic acid (4-HB), a tyrosine derivative. The enzyme(s) responsible for the decarboxylation and hydroxylation step(s) (dashed arrows) at ring position 1 has not been found. Hence, there is uncertainty about the order of steps. The decarboxylation step may precede the Coq6/COQ6 hydroxylation step based on the accumulation of 4-hydroxy-3-polyprenylphenol (4-HP) in yeast and human cells harboring mutations in Coq6/COQ6 data from [14,33,34]. In addition to the yeast Coq and human COQ polypeptides, other polypeptides involved in CoQ biosynthesis include PDSS1 and PDSS2 (decaprenyl diphosphate synthase subunits 1 and 2), Yah1 (yeast ferredoxin), Arh1 (yeast ferredoxin reductase), FDX1 and FDX2 (human ferredoxins 1 and 2), and FDXR, human ferredoxin reductase. Intermediates in the pathway include: DMAPP, dimethylallyl pyrophosphate; IPP, isopentenyl pyrophosphate; HPB, 3-polyprenyl-4-hydroxybenzoic acid; DHPB, 4,5-dihydroxy-3-polyprenylbenzoic acid; HMPB, 4-hydroxy-5-methoxy-3-polyprenylbenzoic acid; DHP, 4,5-dihydroxy-3-polyprenylphenol; $DDMQH_2$, 2-methoxy-6-polyprenyl-1,4-benzohydroquinone; $DMQH_2$, 2-methoxy-5-methyl-6-polyprenyl-1,4-benzohydroquinone; $DMeQH_2$, 3-methyl-6-methoxy-2-polyprenyl-1,4,5-benzenetriol. Note that the intermediates found in *S. cerevisiae* contain a hexaprenyl tail, while humans make decaprenylated CoQ_{10} intermediates. (**B**) The CoQ synthome (Complex Q in humans) is a high-molecular mass protein and lipid complex data from [1], consisting of polypeptides COQ3-COQ9. The PDSS proteins (homologous to *S. cerevisiae* Coq1), COQ2, and the lipid-binding proteins COQ10A and COQ10B do not associate with the complex. Colored hexagons indicate CoQ intermediates; white hexagons indicate the final CoQ product. Polypeptides for which the human protein structures have been solved are highlighted in pink. The COQ8A/COQ8B polypeptides are thought to have a dynamic association with complex Q. Polypeptides are not drawn to scale and their stoichiometry has not been determined.

In this study, we utilized exome and genome sequencing data of large populations, as well as clinical variants reported in the literature and the NCBI ClinVar database [35] to generate a comprehensive list of missense single nucleotide variants (SNVs) found in genes encoding the core CoQ synthome or complex Q (*COQ3*–*COQ7* and *COQ9*). The *COQ8A* and *COQ8B* genes were excluded due to their aforementioned dynamic interactions with the core complex. We structurally and functionally characterized variants that occurred in conserved and functional regions of the protein, using multiple sequence alignment and structural analyses with available models and crystal structures. In addition, clinically reported variants and those with high allele frequency were also included in our analyses. Our final list consisted of 429 variants compiled from gnomAD [36], ClinVar, Missense3D-DB [37], as well as the published research literature. We predicted the pathogenicity of each variant using the Missense3D mutation classifier, which relies purely on structural information and local structural changes [38]. When an experimentally determined structure was not available, as is often the case for the COQ polypeptides, Missense3D presented the advantage of being able to make predictions based on computational models such as those generated by AlphaFold [39]. This is in contrast to other classifier methods, including SIFT [40] and Polyphen-2 [41], that rely on evolutionary conservation and a mixture of sequence- and structure-based predictive features, respectively. In total, Missense3D identified 115 variants that are structurally damaging and potentially pathogenic. Confirmation of these predictions will require biochemical characterization in model systems, such as *Saccharomyces cerevisiae*. The results presented will provide a resource for clinicians with the aim of guiding efforts toward the treatment of primary CoQ_{10} deficiency.

2. Materials and Methods

2.1. Multiple Sequence Alignment

All human COQ polypeptide and orthologous sequences were obtained from NCBI GenBank Release 246.0 [42]. Multiple sequence alignments were generated using the ClustalW package of Clustal Omega [43] and visualized with Jalview2 [44]. Residues were classified as highly conserved if the percent agreement at that position was higher than 80%, as calculated by the built-in feature of Jalview and indicated by a dark blue shading in the sequence alignment. Prior biochemical characterization and crystal structure of *Escherichia coli* ubiquinone biosynthesis *O*-methyltransferase UbiG (the COQ3 ortholog) was used to determine the functional regions in human COQ3 (PDB: 4KDC and 5DPM) [45,46]. Molecular genetic analyses of *S. cerevisiae* Coq4 were used to determine the potential zinc-liganding residues in human COQ4 [47]. Apoenzyme (apo; PDB: 4OBX) and AdoMet-bound (PDB: 4OBW) form of *S. cerevisiae* Coq5 crystal structures were used to determine homologous residue functionality in human COQ5 [48]. Functional residues in human COQ6 were determined using an *S. cerevisiae* Coq6 model [49]. Prior biochemical characterization, a structural model, and a recent structure of human COQ7 were used to identify the functional regions of COQ7 [50–52]. Prior biochemical characterization, crystal structures, and molecular dynamics simulations were used to outline the functional residues in COQ9 (PDB: 6AWL and 6DEW) [50,52].

2.2. Analysis of Single Nucleotide Variants

Human SNVs occurring in the canonical transcripts, as reported in NCBI RefSeq [53] for *COQ3*–*COQ7* and *COQ9*, were gathered from gnomAD v2.1.1 [36], NCBI ClinVar [35], Missense3D-DB v1.5.1 [37], and available literature. Only SNVs that resulted in a missense variant were analyzed. In addition, a filter was applied to retain variants that occur in highly conserved (see Section 2.1) or functional amino acid positions. Variants documented in the ClinVar database or literature, as well as variants with an allele frequency larger than 1.00×10^{-4} as reported in gnomAD v2.1.1 (labeled as "Frequent Polymorphisms"), were also included in our analysis. Finally, exonic variants that are within two nucleotides of a splice site were included as variants of potential interest. Since the Missense3D-DB had already published variant classification using the crystal structure of COQ9, any variant that

was reported as structurally damaging in the database was also included in our analysis, regardless of amino acid position or conservation.

The selected variants were classified with three mutation classifiers, each using a different algorithm. Missense3D (http://missense3d.bc.ic.ac.uk/missense3d/, accessed on 30 March 2022) reports deleteriousness based on local structural feature changes that may be destabilizing [38]. SIFT (https://sift.bii.a-star.edu.sg/, accessed on 30 March 2022) scores variants as "Tolerated" or "Deleterious" based on evolutionary conservation [40]. Polyphen-2 (http://genetics.bwh.harvard.edu/pph2/, accessed on 30 March 2022) uses a Naïve Bayes classifier to report the likelihood of a mutation being damaging based on a combination of sequence- and structure-based criteria, whenever structures are available. Variants are scored as "Benign", "Possibly Damaging", and "Probably Damaging" [41]. Default settings were used whenever applicable. Results and interpretations from the three mutation classifiers can be found in Supplemental Table S1. The pipeline for SNV selection and classification is illustrated in Figure 2.

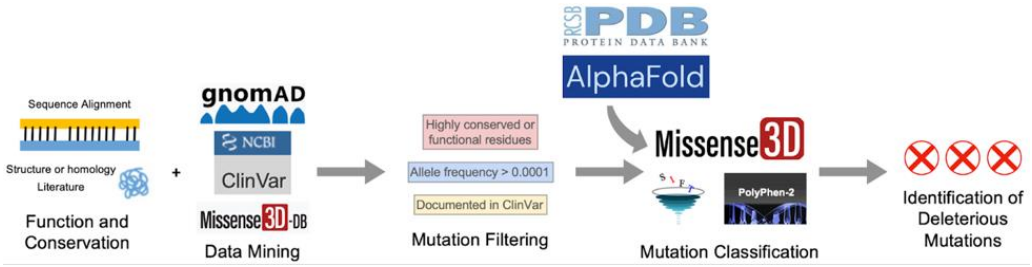

Figure 2. Schematic diagram of the overall approach used in this study.

2.3. Missense3D Analysis

Selected variants were submitted to the Missense3D online server for analysis of structural impact. For COQ3–COQ7, all variants were analyzed using the structural predictions of the human protein obtained from the AlphaFold Protein Structure Database [39,54]. For COQ9, variants occurring in regions modeled by its crystal structure (PDB 6AWL) were assessed using the crystal structure, while the remaining variants were assessed using their AlphaFold models. AlphaFold models used in this study include Q9NZJ6 (COQ3), Q9Y3A0 (COQ4), Q5HYK3 (COQ5), Q9Y2Z9 (COQ6), Q99807 (COQ7), and O75208 (COQ9). Structures were visualized using PyMOL (PyMOL Molecular Graphics System, Version 2.4.2, Schrödinger, LLC, New York, NY, USA).

3. Results

3.1. COQ3

COQ3 is an *S*-adenosyl-L-methionine (AdoMet)-dependent methyltransferase that catalyzes both *O*-methylation steps in CoQ biosynthesis in both *S. cerevisiae* and humans [55–57]. Namely, it is responsible for the conversion of DHPB to HMPB as well as the last step in CoQ biosynthesis, $DMeQH_2$ to $CoQH_2$ (Figure 1A). Overexpression of human COQ3 has been shown to rescue the growth CoQ biosynthesis of respiratory deficient *coq3*Δ yeast [56]. COQ3 and its yeast homolog are required for synthome stabilization, as partial knockdown of COQ3 in human cells results in a significant decrease in the levels of COQ4–COQ9, with the exception of COQ5 [58]. This result is corroborated by studies in yeast harboring a deletion in *COQ3* [59]. Interestingly, Coq3 is stable in *coq4–coq9* null mutant yeast strains studied in the presence of phosphatase and protease inhibitors, and its level is dependent on Coq8 [21,59]. There are currently no crystal structures available for eukaryotic homologs of COQ3. Structures are available for the orthologous *O*-methyltransferase UbiG from *E. coli*, which shares 34% sequence identity with human COQ3 and is part of a soluble ubiquinone/menaquinone biosynthetic complex [60]. Crystal structures of

the apo and S-adenosyl-L-homocysteine (AdoHcy)-bound UbiG monomer have guided subsequent biochemical characterizations and confirmed its seven β-strand Rossmann-fold structure [45,46].

To date, there have not been reported cases of primary CoQ_{10} deficiency associated with mutations in the *COQ3* gene [28–30], and pathogenic SNVs have not been identified. The lack of clinical data is echoed in yeast studies, which have primarily focused on *COQ3* gene deletions. As a result, no point mutations conferring pathogenic effects have been characterized in yeast. However, *COQ3* gene expression was found to be upregulated in esophageal squamous cell carcinoma and was associated with poor prognosis, hinting at a potentially unique role of COQ3 in humans [61,62].

From gnomAD, ClinVar, and Missense3D-DB, we identified 44 missense SNVs of interest (Figure 3; Supplemental Table S1; see Section 2.2 for the selection criteria). Of these variants, 29 coincided with a highly conserved region or functional residue determined from structural and biochemical studies, as well as analyses of sequence conservation [45,46,63]. Sixteen SNVs occurring in highly conserved or functional residues were classified as structurally damaging by Missesense3D. Twelve additional variants from gnomAD that were neither highly conserved nor functional residues were included due to their notable allele frequency. Interestingly, three of these frequent variants were also classified as structurally damaging. V202M was the only variant listed in ClinVar, although its clinical significance was "Likely Benign". Finally, a total of four variants were marked as potential splice site variants in addition to their apparent amino acid sequence change. Since the effect on splicing may be confounding, this group of variants was not subjected to extensive study.

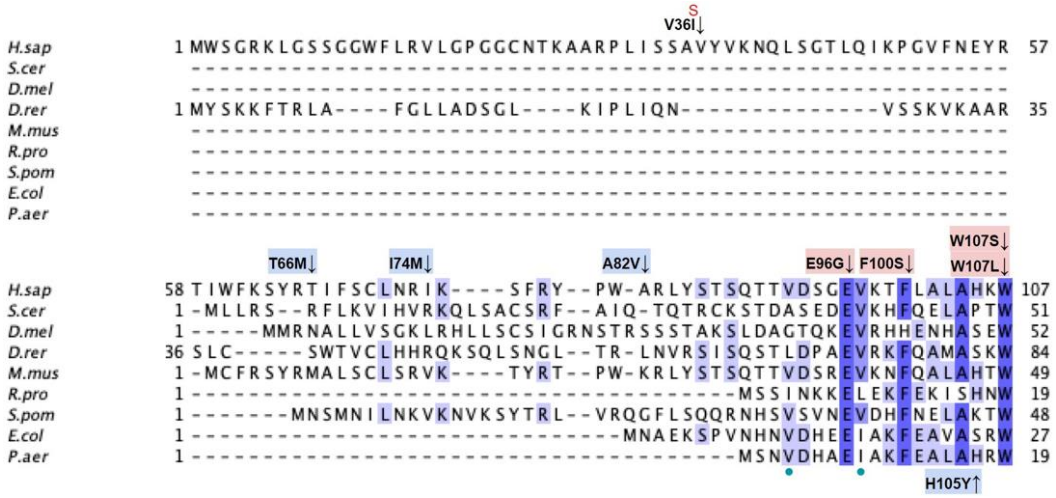

Figure 3. *Cont.*

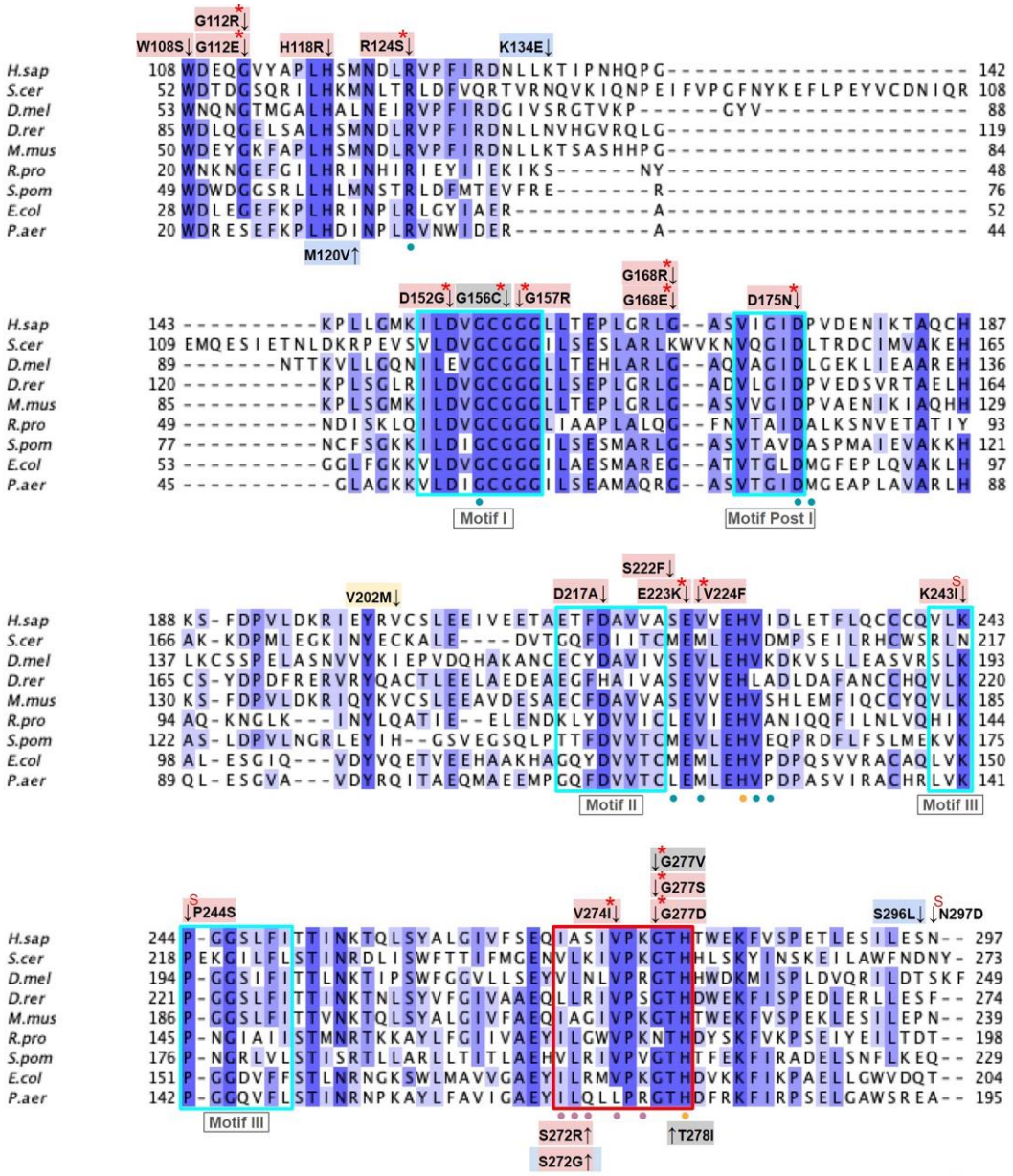

Figure 3. *Cont.*

Figure 3. Labeled and annotated multiple sequence alignment of COQ3. Amino acid sequences of COQ3 were analyzed as described in Materials and Methods and include *Homo sapiens* (NCBI accession number NP_059117.3) and homologs in *Saccharomyces cerevisiae* (NP_014545), *Drosophila melanogaster* (NP_610092.2), *Danio rerio* (NP_001002620.1), *Mus musculus* (NP_766275.1), *Rickettsia prowazekii* (WP_004596275.1), *Schizosaccharomyces pombe* (NP_588239.2), *Escherichia coli* (NP_416735.1), and *Pseudomonas aeruginosa* (WP_003122245.1). See KEY for descriptions of the figure annotations. Putative AdoMet binding residues are denoted by a blue dot, and residues thought to interact with the cell membrane in *E. coli* UbiG are denoted by a purple dot, data from [45,46]. A pair of co-evolving, highly conserved, and structurally nearby histidines may be involved in metal ion coordination (orange dot), data from [63]. Methyltransferase motifs I, post-I, II, and III are boxed in cyan data from [56,64]. The putative membrane-interacting hydrophobic region is boxed in red, data from [45]. For all multiple sequence alignments, conservation is indicated via shaded residues, which represent a percent identity great than 80%, 60%, and 40%, from darkest to lightest. Residues with less than 40% identity are unshaded.

The human COQ3 model was obtained from the AlphaFold Protein Structure Database (Figure 4) [39,54]. The core structure of the model consists of eight α-helices (as rendered by the AlphaFold 3D viewer) and eight β-sheets, flanked by long disordered regions on the N- and C-termini. The overall structure of the model aligned well with the crystal structure of AdoHcy-bound (PDB: 5DPM; Figure 5A) and apo *E. coli* UbiG (PDB: 4KDC; Figure A1). Four sequence motifs shared among class I methyltransferases, motifs I–III and post-I, each form a β-strand that aligns the residues in the AdoMet binding pocket (Figure 5B) [64,65].

In addition to the conserved Rossmann fold structure, the UbiG/COQ3 family contains a hydrophobic stretch of ten residues (residues 270–279 in the human COQ3 sequence) that is thought to interact with the membrane in UbiG [46]. An isolated helix linked to the hydrophobic region is visible in the COQ3 model, while this region was truncated in the crystal structure of UbiG (Figure 5A) [46]. This region is thought to act as a gate to the AdoMet binding pocket, which is consistent with its position in the model (Figure 5B) [46]. However, it is not clear how this putative membrane interaction helix is compatible with the recent structure of the soluble Ubi metabolon [66].

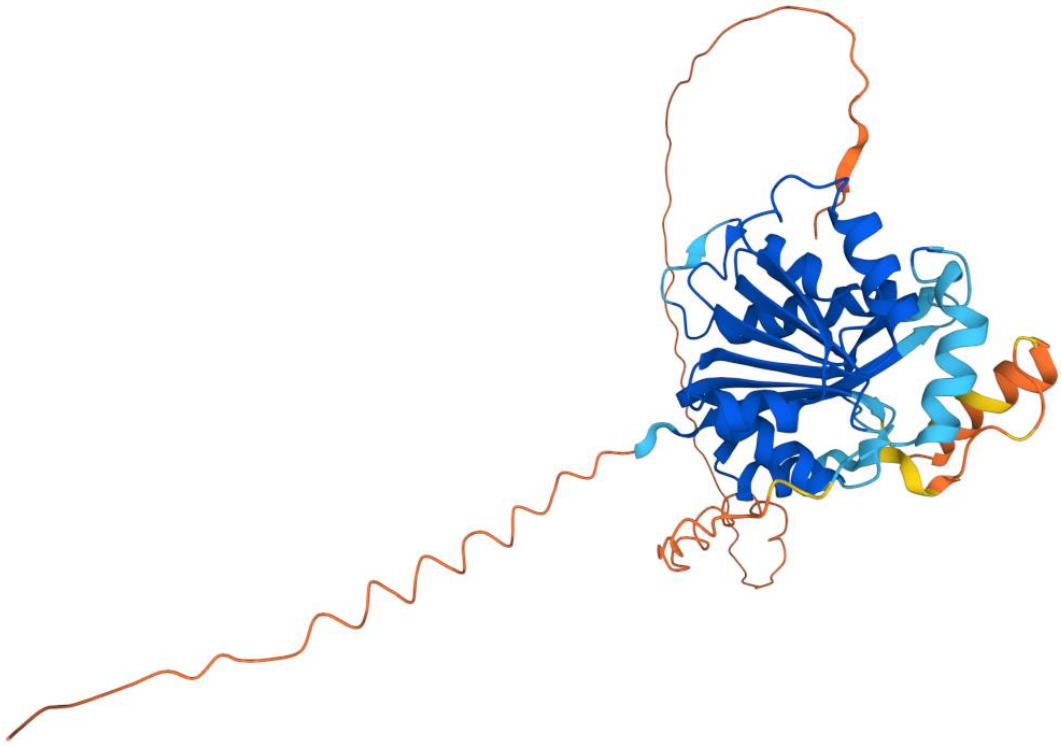

Figure 4. AlphaFold model of human COQ3. Model color corresponds to model confidence in each region. Very high confidence in dark blue (pLDDT > 90); confident in light blue (90 > pLDDT > 70); low confidence in yellow (70 > pLDDT > 50); very low confidence in orange (pLDDT < 50). pLDDT is a measure of per-residue confidence. pLDDT < 50 is a reasonably strong predictor of disorder for the corresponding residue. Figure was generated by the AlphaFold Protein Structure Database; adapted with permission from [39,54].

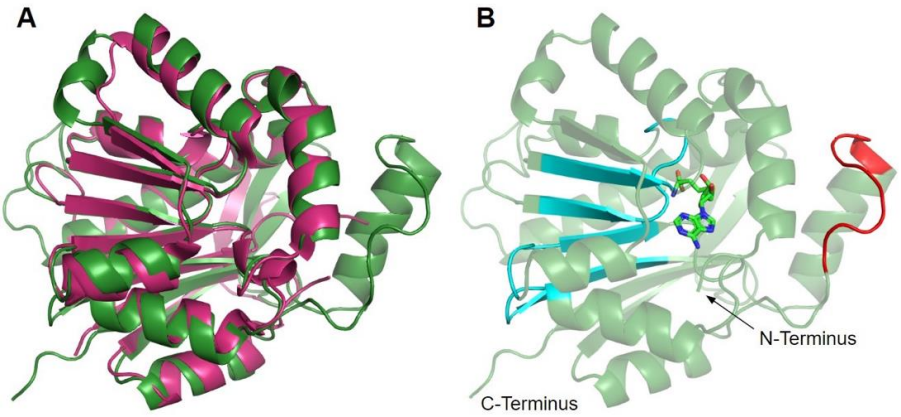

Figure 5. Alignment of AlphaFold-generated model of human COQ3 with existing *E. coli* UbiG crystal structure. (**A**) Superimposition of the human COQ3 model (residues 91–336, shown in dark green), adapted with permission from [39,54], and the crystal structure of AdoHcy-bound *E. coli* UbiG (shown in magenta, PDB: 5DPM). The N- and C-termini of the model were omitted due to low confidence. Note that this and subsequent figures about COQ3 were generated using PyMOL, which classifies a short-coil region as a helix (top left of figure). This gives a total of nine helices as opposed to eight rendered in Figure 4. (**B**) Human COQ3 model with conserved methyltransferase motifs I–III and post-I highlighted in cyan and the hydrophobic region in red. AdoMet (shown in light green) was modeled via structural alignment with PDB 5DPM using PyMOL.

3.1.1. SNVs in Methyltransferase Motifs I and Post I

Motif I (residues I150 to G1158) is found in the first β-strand followed by a Gly-rich loop that extends into the putative AdoMet binding site of COQ3 (Figure 6A) [65]. It closely resembles the nine-residue consensus sequence, with two aliphatic residues followed by a (D/E) (V/I) GXGXG motif [64]. The backbone carbonyl of the G66 in *E. coli* in this motif (G156 in humans) has been shown to form a hydrogen bond with the amino group of AdoHcy in UbiG (PDB: 5DPM) [46].

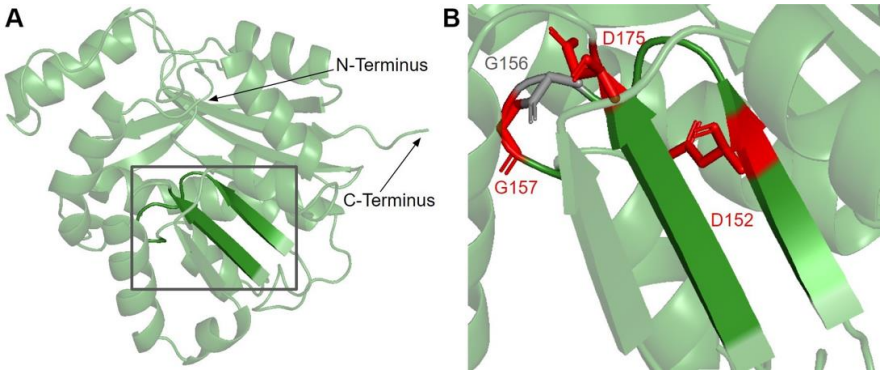

Figure 6. SNVs found in motifs I and post I of COQ3. (**A**) Motifs I (right β-strand and loop, residues I150 to G1158) and post I (left β-strand, residues V171 to D175) highlighted on residues 91–336 of the COQ3 model. N- and C-termini were truncated for simplicity. (**B**) Locations of SNVs in motifs I and post-I are depicted. Residues are colored according to their corresponding SNVs in Figure 3.

There are three SNVs of interest in this region, all of which occur on highly conserved residues (Figures 3 and 6B). D152G from gnomAD maps to the β-strand region, which is critical for the alignment of AdoMet binding residues. Missense3D classifies this variant as structurally damaging due to the replacement of a buried charge and the loss of a buried hydrogen bond. These disruptions may lead to destabilization of the core structure and more profound changes to the CoQ synthome. G156C and G157R were reported in Missense3D-DB and gnomAD, respectively. These two SNVs map to the flexible Gly-rich loop. Missense3D classifies both variants as structurally damaging due to the replacement of buried Gly residues. In addition, G156C was flagged for altering the buried/exposed status of this residue position, which likely refers to the mutant Cys residue protruding into the AdoMet binding site. G157R, on the other hand, introduces a buried charge in proximity with the putative docking region of the amino and carboxyl groups of AdoMet. Indeed, mutating the homologous residue in yeast, G133, to an Ala resulted in partial suppression of respiratory growth and significantly reduced CoQ levels, despite stable expression of the polypeptide [63]. Taken together, these two variants likely affect cofactor binding and enzyme activity.

Motif post-I (V171 to D175) is part of the second β-strand that contains a short stretch of hydrophobic residues followed by a highly conserved acidic residue (Figure 6A) [65]. The acidic residue in *E. coli* UbiG, D85 (D175 in humans) was shown to form hydrogen bonds with the O2′ and O3′ hydroxyl groups on the ribose ring of AdoHcy in the crystal structure of UbiG (PDB: 5DPM), while residue M86 (P176 in humans) immediately following motif post-I interacts with the adenine ring [46]. D175N is the only SNV of interest in this region (Figures 3 and 6B). This variant was classified as structurally damaging by Missense3D due to the replacement of a buried charge, which may disrupt the aforementioned interactions with the ribose ring.

3.1.2. SNVs in Methyltransferase Motifs II and III

Motif II, roughly E214 to A221, maps to residues immediately preceding and including the fourth β-strand (Figure 7A). The sequence of motif II is not as well conserved among COQ3 homologs, although one highly conserved Asp is thought to make contact with motif I (Figure 3) [65]. Aliphatic residues following this Asp mark the start of β4, which leads to a loop containing residues forming a hydrophobic environment for the adenine ring of AdoHcy in UbiG [46]. In addition, this region following motif II is thought to interact with the methyl group in AdoMet as well as the substrate, giving it a possible role in determining substrate specificity [65,67]. This hypothesis is supported by coevolution studies of UbiG/COQ3, in which residue position 196 in yeast Coq3 (222 in humans) was shown to coevolve in other methyltransferases but was distinct in Coq3 and *E. coli* UbiG. One additional residue of interest downstream is H227 in human COQ3. Its homologous residue in UbiG, H134, was shown to be required for growth in *E. coli*, and in the *Arabidopsis thaliana* small RNA 2′-O-methyltransferase HEN1 the homologous residue was described as magnesium-binding [45,68]. Mutating this residue to an Ala in yeast (H201A) completely destabilized the polypeptide [63]. In motif II and the loop following it, there are four SNVs of interest in highly conserved or functional residues, all of which were reported in gnomAD (Figures 3 and 7B). D217A immediately preceding β4 was, while highly conserved, not classified as damaging by Missense3D due to the residue being solvent-exposed in the model. S222F, E223K, and V224F are located in the loop following β4. S222 and V224 are thought to bind the amino group and the adenine ring of AdoMet, respectively, by homology with *E. coli* UbiG (M129 and M131) [46]. However, only V224F was classified as structurally damaging due to a change in cavity size, likely referring to the binding pocket for the adenine ring of AdoMet. S222F and E223K were also solvent-exposed in the model, which resulted in their classification as neutral despite their disruption of hydrogen bonds or salt bridges. In yeast, an Ala mutation in the homologous position of E223 completely destabilized the Coq3 polypeptide and disrupted respiratory growth. Coq4

was also destabilized as a consequence [63]. This strongly suggests that all three variants in the loop are likely disruptive.

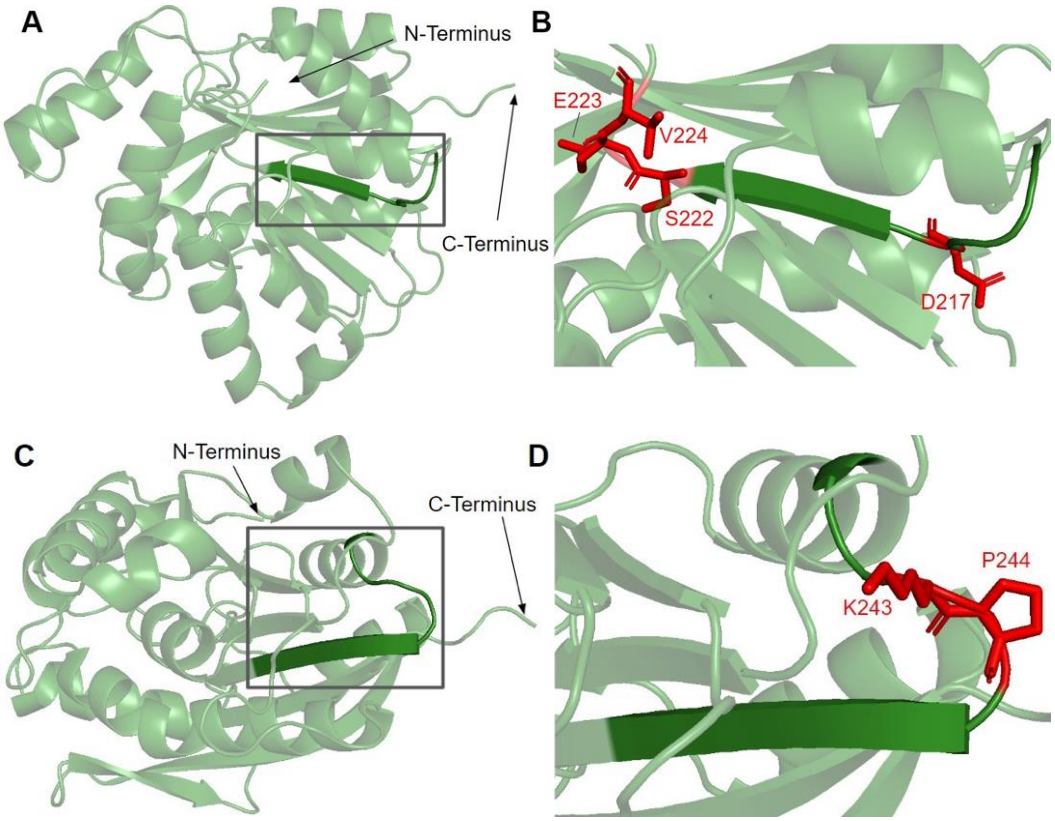

Figure 7. SNVs found in motifs II and III of COQ3. (**A**,**C**) Residues 91–336 of the COQ3 model with E214 to A221 as motif II (**A**) and V241 to I250 as motif III (**C**) are highlighted. (**B**,**D**) Locations of SNVs in motif II and nearby residues (**B**) and motif III (**D**) are depicted. N- and C-termini were truncated for simplicity. Residues are colored according to their corresponding SNVs in Figure 3.

Motif III (V241 to I250) lies on the fifth β-strand as well as the loop and parts of the helix preceding it (Figure 7C). This loop is essential for the alignment of the methyltransferase motifs and consists of Pro and Gly residues to facilitate the turn [65]. GnomAD reported two SNVs, K243I and P244S, in highly conserved residues of this motif (Figure 7D). Neither SNV was classified as structurally damaging by Missense3D. However, it is worth noting that these SNVs occur near a splice junction and may therefore result in more profound changes to protein expression in addition to changes in protein sequence.

3.1.3. SNVs in the Membrane Interacting Hydrophobic Region

Previous studies demonstrated that a region consisting of several hydrophobic and basic residues in *E. coli* UbiG and human COQ3 is required for their interaction with liposomes containing cardiolipin [45]. Furthermore, mutating multiple residues in this region to Ala resulted in reduced growth in *E. coli* [45]. In the human COQ3 model, this region can be seen mapping to a linker connecting an isolated α-helix to the core structure

(Figure 8A). This is consistent with a model in UbiG in which this region acts as a gate to the binding site of the AdoMet cofactor [46]. Upon binding to the membrane, this helix is thought to dissociate from the core structure, allowing the cofactor to diffuse into the active site. Mutating residues in and preceding this region to disrupt its interaction with the core structure indeed resulted in enhanced binding of AdoHcy [46]. Nevertheless, it is worth noting that there are key differences in CoQ biosynthesis in *E. coli* and humans. UbiG is part of a soluble complex in the cytosol, while COQ3 is part of a membrane-associated complex in the mitochondrial matrix [60]. Implications of this membrane interaction in human COQ3 have not been investigated. Its preferential binding to liposomes containing cardiolipin, a unique component of the inner mitochondrial membrane, suggests a similar cofactor gating role in human COQ3. Meanwhile, a more recent coevolution study of the UbiG/COQ3 family identified the His residue at the end of this region (H279 in humans, H254 in yeast) as coevolving with the putative metal binding H201 in yeast (H227 in humans) [63]. The close proximity of the two His residues in our model supports an alternative role of metal binding. However, the functional significance of this region in human COQ3 remains unelucidated.

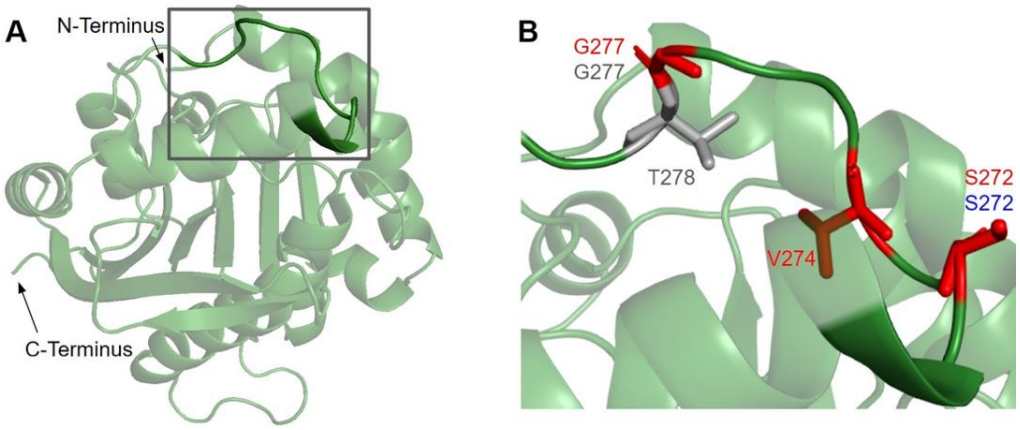

Figure 8. SNVs found in the membrane interacting hydrophobic region of COQ3. (**A**) Residues I270 to H279 are highlighted on residues 91–336 of the COQ3 model. N- and C-termini were truncated for simplicity. (**B**) Locations of SNVs in the hydrophobic region are depicted. Residues are colored according to their corresponding SNVs in Figure 3.

In this region, we have identified seven variants spanning five residue positions from gnomAD and Missense3D-DB (Figure 8B). S272G, S272R, and V274I all coincide with residues known to affect liposome binding in UbiG when mutated [45]. Interestingly, S272G is a frequent polymorphism with an allele frequency of 8.45×10^{-1}, suggesting that this variant may be benign. V274I was classified as structurally damaging by Missense3D due to changes in cavity size, which likely refers to the active site of COQ3. This classification suggests a possible change in either substrate or cofactor binding and therefore activity. G227S, G227V, G227D, and T278I were not tested in UbiG, although the high conservation suggests functional importance. All three variants occurring on G227 were classified as damaging by Missense3D due to disallowed phi/psi angle.

3.1.4. Frequent Polymorphisms in COQ3

In this study, we have defined "frequent polymorphism" as a variant having an allele frequency larger than 1.00×10^{-4}. There are 12 such variants found in COQ3 that do not fall into the previously described functional regions. Most of them occur in regions

of poor conservation such as the N- and C-termini. Two variants, Y329H and K134E, stand out with their exceptionally high allele frequency of 9.84×10^{-1} and 3.03×10^{-1}, respectively. Interestingly, Y329H, located on β7, was classified as structurally damaging by Missense3D due to the introduction of a buried charge. However, given the large number of homozygotes that result from its allele frequency, this variant is unlikely to be detrimental. Two additional variants, G348E (allele frequency 8.14×10^{-4}) and E365D (allele frequency 6.07×10^{-4}), were classified as structurally damaging. The former was flagged for replacement of a Gly residue in a bend, which may affect the flexibility of the region. The latter was flagged for steric clash, which may be an artifact of the Missense3D program since the region is disordered.

3.2. COQ4

COQ4 has not been characterized as having an enzymatic function, though it appears to play an important structural role in organizing the CoQ synthome [13]. Human transcripts encode two *COQ4* isoforms; isoform 2 lacks both the first exon and the mitochondrial leader sequence and fails to rescue yeast *coq4* null mutants [69]. The polypeptide encoded by *COQ4* isoform 1 complements *coq4* null mutant yeast [69]. This demonstrates conserved functionality across species as well as the power of *S. cerevisiae* as a model organism to study human *COQ4* mutations [69]. Human COQ4 is located within mitochondria [69], as is the yeast Coq4 polypeptide that is peripherally associated with the matrix side of the IMM [70].

The first structure determined for a COQ4 homolog, the Alr8543 polypeptide from *Nostoc* sp. (PDB: 3KB4), revealed a geranylgeranyl monophosphate bound between hydrophobic helices. However, PDB: 3KB4 is now obsolete and has been replaced with PDB: 6E12. The Alr8543 protein in the more recent 6E12 structure is in complex with two magnesium ions. Both Mg^{2+} ions are associated with a conserved HDXXH-$(X)_{10–13}$-E signature motif required for COQ4 functionality and is similarly considered to chelate a zinc ion [47]. Mutations in the human *COQ4* gene are associated with primary CoQ_{10} deficiency and with several disease states including a range of neurological afflictions, cardiomyopathy, and respiratory distress [29].

From gnomAD, ClinVar, Missense3D-DB, and literature, we identified 97 missense SNVs of interest (Figure 9; Supplemental Table S1). Of these variants, 60 coincided with a highly conserved region or functional residues, as determined from the multiple sequence alignment as well as structural studies with Alr8543. Of 22 variants classified as structurally damaging by Missense3D, 18 were contained within a highly conserved or functional region. From the ClinVar database and published research literature, 15 missense SNVs were determined to be either pathogenic or likely pathogenic. Four of these pathogenic or likely pathogenic variants were identified by Missense3D to be structurally damaging. Fifteen additional variants from gnomAD were included as frequent polymorphisms. Intriguingly, three of these frequent polymorphisms were identified in the research literature as deleterious. G124S (allele frequency of 1.13×10^{-4}) has been identified as a founder mutation in the southern Chinese population [71]. Another, E161D (allele frequency of 6.03×10^{-3}) was found in a patient who suffered from primary CoQ_{10} deficiency and later died from rhabdomyolysis [72,73]. A third, R240C (allele frequency of 1.79×10^{-4}), occurred in a patient with progressive spasticity, motor impairment, and ataxia [74]. This patient harbored biallelic variants of COQ4 (P193S and R240C), and individual tests of these alleles of human COQ4 in yeast showed that neither variant could rescue a *coq4* yeast mutant [74].

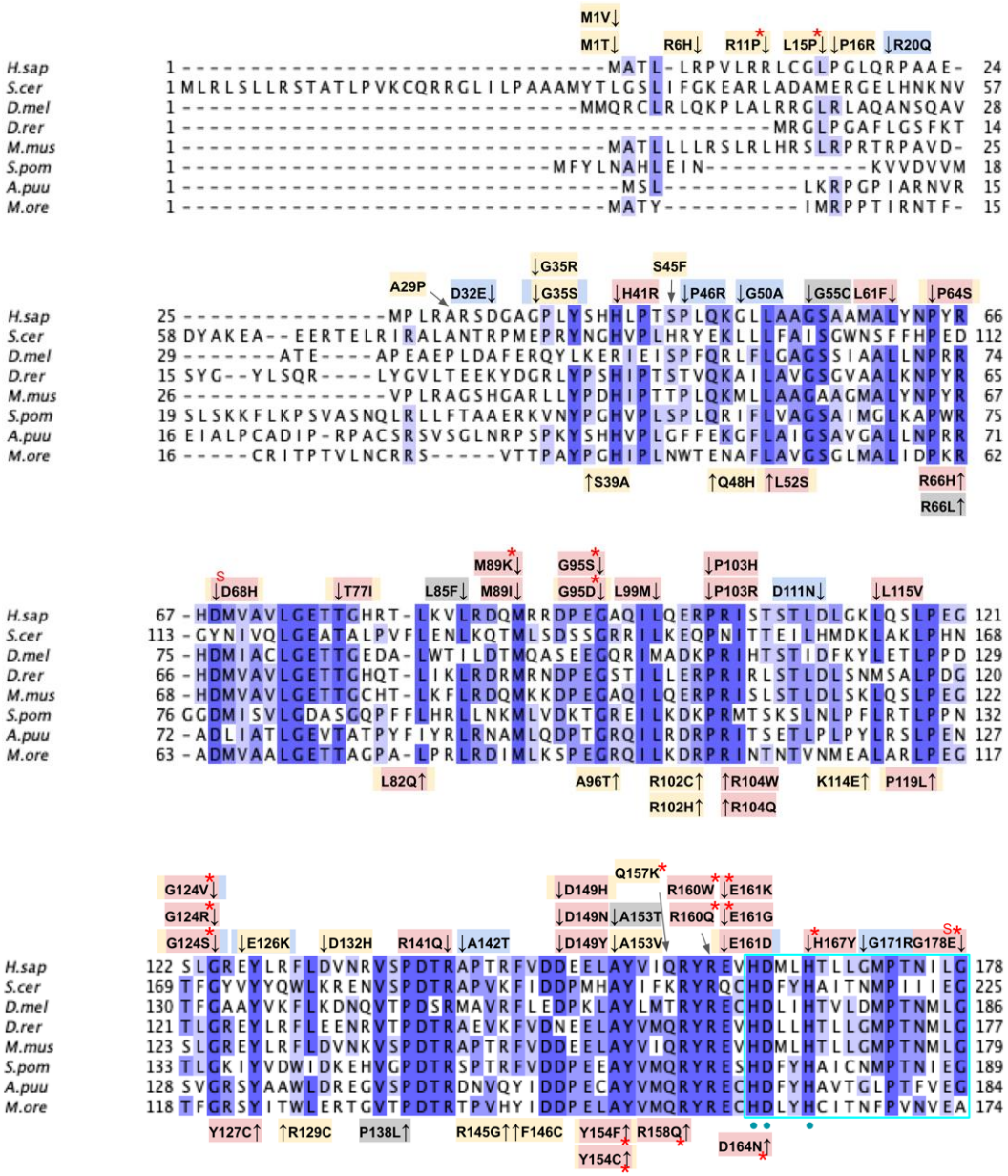

Figure 9. *Cont.*

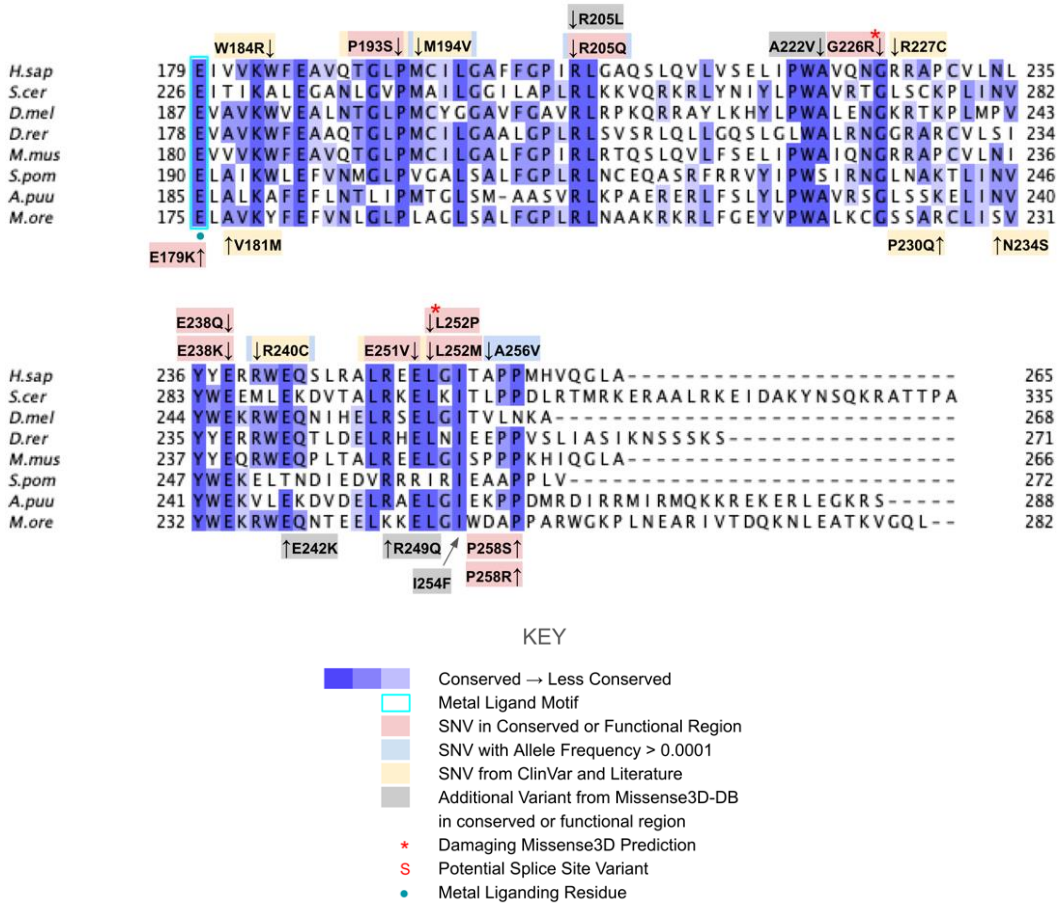

Figure 9. Labeled and annotated multiple sequence alignment of COQ4. Amino acid sequences of COQ4 were analyzed as described in Materials and Methods and include *Homo sapiens* (NCBI accession number NP_057119.3) and homologs in *Saccharomyces cerevisiae* (NP_010490.1), *Drosophila melanogaster* (NP_730270.1), *Danio rerio* (NP_001108192.1), *Mus musculus* (NP_848808.1), *Schizosaccharomyces pombe* (NP_593130.1), *Aspergillus puulaauensis* (XP_041555109.1), and *Marasmius oreades* (XP_043005754.1). See KEY for descriptions of the figure annotations. The metal ligand motif is boxed in cyan, and putative residues that ligand the metal ions are denoted by a blue dot, data from [47].

The human COQ4 model was obtained from the AlphaFold Protein Structure Database (Figure 10A) [39,54]. The per-residue model confidence is shown in Figure 10A. A structural alignment of the human COQ4 AlphaFold model with the PDB 6E12 structure of the Alr8543 polypeptide, a COQ4 homolog from Nostoc sp., is shown in Figure 10B.

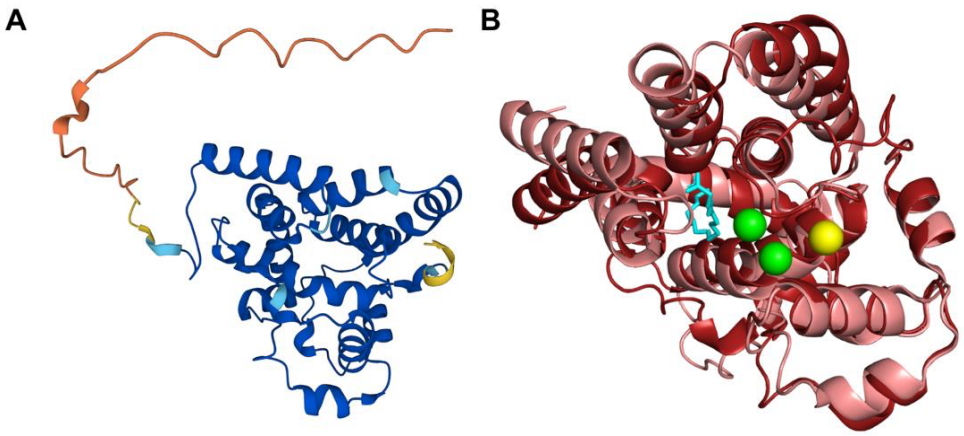

Figure 10. Comparison of the COQ4 AlphaFold model and the structure of Alr8543. (**A**) AlphaFold model of single chain of COQ4. Model color corresponds to model confidence as described in Figure 4. Figure was generated by the AlphaFold Protein Structure Database; adapted with permission from [39,54]. (**B**) Structural alignment of the human COQ4 AlphaFold model (shown in dark red) and Chain B of the crystal structure of Alr8543 protein (shown in salmon, PDB: 6E12) in complex with oleic acid (shown in cyan), Mg^{2+} (shown in green), and Cl^{-} (shown in yellow). Residues 1–44 of the AlphaFold model were omitted due to disordered structure.

3.2.1. SNVs in the Metal Liganding Motif

The amino acid sequence of COQ4 contains the highly conserved HDXXH-$(X)_{11}$-E motif indicative of a metal ligand [47]. While the function and identity of the metal ligand remain unknown, it has been hypothesized that the ligand is sensitive to the redox state of mitochondria. Mutations in this region may destabilize coordination of the metal and CoQ synthome formation [47]. The motif spans residues H163 to E179 (Figure 11A). In the Alr8543 structure, the analogous E136 in the conserved HDXXH-$(X)_{11}$-E motif ligands one Mg^{2+} ion (Figure A2). H124, the second H residue of the motif, forms an interaction with E. The D121 of this motif in Alr8543 ligands the second Mg^{2+} ion.

There are four SNVs reported in Missense3D-DB that occur at highly conserved residues within the metal-liganding motif: D164N, H167Y, G178E, and E179K (Figure 11B). Of these, D164, H167, and E179 correspond to residues predicted to ligand the metal ion. D164 is proposed to be analogous to the Mg^{2+} ion-liganding D121 in Alr8543 (Figure A2). H167 is proposed to be analogous to H120 in Alr8543, which stabilizes interactions with E136 that ligands the Mg^{2+} ion. E179 is proposed to be analogous to E136, which ligands the second Mg^{2+} ion in Alr8543 (Figure A2). A homologous point mutation of E179K in Coq4 of *S. cerevisiae* was unable to form the high molecular mass CoQ synthome [47]. Three SNVs in this region, D164N, H167Y, and G178E, were identified by Missense3D as being structurally damaging. None of these mutations have a reported clinical association on ClinVar.

The most common flags generated by Missense3D relate to the change or introduction of a buried charge, such as at D164 and H167. Such changes may destabilize the tertiary structure of COQ4 and may also affect the ability of COQ4 to interact with metal ligands.

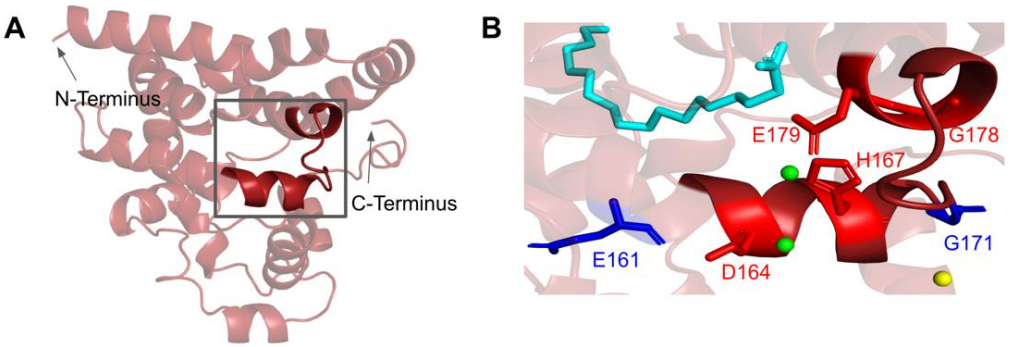

Figure 11. SNVs found in the putative COQ4 metal-liganding motif. (**A**) The metal-liganding motif (encompassing residues H163 to E179) is highlighted in red on the COQ4 model. (**B**) Locations of SNVs are depicted. Structural alignment of Alr8543 and COQ4 identifies the metal-liganding motifs in COQ4. Metal ions and oleic acid were obtained from this structural alignment. Residues are colored according to their corresponding SNVs in Figure 9. Mg^{2+} ions are designated as green spheres and Cl^{-} in yellow. Oleic acid is represented by the cyan structure.

3.2.2. COQ4 Haploinsufficiency

Salviati et al. first identified the *COQ4* gene as being haploinsufficient [75]. This property is unusual because heterozygous carriers harboring a mutation in one of the other *COQ* genes are generally described as asymptomatic and produce normal levels of CoQ. *COQ4* haploinsufficiency was confirmed in both fibroblast and yeast cell models [75]. Intriguingly, one of the SNVs identified as a frequent polymorphism (E161D, Figure 11B) was detected as a heterozygous mutation in a patient with CoQ_{10} deficiency who had minor mental retardation and died of rhabdomyolysis [72,73]. Correction of the sequence variant in a cell culture model with CRISPR-mediated editing rescued the CoQ-deficient phenotype [73]. It is tempting to speculate that the haploinsufficiency of COQ4 may be related to its putative role in "scaffolding" the CoQ synthome, as proteins that serve analogous functions appear to be sensitive to changes in gene dosage [76].

3.3. COQ5

COQ5 is an AdoMet-dependent *C*-methyltransferase and a component of the CoQ synthome [18,77]. It is required for the conversion of $DDMQH_2$ to $DMQH_2$ in both *S. cerevisiae* and humans (Figure 1A) [18,78,79]. The human protein has been shown to rescue Coq5-deficient yeast that harbor stable but inactive Coq5 polypeptides, and it can also rescue *coq5* null mutants that overexpress Coq8 [18,80]. COQ5 is thought to be crucial for the stability of the synthome, as yeast lacking Coq5 are CoQ-less, respiratory-deficient, and do not form an intact synthome [59,80,81]. Partial knockdown of *COQ5* in human cells corroborates the findings observed in yeast *coq5* mutants and supports the crucial role of COQ5 in CoQ synthome formation and CoQ biosynthesis [20]. Crystal structures of the apo and AdoMet-bound yeast Coq5 dimers have been determined [48], revealing its seven β-strand Rossmann fold structure typical of the most common class I methyltransferases [64,82]. These crystal structures, in addition to known methyltransferase motifs [64], have helped elucidate the AdoMet and substrate-binding pockets as well as key residues involved in protein dimerization.

To date, only three patients with a mutation in *COQ5* have been documented. These related patients carried a 9590-bp duplication of the last four exons and part of the 3′ UTR of *COQ5*, resulting in an elongated 3′ UTR. They were deficient in CoQ_{10} and exhibited symptoms exclusive to the central nervous system, including encephalopathy, intellectual disability, ataxia, and cerebellar atrophy. The clinical outcome of long-term CoQ_{10}

supplementation on these patients was equivocal [83]. Meanwhile, pathogenic SNVs in the *COQ5* gene have not been identified, although yeast studies have identified point mutations affecting the activity and stability of the Coq5 polypeptide, all of which resulted in respiratory deficiency [80].

From gnomAD, ClinVar, and Missense3D-DB, we identified 88 missense SNVs of interest (Figure 12; Supplemental Table S1). Of these variants, 76 coincided with a highly conserved region or functional residue, which were determined from the multiple sequence alignment as well as structural studies on yeast Coq5 [48]. All 24 variants classified as structurally damaging by Missense3D were contained in this group. In addition, ten variants from gnomAD that did not occur in highly conserved or functional residues were included as frequent polymorphisms. None of these variants were predicted to be structurally damaging.

The human COQ5 model was obtained from the AlphaFold Protein Structure Database (Figure 13) [39,54]. Compared to the crystal structure of AdoMet-bound yeast Coq5 (PDB: 4OBW) and apo yeast Coq5 (PDB: 4OBX), this model consisted of an additional α-helix N-terminal to the core structure, which was not visible in the yeast Coq5 crystal structure (Figures 14A and A3) [48]. The α3 of the human COQ5 model is extended compared to that of the yeast Coq5 structure and is followed by a loop region containing a shorter helix. This region reflects an insert that spans residues 134–164, found exclusively in vertebrate species (Figure 12). The core seven β-strand structure, as well as the AdoMet and substrate-binding pockets, remain largely similar. In addition to their conserved three-dimensional structure, each of the four methyltransferase motifs (motifs I-III and post-I) in COQ5 approximately correspond to one β-strand connected to loops that make up the AdoMet binding site (Figure 14B) [64,65].

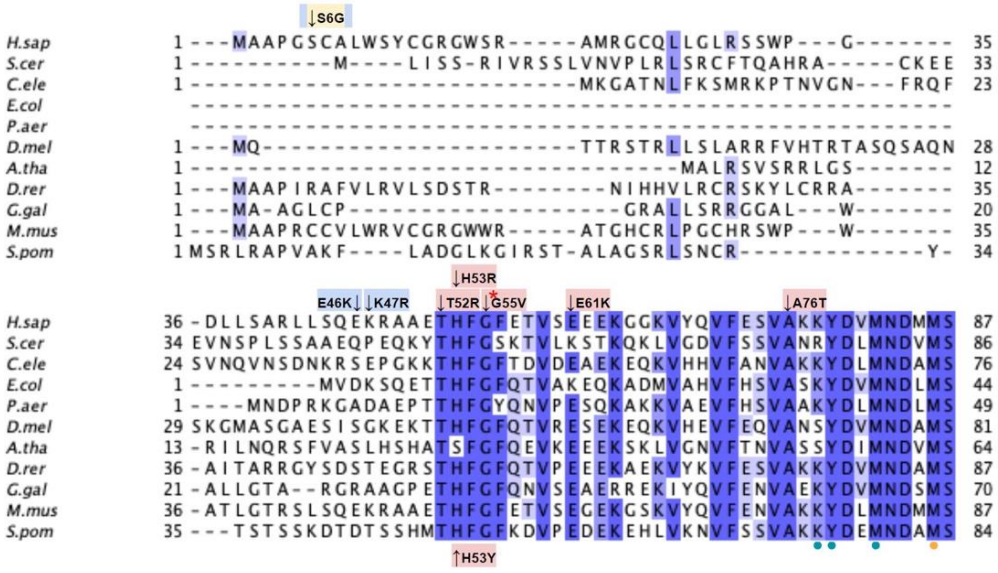

Figure 12. *Cont.*

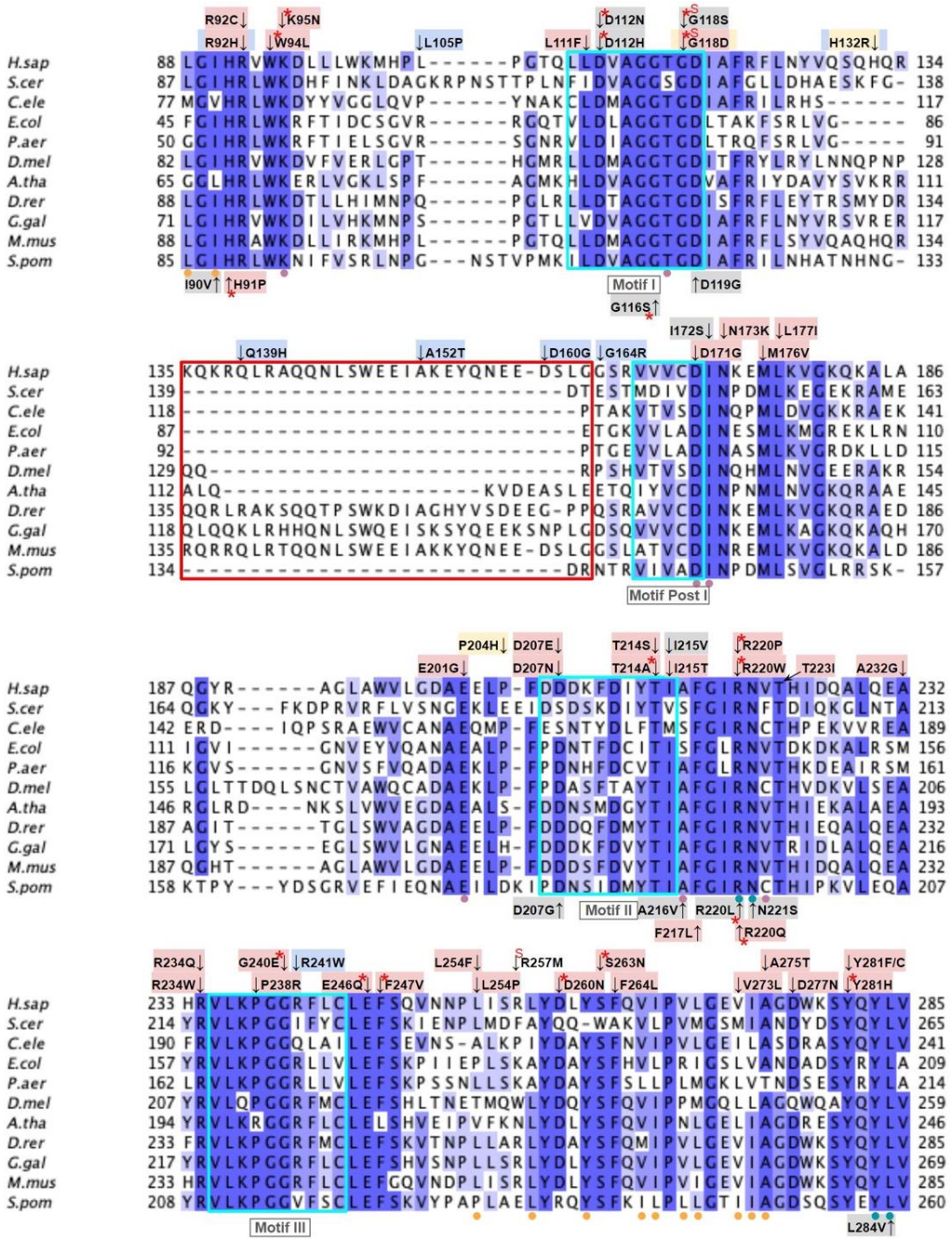

Figure 12. *Cont.*

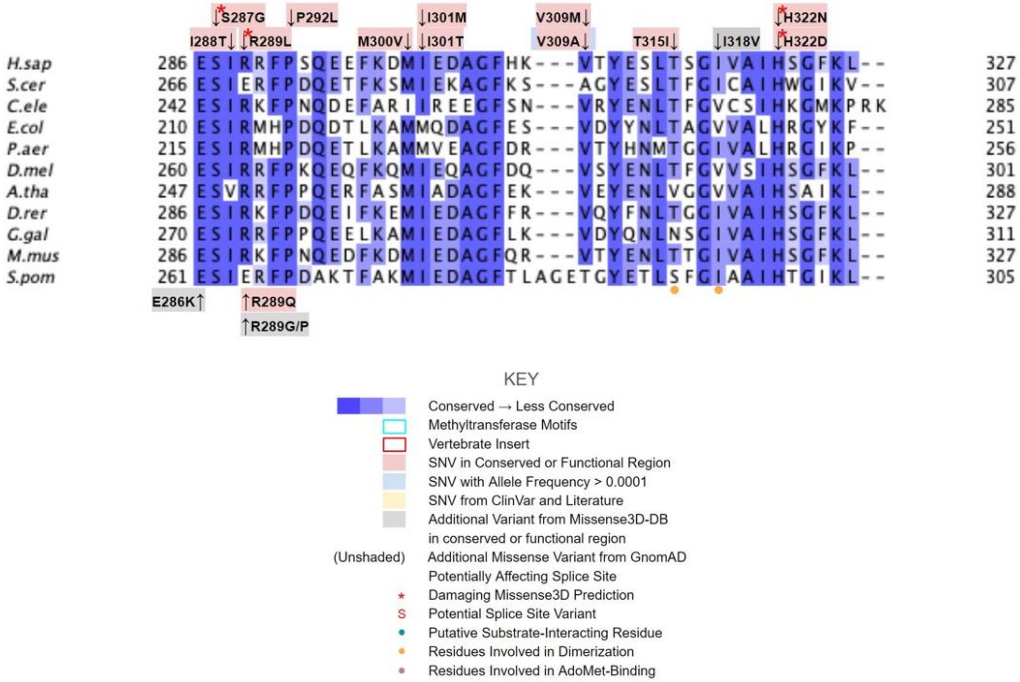

Figure 12. Labeled and annotated multiple sequence alignment of COQ5. Amino acid sequences of COQ5 were analyzed as described in Materials and Methods and include *Homo sapiens* (NCBI accession number NP_115690.3) and homologs in *Saccharomyces cerevisiae* (NP_013597.1), *Caenorhabditis elegans* (NP_498704.1), *Escherichia coli* UbiE (YP_026260.1), *Pseudomonas aeruginosa* UbiE (NP_253750.1), *Drosophila melanogaster* (NP_572865.1), *Arabidopsis thaliana* (NP_200540.1), *Danio rerio* (NP_001004541.1), *Gallus gallus* (NP_001006194.1), *Mus musculus* (NP_080780.1), and *Schizosaccharomyces pombe* (NP_587834.1). See KEY for descriptions of the figure annotations. Functional residues (dotted) were determined from the yeast Coq5 crystal structure (data from [48]). Methyltransferase motifs I, post-I, II, and III are boxed in cyan (data from [18]). An insert exclusively found in vertebrate species is boxed in red. Note that W243 in *S. cerevisiae* (aligned to S263 in the human sequence) is the residue involved in dimerization based on the crystal structure. However, since all other species in the multiple sequence alignment have a Tyr insertion at that position, Y262 was chosen as the functional residue instead due to its similar aromatic nature.

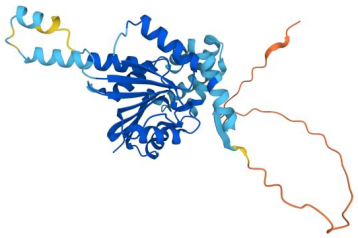

Figure 13. AlphaFold model of the COQ5 monomer. Model color corresponds to model confidence as described in Figure 4. Figure was generated by the AlphaFold Protein Structure Database; adapted with permission from [39,54].

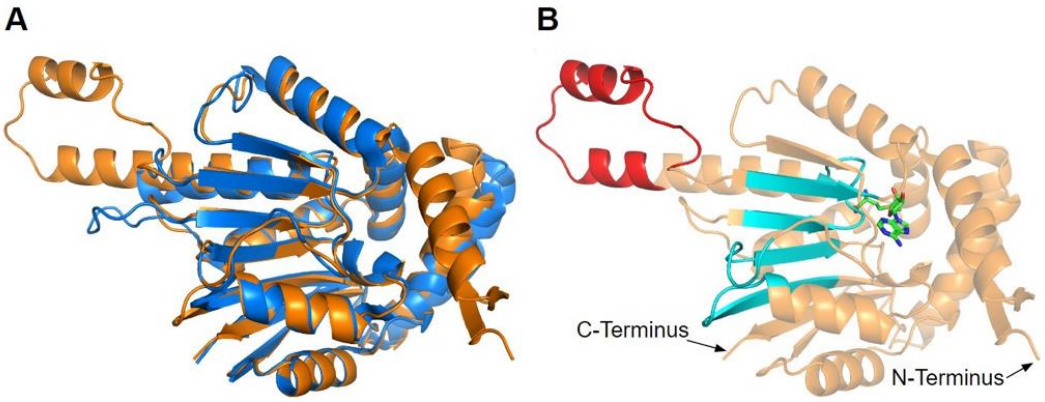

Figure 14. Alignment of AlphaFold-generated model of human COQ5 with existing yeast Coq5 crystal structures. (**A**) Superimposition of the human COQ5 model (shown in orange), adapted with permission from [39,54], and the crystal structure of AdoMet-bound yeast Coq5 (shown in blue, PDB: 4OBW). The first 47 residues of the AlphaFold model, which contains a disordered region with low confidence, were omitted for clarity. (**B**) Human COQ5 model with conserved methyltransferase motifs I-III and post-I highlighted in cyan and vertebrate insert in red. AdoMet (shown in green) was modeled via structural alignment with the crystal structure of AdoMet-bound yeast Coq5 using PyMOL.

3.3.1. SNVs in Methyltransferase Motifs I and Post-I

The first of the four motifs, motif I, is a Gly-rich motif that makes up the first β-strand followed by an extended turn (Figure 15A) [65]. The homologous residue of T117 within this motif (S122 in yeast) has been shown to interact with the amino group of AdoMet in yeast Coq5, while the remaining residues line the AdoMet binding pocket (PDB: 4OBW) [48]. Mutations occurring in this region, which roughly corresponds to residues L110 to D119, may affect the binding of the AdoMet cofactor and therefore enzyme activity. In total, we identified seven SNVs of interest spanning five distinct amino acid positions in this motif, all of which occur on highly conserved residues (Figures 12 and 15B). D112N, D112H, G116S, G118S, and D119G were reported in Missense3D-DB, and all but D119G were classified as structurally damaging by Missense3D. These point mutations may result in the loss of stabilizing interactions within the protein or with the cofactor, as well as the loss of buried Gly residues, which may destabilize the extended turn. L111F and G118D were reported in gnomAD, with G118D having an unknown clinical significance in ClinVar. G118D was classified as structurally damaging due to similar reasons as the previous group of variants, while L111F was neutral. In yeast, a G120R point mutant, homologous to G115 in human COQ5, was found to be structurally stable but catalytically inactive [80], further supporting the Missense3D classifications. However, it is worth noting that the two SNVs at position 118, G118S and G118D, flank the splice sites between exons 2 and 3 on the 5′ and 3′ ends, and may affect splicing in addition to protein structure.

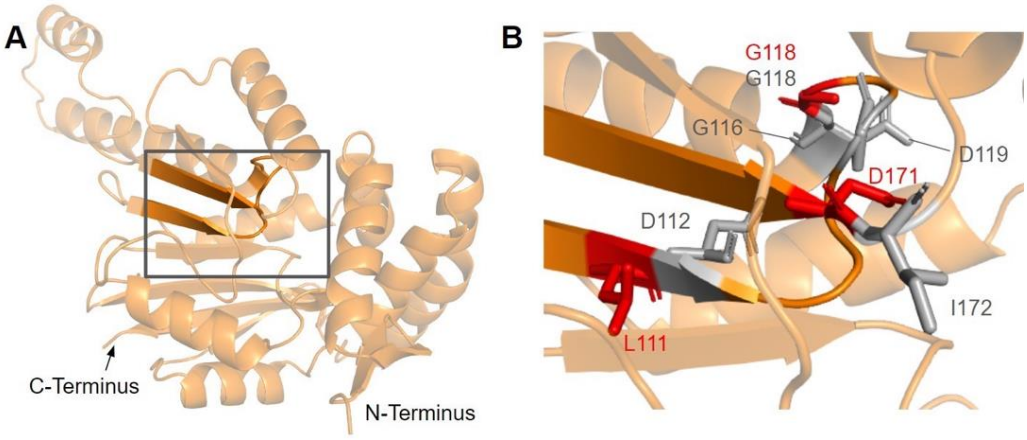

Figure 15. SNVs found in motif I and post-I of COQ5. (**A**) Motif I (lower β-strand, residues L110 to D119) and post-I (upper β-strand, residues V167 to D171) highlighted on the COQ5 model. The first 47 residues were truncated for simplicity. (**B**) Locations of SNVs in motifs I and post-I are depicted. Residues are colored according to their corresponding SNVs Figure 12.

After motif I, the second β-strand is partially composed of motif post-I, which contains a highly conserved acidic residue responsible for interacting with the hydroxyl groups on the ribose ring of AdoMet (Figure 15A) [48,65]. We have defined motif post-I as residues V167 to D171, although flanking residues I172 and N173 are also highly conserved. There are two particular SNVs of interest in the motif post-I region found in gnomAD, namely D171G at the conserved acidic residue and I172S adjacent to it, both of which extend into the AdoMet binding pocket and are annotated as AdoMet-binding (Figures 12 and 15B). These mutations likely abolish interaction with the ribose ring of AdoMet, but were not classified as damaging by Missense3D due to the residues being solvent-exposed in the binding pocket of the model.

3.3.2. SNVs in Methyltransferase Motifs II and III

Motif II (D206 to I215) is located in the fourth β-strand (Figure 16A), where residues K209 to D211 are thought to make extensive contacts with motifs I and III to help align the methyltransferase domain [65]. Residues immediately after motif II form a loop that extends into the AdoMet and substrate-binding pockets. This loop region includes A216 and V222, which are homologous to yeast Coq5 residues interacting with AdoMet, as well as R220 and N221, which are thought to interact with the substrate, $DDMQH_2$ [48]. In motif II and the loop that follows it, there are 15 SNVs of interest spanning eight distinct amino acid positions, all of which are highly conserved (Figures 12 and 16B). D207G, A216V, A215V, R220L, and N221S were reported in Missense3D-DB, although all of them were classified as neutral by Missense3D except for R220L. From gnomAD, we identified variants D207E, D207N, T214S, T214A, I215T, F217L, R220P, R220W, R220Q, and T223I. Of these, T214A, R220P, R220W, and R220Q were classified as deleterious by Missense3D. The most common flags pertain to the loss of buried charges, residue-residue interactions, as well as a change in cavity size (R220). Cavity size likely refers to a change in the substrate binding pocket and is likely to result in a loss of activity. In yeast Coq5, the introduction of G199D (the residue homologous to G218 in human COQ5) resulted in a structurally stable but catalytically inactive mutant that was respiratory-deficient [80], suggesting that mutations in this region are likely pathogenic.

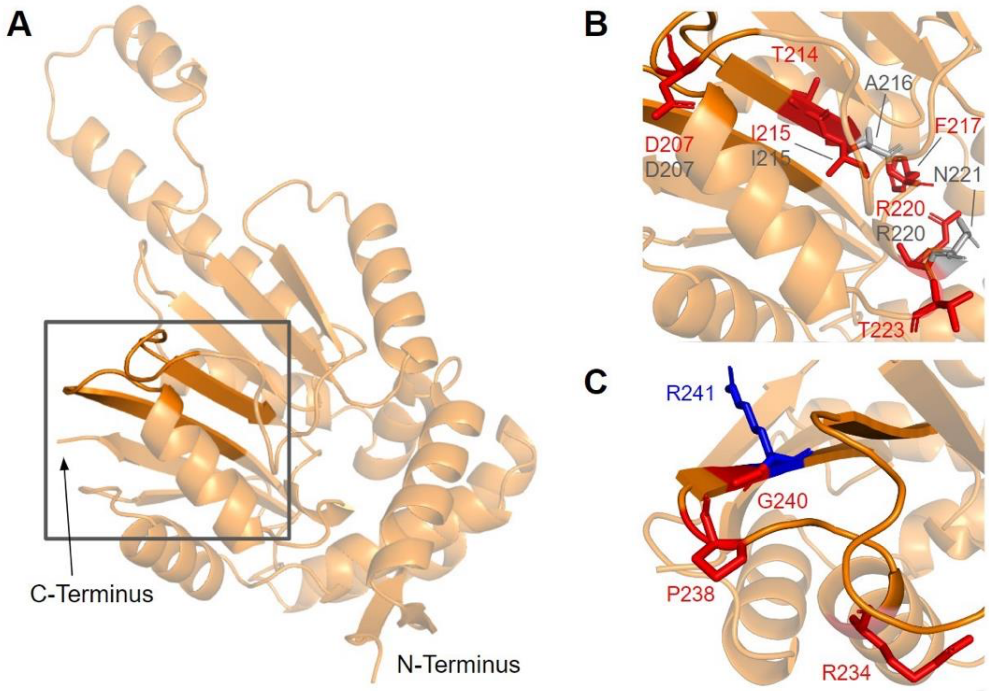

Figure 16. SNVs found in motifs II and III of COQ5. (**A**) Motif II (upper β-strand, residues D206 to I215) and motif III (lower β-strand, residues V235 to F242) highlighted on the COQ5 model. The first 47 residues were truncated for simplicity. (**B**,**C**) Locations of SNVs in motif II (**B**) and motif III (**C**) are depicted. Residues are colored according to their corresponding SNVs in Figure 12.

Motif III (V235 to C244) and the residues preceding it are located in a coil that becomes β-strand five (Figure 16A). The residues in this coil are responsible for aligning the residues in β5 and the active site [65]. From gnomAD, we identified five SNVs of interest spanning four distinct amino acid positions in this region (Figures 12 and 16C). They are R234Q, R234W, P238R, G240E, and R241W, all of which are highly conserved, with the exception of R241W, which is a frequent polymorphism (allele frequency of 4.21×10^{-4}). Only G240E was classified as damaging by Missense3D.

3.3.3. SNVs on the Dimerization Interface

The dimerization interface, as determined from the crystal structures of the yeast Coq5 dimer (PDB: 4OBX and 4OBW), consists of hydrophobic residues homologous to M86, L88, I90, L254, L258, Y262, V266, I267, V269, L270, V273, I274, A275, T315, and I318 [48]. We identified a total of seven SNVs spanning six unique amino acid positions (Figure 17A). Among them, L254F, L254P, V273L, A275T, and T315I were found in gnomAD, while I90V and I318V were found in Missense3D-DB (Figure 17B). None of these variants were flagged as damaging by Missense3D, as the mutant residues were often hydrophobic. It is worth noting that all seven SNVs would appear as surface residues in the COQ5 model, which does not include an oligomeric structure. The effectiveness of Missense3D is limited in this region; thus, we have also provided the SIFT and Polyphen-2 classifications (Supplemental Table S1).

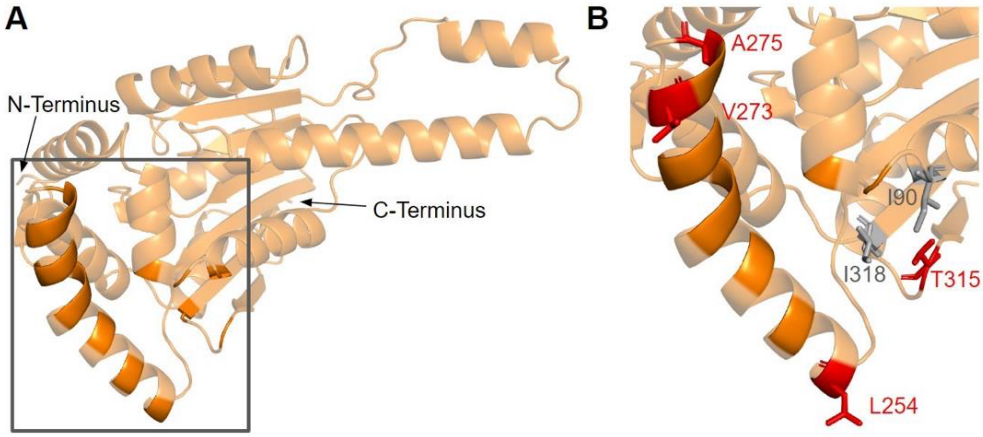

Figure 17. SNVs found in the COQ5 dimerization interface. (**A**) The dimerization interface of COQ5 largely consists of hydrophobic residues located on the α6 helix (left highlight). The first 47 residues were truncated for simplicity. (**B**) Locations of SNVs are depicted. Residues are colored according to their corresponding SNVs in Figure 12.

3.3.4. Additional SNVs in Potentially Significant Regions

Two additional regions on COQ5 are worth noting. The first is an insert roughly located at residues K135 to G163, which is found exclusively in vertebrate species. A BLAST search comprising the amino acid sequence of this region gave no significant hits [84]. Three SNVs with allele frequency larger than 1.00×10^{-4} are found in this region: Q139H, A152T, and D160G (Figure 18A). A152T was estimated to have an allele frequency of 1.18×10^{-1} by gnomAD, the most common among all missense SNVs found in the *COQ5* coding region. While none of these variants were classified as structurally damaging by Missense3D, this region may have evolved new functions, such as protein-protein interactions, that may be affected by these mutations. The second region of interest is the C-terminus of COQ5. Previous studies in yeast have identified a Coq5 point mutant located four residues away from the C-terminus. This mutant resulted in a partially active enzyme that resulted in a decrease in the steady-state levels of Coq3, Coq4, and Coq5, as well as respiratory deficiency [80]. The underlying cause of this phenotype is unclear, although it does suggest that the C-terminus of COQ5 may play a key role in stabilizing Coq5, whether it be through residue-residue interactions or some other means. Two SNVs, H322N and H322D, are found in this region, located just six amino acids away from the C-terminus (Figure 18B). Residue H322 was predicted to interact with Q294 by Missense3D. Both variants were classified as damaging, for reasons related to the loss of buried charges and hydrogen-bonding interactions.

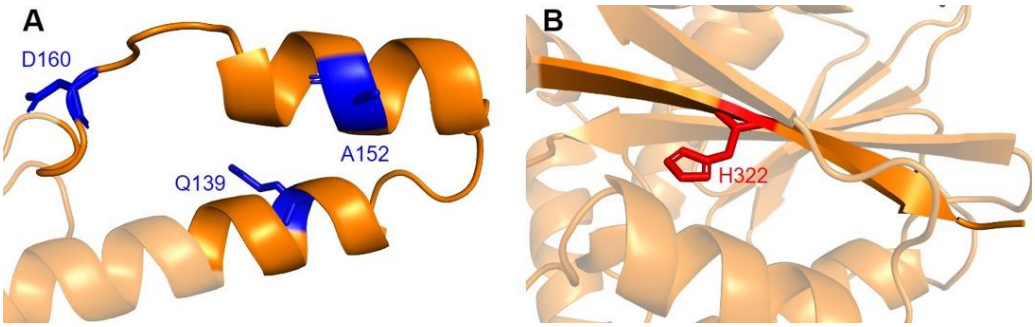

Figure 18. SNVs found in other potentially significant regions of COQ5. Locations of SNVs are depicted in (**A**) the vertebrate insert (left, residues K135 to G163) , and (**B**) in the C-terminus (right, residues V319 to L327). Residues are colored according to their corresponding SNVs in Figure 12.

3.4. COQ6

COQ6 is characterized as a class A flavoprotein monooxygenase with a tightly bound FAD cofactor [33,85,86]. However, unlike typical flavin-dependent monooxygenases which receive electrons directly via an NAD(P)H coenzyme, NAD(P)H instead delivers electrons to yeast Coq6 via ferredoxin Yah1 (FDX1 and FDX2 are human homologs) and ferredoxin reductase Arh1 (FDXR is a human homolog) [13]. It is not yet known if human homologs FDX1, FDX2, and FDXR perform the same electron transfer roles for COQ6. Coq6 is peripherally associated with the IMM and is responsible for the addition of a hydroxyl group to the C5 position on the CoQ ring precursor, converting HPB to DHPB (Figure 1A) [33]. While both humans and yeast use 4-HB as a ring precursor for CoQ biosynthesis, yeast cells also utilize para-aminobenzoic acid (pABA) as a ring precursor to CoQ [87]. Ozeir et al. showed that yeast Coq6, in addition to hydroxylating C5, is also able to deaminate the ring C4 position on the intermediate derived from pABA [88]. Yeast *coq6* null-mutants accumulate 3-hexaprenyl-4-hydroxybenzoic acid (HHB) and 3-hexaprenyl-4-aminobenzoic acid (HAB) [13,89]. Yeast *coq6* point mutants that express a stable but inactive Coq6 polypeptide accumulate 3-hexaprenyl-4-hydroxyphenol (4-HP_6) [33]. The equivalent intermediate, 4-HP_{10}, has also been observed to accumulate in human cells harboring a *COQ6* disruption [34]. This finding indicates that the C1-decarboxylation and C1-hydroxylation steps can occur prior to the C5-hydroxylation step (Figure 1A). Resolving the order of steps will require an in vitro assay for Coq6 and would also benefit from identification of the enzyme(s) that mediate the decarboxylation and hydroxylation at C1. Expression of human COQ6 partially complements yeast lacking Coq6, demonstrating the usefulness of *S. cerevisiae* as a model organism to study human *COQ6* mutations [90].

Mutations in the human *COQ6* gene are associated with primary CoQ_{10} deficiency and are further associated with several disease states, predominantly steroid-resistant nephrotic syndrome (SRNS) and sensorineural hearing loss (SNHL) [29,91–93]. Importantly, supplementation with either 3,4-dihydroxybenzoic acid (3,4-diHB) or vanillic acid (VA) partially restores CoQ biosynthesis in yeast *coq6* null mutants expressing human *COQ6* genes harboring pathogenic mutations; such a bypass of the C5-hydroxylation step with VA or 3,4-diHB also occurs when yeast coq6 null mutants overexpress Coq8 [33,90]. Supplementation with VA may provide a potential avenue of treatment for patients with CoQ_{10} deficiency due to mutations in the *COQ6* gene. However, clinical trials are required to determine both the safety and efficacy of this "bypass" therapy.

Drovandi et al. list 48 patients who likely have pathogenic mutations in COQ6 [91]. While mutations in *COQ6* are rare, they result in severe disease phenotypes across multiple physiological systems. A report by Perrin et al. detailed a case study of a Turkish patient born to consanguineous parents with a missense mutation in *COQ6* [94]. The patient

presented with end-stage renal failure at five years old and subsequently received an organ transplant. At 17 years old, the patient presented with sudden loss of vision. Genetic analysis of the *COQ6* gene revealed the presence of the SNV A353D. The younger brother of this patient harbored the same homozygous mutation and presented with primary CoQ_{10} deficiency with SRNS and SNHL. Replacement therapy with idebenone (a hydrophilic short-chain CoQ_{10} analog) began at an earlier age for the second patient. Doimo et al. expressed the human A353D mutation, amongst others, in *S. cerevisiae coq6* at the corresponding residue A361 [90]. Results indicated that the mutation was hypomorphic, as yeast were viable but showed decreased growth on medium containing a nonfermentable carbon source. A recent study indicates that clusters of the A353D occur in Kazak, Turkish, and Iranian populations, and show a comparatively later disease onset [91]. In contrast, patients with a variant that is predominant in the Middle East (G255R), present with early disease onset, severe phenotype, and higher odds of mortality [91]. Further mutagenesis studies using yeast can help to elucidate the effects of mutations found in patients. In addition to the 13 known pathogenic mutations in *COQ6*, there have also been several reported heterozygous SNVs that may confer deleterious consequences.

From gnomAD, ClinVar, Missense3D-DB, and literature we identified 82 missense SNVs of interest (Figure 19; Supplemental Table S1). Of these variants, 55 SNVs coincided with a highly conserved or functional residue, determined from the multiple sequence alignment and from structural studies on yeast, respectively [49]. Identification of functional residues was performed by in silico prediction of substrate-access tunnels and protein-cofactor interactions [49]. Residues predicted to be functional were subsequently corroborated by site-directed mutagenesis and in vivo functional assays in the yeast model [49]. Of the 27 variants classified as structurally damaging by Missense3D, 21 overlapped with the group of highly conserved or functional residues (Figure 19). From the ClinVar database, seven missense variants were determined to be pathogenic or likely pathogenic. Of those seven variants, three were identified by Missense3D to be structurally damaging. There were 18 SNVs in gnomAD identified as frequent polymorphisms. Intriguingly, one of the frequent polymorphisms T446M (allele frequency of 1.70×10^{-4}) was identified as being structurally damaging by Missense3D.

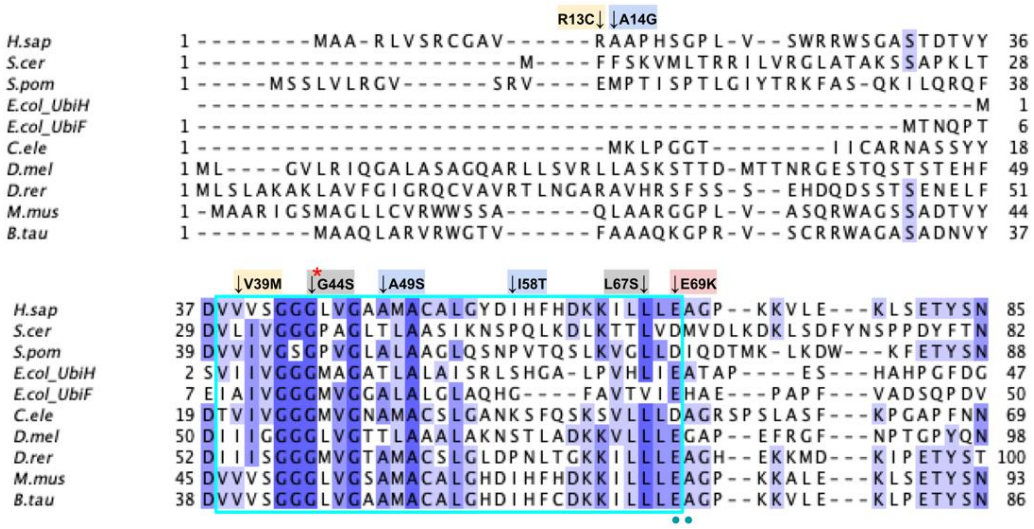

Figure 19. *Cont.*

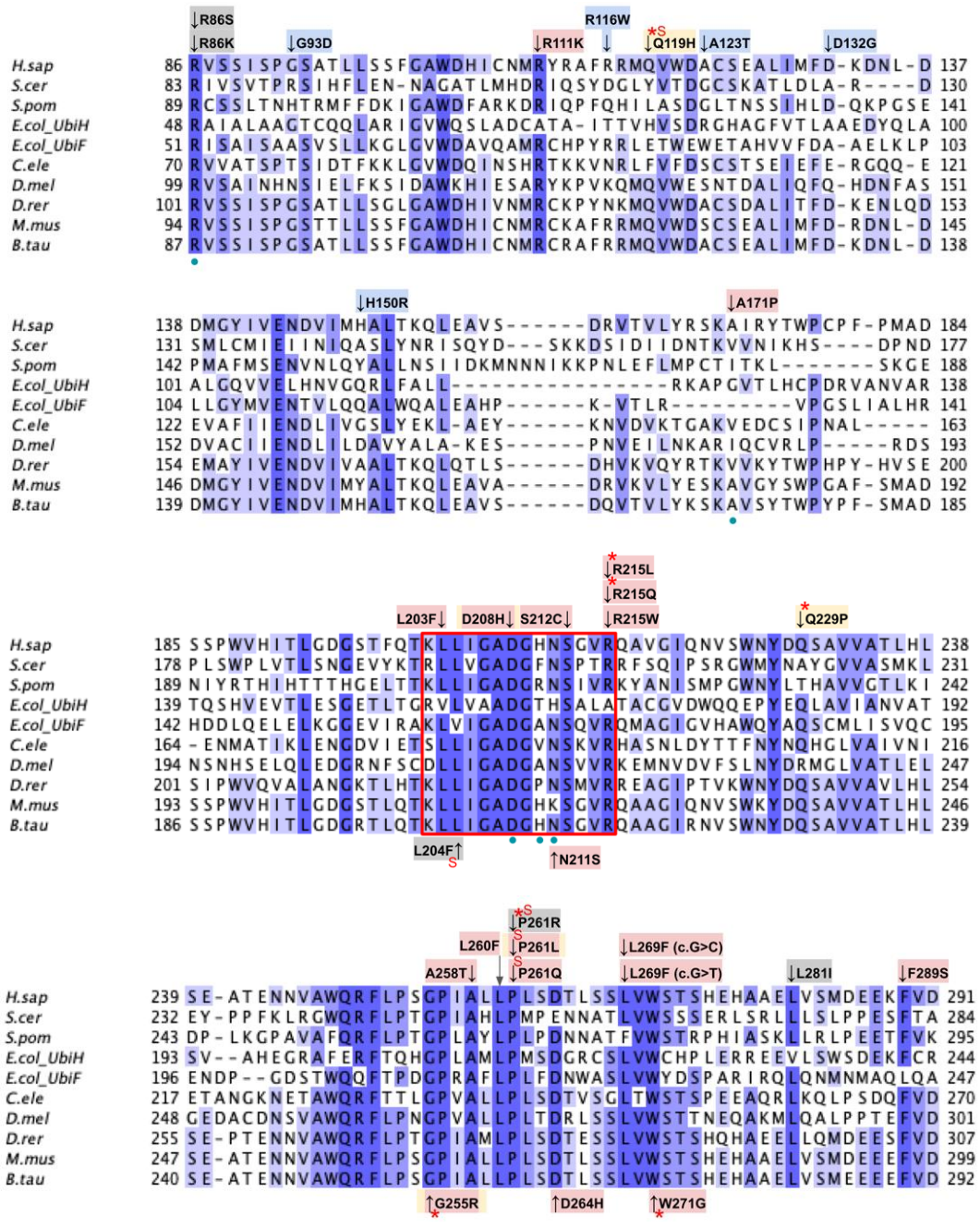

Figure 19. *Cont.*

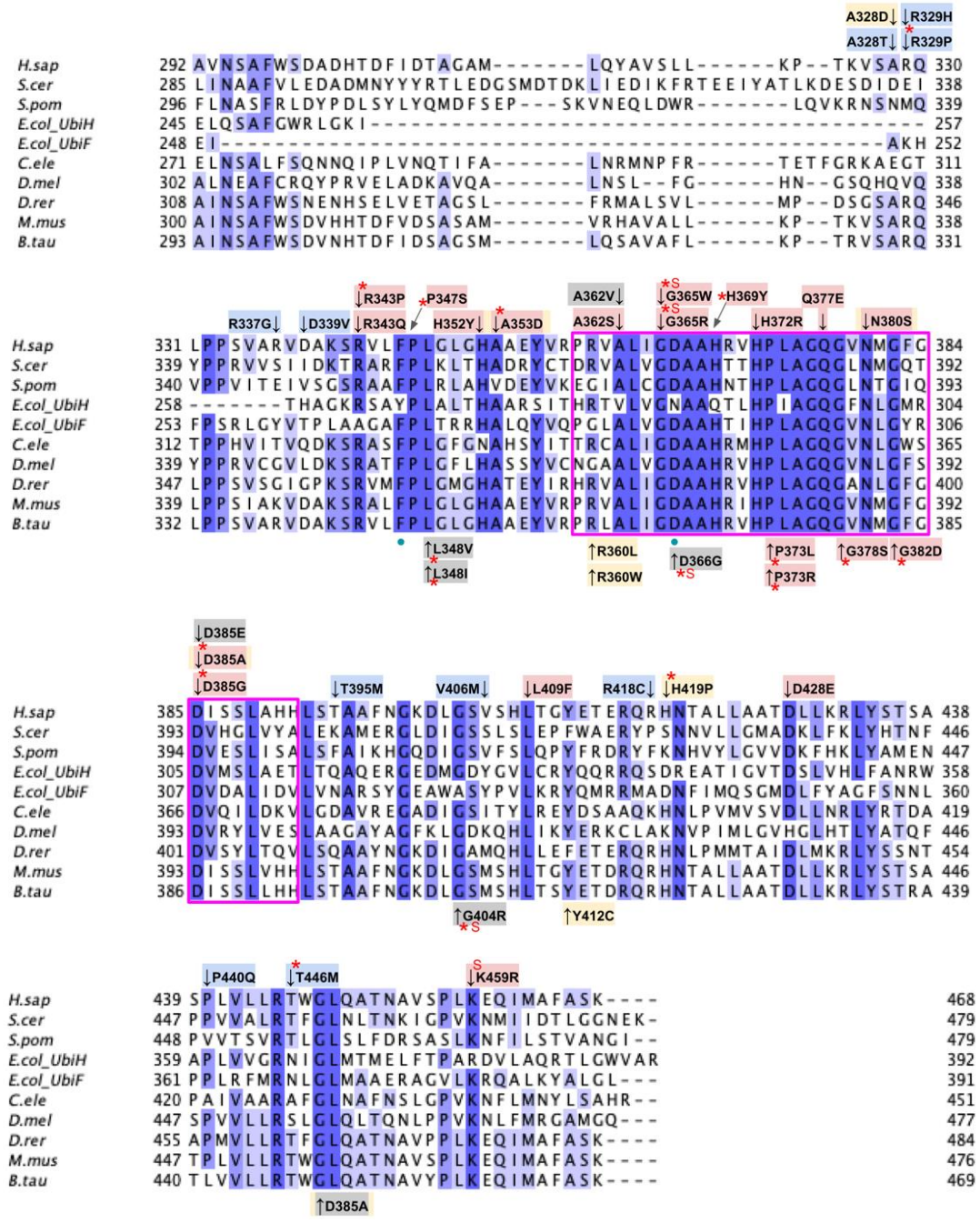

Figure 19. *Cont.*

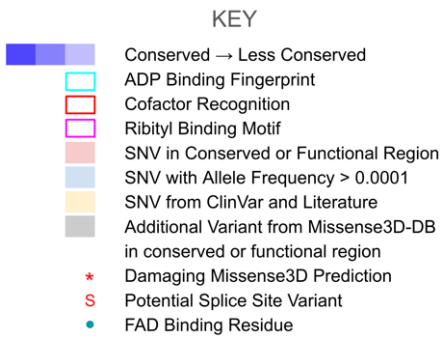

Figure 19. Labeled and annotated multiple sequence alignment of COQ6. Amino acid sequences of COQ6 were analyzed as described in Materials and Methods and include *Homo sapiens* (NCBI accession number NP_872282.1) and homologs in *Saccharomyces cerevisiae* (NP_011771.1), *Schizosaccharomyces pombe* (NP_595401.2), *Escherichia coli* UbiH (NP_417383.1), *Escherichia coli* UbiF (NP_415195.1), *Caenorhabditis elegans* (NP_505415.2), *Drosophila melanogaster* (NP_608934.1), *Danio rerio* (NP_001038869.1), *Mus musculus* (NP_766170.2), and *Bos taurus* (NP_001039558.1). See KEY for descriptions of the figure annotations. The ADP Binding Fingerprint is boxed in cyan, the Cofactor Recognition motif is boxed in red, and the Ribityl Binding motif is boxed in magenta, data from [89]. FAD-binding residues are marked with blue dots, data from [49].

The human COQ6 model was obtained from the AlphaFold Protein Structure Database (Figure 20) [39,54].

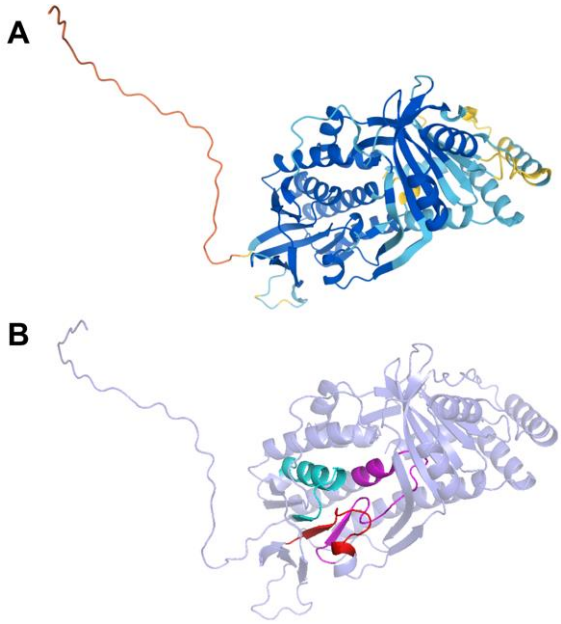

Figure 20. AlphaFold model of single chain of COQ6. (**A**) Model color corresponds to model confidence as described in Figure 4. Figure was generated by the AlphaFold Protein Structure Database [39,54]. (**B**) Structural motifs shown in Figure 19 are highlighted.

3.4.1. SNVs in the ADP-Binding Fingerprint

The COQ6 amino acid sequence contains the characteristic GXGXXG fingerprint necessary for binding the ADP-moiety of the FAD cofactor, along with other conserved residues involved in FAD/NAD^+ recognition [89,95]. The segment forms a characteristic βαβ-fold that binds FAD, which is reflected in the COQ6 multiple sequence alignment and model (Figures 19 and 21A). The βαβ-fold occurs near the N-terminus of COQ6 from residues D37 to E69 (Figure 21A). In this domain, we encounter six SNVs with relevance to this analysis. Mutations occurring in this region may affect COQ6 cofactor-binding capabilities. Two SNVs reported in Missense3D-DB occur at highly conserved residues within the ADP-binding fingerprint: G44S and L67S (Figure 21B). Of these two, G44S was identified by Missense3D as being structurally damaging, due to the replacement of Gly at a bend. Neither mutation has a clinical association listed on ClinVar. In this same motif gnomAD reports a SNV that occurs at a residue identified as FAD-binding: E69K (Figure 21B). This variant is of particular interest because of its potential to disrupt cofactor binding. However, E69K does not have any clinical association with primary CoQ_{10} deficiency, nor is it predicted to be structurally damaging by Missense3D. Two SNVs reported in gnomAD are identified as frequent polymorphisms: A49S and I58T (Figure 21B). Neither of these variants occurs at highly conserved residues. According to the ClinVar database, A49S has been listed as a benign mutation. There is no ClinVar annotation for I58T. Both of these variants are characterized as neutral by Missense3D. One additional SNV is reported in ClinVar in this region: V39M (Figure 21B). This variant has an uncertain significance label on ClinVar and is characterized as structurally neutral by Missense3D.

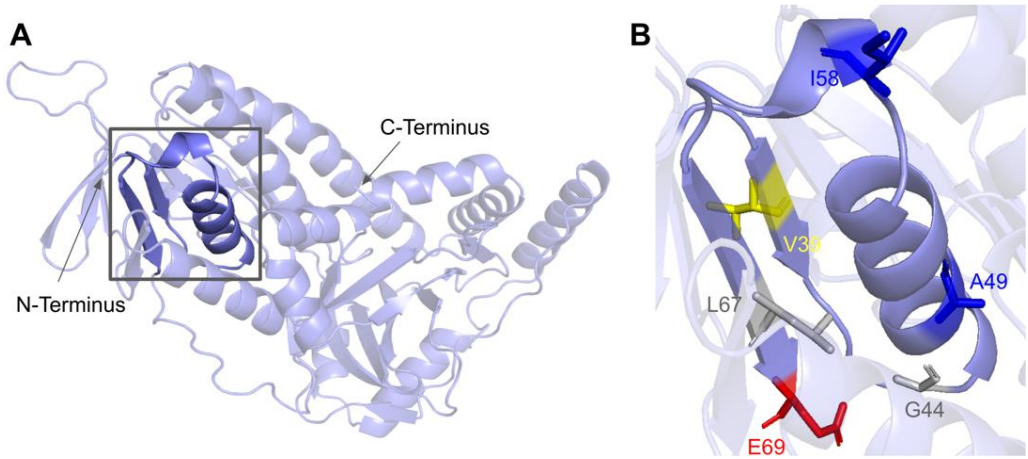

Figure 21. SNVs in the COQ6 ADP-binding fingerprint. (**A**) The ADP-binding βαβ-fold is highlighted on the COQ6 model and includes residues D37 to E69. Residues 1–35 have been truncated. (**B**) Locations of SNVs are depicted. Residues are colored according to their corresponding SNVs in Figure 19.

3.4.2. SNVs in the Cofactor Recognition Structure

This second region on the COQ6 polypeptide is suggested to recognize the pyrophosphate moiety of the FAD cofactor [89]. The cofactor recognition structure occurs from residues K202 to R215 (Figure 22A). In this domain, we encounter eight SNVs with relevance to this analysis. Mutations in functional residues contributing to FAD-binding are predicted to diminish COQ6 function, resulting in a deficiency in CoQ_{10}. There are six SNVs reported in gnomAD that affect highly conserved residues within this region:

L203F, N211S, S212C, R215L, R215Q, and R215W (Figure 22B). Of these six variants, R215L and R215Q were reported as structurally damaging by Missense3D. N211S may disrupt catalytic function, as it occurs at a residue identified as FAD-binding and is flagged by Missense3D as a buried charge replaced. However, this mutation does not have any clinical association. There is one additional SNV reported in Missense3D-DB occurring at a highly conserved residue: L204F (Figure 22B). This mutation is predicted to be structurally neutral by Missense3D. L204F does not have a clinical association with CoQ_{10} deficiency. ClinVar reports one SNV in this region: D208H (Figure 22B). This variant occurs at a highly conserved residue identified as FAD-binding and has a clinical association of unknown significance. This mutation is reported to lead to haploinsufficiency of COQ6, predisposing individuals harboring the mutation to schwannomatosis, which is a rare genetic disorder resulting in multiple benign schwannomas growing on peripheral nerves [96]. However, further studies must be conducted to confirm this link [97].

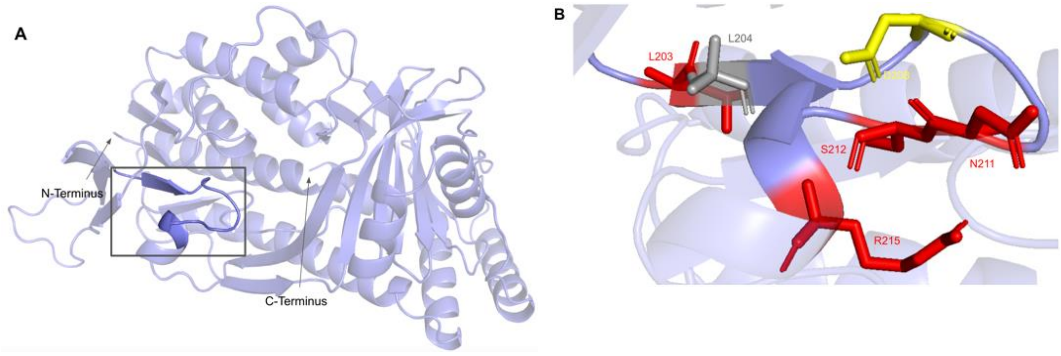

Figure 22. SNVs found in the COQ6 NAD(P)H/FAD recognition sequence. (**A**) NAD(P)H/FAD recognition structure highlighted on COQ6 model, residues K203 to R215. Residues 1–35 have been truncated. (**B**) Locations of SNVs are depicted. Residues are colored according to their corresponding SNVs in Figure 19.

3.4.3. SNVs in the Ribityl Binding Motif

The third region of known importance on the COQ6 polypeptide has been implicated in binding to the ribityl moiety on FAD. It contains the consensus fingerprint for ribityl binding, including the conserved Asp necessary to hydrogen bond with O-3 of the ribityl moiety [89,98]. This region is predicted to reside near the putative catalytic region containing the other amino acid fingerprints necessary for FAD-binding. Mutations in functional residues contributing to coenzyme binding are predicted to diminish COQ6 function, resulting in a deficiency in CoQ_{10}.

This region spans residues P359 to H392 (Figures 19 and 23A). In this domain, we encounter 18 SNVs relevant to this analysis. There are 11 SNVs reported in gnomAD that occur in highly conserved residues within this region. Eight of these 11 variants, G365W, G365R, H369Y, P373L, P373R, G378S, G382D, and D385G are reported to be structurally damaging by Missense3D. The high number of variants predicted to be structurally damaging in this region may be indicative of its structural importance to COQ6 integrity. Three additional SNVs are reported in Missense3D-DB to occur at highly conserved residues: A362V, D366G, and D385E (Figure 23B). Of the three, only D366G is predicted to be structurally damaging by Missense3D. This variant is also located at the conserved Asp predicted to bind FAD and may therefore disrupt COQ6 function. None of these mutations have clinical associations.

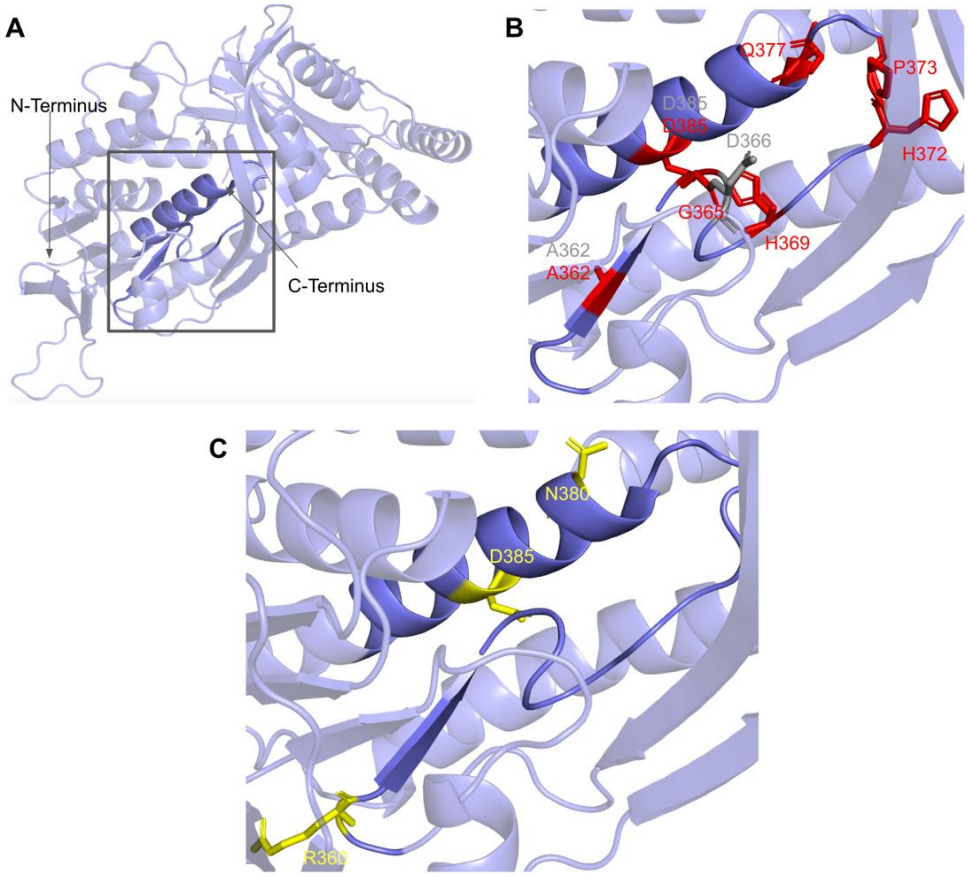

Figure 23. SNVs found in the COQ6 ribityl binding motif. (**A**) Ribityl binding motif is highlighted on the COQ6 model, from residues P359 to H392. Residues 1–35 have been truncated. (**B**) Locations of SNVs in conserved or functional regions are depicted. (**C**) Locations of ClinVar and literature variants are depicted. Residues are colored according to their corresponding SNVs in Figure 19.

In this region, four SNVs are reported in ClinVar and the research literature: R360L, R360W, N380S, and D385A (Figure 23C). R360L is associated with primary CoQ_{10} deficiency and is labeled as likely pathogenic. R360W was found in a compound-heterozygous patient with the frameshift c.804delC mutation and was determined to be pathogenic [99]. Patients homozygous for R360W have been identified in China and Central/Eastern Europe and have been associated with a higher risk of cardiomyopathy, growth retardation, and neurologic involvement [91]. The N380S variant does not have a condition associated with it but is labeled as likely pathogenic by ClinVar. The D385A variant is reported and has been predicted in silico to be deleterious but has not been associated with any clinical manifestations [100]. This D385A variant is the only one of these four SNVs that is predicted to be structurally damaging by Missense3D.

The most common flags generated by Missense3D for this region concern the change of buried residues. The most consequential changes pertain to the replacement of buried charges and Gly residues. Such variants have the potential to disrupt FAD-binding and protein folding.

3.5. COQ7

COQ7 is characterized as a di-iron carboxylate hydroxylase [13]. It is peripherally associated with the matrix side of the IMM and is responsible for the penultimate step of CoQ biosynthesis, hydroxylating $DMQH_2$ to $DMeQH_2$ [101,102]. Addition of 2,4-diHB was shown to restore synthesis of CoQ_6 in the yeast *coq7* null mutant when Coq8 was overexpressed [59]. The overexpression of Coq8 stabilizes the yeast Coq polypeptides that are otherwise degraded in the *coq* null mutants. The use of an alternate ring precursor to "bypass" the blocked Coq7 hydroxylase step in CoQ biosynthesis is similar to the previously described VA bypass of certain yeast *coq6* point mutants, or the *coq6* null mutant overexpressing Coq8 [33,90]. Tests of 2,4-diHB bypass therapy in patient fibroblasts harboring *COQ7* mutations indicated that such a bypass was not uniformly successful and seemed to have the most benefit in cells with a more profound deficiency in COQ7 [103]. Hence, the outcome of such bypass therapies is likely to be quite dependent on the nature of the mutations.

Human COQ7 is able to complement yeast lacking Coq7, demonstrating conserved functionality across species as well as the viability of *S. cerevisiae* as a model organism to study human *COQ7* mutations [104]. Mutations in the human *COQ7* gene are associated with primary CoQ_{10} deficiency and are further associated with several disease states, predominantly hypertonia and sensorineural hearing loss (SNHL) [29].

From gnomAD, ClinVar, Missense3D-DB, and literature we identified 60 missense SNVs of interest (Figure 24; Supplemental Table S1). Of these variants, 47 coincided with a highly conserved region or functional residue, which were determined from the multiple sequence alignment as well as structural studies on human COQ7 [50,52]. Eleven of the twelve variants classified as structurally damaging by Missense3D were contained in this group (Figure 24). From the ClinVar Database and literature, four missense variants were determined to be pathogenic or likely pathogenic. None of these four variants were identified by Missense3D to be structurally damaging. There were 13 SNVs in gnomAD identified as frequent polymorphisms. One of these, R65C (allele frequency of 2.76×10^{-4}) was identified as being structurally damaging by Missense3D.

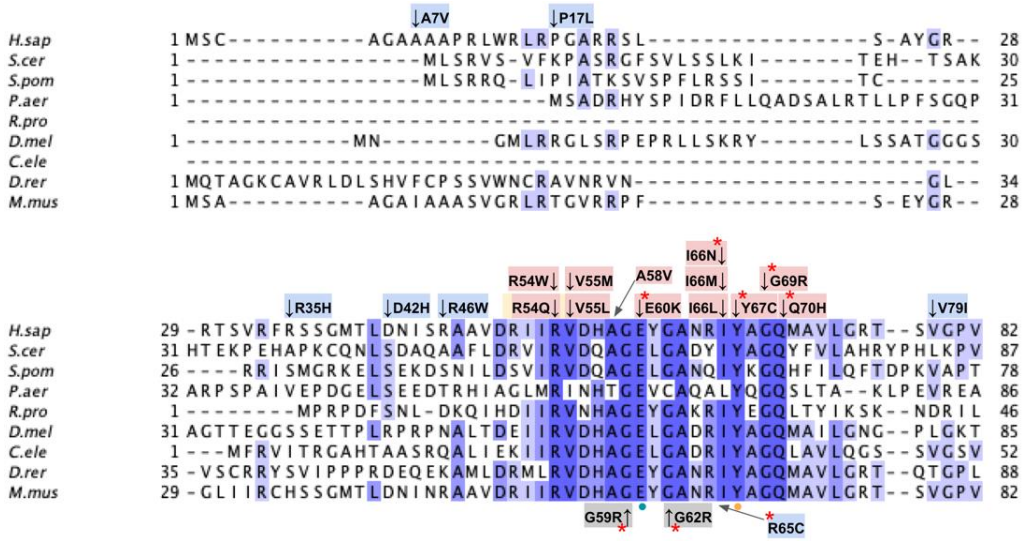

Figure 24. *Cont.*

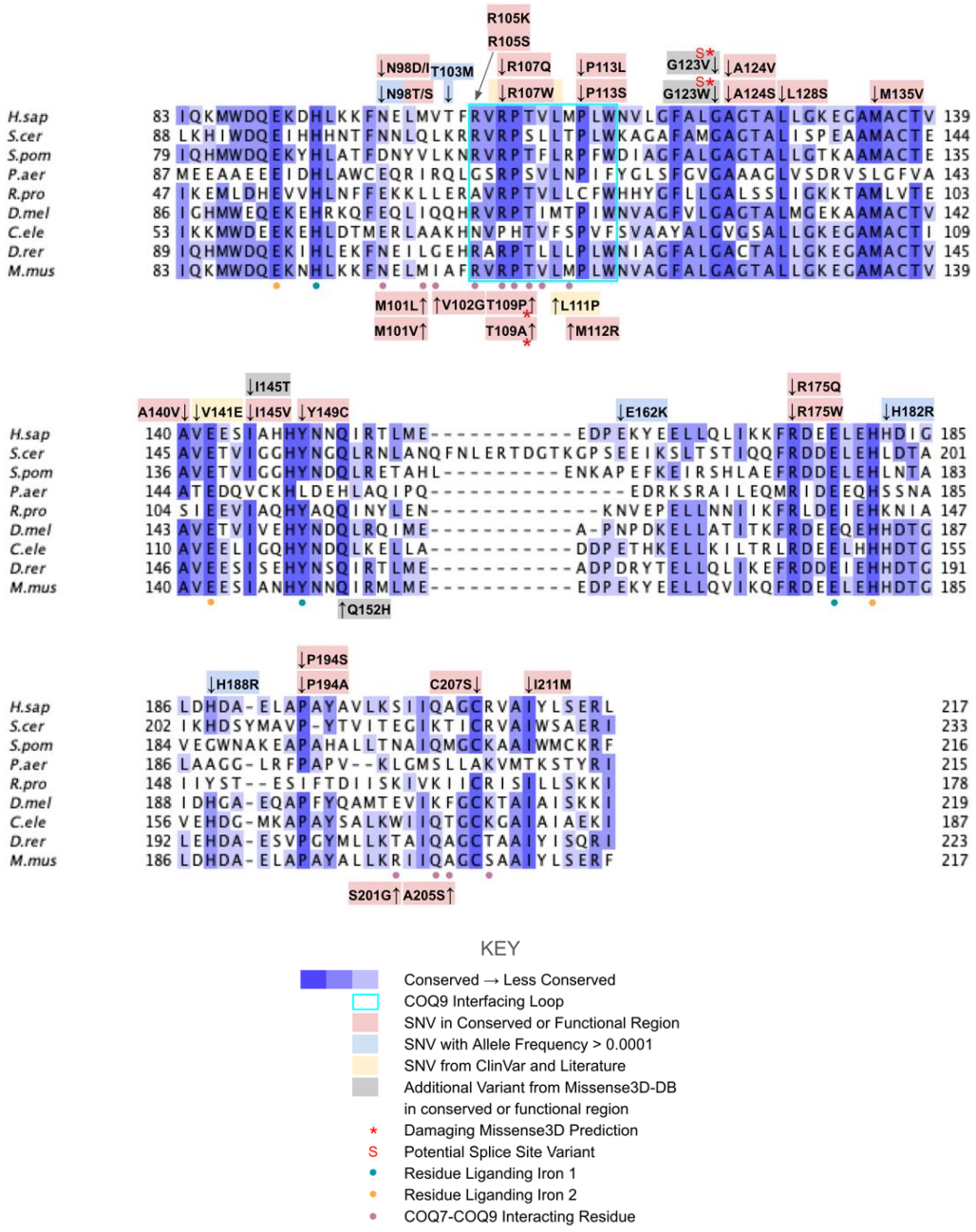

Figure 24. Labeled and annotated multiple sequence alignment of COQ7. Amino acid sequences of COQ7 were analyzed as described in Materials and Methods and include *Homo sapiens* (NCBI accession number NP_057222.2) and homologs in *Saccharomyces cerevisiae* (NP_014768.2), *Schizosaccharomyces*

pombe (NP_595416), *Pseudomonas aeruginosa* (QLJ91605.1), *Rickettsia prowazekii* (ADE29699), *Drosophila melanogaster* (NP_651967.2), *Caenorhabditis elegans* (NP_498128.1), *Danio rerio* (NP_001076480.1), and *Mus musculus* (NP_034070.1). See KEY for descriptions of the figure annotations. The COQ9 interfacing loop is boxed in cyan, data from [50]. Residues that ligand iron 1 are marked with blue dots, and those that ligand iron 2 are marked with orange dots, data from [52]. COQ7-COQ9 interacting residues are marked with purple dots, data from [50,52].

The human COQ7 model was obtained from the AlphaFold Protein Structure Database (Figure 25) [39,54]. The structure of a human COQ7:COQ9 complex was recently determined (PDB: 7SSS and 7SSP) [52].

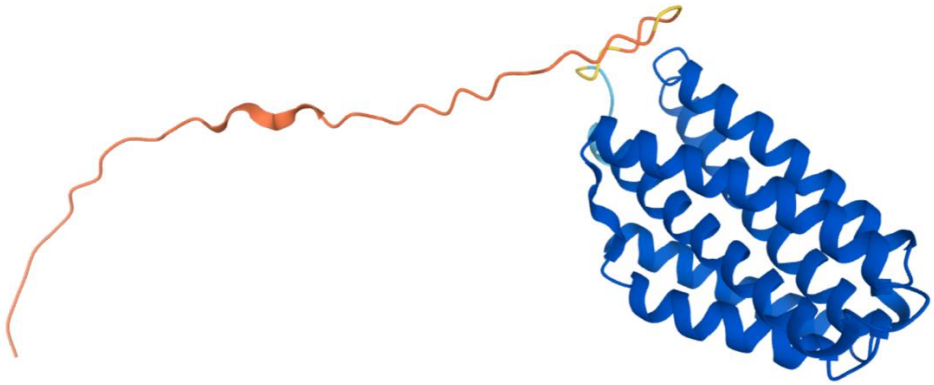

Figure 25. AlphaFold model of single chain of COQ7. Model color corresponds to model confidence as described in Figure 4. Figure was generated by the AlphaFold Protein Structure Database [39,54].

3.5.1. SNVs in a Loop of COQ7 That Interfaces with COQ9

The COQ7 polypeptide contains a loop (residues R105 to W115) that is situated between α-helix 1 and α-helix 2 and is composed predominantly of residues with hydrophobic side-chains. This loop was predicted to interact with COQ9 [50] and was recently observed at the interface between COQ7 and COQ9 in the structure determined for an octameric COQ7:COQ9 complex [52]. The residues in this loop are situated on the outer face of COQ7 (Figure 26A). In this domain, we encounter six SNVs with relevance to this analysis. Mutations in this region have the potential to decrease COQ7-COQ9 hydrophobic, hydrogen-bonding, and salt bridge interactions noted by [52]. There are nine SNVs reported in gnomAD occurring at highly conserved or functional residues in this region (Figure 26B). Of these nine SNVs from gnomAD, only variants at T109 were flagged by Missense3D as structurally damaging (buried H-bond breakage). None of these variants are present as homozygotes in gnomAD, nor are they associated with a deficiency in CoQ_{10}. The variant R107W was identified in ClinVar as having uncertain significance and occurs at a highly conserved residue (Figure 26B). This variant is adjacent to P108, a key residue predicted to interact with COQ9 [50]. Missense3D characterizes R107W as neutral. L111P was identified as a homozygous mutation in a six-year-old girl presenting with SNHL and spasticity by Wang et al. (Figure 26B) [103]. However, the severity of this mutation was determined to be dependent on the presence of another variant, T103M, which is identified here as a frequent polymorphism (allele frequency of 6.24×10^{-1}). Missense3D characterizes T103M as neutral.

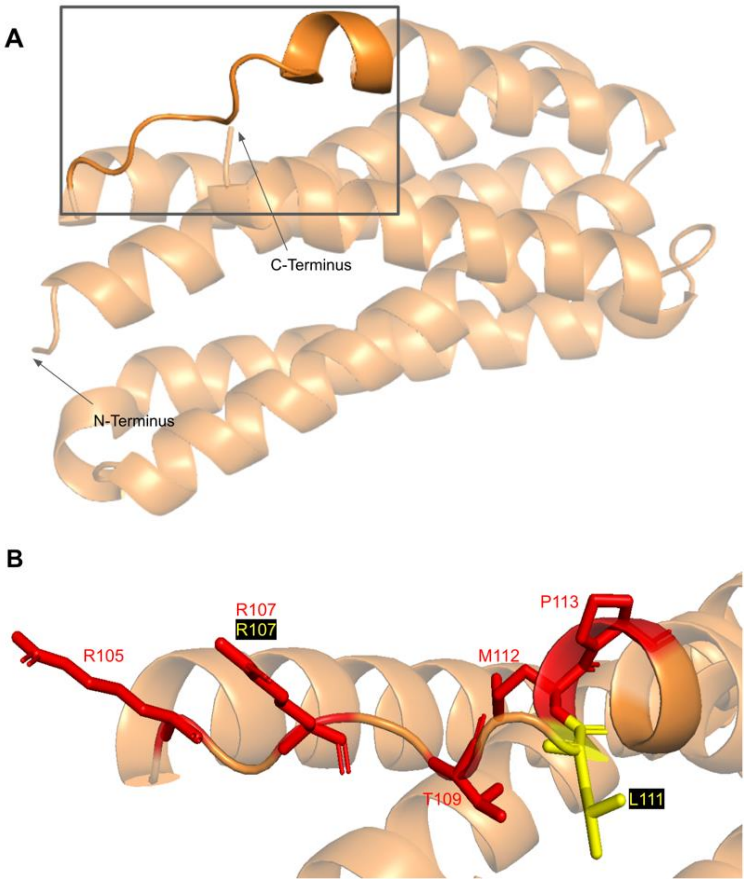

Figure 26. SNVs found in the COQ7 loop that interfaces with COQ9. (**A**) The loop (residues R105 to W115) that interfaces with COQ9 are highlighted on the COQ7 model. Residues 1–43 have been truncated. (**B**) Locations of SNVs are depicted. Residues are colored according to their corresponding SNVs in Figure 24.

3.5.2. Residues near the C-terminus of COQ7 That Form Contacts with COQ9

The COQ7:COQ9 complex co-crystallized with a core of phospholipids, suggesting that membrane association is crucial for complex formation [52]. Four residues located in the C-terminal α-helix 6 make additional contacts with COQ9: S201, Q204, A205, and R208. It seems possible that the variant C207S, nestled among these residues and occurring at a highly conserved Cys, might impact the association of COQ7 with COQ9. There are also two variants that occur at reported interacting residues: S201G and A205S. Both variants are characterized by Missense 3D as neutral but may have the potential to disrupt COQ7:COQ9 interaction.

3.5.3. SNVs in the Predicted Iron-Liganding Motif

COQ7 was first identified as a di-iron protein with the motif E X_{n1} EXXH X_{n2} E X_{n3} EXXH, where n represents a variable number of connecting residues [51]. These residues form carboxylate ligands that are predicted to bind to two Fe (II) atoms located within the four-helix bundle of COQ7 [101]. Using three-dimensional mapping of their COQ7 cryo-EM

structure, Manicki et al. suggested that the motif E X_6 Y X_{22} E X_2 H X_{48} E X_6 Y X_{28} E X_2 H is functionally important in forming these di-iron carboxylate ligands [52]. However, it is important to note that the structure determined for COQ7 did not possess metals, hence the residues that function to ligand the di-iron are surmised based on structural similarity to other di-iron carboxylate proteins [52]. SNVs at or near residues in the motif are predicted to disrupt the ability of COQ7 to ligand iron atoms. We encounter three SNVs at or near residues in the predicted di-iron-liganding motif. G59R and E60K occur at or adjacent to E60, which ligands iron 1 (Figure 27B). G59R was reported in Missense3D-DB and was characterized as altering a cavity by Missense3D. This is likely to reduce substrate access to the active site. E60K was reported in gnomAD and was characterized as switching a buried charge by Missense3D. It is important to note that Missense3D does not take into account the roles played by residues that act as metal ligands when making predictions about functionality.

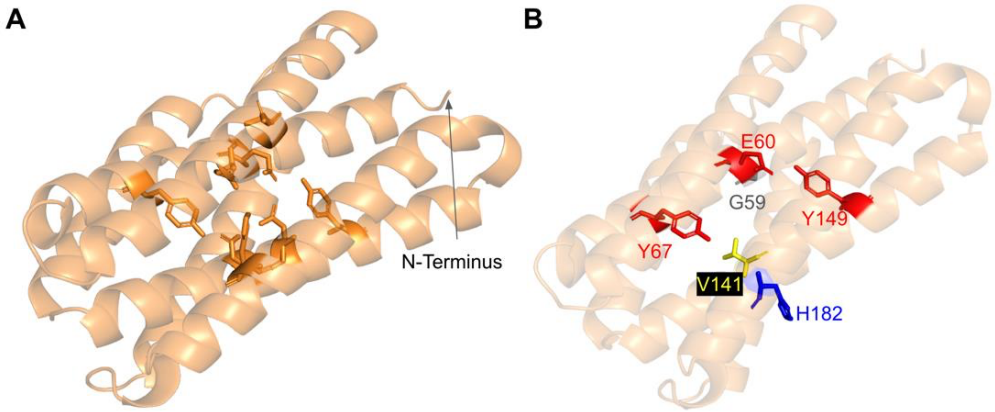

Figure 27. SNVs found in COQ7 residues that are adjacent to or that ligand the iron atoms. (**A**) The residues predicted to ligand the Fe (II) atoms are depicted in orange on the COQ7 model; E60, Y67, E90, H93, E142, Y149, E178, and H181. (**B**) Locations of SNVs are depicted. Residues are colored according to their corresponding SNVs in Figure 24. Residues 1–43 have been truncated in both panels.

The V141E variant occurs adjacent to E142, which is predicted to ligand iron 2 (Figure 27B). This variant was reported in the ClinVar database and is labeled as deleterious. Missense3D characterizes this variant as neutral. It is likely that V141E disrupts ligand formation with the iron.

3.5.4. SNVs Predicted to Impact Redox Chemistry of COQ7

COQ7 utilizes NADH to reduce the iron atoms, which then activate O_2 to perform the hydroxylation step of the DMQ substrate [101]. Several of the residues predicted to act as ligands for the two iron atoms (E60, H148, Y149) are thought to mediate a sequential electron-proton-electron relay [101], and a DMQ quinone may act as a conduit between NADH and the di-iron site [105]. Intriguingly, Manicki et al. observed that the NADH cofactor is localized adjacent to a water-filled channel formed by the triad [52]. The variants E60K and Y149C discussed previously (Figure 27) likely disrupt this redox chemistry.

3.6. COQ9

COQ9 is peripherally associated with the IMM and is shown to be essential for CoQ synthome formation and stabilization in both human and yeast cells [50,106]. COQ9 homologs play slightly different roles in different organisms. Coq9, the yeast COQ9 homolog,

plays a supportive role in the hydroxylation steps mediated by Coq6 and Coq7 [13]. Certain *coq9* yeast mutants accumulate demethoxy-Q (DMQ), the penultimate intermediate of the CoQ biosynthetic pathway [107]. In humans, COQ9 plays a supportive role in the COQ7 hydroxylation of DMQ in addition to the stabilization of the CoQ synthome [25]. Patients with deficiencies in COQ9 have been shown to accumulate DMQ_{10}, the same intermediate that accumulates in COQ7-deficient cells [108].

To date, pathogenic cases of genetic variants in the *COQ9* gene have been identified in seven patients across four families [29]. While the determination of pathogenic variants in *COQ9* is rare, mutations in the *COQ9* gene are associated with primary CoQ_{10} deficiency and are further associated with several disease states, predominantly encephalomyopathy and an autosomal-recessive neonatal-onset CoQ_{10} deficiency [29]. Low levels of CoQ_{10} in human cells resulting from COQ9 deficiency can be partially restored by treatment with 2,4-diHB or VA [109]. For 2,4-diHB, the addition of the hydroxyl group at the 2-carbon position allows it to bypass the COQ7 hydroxylation step in COQ7-deficient cells. VA was shown to increase the production of CoQ_{10} in COQ9-deficient cells [109]. Neither 2,4-diHB nor VA have been used as treatments in patients.

From gnomAD, ClinVar, and Missense3D-DB, we identified 52 missense SNVs of interest (Figure 28; Supplemental Table S1). Of these variants, 17 coincided with a highly conserved region or functional residue, which were determined from the multiple sequence alignment as well as structural studies on human COQ9 [50,52]. Two of the twelve variants classified as structurally damaging by Missense3D were contained in this group (Figure 28). From the ClinVar Database and literature, 11 missense variants were determined to be pathogenic or likely pathogenic. Two of these variants (P55T and H148P) were identified by Missense3D to be structurally damaging. There were 17 SNVs in gnomAD identified as frequent polymorphisms. Two of these, N252K and M281V (allele frequencies of 1.41×10^{-4} and 1.70×10^{-4}, respectively), were identified as being structurally damaging by Missense3D.

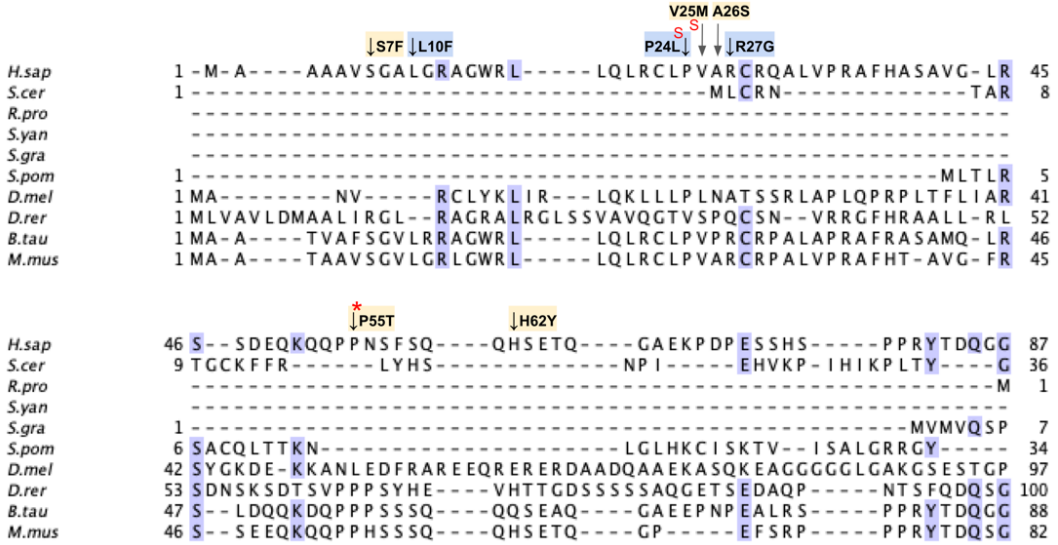

Figure 28. *Cont.*

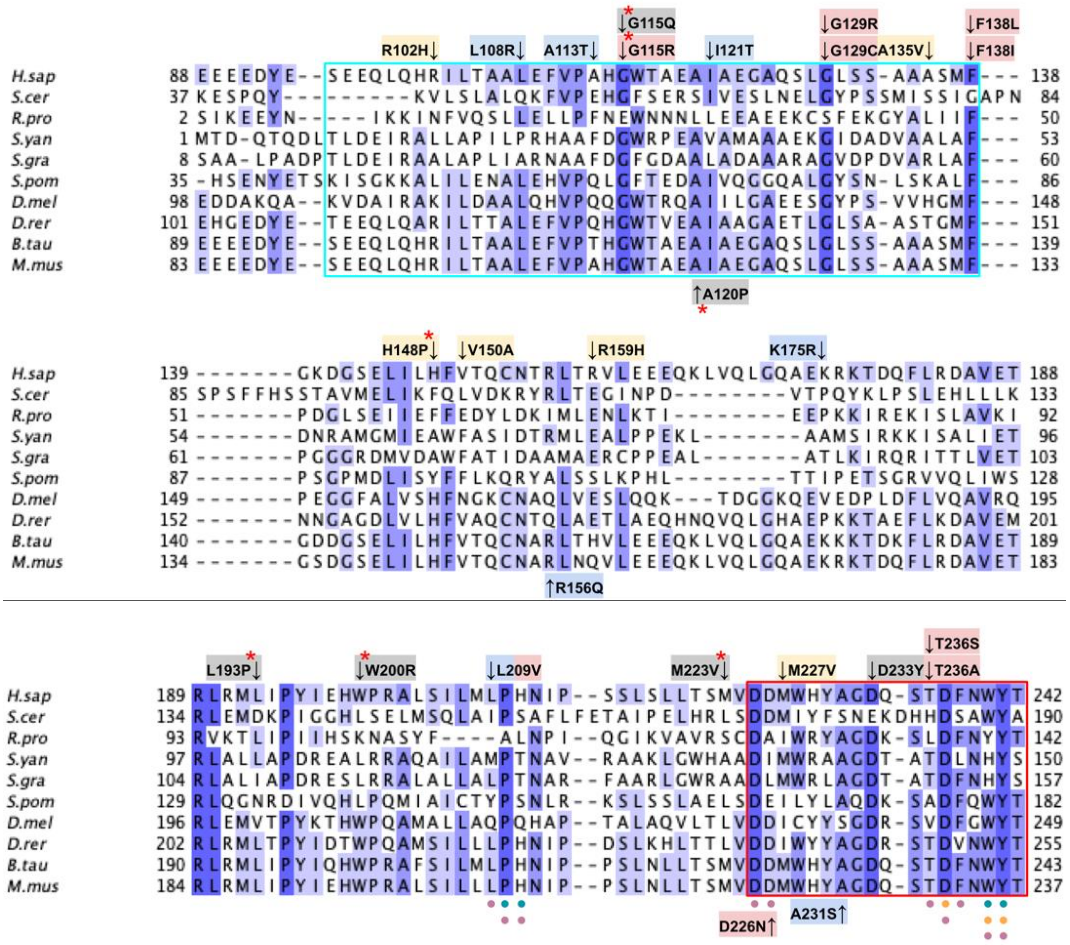

Figure 28. *Cont.*

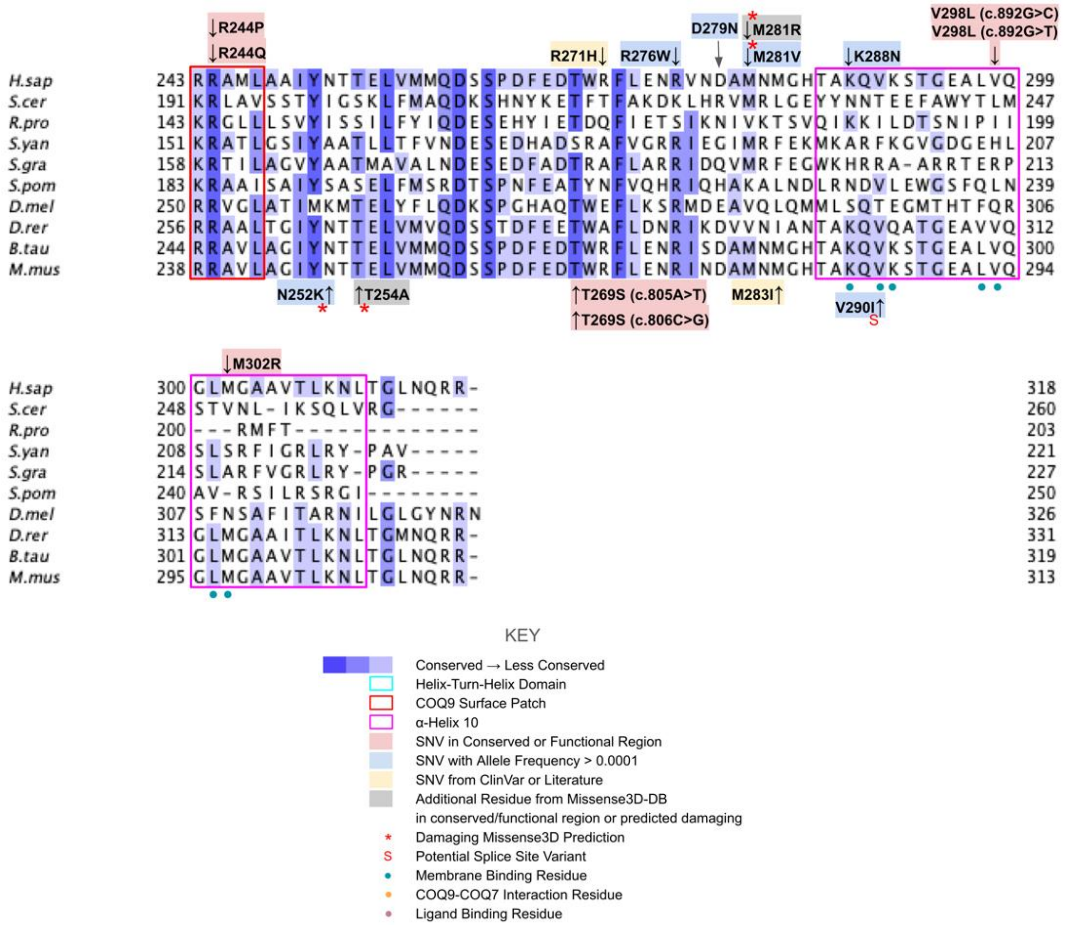

Figure 28. Labeled and annotated multiple sequence alignment of COQ9. Amino acid sequences of COQ7 were analyzed as described in Materials and Methods and include *Homo sapiens* (NCBI accession number NP_064708.1) and homologs in *Saccharomyces cerevisiae* (QHB10353.1), *Rickettsia prowazekii* (WP_004596292.1), *Sphingomonas yanoikuyae* (EKU74250.1), *Sphingopyxis granuli* (WP_082737038.1), *Schizosaccharomyces pombe* (NP_594426.1), *Drosophila melanogaster* (NP_724594.1), *Danio rerio* (NP_001092216.1), *Bos taurus* (NP_001039767.1), and *Mus musculus* (NP_080728.1). See KEY for descriptions of the figure annotations. Residues in the HTH domain are boxed in cyan and COQ9 surface patch in red, data from [25]. COQ7 interaction residues are marked with orange dots, data from [52]. Ligand-binding residues are marked with purple dots, data from [50].

The human COQ9 structure determined by X-ray diffraction at 2.00 Å resolution by Lohman et al. (PDB: 6AWL) was used as a model for visualizing the protein in PyMOL [50]. The COQ9 protein exists as a dimer with a hydrophobic cavity. Two co-crystallized molecules are visible in this structure: phosphatidylethanolamine and bis-tris (Figure 29A). A second COQ9 structure, determined by X-ray diffraction at 2.00 Å resolution by Lohman et al., PDB: 6DEW, co-crystallized with various isoprenes (Figure 29B) [50]. Additionally, Lohman et al. expressed COQ9$^{\Delta N79}$ (lacking the amino-terminal 79 residues)

in *E. coli* and found six co-purified enriched lipids including CoQ_8, menaquinone-8, and 2-octaprenyl phenol, which had the highest intensity signal of any lipid.

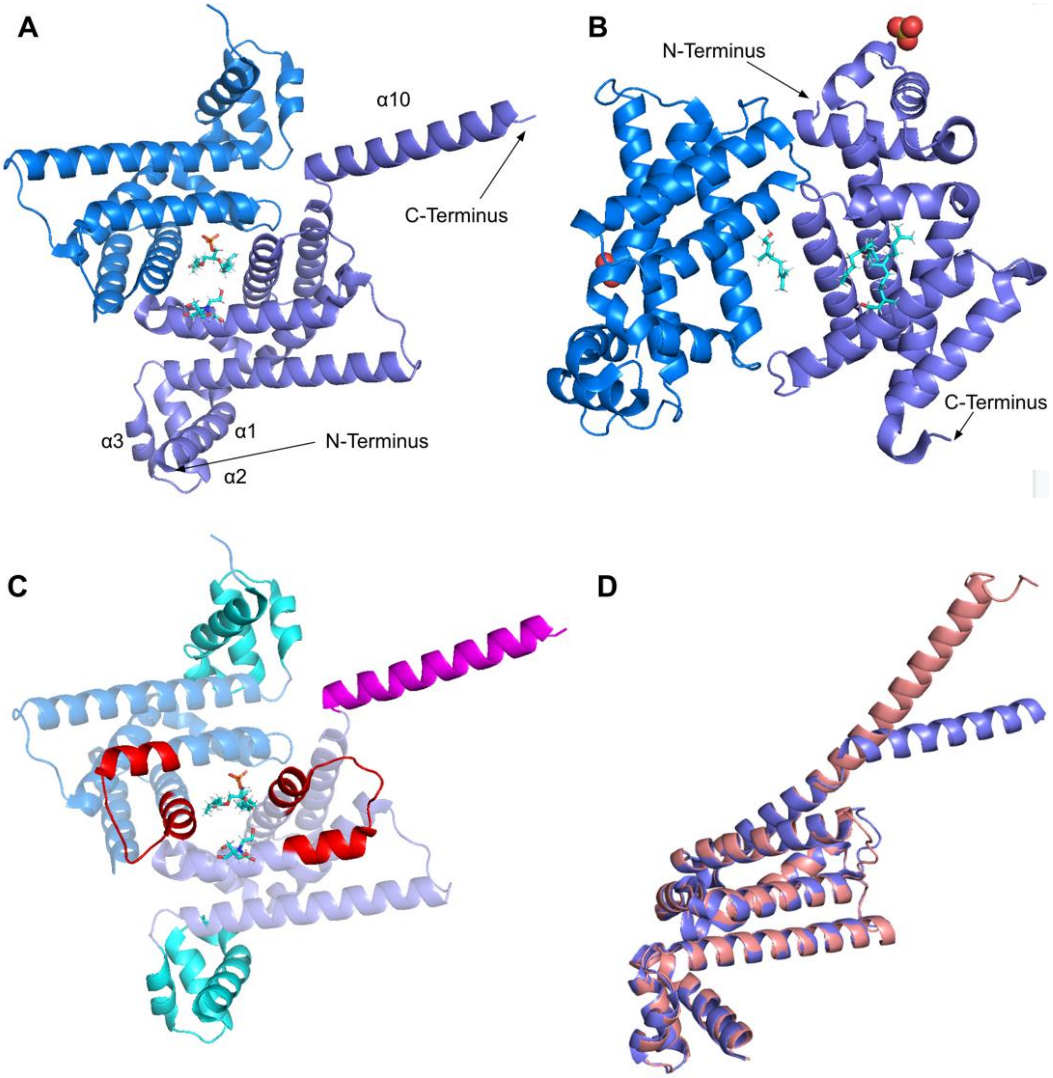

Figure 29. Comparison of existing structures of COQ9 and the AlphaFold model of COQ9 (**A**) PDB: 6AWL structure of $COQ9^{\Delta N79}$ with co-crystallized phosphatidylethanolamine and bis-tris shown in cyan, data from [50]. Chain A colored in purple, chain B colored in blue. (**B**) PDB: 6DEW structure of $COQ9^{\Delta N79,\Delta C36}$ with co-crystallized geraniol, cis-trans-farnesol, trans-trans-farnesol, and cis-cis-farnesol shown in cyan and sulfate molecules shown as ball structures; Chain A colored in purple, chain B colored in blue, data from [50]. (**C**) Structural motifs shown on 6AWL structure. Colors match Figure 28. (**D**) Structural alignment of 6AWL chain A shown in purple with the AlphaFold model obtained from the AlphaFold Protein Structure Database [39,54], shown in pink.

This indicates COQ9 as lipid-binding and its hydrophobic pocket as a potential binding site. Structural motifs noted in Figure 28 are designated on the 6AWL structure (Figure 29C). A model for human COQ9 was obtained using the AlphaFold Protein Structure Database (Figure A4) [39,54]. This model shows 79 residues at the N-terminus that the crystal structure for COQ9 (PDB: 6AWL) lacked (Figure 29D).

3.6.1. SNVs in the Helix-Turn-Helix Domain

COQ9 has been determined to have structural homology to proteins in the TetR family of regulators (TFRs) [25]. TFR proteins are typically found in prokaryotes with small-molecule binding capability, allowing many in the family to regulate transcription [110]. All TFR proteins consist of an N-terminal helix-turn-helix (HTH)-domain DNA binding motif consisting of α-helices 1–3, or residues E91-F138 (Figure 30A) and a larger C-terminal ligand-binding motif consisting of α-helices 4–9 (Figure 29A). However, COQ9 is not predicted to bind DNA, making it an atypical TFR protein [25].

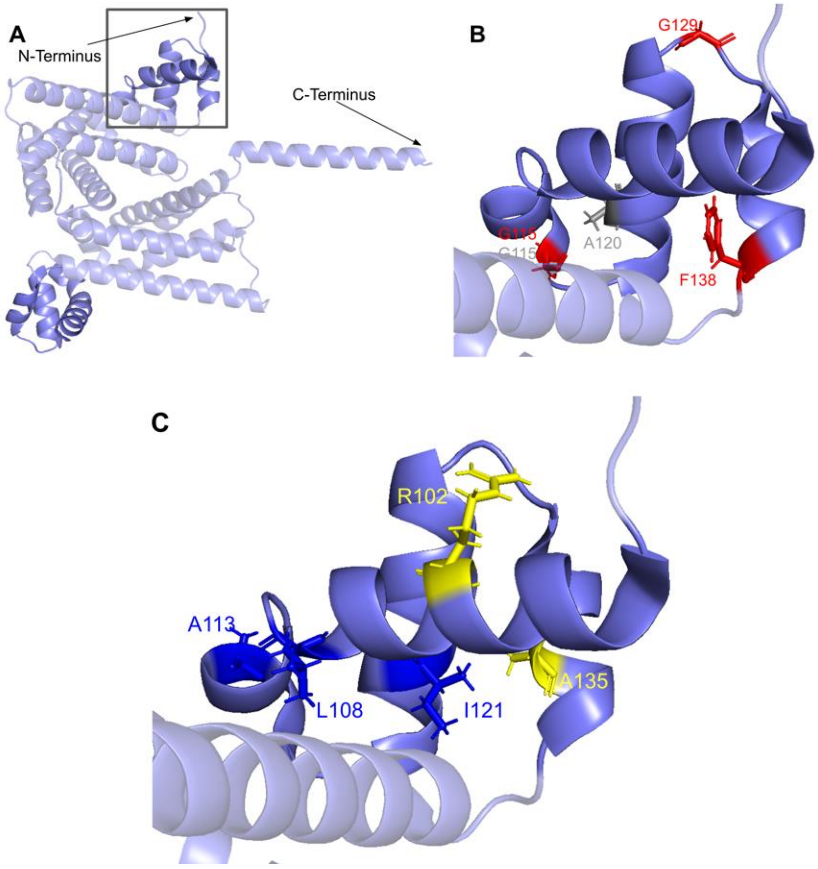

Figure 30. SNVs in the HTH-domain of COQ9. (**A**) N-terminal HTH-domains highlighted on the COQ9 dimer structure (PDB:6AWL), corresponding to residues S95 to F138 and D92 to F138, on chains A and B, respectively. (**B**) Locations of SNVs in conserved or functional regions are depicted. (**C**) Locations of ClinVar variants and frequent polymorphisms are depicted. Residues are colored according to their corresponding SNVs in Figure 28.

In the COQ9 HTH domain, we encounter twelve SNVs with relevance to this analysis. There are five SNVs reported in gnomAD occurring at highly conserved residues in this segment of amino acids: G115R, G129R, G129C, F138L, and F138I (Figure 30B). Of these five SNVs from gnomAD, only G115R was flagged by Missense3D as damaging. None of these variants are present as homozygotes in gnomAD, nor are they associated with a deficiency in CoQ_{10}. Additionally, there are two SNVs reported in Missense3D-DB that are predicted to be structurally damaging by Missense3D: G115Q and A120P.

Three SNVs reported in gnomAD are identified as frequent polymorphisms: L108R, A113T, and I121T (Figure 30C). Only one variant, L108R, occurs at a highly conserved residue. According to the ClinVar database, one report states that L108R is likely benign whereas four others list an uncertain significance. Two of the four uncertain significance interpretations list primary CoQ_{10} deficiency as the associated condition. The L108R variant is of particular interest because of its frequency and possible pathogenicity; however, no homozygotes have been reported to date. A113T has been determined to be a likely benign SNV. I121T occurs at a semi-conserved residue, and there are conflicting reports ranging from being likely benign to having uncertain significance. All of these variants are characterized as neutral by Missense3D. Two additional SNVs are reported in ClinVar in the HTH-domain: R102H and A135V (Figure 30C). Both of these variants potentially lead to primary CoQ_{10} deficiency; however, the association must be investigated further in order to elucidate a certain link. Both SNVs are characterized as neutral by Missense3D.

3.6.2. SNVs in the COQ9 Surface Patch

The second motif present in typical TFR proteins is a C-terminal ligand-binding domain [110]. The COQ9 surface patch is comprised of several highly conserved residues necessary for interaction with COQ7, ranging from residues D225 to L247 [25]. The surface patch resides near the lipid-binding pocket (Figure 31A). Mutagenesis of conserved residues in this region of COQ9 and co-purification with COQ7 has been shown to disrupt COQ9-COQ7 interaction, resulting in reduced production of CoQ and accumulation of the COQ7 substrate DMQ. Thus, we predict that mutations in highly conserved regions along the surface patch may result in either disruption of protein-protein interaction within the CoQ synthome or destabilization of the COQ9 protein itself. Variants in this region are not likely to disrupt protein stability, as these are solvent-exposed and will thus appear neutral to Missense3D.

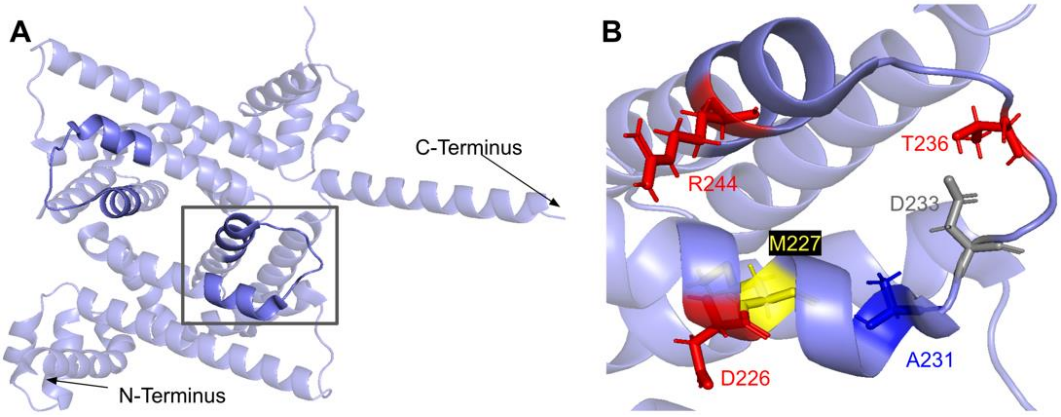

Figure 31. SNVs found in the COQ9 surface patch. (**A**) Surface patch highlighted on the COQ9 dimer (PDB:6AWL), corresponding to residues D225 to L247. (**B**) Locations of SNVs are depicted. Residues are colored according to their corresponding SNVs in Figure 28.

In COQ9, the surface patch stretches from the end of α-helix 7 and the beginning of α-helix 8. In this domain, we encounter eight SNVs with relevance to this analysis. There are five SNVs reported in gnomAD occurring at highly conserved or functional residues in this segment of amino acids (Figure 31B). None of these mutations are predicted to be structurally damaging by Missense3D. None of these mutations has a clinical association with CoQ_{10} deficiency.

There is one additional SNV reported in Missense3D-DB occurring at a highly conserved residue: D233Y. This mutation is predicted to be structurally neutral by Missense3D. D233Y does not have a clinical association with CoQ_{10} deficiency. Another SNV reported in gnomAD is identified as a frequent polymorphism, A231S. This variant does not occur at a highly conserved residue. It is predicted to be neutral by Missense3D and has been labeled as likely benign by ClinVar. There is one SNV reported in ClinVar in the surface patch region, M227V (Figure 31B). This variant is associated with primary CoQ_{10} deficiency; however, it has been labeled as having unknown significance in ClinVar. M227V is characterized as neutral by Missense3D.

3.6.3. SNVs in α-Helix 10

α-helix 10 (α10), a C-terminal amphipathic helix not present in typical TFR proteins, has been found to have importance in membrane binding [50]. Lohman et al. found that COQ9 binds the matrix side of the IMM in a series of five steps. In the second step, the hydrophobic residues along α10 associate with the membrane phospholipids. Mutating these hydrophobic residues to Ser significantly reduced liposome association. We predict that, despite low evolutionary conservation of residues along α10, mutations occurring at residues implicated in membrane binding may result in reduced membrane association and lower levels of synthome formation, thus resulting in lowered CoQ production.

α10 occurs at the C-terminus of COQ9 from T286 to R311 (Figure 32A). In this domain, we encounter five SNVs with relevance to this analysis. Three SNVs reported in gnomAD occur at residues implicated in membrane binding: V298L (c.892G>C and c.892G>T) and M302R (Figure 32B). Both variants are characterized as neutral by Missense3D and neither are clinically associated with primary CoQ_{10} deficiency. For V298L, the SNV mutates a hydrophobic residue to another hydrophobic residue, minimizing the impact of the change. For M302R, the SNV mutates a hydrophobic residue to a positively charged residue, which may potentially have a large impact on membrane binding ability. There are two SNVs reported in gnomAD that were identified as frequent polymorphisms: K288N and V290I. Both variants are characterized as neutral by Missense3D and K288N is labeled as benign by ClinVar. V290I did not appear in ClinVar.

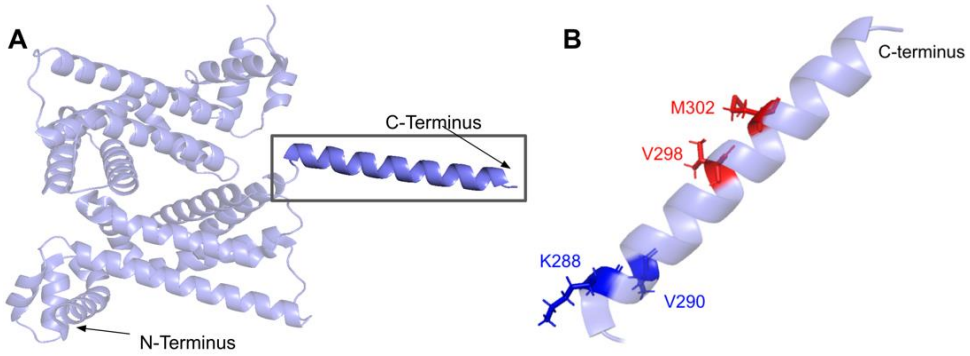

Figure 32. SNVs found in α10 of COQ9. (**A**) α10 highlighted on COQ9 dimer structure (PDB: 6AWL), corresponding to residues T286 to L311. (**B**) Locations of SNVs are depicted. Residues are colored according to their corresponding SNVs in Figure 28.

4. Discussion

Herein, we analyzed the functional and structural impacts of missense SNVs in *COQ3–COQ7* and *COQ9*. From a large pool of genome and exome sequencing data (gnomAD and Missense3D-DB), as well as clinically documented variants (NCBI ClinVar and literature), 429 variants were selected; these consisted of SNVs in conserved and functional regions, with potential clinical significance or with high allele frequency. Of these, 115 SNVs were classified as potentially structurally damaging by the Missense3D server. AlphaFold models were used for classification wherever crystal structures were not available. As expected, we found frequent polymorphisms to be less deleterious than those found in highly conserved or functional residues. The mutation classifiers used, Missense3D, SIFT, and PolyPhen-2, often had disagreements with their respective assessments. Some of this disagreement can be attributed to the assessment criteria used by each classifier. Missense3D is more stringent in its structural consequence criteria whereas the SIFT and PolyPhen-2 algorithms are less conservative when classifying a mutation as deleterious. Nevertheless, when the data obtained across classifiers are compared in the context of function, one can make an educated prediction based on the considerations described here.

It is imperative to note that predicted models may not accurately reflect the true physiological structures. The dynamic residue-residue interactions between polypeptides may result in different local conformations that are not represented in the individual structural models, including disordered regions. A further consequence of this limitation is that mutation classifiers such as the ones used in this study cannot predict the extent to which the activity of an enzyme is affected. Additionally, mutation classifiers may underestimate the deleteriousness of certain mutations, such as point mutations within binding pockets deemed "benign" that may impair essential cofactor or substrate binding, polymorphisms within the mitochondrial targeting sequence that may affect localization, or surface mutations that may alter protein-protein interaction interfaces. In the case of Missense3D, it is currently unable to model mutations at a protein-protein or protein-ligand interaction interface, as additional polypeptide chains or ligands in the provided structure are removed during analysis. One example of a mutation that was overlooked by Missense3D is the D208H mutation in COQ6, which occurs at a putative FAD-binding residue. This mutation has been associated with schwannomatosis in a family of patients [96]. While this linkage has been contested, it has been shown that human COQ6 harboring this mutation is unable to rescue *coq6* null yeast, suggesting a loss of function. However, Missense 3D had classified the mutation as neutral.

Differential gene expression in distinct tissues may also account for pathogenic effects that cannot be characterized solely by predicted structures. For example, mutations associated with the atypical kinase COQ8B present a perplexing case where the pathogenic phenotypes appear to be kidney-specific [29]. While the methods described in this study can identify potentially pathogenic SNVs, they cannot predict the extent to which a structurally destabilizing mutation decreases protein levels in a given tissue, nor whether a resulting decrease is sufficient to affect tissue function. It is also worth noting that distinct cell types may also be differentially impacted by CoQ deficiency due to particular energy demands or exposure to oxidative damage.

Despite these limitations, multiple sequence alignments and structural models have revealed highly conserved and functionally relevant residues, which allowed us to narrow our search in identifying variants with potential clinical significance. The pipeline used in this work may also serve as a scaffold for future SNV studies. Multiple sequence alignments can help identify highly conserved regions of unknown function such as post-translational modification sites. Meanwhile, structural models can be used in computational studies to predict protein-protein interaction interfaces as well as the effect of SNVs on ligand binding and catalysis. All of these studies are invaluable in elucidating the regulatory mechanisms of CoQ biosynthesis. Furthermore, our pipeline provides a structural basis for analyzing existing pathogenic mutations. For example, Ling et al. identified a patient with a homozygous mutation G124S in COQ4 inherited from heterozygous parents. Skin

fibroblasts isolated from the patient exhibited low CoQ_{10} content [111]. A separate study found another patient homozygous for the G124S allele with poor cardiac contractility and developmental delays [71]. In silico analyses from Missense3D, SIFT, and Polyphen-2 all correctly predicted the deleterious nature of this mutation. In particular, Missense3D classified the mutation as damaging due to the replacement of a buried Gly, suggesting deleterious structural consequence. Additionally, this pipeline can be combined with other publicly available high-throughput data, such as gene expression profiles of different human tissues, to yield further insight into the phenotype variability in primary CoQ deficiencies.

Primary CoQ_{10} deficiency is often caused by autosomal recessive mutations. Compounded with the limited accessibility to genome sequencing, it is likely that a significant portion of pathogenic variants has not been identified. Furthermore, early intervention of primary CoQ_{10} deficiency has shown to be effective [32], illuminating the importance of detecting such mutations early. As the cost of genetic sequencing declines over time, we expect more variants to be identified in the future.

To aid the prompt diagnosis of pathogenic variants causing primary CoQ_{10} deficiency, further in vitro and in vivo biochemical characterizations in model organisms such as *S. cerevisiae* are required to validate the SNV classifications made in this study. Regarding COQ3 and COQ5, there has been little to no clinical information on *COQ3*- and *COQ5*-associated primary CoQ_{10} deficiency. This may appear to suggest that COQ3 and COQ5 mutations are not pathogenic. However, we speculate that many structurally damaging variants may be embryonic lethal, resulting in an apparent lack of known pathogenic variants. Conversely, mutations in the COQ8A and COQ8B polypeptides are reported to have several pathogenic effects [29], likely due to the aforementioned dynamic interactions and/or redundancy of function. For this reason, the clinical effects of mutations in the COQ8A and COQ8B polypeptides would require a more elaborate structural analysis and stringent biochemical characterization to fully understand the consequences of such SNVs.

Current treatment for CoQ deficiency relies on oral supplementation with CoQ_{10}. However, this method is only partially successful due to poor uptake of this extraordinarily hydrophobic lipid molecule. It will be important to identify the gene products responsible for the cellular trafficking of both exogenous and endogenous CoQ and its delivery to the mitochondria [112,113]. A potential alternative is a "bypass" treatment, in which a CoQ precursor can be administered to circumvent any faulty enzymatic steps in the biosynthetic pathway, as demonstrated previously in yeast [90], mice [114], and human fibroblasts [115]. Unfortunately, the success of this potential avenue is contingent upon the nature of the mutation. The COQ polypeptide harboring the SNV must be able to retain a structurally stable CoQ complex. Given the extensive interactions between the COQ polypeptides, membrane association, and binding of CoQ and CoQ-biosynthetic intermediates in the high molecular mass CoQ synthome, it seems likely that many surface residue SNVs may impact these interactions.

Similar to the bypass approach, another option for treating CoQ deficiency is supplementation with MitoQ. MitoQ is composed of the lipid molecule conjugated to a triphenylphosphonium cation, which enables the antioxidant to be targeted to the mitochondria [116]. Recently, clinical studies involving the supplementation of this CoQ derivative have been shown to attenuate mitochondrial DNA damage in skeletal muscle [117,118], although the direct role of MitoQ in this protective effect remains unclear. Given that MitoQ does not support the respiratory electron transport function of CoQ, it is unlikely on its own to rescue primary CoQ_{10} deficiency [119].

A recent innovative method to serve as a potential therapy for mitochondria-related diseases is mitochondria transplantation. The fusion and fission of mitochondria within the cell are essential for the maintenance of healthy mitochondrial functions [120], and such dynamics are an attractive process to exploit for therapeutic applications. Recent studies explored the potential for mitochondrial transplants as a targeted therapy for repairing defunct mitochondria in different cells and, in a larger application, tissue revital-

ization [121,122]. Similarly, given the association of mitochondrial dysfunction with disease, another avenue for therapeutics involves the design of drugs that induce mitochondrial biogenesis, thereby promoting the turnover of defunct mitochondria and subsequently the emergence of healthy mitochondria. Several naturally occurring polyphenols have been identified as mitochondrial biogenesis inducers, such as resveratrol and phytoestrogens [123]. However, similar to oral CoQ_{10} supplements, the therapeutic advantage of these inducers is limited by poor absorption. To target mitochondrial biogenesis from a transcriptional approach, a number of nuclear transcription factors have also been implicated in promoting mitochondrial biogenesis, which would help coordinate the expression of both mitochondrial-encoded genes as well as those that are nuclear-encoded, such as our *COQ* genes [123,124]. Unfortunately, the response resulting from this approach would be nonspecific, as targeting the induction of transcription factors would activate several other pathways, potentially leading to more severe side effects. Currently, targeting mitochondrial disease through the induction of mitochondrial biogenesis remains unsuccessful. While these approaches may have promise for treating mitochondrial dysfunctions, primary CoQ_{10} deficiencies result from mutations in the nuclear-encoded *COQ* genes, making this method suitable for only certain types of secondary CoQ_{10} deficiencies.

In summary, this work provides a thorough structural and functional analysis of clinically relevant SNVs in several of the *COQ* genes. We have identified 115 SNVs that are likely pathogenic due to structural perturbations, using multiple sequence alignments, mutation classifiers, and predicted or solved protein structures. This analysis highlights the intricate interactions in local regions of a given protein, as well as the large-scale dynamic interactions between the individual constituents of protein complexes. Together, this serves as a scaffold for future studies that seek to characterize the biochemical consequences of SNVs that result in pathogenic effects caused by primary CoQ_{10} deficiencies. Finally, the approach employed takes advantage of recent advances in protein tertiary structure prediction and should be applicable to any human gene with identified homologs and reported SNVs.

Supplementary Materials: The following supporting information can be downloaded at: https://www.mdpi.com/article/10.3390/antiox11122308/s1, Table S1: Comprehensive list of analyzed variants. References [71,72,74,90–93,96,99,100,103,111,115,125–148] were cited in supplementary.

Author Contributions: Conceptualization, F.T., S.W. and C.F.C.; methodology, S.W., A.J., F.T. and C.F.C.; validation, A.J. and S.W.; formal analysis, A.J. and S.W.; investigation, A.J. and S.W.; data curation, A.J., S.W. and A.N.N.; writing—original draft preparation, A.J., S.W. and N.A.N.; writing—review and editing, C.F.C., A.J., S.W., N.A.N., F.T. and A.N.N.; visualization, S.W. and A.J.; supervision, C.F.C.; project administration, C.F.C. All authors have read and agreed to the published version of the manuscript.

Funding: This research was funded by the UCLA Graduate Division and the UCLA Edwin W. Pauley Fellowship (S.W.) and by the UCLA Department of Chemistry & Biochemistry Summer Undergraduate Research Fellowships to A.J., A.N. and F.T. We also acknowledge funding from the National Science Foundation grant MCB-1714569.

Institutional Review Board Statement: Not applicable.

Informed Consent Statement: Not applicable.

Data Availability Statement: All models and crystal structures used in Missense3D analysis were obtained from the AlphaFold Protein Structure database (https://alphafold.ebi.ac.uk/ accessed on 14 October 2022) and the Protein Data Bank (https://www.rcsb.org/ accessed on 14 October 2022), respectively. Accession numbers of these structures can be found in the Materials & Methods. Accession numbers of the protein sequences analyzed in this study can be found in the captions of Figures showing the respective multiple sequence alignments. All SNVs analyzed in this study were obtained from gnomAD (https://gnomad.broadinstitute.org/ accessed on 30 March 2022), ClinVar (https://www.ncbi.nlm.nih.gov/clinvar/ accessed on 30 March 2022), and Missense3D-DB (http://missense3d.bc.ic.ac.uk:8080/ accessed on 30 March 2022). A full list can be found in Table S1.

Acknowledgments: We thank the UCLA Division of Physical Sciences for supporting this project. We also thank Michael Guile for helpful advice during the initial phase of this project, as well as Robert Clubb and Steven G. Clarke for advice on structures and methyltransferases. S.W. participates in the UCLA Chemistry-Biology Interface Predoctoral Training Program funded by NIH NIGMS award T32GM36614. The content is solely the responsibility of the authors and does not necessarily represent the official views of the National Institutes of Health.

Conflicts of Interest: The authors declare no conflict of interest. The funders had no role in the design of the study; in the collection, analyses, or interpretation of data; in the writing of the manuscript; or in the decision to publish the results.

Abbreviations

AdoHcy, S-adenosyl-L-homocysteine; AdoMet, *S*-adenosyl-L-methionine; apo, apoenzyme; *APTX*, gene encoding aprataxin; Arh1, yeast ferredoxin reductase; *BRAF*, gene encoding B-Raf; CoQ, coenzyme Q or ubiquinone; $CoQH_2$, reduced $CoQH_2$ hydroquinone or ubiquinol; CoQn, n = number of isoprene units in polyprenyl tail; $DDMQH_2$, 2-methoxy-6-polyprenyl-1,4-benzohydroquinone; DHP, 4,5-dihydroxy-3-polyprenylphenol; DHPB, 4,5-dihydroxy-3-polyprenylbenzoic acid; 2,4,-diHB, 2,4-dihydroxybenzoic acid; 3,4-diHB, 3,4-dihydroxybenzoic acid; DMAPP, dimethylallyl pyrophosphate; $DMeQH_2$, 3-methyl-6-methoxy-2-polyprenyl-1,4,5-benzenetriol; $DMQH_2$, 2-methoxy-5-methyl-6-polyprenyl-1,4-benzohydroquinone; *ETFDH*, gene encoding mitochondrial electron transfer flavoprotein-ubiquinone oxidoreductase; FDX1, human ferredoxin 1; FDX2, human ferredoxin 2; FDXR, human ferredoxin reductase; HAB, 3-hexaprenyl-4-aminobenzoic acid; 4-HB, 4-hydroxybenzoic acid; HHB, 3-hexaprenyl-4-hydroxybenzoic acid; HMPB, 4-hydroxy-5-methoxy-3-polyprenylbenzoic acid; 4-HP, 4-hydroxy-3-polyprenylphenol; $4\text{-}HP_6$, 3-hexaprenyl-4-hydroxyphenol; HPB, 3-polyprenyl-4-hydroxybenzoic acid; IMM, inner mitochondrial membrane; IPP, isopentenyl pyrophosphate; *MUT*, gene encoding methylmalonyl-CoA mutase; pABA, para-hydroxybenzoic acid; PDB, protein data bank; PDSS1, decaprenyl diphosphate synthase subunit 1; PDSS2, decaprenyl diphosphate subunit 2; SNV, single nucleotide variant; SNHL, sensorineural hearing loss; SRNS, steroid-resistant nephrotic syndrome; TFRs, TetR family of regulators; UbiG, *E. coli* ubiquinone biosynthesis *O*-methyltransferase; VA, vanillic acid; Yah1, yeast ferredoxin.

Appendix A

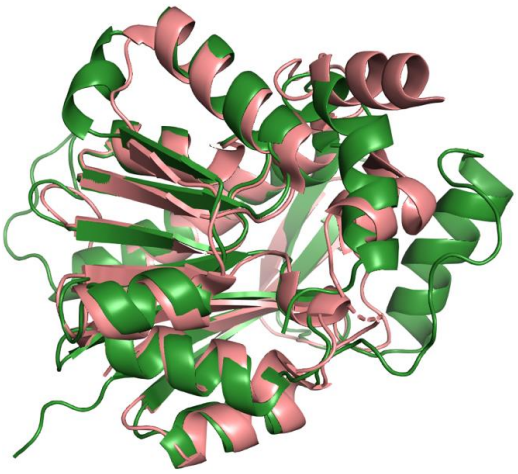

Figure A1. Structural alignment of the human COQ3 model (shown in dark green) and the crystal structure of *E. coli* UbiG, apo form (shown in pink, PDB: 4KDC). Residues 1–90 and 337–369 of the AlphaFold model were omitted due to disordered structure. Alignment was performed using PyMOL.

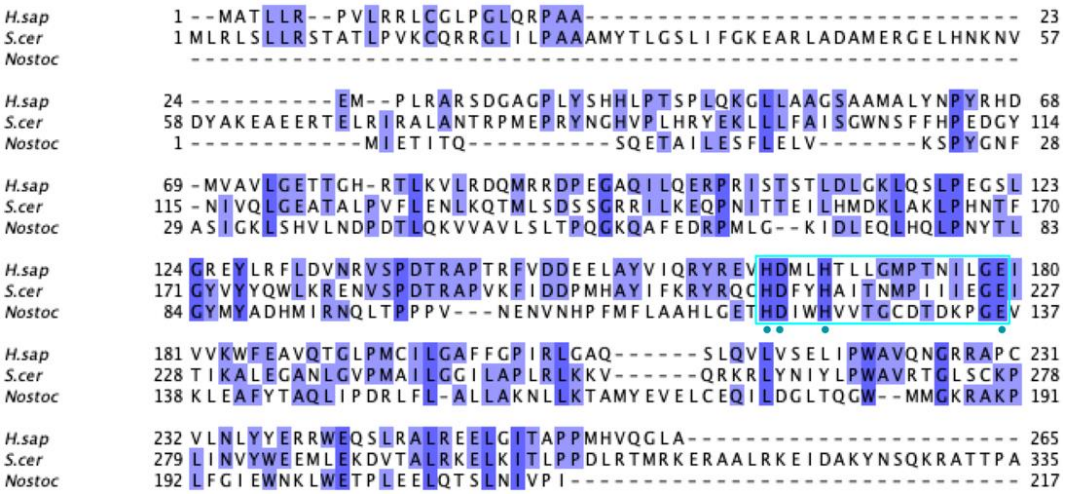

Figure A2. Multiple sequence alignment of *H. sapiens* COQ4, *S. cerevisiae* COQ4, and *Nostoc sp.* homolog Alr8543 (NCBI accession number: WP_010999537.1). Metal-liganding motif is boxed in cyan, and residues in Alr8543 (H120, D121, H124, and E136) that act to ligand the Mg^{2+} ions are marked with blue dots.

Figure A3. Structural alignment of the human COQ5 model (shown in orange) and the crystal structure of *S. cerevisiae* Coq5, apo form (shown in teal, PDB: 4OBX). Residues 1–47 of the AlphaFold model were omitted due to disordered structure. Alignment was performed using PyMOL.

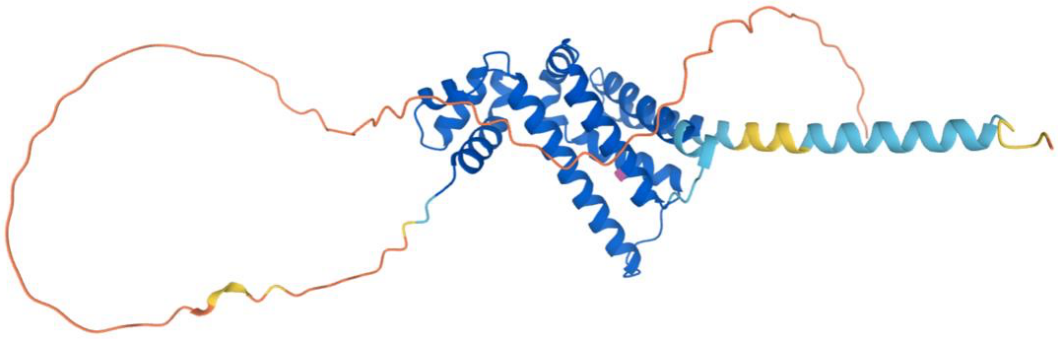

Figure A4. AlphaFold model of single chain of COQ9. Model color corresponds to the model confidence described in Figure 4. Figure was generated by the AlphaFold Protein Structure Database [39,54].

References

1. Stefely, J.A.; Pagliarini, D.J. Biochemistry of Mitochondrial Coenzyme Q Biosynthesis. *Trends Biochem. Sci.* **2017**, *42*, 824–843. [CrossRef] [PubMed]
2. Banerjee, R.; Purhonen, J.; Kallijarvi, J. The mitochondrial coenzyme Q junction and complex III: Biochemistry and pathophysiology. *FEBS J.* **2021**, *289*, 6936–6958. [CrossRef] [PubMed]
3. Turunen, M.; Olsson, J.; Dallner, G. Metabolism and function of coenzyme Q. *Biochim. Biophys. Acta* **2004**, *1660*, 171–199. [CrossRef] [PubMed]
4. Frei, B.; Kim, M.C.; Ames, B.N. Ubiquinol-10 is an effective lipid-soluble antioxidant at physiological concentrations. *Proc. Natl. Acad. Sci. USA* **1990**, *87*, 4879–4883. [CrossRef]
5. Maroz, A.; Anderson, R.F.; Smith, R.A.; Murphy, M.P. Reactivity of ubiquinone and ubiquinol with superoxide and the hydroperoxyl radical: Implications for in vivo antioxidant activity. *Free Radic. Biol. Med.* **2009**, *46*, 105–109. [CrossRef]
6. Stocker, R.; Bowry, V.W.; Frei, B. Ubiquinol-10 protects human low density lipoprotein more efficiently against lipid peroxidation than does alpha-tocopherol. *Proc. Natl. Acad. Sci. USA* **1991**, *88*, 1646–1650. [CrossRef]
7. Do, T.Q.; Schultz, J.R.; Clarke, C.F. Enhanced sensitivity of ubiquinone-deficient mutants of Saccharomyces cerevisiae to products of autoxidized polyunsaturated fatty acids. *Proc. Natl. Acad. Sci. USA* **1996**, *93*, 7534–7539. [CrossRef]
8. Poon, W.W.; Do, T.Q.; Marbois, B.N.; Clarke, C.F. Sensitivity to treatment with polyunsaturated fatty acids is a general characteristic of the ubiquinone-deficient yeast coq mutants. *Mol. Asp. Med.* **1997**, *18*, S121–S127. [CrossRef]
9. Kagan, V.; Serbinova, E.; Packer, L. Antioxidant effects of ubiquinones in microsomes and mitochondria are mediated by tocopherol recycling. *Biochem. Biophys. Res. Commun.* **1990**, *169*, 851–857. [CrossRef]
10. Bersuker, K.; Hendricks, J.M.; Li, Z.; Magtanong, L.; Ford, B.; Tang, P.H.; Roberts, M.A.; Tong, B.; Maimone, T.J.; Zoncu, R.; et al. The CoQ oxidoreductase FSP1 acts parallel to GPX4 to inhibit ferroptosis. *Nature* **2019**, *575*, 688–692. [CrossRef]
11. Doll, S.; Freitas, F.P.; Shah, R.; Aldrovandi, M.; da Silva, M.C.; Ingold, I.; Goya Grocin, A.; Xavier da Silva, T.N.; Panzilius, E.; Scheel, C.H.; et al. FSP1 is a glutathione-independent ferroptosis suppressor. *Nature* **2019**, *575*, 693–698. [CrossRef] [PubMed]
12. Olson, R.E.; Dialamieh, G.H.; Bentley, R.; Springer, C.M.; Ramsey, V.G. Studies on Coenzyme Q. Pattern of Labeling in Coenzyme Q9 after Administration of Isotopic Acetate and Aromatic Amino Acids to Rats. *J. Biol. Chem.* **1965**, *240*, 514–523. [CrossRef]
13. Awad, A.M.; Bradley, M.C.; Fernandez-Del-Rio, L.; Nag, A.; Tsui, H.S.; Clarke, C.F. Coenzyme Q10 deficiencies: Pathways in yeast and humans. *Essays Biochem.* **2018**, *62*, 361–376. [CrossRef] [PubMed]
14. Pierrel, F.; Hamelin, O.; Douki, T.; Kieffer-Jaquinod, S.; Muhlenhoff, U.; Ozeir, M.; Lill, R.; Fontecave, M. Involvement of Mitochondrial Ferredoxin and Para-Aminobenzoic Acid in Yeast Coenzyme Q Biosynthesis. *Chem. Biol.* **2010**, *17*, 449–459. [CrossRef] [PubMed]
15. Saiki, R.; Nagata, A.; Kainou, T.; Matsuda, H.; Kawamukai, M. Characterization of solanesyl and decaprenyl diphosphate synthases in mice and humans. *Febs J.* **2005**, *272*, 5606–5622. [CrossRef] [PubMed]
16. Floyd, B.J.; Wilkerson, E.M.; Veling, M.T.; Minogue, C.E.; Xia, C.; Beebe, E.T.; Wrobel, R.L.; Cho, H.; Kremer, L.S.; Alston, C.L.; et al. Mitochondrial Protein Interaction Mapping Identifies Regulators of Respiratory Chain Function. *Mol. Cell* **2016**, *63*, 621–632. [CrossRef] [PubMed]
17. Ashraf, S.; Gee, H.Y.; Woerner, S.; Xie, L.X.; Vega-Warner, V.; Lovric, S.; Fang, H.; Song, X.; Cattran, D.C.; Avila-Casado, C.; et al. *ADCK4* mutations promote steroid-resistant nephrotic syndrome through CoQ_{10} biosynthesis disruption. *J. Clin. Investig.* **2013**, *123*, 5179–5189. [CrossRef]

18. Nguyen, T.P.; Casarin, A.; Desbats, M.A.; Doimo, M.; Trevisson, E.; Santos-Ocana, C.; Navas, P.; Clarke, C.F.; Salviati, L. Molecular characterization of the human COQ5 C-methyltransferase in Coenzyme Q biosynthesis. *Biochim. Biophys. Acta* **2014**, *1841*, 1628–1638. [CrossRef]
19. Stefely, J.A.; Licitra, F.; Laredj, L.; Reidenbach, A.G.; Kemmerer, Z.A.; Grangeray, A.; Jaeg-Ehret, T.; Minogue, C.E.; Ulbrich, A.; Hutchins, P.D.; et al. Cerebellar Ataxia and Coenzyme Q Deficiency through Loss of Unorthodox Kinase Activity. *Mol. Cell* **2016**, *63*, 608–620. [CrossRef]
20. Yen, H.C.; Liu, Y.C.; Kan, C.C.; Wei, H.J.; Lee, S.H.; Wei, Y.H.; Feng, Y.H.; Chen, C.W.; Huang, C.C. Disruption of the human COQ5-containing protein complex is associated with diminished coenzyme Q_{10} levels under two different conditions of mitochondrial energy deficiency. *Biochim. Biophys. Acta* **2016**, *1860*, 1864–1876. [CrossRef]
21. Tauche, A.; Krause-Buchholz, U.; Rodel, G. Ubiquinone biosynthesis in *Saccharomyces cerevisiae*: The molecular organization of *O*-methylase Coq3p depends on Abc1p/Coq8p. *FEMS Yeast Res.* **2008**, *8*, 1263–1275. [CrossRef] [PubMed]
22. Xie, L.X.; Hsieh, E.J.; Watanabe, S.; Allan, C.M.; Chen, J.Y.; Tran, U.C.; Clarke, C.F. Expression of the human atypical kinase ADCK3 rescues coenzyme Q biosynthesis and phosphorylation of Coq polypeptides in yeast *coq8* mutants. *Biochim. Biophys. Acta* **2011**, *1811*, 348–360. [CrossRef] [PubMed]
23. Allan, C.M.; Awad, A.M.; Johnson, J.S.; Shirasaki, D.I.; Wang, C.; Blaby-Haas, C.E.; Merchant, S.S.; Loo, J.A.; Clarke, C.F. Identification of Coq11, a new coenzyme Q biosynthetic protein in the CoQ-Synthome in *Saccharomyces cerevisiae*. *J. Biol. Chem.* **2015**, *290*, 7517–7534. [CrossRef] [PubMed]
24. Subramanian, K.; Jochem, A.; Le Vasseur, M.; Lewis, S.; Paulson, B.R.; Reddy, T.R.; Russell, J.D.; Coon, J.J.; Pagliarini, D.J.; Nunnari, J. Coenzyme Q biosynthetic proteins assemble in a substrate-dependent manner into domains at ER-mitochondria contacts. *J. Cell Biol.* **2019**, *218*, 1353–1369. [CrossRef] [PubMed]
25. Lohman, D.C.; Forouhar, F.; Beebe, E.T.; Stefely, M.S.; Minogue, C.E.; Ulbrich, A.; Stefely, J.A.; Sukumar, S.; Luna-Sanchez, M.; Jochem, A.; et al. Mitochondrial COQ9 is a lipid-binding protein that associates with COQ7 to enable coenzyme Q biosynthesis. *Proc. Natl. Acad. Sci. USA* **2014**, *111*, E4697–E4705. [CrossRef]
26. Reidenbach, A.G.; Kemmerer, Z.A.; Aydin, D.; Jochem, A.; McDevitt, M.T.; Hutchins, P.D.; Stark, J.L.; Stefely, J.A.; Reddy, T.; Hebert, A.S.; et al. Conserved Lipid and Small-Molecule Modulation of COQ8 Reveals Regulation of the Ancient Kinase-like UbiB Family. *Cell Chem. Biol.* **2018**, *25*, 154–165. [CrossRef]
27. Stefely, J.A.; Kwiecien, N.W.; Freiberger, E.C.; Richards, A.L.; Jochem, A.; Rush, M.J.P.; Ulbrich, A.; Robinson, K.P.; Hutchins, P.D.; Veling, M.T.; et al. Mitochondrial protein functions elucidated by multi-omic mass spectrometry profiling. *Nat. Biotechnol.* **2016**, *34*, 1191–1197. [CrossRef]
28. Alcazar-Fabra, M.; Trevisson, E.; Brea-Calvo, G. Clinical syndromes associated with Coenzyme Q10 deficiency. *Essays Biochem.* **2018**, *62*, 377–398. [CrossRef]
29. Alcazar-Fabra, M.; Rodriguez-Sanchez, F.; Trevisson, E.; Brea-Calvo, G. Primary Coenzyme Q deficiencies: A literature review and online platform of clinical features to uncover genotype-phenotype correlations. *Free Radic. Biol. Med.* **2021**, *167*, 141–180. [CrossRef]
30. Desbats, M.; Lunardi, G.; Doimo, M.; Trevisson, E.; Salviati, L. Genetic bases and clinical manifestations of coenzyme Q10 (CoQ10) deficiency. *J. Inherit. Metab Dis* **2015**, *38*, 145–156. [CrossRef]
31. Garrido-Maraver, J.; Cordero, M.D.; Oropesa-Avila, M.; Fernandez Vega, A.; de la Mata, M.; Delgado Pavon, A.; de Miguel, M.; Perez Calero, C.; Villanueva Paz, M.; Cotan, D.; et al. Coenzyme q10 therapy. *Mol. Syndr.* **2014**, *5*, 187–197. [CrossRef] [PubMed]
32. Montini, G.; Malaventura, C.; Salviati, L. Early coenzyme Q10 supplementation in primary coenzyme Q10 deficiency. *N. Engl. J. Med.* **2008**, *358*, 2849–2850. [CrossRef] [PubMed]
33. Ozeir, M.; Muhlenhoff, U.; Webert, H.; Lill, R.; Fontecave, M.; Pierrel, F. Coenzyme Q Biosynthesis: Coq6 Is Required for the C5-Hydroxylation Reaction and Substrate Analogs Rescue Coq6 Deficiency. *Chem. Biol.* **2011**, *18*, 1134–1142. [CrossRef] [PubMed]
34. Acosta Lopez, M.J.; Trevisson, E.; Canton, M.; Vazquez-Fonseca, L.; Morbidoni, V.; Baschiera, E.; Frasson, C.; Pelosi, L.; Rascalou, B.; Desbats, M.A.; et al. Vanillic Acid Restores Coenzyme Q Biosynthesis and ATP Production in Human Cells Lacking COQ6. *Oxid Med. Cell Longev.* **2019**, *2019*, 3904905. [CrossRef] [PubMed]
35. Landrum, M.J.; Lee, J.M.; Benson, M.; Brown, G.; Chao, C.; Chitipiralla, S.; Gu, B.; Hart, J.; Hoffman, D.; Hoover, J.; et al. ClinVar: Public archive of interpretations of clinically relevant variants. *Nucleic Acids Res.* **2016**, *44*, D862–868. [CrossRef] [PubMed]
36. Karczewski, K.J.; Francioli, L.C.; Tiao, G.; Cummings, B.B.; Alfoldi, J.; Wang, Q.; Collins, R.L.; Laricchia, K.M.; Ganna, A.; Birnbaum, D.P.; et al. The mutational constraint spectrum quantified from variation in 141,456 humans. *Nature* **2020**, *581*, 434–443. [CrossRef]
37. Khanna, T.; Hanna, G.; Sternberg, M.J.E.; David, A. Missense3D-DB web catalogue: An atom-based analysis and repository of 4M human protein-coding genetic variants. *Hum. Genet.* **2021**, *140*, 805–812. [CrossRef]
38. Ittisoponpisan, S.; Islam, S.A.; Khanna, T.; Alhuzimi, E.; David, A.; Sternberg, M.J.E. Can Predicted Protein 3D Structures Provide Reliable Insights into whether Missense Variants Are Disease Associated? *J. Mol. Biol.* **2019**, *431*, 2197–2212. [CrossRef]
39. Jumper, J.; Evans, R.; Pritzel, A.; Green, T.; Figurnov, M.; Ronneberger, O.; Tunyasuvunakool, K.; Bates, R.; Zidek, A.; Potapenko, A.; et al. Highly accurate protein structure prediction with AlphaFold. *Nature* **2021**, *596*, 583–589. [CrossRef]
40. Sim, N.L.; Kumar, P.; Hu, J.; Henikoff, S.; Schneider, G.; Ng, P.C. SIFT web server: Predicting effects of amino acid substitutions on proteins. *Nucleic Acids Res.* **2012**, *40*, W452–W457. [CrossRef]

41. Adzhubei, I.; Jordan, D.M.; Sunyaev, S.R. Predicting functional effect of human missense mutations using PolyPhen-2. *Curr. Protoc. Hum. Genet.* **2013**, *76*, 7.20.1–7.20.41. [CrossRef] [PubMed]
42. Benson, D.A.; Cavanaugh, M.; Clark, K.; Karsch-Mizrachi, I.; Lipman, D.J.; Ostell, J.; Sayers, E.W. GenBank. *Nucleic Acids Res.* **2013**, *41*, D36–D42. [CrossRef]
43. Sievers, F.; Higgins, D.G. Clustal Omega for making accurate alignments of many protein sequences. *Protein Sci* **2018**, *27*, 135–145. [CrossRef] [PubMed]
44. Waterhouse, A.M.; Procter, J.B.; Martin, D.M.; Clamp, M.; Barton, G.J. Jalview Version 2–a multiple sequence alignment editor and analysis workbench. *Bioinformatics* **2009**, *25*, 1189–1191. [CrossRef]
45. Zhu, Y.; Wu, B.; Zhang, X.; Fan, X.; Niu, L.; Li, X.; Wang, J.; Teng, M. Structural and biochemical studies reveal UbiG/Coq3 as a class of novel membrane-binding proteins. *Biochem. J.* **2015**, *470*, 105–114. [CrossRef] [PubMed]
46. Zhu, Y.; Jiang, X.; Wang, C.; Liu, Y.; Fan, X.; Zhang, L.; Niu, L.; Teng, M.; Li, X. Structural insights into the methyl donor recognition model of a novel membrane-binding protein UbiG. *Sci. Rep.* **2016**, *6*, 23147. [CrossRef]
47. Marbois, B.; Gin, P.; Gulmezian, M.; Clarke, C.F. The yeast Coq4 polypeptide organizes a mitochondrial protein complex essential for coenzyme Q biosynthesis. *Biochim. Biophys. Acta* **2009**, *1791*, 69–75. [CrossRef]
48. Dai, Y.N.; Zhou, K.; Cao, D.D.; Jiang, Y.L.; Meng, F.; Chi, C.B.; Ren, Y.M.; Chen, Y.X.; Zhou, C.Z. Crystal structures and catalytic mechanism of the C-methyltransferase Coq5 provide insights into a key step of the yeast coenzyme Q synthesis pathway. *Acta Crystallogr. Sect. D-Biol. Crystallogr.* **2014**, *70*, 2085–2092. [CrossRef]
49. Ismail, A.; Leroux, V.; Smadja, M.; Gonzalez, L.; Lombard, M.; Pierrel, F.; Mellot-Draznieks, C.; Fontecave, M. Coenzyme Q Biosynthesis: Evidence for a Substrate Access Channel in the FAD-Dependent Monooxygenase Coq6. *PLoS Comput. Biol.* **2016**, *12*, e1004690. [CrossRef]
50. Lohman, D.C.; Aydin, D.; Von Bank, H.C.; Smith, R.W.; Linke, V.; Weisenhorn, E.; McDevitt, M.T.; Hutchins, P.; Wilkerson, E.M.; Wancewicz, B.; et al. An Isoprene Lipid-Binding Protein Promotes Eukaryotic Coenzyme Q Biosynthesis. *Mol. Cell* **2019**, *73*, 763–774. [CrossRef]
51. Stenmark, P.; Grunler, J.; Mattsson, J.; Sindelar, P.J.; Nordlund, P.; Berthold, D.A. A new member of the family of di-iron carboxylate proteins. Coq7 (clk-1), a membrane-bound hydroxylase involved in ubiquinone biosynthesis. *J. Biol. Chem.* **2001**, *276*, 33297–33300. [CrossRef] [PubMed]
52. Manicki, M.; Aydin, H.; Abriata, L.A.; Overmyer, K.A.; Guerra, R.M.; Coon, J.J.; Dal Peraro, M.; Frost, A.; Pagliarini, D.J. Structure and functionality of a multimeric human COQ7:COQ9 complex. *Mol. Cell* **2022**, *82*, 1–17. [CrossRef] [PubMed]
53. O'Leary, N.A.; Wright, M.W.; Brister, J.R.; Ciufo, S.; Haddad, D.; McVeigh, R.; Rajput, B.; Robbertse, B.; Smith-White, B.; Ako-Adjei, D.; et al. Reference sequence (RefSeq) database at NCBI: Current status, taxonomic expansion, and functional annotation. *Nucleic Acids Res.* **2016**, *44*, D733–D745. [CrossRef] [PubMed]
54. Varadi, M.; Anyango, S.; Deshpande, M.; Nair, S.; Natassia, C.; Yordanova, G.; Yuan, D.; Stroe, O.; Wood, G.; Laydon, A.; et al. AlphaFold Protein Structure Database: Massively expanding the structural coverage of protein-sequence space with high-accuracy models. *Nuc. Acid. Res.* **2022**, *50*, D439–D444. [CrossRef] [PubMed]
55. Clarke, C.F.; Williams, W.; Teruya, J.H. Ubiquinone biosynthesis in *Saccharomyces cerevisiae*. Isolation and sequence of *COQ3*, the 3,4-dihydroxy-5-hexaprenylbenzoate methyltransferase gene. *J. Biol. Chem.* **1991**, *266*, 16636–16644. [CrossRef]
56. Jonassen, T.; Clarke, C.F. Isolation and functional expression of human *COQ3*, a gene encoding a methyltransferase required for ubiquinone biosynthesis. *J. Biol. Chem.* **2000**, *275*, 12381–12387. [CrossRef]
57. Poon, W.W.; Barkovich, R.J.; Hsu, A.Y.; Frankel, A.; Lee, P.T.; Shepherd, J.N.; Myles, D.C.; Clarke, C.F. Yeast and rat Coq3 and *Escherichia coli* UbiG polypeptides catalyze both *O*-methyltransferase steps in coenzyme Q biosynthesis. *J. Biol. Chem.* **1999**, *274*, 21665–21672. [CrossRef]
58. Yen, H.C.; Yeh, W.Y.; Lee, S.H.; Feng, Y.H.; Yang, S.L. Characterization of human mitochondrial PDSS and COQ proteins and their roles in maintaining coenzyme Q10 levels and each other's stability. *Biochim. Biophys. Acta Bioenerg.* **2020**, *1861*, 148192. [CrossRef]
59. Xie, L.X.; Ozeir, M.; Tang, J.Y.; Chen, J.Y.; Jaquinod, S.K.; Fontecave, M.; Clarke, C.F.; Pierrel, F. Overexpression of the Coq8 kinase in *Saccharomyces cerevisiae coq* null mutants allows for accumulation of diagnostic intermediates of the coenzyme Q_6 biosynthetic pathway. *J. Biol. Chem.* **2012**, *287*, 23571–23581. [CrossRef] [PubMed]
60. Pierrel, F.; Burgardt, A.; Lee, J.H.; Pelosi, L.; Wendisch, V.F. Recent advances in the metabolic pathways and microbial production of coenzyme Q. *World J. Microbiol. Biotechnol.* **2022**, *38*, 58. [CrossRef]
61. King, R.J.; Qiu, F.; Yu, F.; Singh, P.K. Metabolic and Immunological Subtypes of Esophageal Cancer Reveal Potential Therapeutic Opportunities. *Front. Cell Dev. Biol* **2021**, *9*, 667852. [CrossRef] [PubMed]
62. Shao, M.; Li, W.; Wang, S.; Liu, Z. Identification of key genes and pathways associated with esophageal squamous cell carcinoma development based on weighted gene correlation network analysis. *J. Cancer* **2020**, *11*, 1393–1402. [CrossRef] [PubMed]
63. Paulela, J.A.; Gomes, F.; Camandona, V.L.; Alegria, T.G.P.; Netto, L.E.S.; Bleicher, L.; Barros, M.H.; Ferreira-Junior, J.R. Coq3p relevant residues for protein activity and stability. *FEMS Yeast Res.* **2021**, *21*, foab055. [CrossRef] [PubMed]
64. Kagan, R.M.; Clarke, S. Widespread occurrence of three sequence motifs in diverse S-adenosylmethionine-dependent methyltransferases suggests a common structure for these enzymes. *Arch. Biochem. Biophys.* **1994**, *310*, 417–427. [CrossRef]
65. Petrossian, T.C.; Clarke, S.G. Multiple Motif Scanning to identify methyltransferases from the yeast proteome. *Mol. Cell Proteom.* **2009**, *8*, 1516–1526. [CrossRef] [PubMed]

66. Hajj Chehade, M.; Pelosi, L.; Fyfe, C.D.; Loiseau, L.; Rascalou, B.; Brugiere, S.; Kazemzadeh, K.; Vo, C.D.; Ciccone, L.; Aussel, L.; et al. A Soluble Metabolon Synthesizes the Isoprenoid Lipid Ubiquinone. *Cell Chem. Biol.* **2019**, *26*, 482–492. [CrossRef]
67. Martin, J.L.; McMillan, F.M. SAM (dependent) I AM: The S-adenosylmethionine-dependent methyltransferase fold. *Curr. Opin. Struct Biol.* **2002**, *12*, 783–793. [CrossRef]
68. Huang, Y.; Ji, L.; Huang, Q.; Vassylyev, D.G.; Chen, X.; Ma, J.B. Structural insights into mechanisms of the small RNA methyltransferase HEN1. *Nature* **2009**, *461*, 823–827. [CrossRef]
69. Casarin, A.; Jimenez-Ortega, J.C.; Trevisson, E.; Pertegato, V.; Doimo, M.; Ferrero-Gomez, M.L.; Abbadi, S.; Artuch, R.; Quinzii, C.; Hirano, M.; et al. Functional characterization of human *COQ4*, a gene required for Coenzyme Q_{10} biosynthesis. *Biochem. Biophys. Res. Commun.* **2008**, *372*, 35–39. [CrossRef]
70. Belogrudov, G.I.; Lee, P.T.; Jonassen, T.; Hsu, A.Y.; Gin, P.; Clarke, C.F. Yeast *COQ4* Encodes a Mitochondrial Protein Required for Coenzyme Q Synthesis. *Arch. Biochem. Biophys.* **2001**, *392*, 48–58. [CrossRef]
71. Yu, M.H.; Tsang, M.H.; Lai, S.; Ho, M.S.; Tse, D.M.L.; Willis, B.; Kwong, A.K.; Chou, Y.Y.; Lin, S.P.; Quinzii, C.M.; et al. Primary coenzyme Q10 deficiency-7: Expanded phenotypic spectrum and a founder mutation in southern Chinese. *NPJ Genom. Med.* **2019**, *4*, 18. [CrossRef] [PubMed]
72. Romero-Moya, D.; Castano, J.; Santos-Ocana, C.; Navas, P.; Menendez, P. Generation, genome edition and characterization of iPSC lines from a patient with coenzyme Q10 deficiency harboring a heterozygous mutation in COQ4 gene. *Stem Cell Res.* **2017**, *24*, 144–147. [CrossRef] [PubMed]
73. Romero-Moya, D.; Santos-Ocana, C.; Castano, J.; Garrabou, G.; Rodriguez-Gomez, J.A.; Ruiz-Bonilla, V.; Bueno, C.; Gonzalez-Rodriguez, P.; Giorgetti, A.; Perdiguero, E.; et al. Genetic Rescue of Mitochondrial and Skeletal Muscle Impairment in an Induced Pluripotent Stem Cells Model of Coenzyme Q_{10} Deficiency. *Stem Cells* **2017**, *35*, 1687–1703. [CrossRef] [PubMed]
74. Mero, S.; Salviati, L.; Leuzzi, V.; Rubegni, A.; Calderan, C.; Nardecchia, F.; Galatolo, D.; Desbats, M.A.; Naef, V.; Gemignani, F.; et al. New pathogenic variants in COQ4 cause ataxia and neurodevelopmental disorder without detectable CoQ10 deficiency in muscle or skin fibroblasts. *J. Neurol.* **2021**, *268*, 3381–3389. [CrossRef] [PubMed]
75. Salviati, L.; Trevisson, E.; Rodriguez Hernandez, M.A.; Casarin, A.; Pertegato, V.; Doimo, M.; Cassina, M.; Agosto, C.; Desbats, M.A.; Sartori, G.; et al. Haploinsufficiency of *COQ4* causes coenzyme Q_{10} deficiency. *J. Med. Genet.* **2012**, *49*, 187–191. [CrossRef]
76. Morrill, S.A.; Amon, A. Why haploinsufficiency persists. *Proc. Natl. Acad. Sci. USA* **2019**, *116*, 11866–11871. [CrossRef]
77. Chen, S.W.; Liu, C.C.; Yen, H.C. Detection of suppressed maturation of the human COQ5 protein in the mitochondria following mitochondrial uncoupling by an antibody recognizing both precursor and mature forms of COQ5. *Mitochondrion* **2013**, *13*, 143–152. [CrossRef]
78. Barkovich, R.J.; Shtanko, A.; Shepherd, J.A.; Lee, P.T.; Myles, D.C.; Tzagoloff, A.; Clarke, C.F. Characterization of the *COQ5* gene from *Saccharomyces cerevisiae*. Evidence for a C-methyltransferase in ubiquinone biosynthesis. *J. Biol. Chem.* **1997**, *272*, 9182–9188. [CrossRef]
79. Dibrov, E.; Robinson, K.M.; Lemire, B.D. The *COQ5* gene encodes a yeast mitochondrial protein necessary for ubiquinone biosynthesis and the assembly of the respiratory chain. *J. Biol. Chem.* **1997**, *272*, 9175–9181. [CrossRef]
80. Baba, S.W.; Belogrudov, G.I.; Lee, J.C.; Lee, P.T.; Strahan, J.; Shepherd, J.N.; Clarke, C.F. Yeast Coq5 C-methyltransferase is required for stability of other polypeptides involved in coenzyme Q biosynthesis. *J. Biol. Chem.* **2004**, *279*, 10052–10059. [CrossRef]
81. He, C.H.; Xie, L.X.; Allan, C.M.; Tran, U.C.; Clarke, C.F. Coenzyme Q supplementation or over-expression of the yeast Coq8 putative kinase stabilizes multi-subunit Coq polypeptide complexes in yeast *coq* null mutants. *Biochim. Biophys. Acta (BBA)-Mol. Cell Biol. Lipids* **2014**, *1841*, 630–644. [CrossRef]
82. Schubert, H.L.; Blumenthal, R.M.; Cheng, X. Many paths to methyltransfer: A chronicle of convergence. *Trends Biochem. Sci.* **2003**, *28*, 329–335. [CrossRef]
83. Malicdan, M.C.V.; Vilboux, T.; Ben-Zeev, B.; Guo, J.; Eliyahu, A.; Pode-Shakked, B.; Dori, A.; Kakani, S.; Chandrasekharappa, S.C.; Ferreira, C.R.; et al. A novel inborn error of the coenzyme Q_{10} biosynthesis pathway: Cerebellar ataxia and static encephalomyopathy due to COQ5 C-methyltransferase deficiency. *Hum. Mutat.* **2018**, *39*, 69–79. [CrossRef] [PubMed]
84. Altschul, S.F.; Gish, W.; Miller, W.; Myers, E.W.; Lipman, D.J. Basic local alignment search tool. *J. Mol. Biol.* **1990**, *215*, 403–410. [CrossRef]
85. Huijbers, M.M.; Montersino, S.; Westphal, A.H.; Tischler, D.; van Berkel, W.J. Flavin dependent monooxygenases. *Arch. Biochem. Biophys.* **2014**, *544*, 2–17. [CrossRef]
86. van Berkel, W.J.; Kamerbeek, N.M.; Fraaije, M.W. Flavoprotein monooxygenases, a diverse class of oxidative biocatalysts. *J. Biotechnol.* **2006**, *124*, 670–689. [CrossRef]
87. Marbois, B.; Xie, L.X.; Choi, S.; Hirano, K.; Hyman, K.; Clarke, C.F. para-Aminobenzoic acid is a precursor in coenzyme Q_6 biosynthesis in *Saccharomyces cerevisiae*. *J. Biol. Chem.* **2010**, *285*, 27827–27838. [CrossRef]
88. Ozeir, M.; Pelosi, L.; Ismail, A.; Mellot-Draznieks, C.; Fontecave, M.; Pierrel, F. Coq6 is responsible for the C4-deamination reaction in coenzyme Q biosynthesis in *Saccharomyces cerevisiae*. *J. Biol. Chem.* **2015**, *290*, 24140–24151. [CrossRef]
89. Gin, P.; Hsu, A.Y.; Rothman, S.C.; Jonassen, T.; Lee, P.T.; Tzagoloff, A.; Clarke, C.F. The *Saccharomyces cerevisiae COQ6* gene encodes a mitochondrial flavin-dependent monooxygenase required for coenzyme Q biosynthesis. *J. Biol. Chem.* **2003**, *278*, 25308–25316. [CrossRef]

90. Doimo, M.; Trevisson, E.; Airik, R.; Bergdoll, M.; Santos-Ocana, C.; Hildebrandt, F.; Navas, P.; Pierrel, F.; Salviati, L. Effect of vanillic acid on *COQ6* mutants identified in patients with coenzyme Q_{10} deficiency. *Biochim. Biophys. Acta-Mol. Basis Dis.* **2014**, *1842*, 1–6. [CrossRef]
91. Drovandi, S.; Lipska-Zietkiewicz, B.S.; Ozaltin, F.; Emma, F.; Gulhan, B.; Boyer, O.; Trautmann, A.; Zietkiewicz, S.; Xu, H.; Shen, Q.; et al. Variation of the clinical spectrum and genotype-phenotype associations in Coenzyme Q10 deficiency associated glomerulopathy. *Kidney Int.* **2022**, *102*, 592–603. [CrossRef] [PubMed]
92. Heeringa, S.F.; Chernin, G.; Chaki, M.; Zhou, W.; Sloan, A.J.; Ji, Z.; Xie, L.X.; Salviati, L.; Hurd, T.W.; Vega-Warner, V.; et al. *COQ6* mutations in human patients produce nephrotic syndrome with sensorineural deafness. *J. Clin. Investig.* **2011**, *121*, 2013–2024. [CrossRef] [PubMed]
93. Yuruk Yildirim, Z.; Toksoy, G.; Uyguner, O.; Nayir, A.; Yavuz, S.; Altunoglu, U.; Turkkan, O.N.; Sevinc, B.; Gokcay, G.; Kurkcu Gunes, D.; et al. Primary coenzyme Q10 Deficiency-6 (COQ10D6): Two siblings with variable expressivity of the renal phenotype. *Eur. J. Med. Genet.* **2020**, *63*, 103621. [CrossRef] [PubMed]
94. Justine Perrin, R.; Rousset-Rouviere, C.; Garaix, F.; Cano, A.; Conrath, J.; Boyer, O.; Tsimaratos, M. COQ6 mutation in patients with nephrotic syndrome, sensorineural deafness, and optic atrophy. *JIMD Rep.* **2020**, *54*, 37–44. [CrossRef]
95. Wierenga, R.K.; Terpstra, P.; Hol, W.G. Prediction of the occurrence of the ADP-binding beta alpha beta-fold in proteins, using an amino acid sequence fingerprint. *J. Mol. Biol.* **1986**, *187*, 101–107. [CrossRef]
96. Zhang, K.; Lin, J.W.; Wang, J.; Wu, X.; Gao, H.; Hsieh, Y.C.; Hwu, P.; Liu, Y.R.; Su, L.; Chiou, H.Y.; et al. A germline missense mutation in COQ6 is associated with susceptibility to familial schwannomatosis. *Genet. Med. Off. J. Am. Coll. Med. Genet.* **2014**, *16*, 787–792. [CrossRef]
97. Trevisson, E.; Clementi, M.; Salviati, L. Is there a link between COQ6 and schwannomatosis? *Genet. Med. Off. J. Am. Coll. Med. Genet.* **2015**, *17*, 312–313. [CrossRef]
98. Eggink, G.; Engel, H.; Vriend, G.; Terpstra, P.; Witholt, B. Rubredoxin reductase of Pseudomonas oleovorans. Structural relationship to other flavoprotein oxidoreductases based on one NAD and two FAD fingerprints. *J. Mol. Biol.* **1990**, *212*, 135–142. [CrossRef]
99. Stanczyk, M.; Balasz-Chmielewska, I.; Lipska-Zietkiewicz, B.; Tkaczyk, M. CoQ10-related sustained remission of proteinuria in a child with COQ6 glomerulopathy-a case report. *Pediatr. Nephrol.* **2018**, *33*, 2383–2387. [CrossRef]
100. Sadowski, C.E.; Lovric, S.; Ashraf, S.; Pabst, W.L.; Gee, H.Y.; Kohl, S.; Engelmann, S.; Vega-Warner, V.; Fang, H.; Halbritter, J.; et al. A single-gene cause in 29.5% of cases of steroid-resistant nephrotic syndrome. *J. Am. Soc. Nephrol.* **2015**, *26*, 1279–1289. [CrossRef]
101. Behan, R.K.; Lippard, S.J. The aging-associated enzyme CLK-1 is a member of the carboxylate-bridged diiron family of proteins. *Biochemistry* **2010**, *49*, 9679–9681. [CrossRef] [PubMed]
102. Marbois, B.N.; Clarke, C.F. The *COQ7* gene encodes a protein in *Saccharomyces cerevisiae* necessary for ubiquinone biosynthesis. *J. Biol. Chem.* **1996**, *271*, 2995–3004. [CrossRef] [PubMed]
103. Wang, Y.; Smith, C.; Parboosingh, J.S.; Khan, A.; Innes, M.; Hekimi, S. Pathogenicity of two *COQ7* mutations and responses to 2,4-dihydroxybenzoate bypass treatment. *J. Cell. Mol. Med.* **2017**, *21*, 2329–2343. [CrossRef] [PubMed]
104. Vajo, Z.; King, L.M.; Jonassen, T.; Wilkin, D.J.; Ho, N.; Munnich, A.; Clarke, C.F.; Francomano, C.A. Conservation of the *Caenorhabditis elegans* timing gene *clk-1* from yeast to human: A gene required for ubiquinone biosynthesis with potential implications for aging. *Mamm. Genome* **1999**, *10*, 1000–1004. [CrossRef]
105. Lu, T.T.; Lee, S.J.; Apfel, U.P.; Lippard, S.J. Aging-associated enzyme human clock-1: Substrate-mediated reduction of the diiron center for 5-demethoxyubiquinone hydroxylation. *Biochemistry* **2013**, *52*, 2236–2244. [CrossRef]
106. Hsieh, E.J.; Gin, P.; Gulmezian, M.; Tran, U.C.; Saiki, R.; Marbois, B.N.; Clarke, C.F. *Saccharomyces cerevisiae* Coq9 polypeptide is a subunit of the mitochondrial coenzyme Q biosynthetic complex. *Arch. Biochem. Biophys.* **2007**, *463*, 19–26. [CrossRef]
107. He, C.H.; Black, D.S.; Nguyen, T.P.; Wang, C.; Srinivasan, C.; Clarke, C.F. Yeast Coq9 controls deamination of coenzyme Q intermediates that derive from para-aminobenzoic acid. *Biochim. Biophys. Acta* **2015**, *1851*, 1227–1239. [CrossRef]
108. Danhauser, K.; Herebian, D.; Haack, T.B.; Rodenburg, R.J.; Strom, T.M.; Meitinger, T.; Klee, D.; Mayatepek, E.; Prokisch, H.; Distelmaier, F. Fatal neonatal encephalopathy and lactic acidosis caused by a homozygous loss-of-function variant in COQ9. *Eur. J. Hum. Genet. EJHG* **2016**, *24*, 450–454. [CrossRef]
109. Herebian, D.; Seibt, A.; Smits, S.H.J.; Bunning, G.; Freyer, C.; Prokisch, H.; Karall, D.; Wredenberg, A.; Wedell, A.; Lopez, L.C.; et al. Detection of 6-demethoxyubiquinone in CoQ_{10} deficiency disorders: Insights into enzyme interactions and identification of potential therapeutics. *Mol. Genet. Metab.* **2017**, *121*, 216–223. [CrossRef]
110. Cuthbertson, L.; Nodwell, J.R. The TetR family of regulators. *Microbiol. Mol. Biol. Rev.* **2013**, *77*, 440–475. [CrossRef]
111. Ling, T.K.; Law, C.Y.; Yan, K.W.; Fong, N.C.; Wong, K.C.; Lee, K.L.; Chu, W.C.; Brea-Calvo, G.; Lam, C.W. Clinical whole-exome sequencing reveals a common pathogenic variant in patients with CoQ10 deficiency: An underdiagnosed cause of mitochondriopathy. *Clin. Chim. Acta* **2019**, *497*, 88–94. [CrossRef] [PubMed]
112. Kemmerer, Z.A.; Robinson, K.P.; Schmitz, J.M.; Manicki, M.; Paulson, B.R.; Jochem, A.; Hutchins, P.D.; Coon, J.J.; Pagliarini, D.J. UbiB proteins regulate cellular CoQ distribution in Saccharomyces cerevisiae. *Nat. Commun.* **2021**, *12*, 4769. [CrossRef] [PubMed]
113. Fernandez-Del-Rio, L.; Kelly, M.E.; Contreras, J.; Bradley, M.C.; James, A.M.; Murphy, M.P.; Payne, G.S.; Clarke, C.F. Genes and lipids that impact uptake and assimilation of exogenous coenzyme Q in Saccharomyces cerevisiae. *Free Radic. Biol. Med.* **2020**, *154*, 105–118. [CrossRef] [PubMed]

114. Luna-Sanchez, M.; Diaz-Casado, E.; Barca, E.; Tejada, M.A.; Montilla-Garcia, A.; Cobos, E.J.; Escames, G.; Acuna-Castroviejo, D.; Quinzii, C.M.; Lopez, L.C. The clinical heterogeneity of coenzyme Q_{10} deficiency results from genotypic differences in the *Coq9* gene. *EMBO Mol. Med.* **2015**, *7*, 670–687. [CrossRef] [PubMed]
115. Freyer, C.; Stranneheim, H.; Naess, K.; Mourier, A.; Felser, A.; Maffezzini, C.; Lesko, N.; Bruhn, H.; Engvall, M.; Wibom, R.; et al. Rescue of primary ubiquinone deficiency due to a novel *COQ7* defect using 2,4-dihydroxybensoic acid. *J. Med. Genet.* **2015**, *52*, 779–783. [CrossRef] [PubMed]
116. Murphy, M.P.; Smith, R.A.J. Targeting antioxidants to mitochondria by conjugation to lipophilic cations. *Ann. Rev. Pharm. Toxicol* **2007**, *47*, 629–656. [CrossRef]
117. Broome, S.C.; Pham, T.; Braakhuis, A.J.; Narang, R.; Wang, H.W.; Hickey, A.J.R.; Mitchell, C.J.; Merry, T.L. MitoQ supplementation augments acute exercise-induced increases in muscle PGC1alpha mRNA and improves training-induced increases in peak power independent of mitochondrial content and function in untrained middle-aged men. *Redox Biol.* **2022**, *53*, 102341. [CrossRef]
118. Williamson, J.; Hughes, C.M.; Cobley, J.N.; Davison, G.W. The mitochondria-targeted antioxidant MitoQ, attenuates exercise-induced mitochondrial DNA damage. *Redox Biol.* **2020**, *36*, 101673. [CrossRef]
119. James, A.M.; Cocheme, H.M.; Smith, R.A.; Murphy, M.P. Interactions of mitochondria-targeted and untargeted ubiquinones with the mitochondrial respiratory chain and reactive oxygen species. Implications for the use of exogenous ubiquinones as therapies and experimental tools. *J. Biol. Chem.* **2005**, *280*, 21295–21312. [CrossRef]
120. Westermann, B. Mitochondrial fusion and fission in cell life and death. *Nat. Rev. Mol. Cell Biol.* **2010**, *11*, 872–884. [CrossRef]
121. Gabelein, C.G.; Feng, Q.; Sarajlic, E.; Zambelli, T.; Guillaume-Gentil, O.; Kornmann, B.; Vorholt, J.A. Mitochondria transplantation between living cells. *PLoS Biol.* **2022**, *20*, e3001576. [CrossRef] [PubMed]
122. Liu, D.; Gao, Y.; Liu, J.; Huang, Y.; Yin, J.; Feng, Y.; Shi, L.; Meloni, B.P.; Zhang, C.; Zheng, M.; et al. Intercellular mitochondrial transfer as a means of tissue revitalization. *Signal. Transduct Target.* **2021**, *6*, 65. [CrossRef] [PubMed]
123. Cameron, R.B.; Beeson, C.C.; Schnellmann, R.G. Development of Therapeutics That Induce Mitochondrial Biogenesis for the Treatment of Acute and Chronic Degenerative Diseases. *J. Med. Chem.* **2016**, *59*, 10411–10434. [CrossRef] [PubMed]
124. Scarpulla, R.C. Transcriptional paradigms in mammalian mitochondrial biogenesis and function. *Physiol. Rev.* **2008**, *88*, 611–638. [CrossRef] [PubMed]
125. Bertoli-Avella, A.M.; Beetz, C.; Ameziane, N.; Rocha, M.E.; Guatibonza, P.; Pereira, C.; Calvo, M.; Herrera-Ordonez, N.; Segura-Castel, M.; Diego-Alvarez, D.; et al. Successful Application of Genome Sequencing in a Diagnostic Setting: 1007 Index Cases from a Clinically Heterogeneous Cohort. *Eur. J. Hum. Genet.* **2021**, *29*, 141–153. [CrossRef]
126. Bosch, A.M.; Kamsteeg, E.-J.; Rodenburg, R.J.; van Deutekom, A.W.; Buis, D.R.; Engelen, M.; Cobben, J.-M. Coenzyme Q10 Deficiency Due to a COQ4 Gene Defect Causes Childhood-Onset Spinocerebellar Ataxia and Stroke-like Episodes. *Mol. Genet. Metab. Rep.* **2018**, *17*, 19–21. [CrossRef]
127. Brea-Calvo, G.; Haack, T.B.; Karall, D.; Ohtake, A.; Invernizzi, F.; Carrozzo, R.; Kremer, L.; Dusi, S.; Fauth, C.; Scholl-Bürgi, S.; et al. COQ4 Mutations Cause a Broad Spectrum of Mitochondrial Disorders Associated with CoQ10 Deficiency. *Am. J. Hum. Genet.* **2015**, *96*, 309–317. [CrossRef]
128. Caglayan, A.O.; Gumus, H.; Sandford, E.; Kubisiak, T.L.; Ma, Q.; Ozel, A.B.; Per, H.; Li, J.Z.; Shakkottai, V.G.; Burmeister, M. COQ4 Mutation Leads to Childhood-Onset Ataxia Improved by CoQ10 Administration. *Cerebellum* **2019**, *18*, 665–669. [CrossRef]
129. Cao, Q.; Li, G.M.; Xu, H.; Shen, Q.; Sun, L.; Fang, X.Y.; Liu, H.M.; Guo, W.; Zhai, Y.H.; Wu, B.B. Coenzyme Q(10) treatment for one child with COQ6 gene mutation induced nephrotic syndrome and literature review. *Zhonghua Er Ke Za Zhi Chin. J. Pediatr.* **2017**, *55*, 135–138. [CrossRef]
130. Chung, W.K.; Martin, K.; Jalas, C.; Braddock, S.R.; Juusola, J.; Monaghan, K.G.; Warner, B.; Franks, S.; Yudkoff, M.; Lulis, L.; et al. Mutations in COQ4, an Essential Component of Coenzyme Q Biosynthesis, Cause Lethal Neonatal Mitochondrial Encephalomyopathy. *J. Med. Genet.* **2015**, *52*, 627–635. [CrossRef]
131. Fung, J.L.F.; Yu, M.H.C.; Huang, S.; Chung, C.C.Y.; Chan, M.C.Y.; Pajusalu, S.; Mak, C.C.Y.; Hui, V.C.C.; Tsang, M.H.Y.; Yeung, K.S.; et al. A Three-Year Follow-up Study Evaluating Clinical Utility of Exome Sequencing and Diagnostic Potential of Reanalysis. *NPJ Genom. Med.* **2020**, *5*, 1–11. [CrossRef]
132. Gigante, M.; Diella, S.; Santangelo, L.; Trevisson, E.; Acosta, M.J.; Amatruda, M.; Finzi, G.; Caridi, G.; Murer, L.; Accetturo, M.; et al. Further Phenotypic Heterogeneity of CoQ10 Deficiency Associated with Steroid Resistant Nephrotic Syndrome and Novel COQ2 and COQ6 Variants: Letter to the Editor. *Clin. Genet.* **2017**, *92*, 224–226. [CrossRef]
133. Helbig, K.L.; Farwell Hagman, K.D.; Shinde, D.N.; Mroske, C.; Powis, Z.; Li, S.; Tang, S.; Helbig, I. Diagnostic Exome Sequencing Provides a Molecular Diagnosis for a Significant Proportion of Patients with Epilepsy. *Genet. Med.* **2016**, *18*, 898–905. [CrossRef]
134. Kakiuchi, T.; Ohtsuka, Y.; Sato, T.; Nakayama, A.; Jinnouchi, K.; Oka, M.; Matsuo, M. Association between Crohn's Disease and AarF Domain-Containing Kinase 4 Glomerulopathy. *Clin. J. Gastroenterol.* **2019**, *12*, 263–268. [CrossRef]
135. Korkmaz, E.; Lipska-Ziętkiewicz, B.S.; Boyer, O.; Gribouval, O.; Fourrage, C.; Tabatabaei, M.; Schnaidt, S.; Gucer, S.; Kaymaz, F.; Arici, M.; et al. ADCK4-Associated Glomerulopathy Causes Adolescence-Onset FSGS. *J. Am. Soc. Nephrol.* **2016**, *27*, 63–68. [CrossRef]
136. Koyun, M.; Çomak, E.; Akman, S. CoenzymeQ10 Therapy in Two Sisters with CoQ6 Mutations with Long-Term Follow-Up. *Pediatr. Nephrol.* **2019**, *34*, 737–738. [CrossRef] [PubMed]
137. Kwong, A.K.-Y.; Chiu, A.T.-G.; Tsang, M.H.-Y.; Lun, K.; Rodenburg, R.J.T.; Smeitink, J.; Chung, B.H.-Y.; Fung, C. A Fatal Case of COQ7 -associated Primary Coenzyme Q 10 Deficiency. *JIMD Reports* **2019**, *47*, 23–29. [CrossRef] [PubMed]

138. Landis, B.J.; Lai, D.; Guo, D.-C.; Corvera, J.S.; Idrees, M.T.; Stadler, H.W.; Cuevas, C.; Needler, G.U.; Vujakovich, C.E.; Milewicz, D.M.; et al. Identification of a Common Polymorphism in COQ8B Acting as a Modifier of Thoracic Aortic Aneurysm Severity. *HGG Adv.* **2022**, *3*, 100057. [CrossRef]
139. Li, G.; Cao, Q.; Shen, Q.; Sun, L.; Zhai, Y.; Liu, H.; An, Y.; Xu, H. Gene Mutation Analysis in 12 Chinese Children with Congenital Nephrotic Syndrome. *BMC Nephrol.* **2018**, *19*, 382. [CrossRef]
140. Liang, Y.; Wei, H.; Yu, X.; Huang, W.; Luo, X.P. Rapidly progressive puberty in a patient with mosaic Turner syndrome: A case report and literature review. *Zhonghua Er Ke Za Zhi Chin. J. Pediatr.* **2017**, *55*, 125–130. [CrossRef]
141. Lu, M.; Zhou, Y.; Wang, Z.; Xia, Z.; Ren, J.; Guo, Q. Clinical Phenotype, in Silico and Biomedical Analyses, and Intervention for an East Asian Population-Specific c.370G>A (p.G124S) COQ4 Mutation in a Chinese Family with CoQ10 Deficiency-Associated Leigh Syndrome. *J. Hum. Genet.* **2019**, *64*, 297–304. [CrossRef]
142. Malinowski, J.R.; Denny, J.C.; Bielinski, S.J.; Basford, M.A.; Bradford, Y.; Peissig, P.L.; Carrell, D.; Crosslin, D.R.; Pathak, J.; Rasmussen, L.; et al. Genetic Variants Associated with Serum Thyroid Stimulating Hormone (TSH) Levels in European Americans and African Americans from the EMERGE Network. *PLoS ONE* **2014**, *9*, e111301. [CrossRef]
143. McKnight, A.J.; Currie, D.; Patterson, C.C.; Maxwell, A.P.; Fogarty, D.G. Targeted Genome-Wide Investigation Identifies Novel SNPs Associated with Diabetic Nephropathy. *Hugo J.* **2009**, *3*, 77–82. [CrossRef]
144. Nykamp, K.; Anderson, M.; Powers, M.; Garcia, J.; Herrera, B.; Ho, Y.-Y.; Kobayashi, Y.; Patil, N.; Thusberg, J.; Westbrook, M.; et al. Sherloc: A Comprehensive Refinement of the ACMG–AMP Variant Classification Criteria. *Genet. Med.* **2017**, *19*, 1105–1117. [CrossRef]
145. Park, E.; Ahn, Y.H.; Kang, H.G.; Yoo, K.H.; Won, N.H.; Lee, K.B.; Moon, K.C.; Seong, M.-W.; Gwon, T.; Park, S.S.; et al. COQ6 Mutations in Children With Steroid-Resistant Focal Segmental Glomerulosclerosis and Sensorineural Hearing Loss. *Am. J. Kidney Dis.* **2017**, *70*, 139–144. [CrossRef]
146. Richards, S.; Aziz, N.; Bale, S.; Bick, D.; Das, S.; Gastier-Foster, J.; Grody, W.W.; Hegde, M.; Lyon, E.; Spector, E.; et al. Standards and Guidelines for the Interpretation of Sequence Variants: A Joint Consensus Recommendation of the American College of Medical Genetics and Genomics and the Association for Molecular Pathology. *Genet. Med.* **2015**, *17*, 405–424. [CrossRef]
147. Salviati, L.; Trevisson, E.; Doimo, M.; Navas, P. Primary Coenzyme Q10 Deficiency. In *Gene Reviews*; Adam, M.P., Ardinger, H.H., Pagon, R.A., Wallace, S.E., Bean, L.J., Gripp, K.W., Mirzaa, G.M., Amemiya, A., Eds.; University of Washington, Seattle: Seattle, WA, USA, 2017; pp. 1–28.
148. Sondheimer, N.; Hewson, S.; Cameron, J.M.; Somers, G.R.; Broadbent, J.D.; Ziosi, M.; Quinzii, C.M.; Naini, A.B. Novel Recessive Mutations in COQ4 Cause Severe Infantile Cardiomyopathy and Encephalopathy Associated with CoQ 10 Deficiency. *Mol. Genet. Metab. Rep.* **2017**, *12*, 23–27. [CrossRef]